HEALTH MONITORING OF RC BEAM-COLUMN JOINTS USING ACOUSTIC EMISSION TECHNIQUE

A Thesis

Submitted in partial fulfilment of the requirement

for the award of the degree of

DOCTOR OF PHILOSOPHY
IN
CIVIL ENGINEERING

Submitted by
Shamsher Singh
Roll No. 951002001

Dr Naveen Kwatra
Professor

Dr Shruti Sharma
Professor

DEPARTMENT OF CIVIL ENGINEERING,
THAPAR INSTITUTE OF ENGINEERING & TECHNOLOGY,
(Deemed to be University), PATIALA-147004,
PUNJAB (INDIA)

May 2022

CERTIFICATE

It is certified that the thesis report entitled "Health Monitoring of RC Beam-Column Joints Using Acoustic Emission Technique", which is being submitted herewith by Shamsher Singh, in partial fulfilment for the award of degree in Doctoral of Civil Engineering (Structures) at Thapar Institute of Engineering and Technology, Patiala is an authentic record of student's work carried out under my supervision and guidance. The matter presented in the thesis has reached the standards fulfilling the regulatory requirements for the award of said degree.

Dr Naveen Kwatra
Professor,
Civil Engineering Department,
TIET, Patiala
(Supervisor)

Dr Shruti Sharma
Professor,
Civil Engineering Department,
TIET, Patiala
(Supervisor)

DECLARATION

It is hereby certified that the work which is being submitted in this thesis, entitled "**Health Monitoring of RC Beam-Column joints using Acoustic Emission Technique**", in fulfilment of the requirement for the award of the degree of Doctor of Philosophy in Civil Engineering submitted to Civil Engineering Department of Thapar Institute of Engineering and Technology, Patiala is an authentic record of my work carried out under my supervision and guidance of Dr Naveen Kwatra and Dr Shruti Sharma. Wherever other research work is referred, it is indexed in the list of references.

The matter presented in this thesis has not been submitted in part or whole to any other university or institute to award any degree in India or abroad.

(Shamsher Singh)

ACKNOWLEDGEMENTS

Writing this dissertation has been a great learning experience because Acoustic Emission monitoring, the core subject of my PhD work, is a fast-developing and challenging field for damage detection in concrete structures. It would not have been possible to complete this project without the support and guidance of my guides, teachers, family members, lab assistants, friends and many others.

I am greatly indebted to Dr Naveen Kwatra and Dr Shruti Sharma, my research advisors, for their deep insight, encouragement, support and immense patience during the entire research period. Their expertise was invaluable in formulating research questions and methodology. They have continuously inspired and encouraged me to sharpen my thinking and enhance my professional skills.

I am also grateful to Dr Prem Pal Bansal, Head of the Department of Civil Engineering, for providing the facilities required for experimental works. Special thanks to Dr Rafat Siddique, Sr. Professor and Dean of Research and Sponsored Projects, for helping me develop concrete mix design skills. Suggestions provided by Dr Shweta Goyal were essential in the timely completion of this project. Special thanks to Doctoral committee members Dr Naveen Kwatra, Dr Shruti Sharma, Dr Shweta Goel, Dr Rajesh Kumar, Dr Trishna Choudhury, and Dr A. B. Daine Roy for their joyful inspiration, admirable guidance and significant remarks.

Additionally, I would like to thank Dr Kirti Vardhan and Priya Goyal, my PhD colleague, Varinder Kumar, Lab Technician, and all my Thapar PG/PhD friends for helping me with acoustic emission testing. Special thanks to Dr Anil Kumar, Satya Singh, and Ram Bhawan, working in Punjab State Corporation Limited, for their immense support in my experimental work.

While writing this manuscript, I received prodigious support and assistance from my near and dear ones. My family members demanded more attention, but none let me realise their issues and continuously helped and encouraged me to undertake this challenging task. My son

Architect Japjeet Singh, daughter, Architect Japleen Kaur, and son-in-law Satbir Singh (Assistant Commandant, CISF), have helped me a lot in finalising and finishing this herculean task. I received immense support from my better half, Harkiranjit Kaur, for encouraging and cheering me up whenever it was required.

The timely completion of this challenging project would not have been possible without the blessing of Darji, the head of our family. Big thanks to my brother Dr Manjit Singh (Retired Prof Head of Orthopaedic Department, Rajindra hospital Patiala), Dr Parneet Kaur Head of Gynaecological dept), Dr Manmohan Singh (Prof Department of Neurosurgery & Gamma Knife Centre, AIIMS) and our most loveable family friend Hussan Lal (IAS) for their encouragement and support.

The Thapar Institute Management deserve special thanks for developing excellent library facilities and a conducive environment for experimental work. My PhD work would have been incomplete without a mathematical tool like MATLAB. I am incredibly thankful to the developers of this excellent software, having every possible facility for massive data management. A user-friendly facility for creating figure works within the MATLAB environment has helped me handle extensive data. Numerous people and teams continuously work behind the scenes by sharing useful MATLAB functions. These selfless people deserve special praise for helping me develop new functions and refining my figure work.

Lastly, I dedicate this project to my mother and father, who left for a heavenly abode much before starting this project. Their blessings have helped me complete this thesis.

(Shamsher Singh)

LIST OF PUBLICATION

Title	: Damage progression in RC Beam-Column Joints under cyclic loading using acoustic emission technique
Authors	: Shamsher Singh, Shruti Sharma and Naveen Kwatra
Date of Acceptance	: 16 August 2021
Journal	: Structural Concrete, DOI: 10.1002/suco.202000713
Impact Factor	: 2.793 (updated 2023)

Title	: A novel damage index for reinforced concrete beam-column joints using acoustic emission Technique
Authors	: Shamsher Singh, Shruti Sharma and Naveen Kwatra
Date of Publication	: 22 Jan 2022
Journal	: European Journal of Environmental and Civil Engineering, DOI: 10.1080/19648189.2021.2023653
Impact Factor	: 2.178 (updated 2023)

Title	: Health monitoring of ECC retrofitted beam-column joints using acoustic emission technique.
Authors	: Shamsher Singh, Shruti Sharma and Naveen Kwatra
Journal	: Manuscript under preparation

ABSTRACT

Structural Health Monitoring (SHM) is an important field to investigate the current state of structures and check the damages caused by devastating forces such as an earthquake. Various non-destructive techniques (NDT) have been employed to monitor the health of the structural system. The existing SHM techniques are capable of detecting the damage with limited precision. Apart from damage detection, quantification of damage is also very important. Load and deformation responses are essential parameters used in damage detection but these parameters are extremely difficult to measure especially in structures damaged due to seismic forces. The various techniques do suffer from certain deficiencies in estimating these parameters after the occurrence of an earthquake. To fill these gaps in research, the current study aims to identify and quantify damage in the reinforced concrete (RC) structural elements by exploring Acoustic Emission (AE) technique. The use of the AE technique is gaining popularity in monitoring various structural applications. It is a passive monitoring technique that is often used to obtain a qualitative and qualitative estimation of damage by studying the variation of AE parameters. The acoustic Emission Technique (AET) is susceptible to crack growth and can locate the source of the AE waveform initiated from the point of damage. This technique can perform real-time monitoring by detecting cracks as it occurs or grows. Despite these advantages, challenges still exist in using the AET, especially in analysing large volumes of AE data recorded during AE monitoring. Primarily this technique has three objectives. Firstly, it helps to locate the source of damage accurately. Secondly, it helps identify and differentiate signals from different sources of AE; lastly, it is capable of quantifying the extent of damage to structures. The study has given inspiring results for analysing test data, thereby opening an opportunity for its use in real-life structures.

This research effort has focused on quantifying damage by developing a novel damage index using the AE technique for Beam-Column Joints (BCJ) subjected to cyclic loading with and without ductile detailing. The deformation and load responses have been studied to get

energy dissipated during cyclic loading. The variation in trends of energy dissipated vis-a-vis acoustic energy has been observed, and a close relationship has been observed between these two energy parameters. A novel damage index has been developed to quantify damage in the BCJ subjected to cyclic loads based on the Acoustic Energy parameter. Further, BCJ was repaired using Engineering Cementitious Composites (ECC). This retrofitting composite has excellent behaviour under tensile and shear loading and helps improve the structures' ductility by distributing cracks uniformly. MATLAB mathematical models have been developed to find the relationship between AE energy and dissipated energy. MATLAB programmes have also been developed for the post-processing of AE data and drawing graphs to predict the damage in BCJ before and after the retrofit. The study has yielded significant results for health monitoring of BCJ designed with and without ductile detailing subjected to cyclic loads and further repaired with ECC as summarised below:

- From the load-deformation characteristics, the Energy Dissipation in ductile BCJ samples is about 3 to 4 times more than in the non-ductile BCJ when subjected to cyclic load. The ductility factor is a valuable parameter for checking the ductile behaviour of BCJ samples. The ductility factor of the ductile BCJ sample is about three times more than the non-ductile BCJ sample.
- The variation of the energy dissipation curve closely matches the AE energy curve at various stages of damage of BCJ subjected to cyclic loading. A relationship has been developed between these two parameters using MATLAB. Thus, the energy dissipation can be estimated using AE energy obtained from AE testing.
- The Improved b-value analysis, primarily based on Gutenberg-Richter law, helps recognise different stages of damage in the structures and evaluate the presence of macro cracks. Ib-value <1 indicates the occurrence of severe damage, and a value from 1-2 shows intermediate damage. Ib-value > 2 is an indication of minor damage. BCJ members designed for ductility formed about two times more additional AE hits

corresponding to severe damage than a non-ductile sample and about three times higher hits corresponding to moderate damage.

- The Felicity Ratio (FR), which is defined as the ratio of load at the start of AE activities to the previous cycle's maximum load, is a powerful tool for observing damage in beam-column joints. A Felicity ratio greater than or equal to one indicates no damage. A Felicity Ratio of 0.75 to 1 is indicative of minor damage. FR lying between 0.5 and 0.75 is indicative of major damage. But FR doesn't provide a true damage state when BCJ is deformed beyond displacement corresponding to peak load.
- Based on AE energy, a novel damage index has been developed in this study for quantifying damage in BCJ. This damage index is a function of two non-dimensional variables, i.e. the δ_i / δ_u and E_i/E_u where δ_i is the displacement at the end of i^{th} load cycle; δ_u is the ultimate displacement capacity of BCJ; E_i is the total AE energy at the end of i^{th} load cycle; and E_u is the ultimate acoustic energy capacity of BCJ. New damage states have been proposed. A damage index (DI_{AE}) value up to 0.5 is an indication of minor damage, DI_{AE} value from 0.5 to 0.75 points towards moderate damage and DI_{AE} value of more than 0.75 represents major damage. The DI_{AE} value of more than unity shows the collapse stage of the BCJ.
- The ultimate load-carrying capacity of ECC-strengthened non-ductile BCJ is higher than control BCJ samples. In comparison, strengthened ductile BCJ is less than the control sample. In both cases, the load-carrying capacity is higher than the design load-carrying capacity of BCJ. Thus, it can be concluded that ECC material can be successfully used to restore the design load capacity of the BCJ.
- Rise-Angle (RA) Vs Average-Frequency (AF) plots help distinguish between different types of cracks, i.e., tensile or shear cracks. The number of tensile hits in an ECC retrofitted non-ductile BCJ is about 3 times more than in a control BCJ. The number of tensile hits in an ECC-repaired ductile BCJ is about 0.3 times that of the control BCJ.

From these results, it can be concluded that there is a reduction in tensile cracks in ductile BCJ samples and an increase in tensile cracks in non-ductile samples. Thus, ECC helps to improve the tensile capacity of ductile BCJ.

- The number of shear hits in an ECC retrofitted non-ductile BCJ up to the unity damage index was three times more than that of a controlled BCJ. The number of shear hits in an ECC retrofitted ductile BCJ up to the unity damage index was reduced by about 0.2 times that of the controlled BCJ. From these results, it can be concluded that there is a reduction in shear cracks in ductile BCJ samples and an increase in tensile cracks in non-ductile samples. Thus, ECC helps to improve the shear capacity of ductile BCJ.
- The total AE Energy of the ECC retrofitted non-ductile BCJ was about four times higher than the corresponding control BCJ. The total AE Energy of the ECC retrofitted ductile BCJ was about 3.2 times higher than the corresponding control beam-column joints. Thus, it can be concluded that ECC material can be successfully used to retrofit the BCJ to achieve Acoustic Energy capacity.

TABLE OF CONTENTS

LIST OF FIGURES

LIST OF TABLES

CHAPTER-1. INTRODUCTION

1.1 GENERAL

Structural Health Monitoring (SHM) is a process used for damage detection and to check the performance of an existing structural system affected by external factors and get feedback for improvement in future design. SHM is particularly helpful in assessing the integrity of buildings after a catastrophic earthquake to develop performance-based design philosophy. Depending on the damage state, identifying damage and its location is paramount in SHM. The monitoring of structures is also helpful in assessing the remaining life of the buildings. The health of reinforced concrete (RC) structures is vital because of their brittle nature and tendency to collapse without giving sufficient warning to the occupants, especially under seismic forces. The structures may deteriorate much before the life span whenever they are subjected to forces beyond design expectations. Such forces may be seismic loads, live loads, wind loads, harsh environmental conditions etc. The quality of construction work is also necessary to increase the life span of structures.

Beam-column joints (BCJ) are critical zones in Reinforced Concrete (RC) buildings and play a significant role in the structure's overall stability, especially under seismic forces. The main reasons for the failure of BCJ are improper ductile detailing, insufficient transverse reinforcement in the BCJ core, use of plain bars and low-strength concrete etc. Beam-column connections substantially contribute to RC structures' overall load-carrying and displacement capacities. The performance of BCJ also depends upon the confining reinforcement. Many experimental evaluations and theoretical studies have been carried out to examine the beam-column joints to find resistance against seismic forces. While analysing the RC multistorey buildings, the BCJs joints are generally assumed as rigid. The ductile detailing has been neglected in the older RC design codes, where attention is restricted to providing longitudinal reinforcement in the beam. Under gravity loads, these provisions may be acceptable. However, many disastrous failures of RC structures have been noticed in past earthquakes. For example,

the 1999 earthquakes in Turkey and Taiwan caused massive damage to buildings because of deficiencies in the design of BCJ. The severity of damage in RC frames is intensified by the high demand imposed by the connecting flexural members on the BCJ because they lack dissipating seismic energy. Improper provision of ductile reinforcement within the joint region may endanger the whole structure, even if individual structural elements such as beams and columns conform to the seismic design requirements. Reinforcing detailing/anchorage of bars and stirrups arrangements have a significant effect on the seismic behaviour of BCJ. Thus, health monitoring of BCJ is critical in identifying damage in a building and checking the deficiencies in the structure.

Various damage detection techniques for RC structures have been reported in the literature, such as visual inspection, tap test, vibration monitoring technique, fibre optic technique, magnetic particle testing, eddy current testing, radiographic technique, ultrasonic technique etc. These techniques suffer in one way or other from the practical implementation of large-scale civil engineering structures. Recently, for the non-destructive evaluation of damage in RC structures, the Acoustic Emission (AE) technique has been recognised as an excellent qualitative and quantitative analysis tool.[1] The damage or deformities produce AE waves in a structure that radiates from the source of origin. These waves are detected by the sensors placed on the surface of the structure. The waveform data is collected and further interpreted to locate the source of damage and its quantification using various AE waveform parameters. Commonly used AE parameters to quantify damage in RC structures include; Intensity Analysis (IA), Improved b-value analysis (Ib-value), Felicity Ratio and Calm Ratio[2]. The IA technique characterises the damage level based on the intensity charts. These charts are plotted between the Historic Index (HI) and Severity Index (Sr)[3, 4].

The Ib-value analysis, based on the Gutenberg-Richter law to find the frequency of earthquakes, helps identify different stages of damage in the structures and assess the presence of macro cracks. The Ib-value close to unity represents damage[5, 6]. The damage assessment

based on Ib-value is also doubtful because of the shortcomings of the Gutenberg-Richter law[7]. Further, a criterion of quantitative analysis of AE signals has been reported by Ohtsu et al.[8, 9] using Load-Ratio & Calm-Ratio based on the Kaiser-Effect. Load-Ratio is defined as the ratio of load at the onset of AE activity to the previous maximum load, and Calm-Ratio is the ratio of cumulative AE activity during the unloading process to total AE activity during the last loading cycle. These ratios are further plotted into a chart to identify the severity of the damage. The AE technique is also helpful in classifying the type of cracks in the structure, i.e., tensile or shear.[10] Classification of the type of damage is carried out using rise angle (RA) and average frequency (AF) values. RA is the ratio of rise-time to maximum amplitude, and AF is the ratio of AE counts to duration [11]. These parameters only indicate the presence of damage but do not provide sufficient information to quantify damage [12, 13]. Thus, there is a need to develop a damage quantification technique based on AE monitoring to assess the overall damage, locate the damage and accurately quantify it in RC BCJ.

Many researchers have developed damage index models depending on response parameters. These damage indices are widely used to predict vulnerability due to seismic damage and make decisions regarding the repair and retrofitting of structures. Researchers have also provided elaborative classification based on damage indices. Frequently used damage index models to quantify the severity of damage are; Park and Ang Damage Index[14], Stiffness Damage Index[15], Drift Ratio[30], Stiffness Degradation[33], low cycle fatigue damage index, plastic energy-based damage index, displacement-based damage index etc. The load and displacement parameters are required to evaluate these damage indices. The DI presented by Park and Ang is the most popular, which considers both cumulative energy demand and ductility demand. It is difficult to evaluate these damage indices because of limitations in measuring energy dissipated in a seismically damaged structure. A few studies have investigated the implementation of AE energy to develop damage quantification[16], [17], [18]. Benavent et al.[16] have interrelated the AE energy with energy dissipated and developed damage index (DI). This

damage index does not consider the effect of displacement response; hence can't represent the actual damage state.

Most of the techniques based on AE data use energy parameters to evaluate the damage. But, in addition to AE energy, the structural displacement parameters also contribute significantly to the structural performance. Hence, structural damage is a combined function of deformation response and energy dissipated. Therefore, both AE energy and displacement parameters should be considered to represent a damage index.

The damages observed in structures during an earthquake initiate the need to explore the possibilities of new techniques for retrofitting and strengthening the structures. The existing structure must also be upgraded to satisfy the current codal requirements. Generally, retrofitting buildings includes adding new members such as shear walls and bracing or strengthening existing members with Fibre Reinforced Polymer (FRP). Commonly used FRP are Glass Fibre Reinforced Polymer (GFRP) and Carbon Fibre Reinforced Polymer (CFRP), steel or RC jacketing etc. The FRP is a key technique used for strengthening an existing structure. This technique is preferred because of its lesser weight, high strength and easy workmanship. Glass Fibre Reinforced Polymers (GFRP) and Carbon Fibre Reinforced Polymers (CFRP) are preferred as better alternatives to commonly used steel reinforcements for RC structures. Recently Engineered Cementitious Composites (ECC) have contributed to safer, more durable, and sustainable concrete infrastructure that is cost-effective and constructed with conventional construction equipment. ECC has been used very effectively for retrofitting various components of RC structures and has shown excellent behaviour under tensile and shear loading that possesses high fracture energy[19],[20]. Therefore, ECC can be considered an ideal material for various structural applications. To verify the performance of ECC being a satisfactory repairing composite, there is a need to study its behaviour and monitor damage progression using the AE technique.

Very little research is available for damage monitoring of RC BCJ using the acoustic

emission technique. The main objective of this research is to monitor the health of BCJ and quantify damage by developing a new damage index model using the AE parameters. The proposed damage index model includes various response parameters such as displacement response, load response and ultimate displacement capacity of the BCJ. The deformation and load response parameters can be obtained by performing a cyclic load test of BCJ. The third parameter i.e., the ultimate capacity of BCJ is obtained by performing a monotonic load test as per the procedure laid down in Park and Ang model.

Further, cyclic load tests have been performed up to the damage level of BCJ to study the behaviour of BCJ reinforced with and without ductile detailing. The damaged samples have been retrofitted using ECC and tested using the AE technique to check the effectiveness of ECC for samples detailed with and without ductile detailing. It is targeted to develop a novel damage index for control and as well as ECC repaired BCJ.

1.2 OBJECTIVES OF STUDY

Considering these gaps in the research following objectives have been laid down in this research work:

- Experimental study of load-deformation characteristics of RC beam-column joints subjected to monotonic load, reinforced with and without ductile detailing.
- Experimental study of the RC beam-column joints subjected to cyclic loads, reinforced with and without ductile detailing, before and after retrofitting.
- Damage monitoring of RC beam-column joints using acoustic emission technique reinforced with and without ductile detailing before and after retrofitting.
- Development of a novel damage index model based on the AE technique.

1.3 ORGANISATION OF THESIS

This thesis has been presented in the following seven chapters:

Chapter-1: Introduction to the importance of beam-column joints in the moment-resisting RC frames, the need for health monitoring and choosing Acoustic emission as an

SHM technique. Various objectives of the research have been laid down.

Chapter-2: This chapter has discussed a detailed literature review about the behaviour of beam-column joints subjected to seismic forces and monotonic loads, structural health monitoring techniques, and relevant parameters under the applied loads. Commonly used damage quantification methods have been elaborated. The literature has also been reviewed regarding work done by various research scholars in the field of retrofitting strategies for the repair of BCJ.

Chapter-3: Detailed discussions about the need for SHM and various techniques used in SHM have been discussed in brief. The acoustic emission technique, its historical background, application for damage detection, advantages and disadvantages, parameters used for damage detection, and the source of damage detection with AE parameters have been carried out in detail.

Chapter-4: This chapter discusses the detailed scheme for the experimental programme, materials used for casting of BCJ, mechanical properties of the material used such as cement, concrete, and steel reinforcement and retrofitting material used to retrofit the BCJ such as GFRP, ECC etc. Retrofitting procedure for repairing BCJ has been laid down.

Chapter-5: This chapter exclusively focuses on the performance of beam-column joints. Experimental results regarding the behaviour of BCJ under monotonic loads and cyclic loads have been presented for control and retrofitted samples. The results based on AE monitoring and load-deformation response have been compared for control and retrofitted samples.

Chapter-6: This chapter discusses various damage quantification techniques used in this research work. Quantification of damage has been carried out based on experimental results from the load-deformation response and AE parameters for control and retrofitted samples.

Chapter-7: Various conclusions from the experimental results have been discussed in

this chapter, such as load-deformation characteristics of BCJ, Monitoring of BCJ using AE parameters, damage index based on AE parameters, and behaviour of ECC retrofitted BCJ and the scope for future work.

Appendix A: A MATLAB function has been created to plot Rise-Angle Vs Average-Frequency to identify the type of cracking in BCJ.

Appendix B: A MATLAB function has been created to find out Ib-values for a group of hit data.

Appendix C: This MATLAB function has been developed to filter data belonging to different damage levels based on Ib-value. Based on this data, a coloured plot can be drawn to see the variation of cumulative hits belonging to three types of damage levels.

Appendix D: Design calculations for RCC detailing of the beam-column joint based on Indian standard code IS 456:2000 for normal detailing (non-ductile design) and IS 13920:1993 for ductile detailing have been carried out in this appendix.

CHAPTER-2. BEHAVIOUR OF BEAM-COLUMN JOINTS

2.1 GENERAL

The beam-column joint (BCJ) can be defined as a part of the column connected with beams on two or more faces[21]. The BCJ has been divided into two types: Type 1 joints are those subjected to gravity and horizontal loads without any significant inelastic joint deterioration, whereas Type 2 joints are subjected to repeated load reversals (as those due to seismic forces) which cause inelastic deformations. There are three types of joints in an RC multistorey framed structure, i.e., interior joint, exterior joint, and corner joint. In an interior BCJ, four beams join the vertical faces of a column. In an exterior BCJ, three beams member perpendicularly connects to the vertical face of the column. In a corner joint two beams, perpendicular to each other, frame into the vertical face of the column. The Impact of forces transferred from the adjoining beams requires a better understanding of BCJ under seismic forces. These forces acting on the BCJ develop complex mechanisms involving bond and shear within the BCJ region.

The reverse cyclic loading caused by seismic forces leads to huge inelastic deformations in the BCJ in reinforced concrete framed structures. The performance of BCJ can be significantly affected if the BCJ are not designed and detailed adequately. The limited space available in the BCJ region requires more attention from the design engineers. In the design of framed structures, it is assumed that BCJ is strong enough to sustain forces generated by the seismic forces and transfer these forces from one structural element to another. The assumption regarding the rigidity of BCJ doesn't consider the effect of high shear forces developed within the BCJ.[22]

Recent failures caused by seismic forces have demonstrated that even when the beam or a column member of any RC framed structure remains intact, the integrity of the whole structure is doubtful if the BCJ fail. The joints are susceptible to failure earlier than the adjacent members due to the failure of the joint zone. The external BCJ are prone to suffer damage

before the other BCJ of the framed structure. Therefore, the ductility and energy absorption capacity of the BCJ plays an essential role in the overall seismic performance of structures.[23] The reinforcing bars should have sufficient strength and ductility under repeated cyclic deformations. It is also essential to verify the shear resistance and anchorage requirement of the reinforcement passing through the joint region. If the BCJ is not designed adequately, the system fails to dissipate energy, and the entire structure may collapse even if other structural members conform to the design requirements.

The design and ductility requirement of RC structures subjected to seismic forces has been incorporated in the Indian standard code of practice, IS 13920. The design of BCJ demands that the columns meeting at a joint should have sufficient flexural strength in the event of overstressing the adjoining beams. The flexural strength ratio of column and beam is an important parameter to ensure that the plastic hinge occurs in the beams rather than in the columns or the joint region. The BCJ should also have satisfactory shear strength to avoid the possibility of shear failure.

The transverse reinforcement and the shear transfer mechanism in a BCJ also play an important role when subjected to seismic forces.[24] IS-13920 (BIS, 1993) assumes the role of hoops to confine the joint core. Confining reinforcement has three important roles. First, it provides shear resistance to the member. Secondly, it helps to confine the concrete core and enhance the ultimate strain of concrete. This results in better ductility and the ability to undergo large deformations. Thirdly, it provides a lateral check against buckling to the compression steel. Karayannis et al., 2005[25] have demonstrated that the use of rectangular spiral reinforcement significantly improves the seismic capacity of external BCJ.

2.2 RESPONSE PARAMETERS

2.2.1 Stiffness

In civil engineering structures, stiffness may be defined as the ability of structural members to resist deformation under load. It is the ratio of the applied load to the deformation

response. Therefore, the stiffness does not have a constant value and keeps on changing with its deterioration. In Figure 2.1, K_i is the stiffness at a required deformation Δ_i and corresponds to the resistance to the force P_i. For conventional materials, the value of the initial stiffness K_0 is higher than the secant stiffness K_s. Deviations in stiffness in the inelastic range are often expressed by the tangent stiffness K_t, which is the slope of the tangent to the response curve for a given pair[26, 27]. A decrease in K_t values show that softening of the structure occurs.

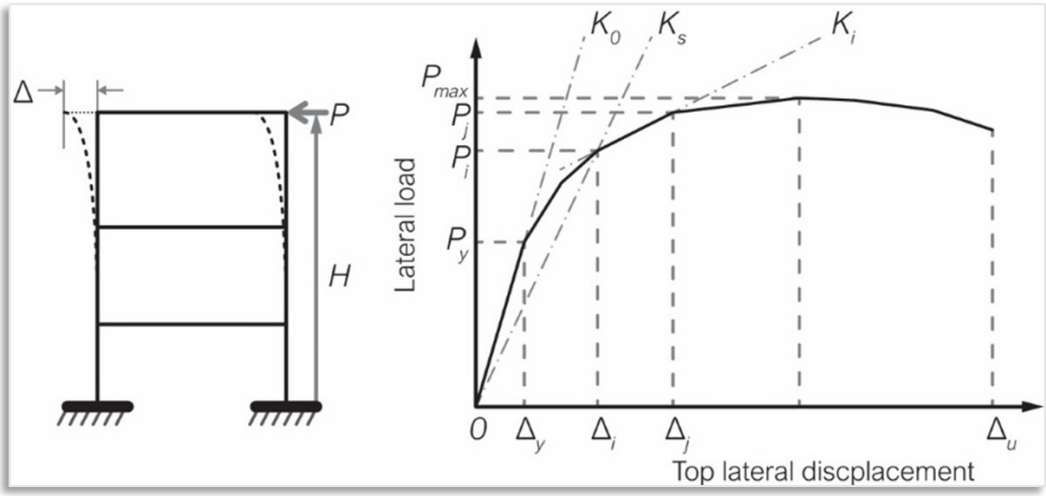

Figure 2.1: Definition of initial, secant and tangent stiffness[27]

2.2.2 Strength

The strength of a material is its capability to resist an applied load without failure or plastic deformation. It is a function of internal forces, deformation, and external loads. The applied forces cause stresses and strains in the material, which results in a change in the shape and size of the material. The stress represents force per unit area, and stress represents a change in dimensions compared to the original dimensions. In designing RC structures, it is essential to consider these factors so that the material selected has sufficient strength to resist applied loads or forces and the original shape and size remain intact. When the load is applied axially, as in the case of a column, the resulting stress may be tensile or compressive. The applied forces also create shearing and bending stresses in the material. The knowledge of analysing a structure to obtain these forces is essential to obtaining load-carrying capacity, displacement capacity and stability.

2.2.3 Ductility

Ductility is the ability of a material to undergo large deformations while the structure is still able to resist loads without collapse. In RCC structures, the concrete is a brittle material and does not contribute to the ductility of the structure. The presence of steel is mainly responsible for attaining the desired ductility in RCC structures. Ductility is very important in structures falling in seismic zones. The performance of RCC structures depends upon the dissipation capacity when subjected to seismic forces. The brittle structures collapse after minimal inelastic deformation, whereas larger lateral deformations are noticed at the collapse in ductile structural systems (Refer to Figure 2.2).

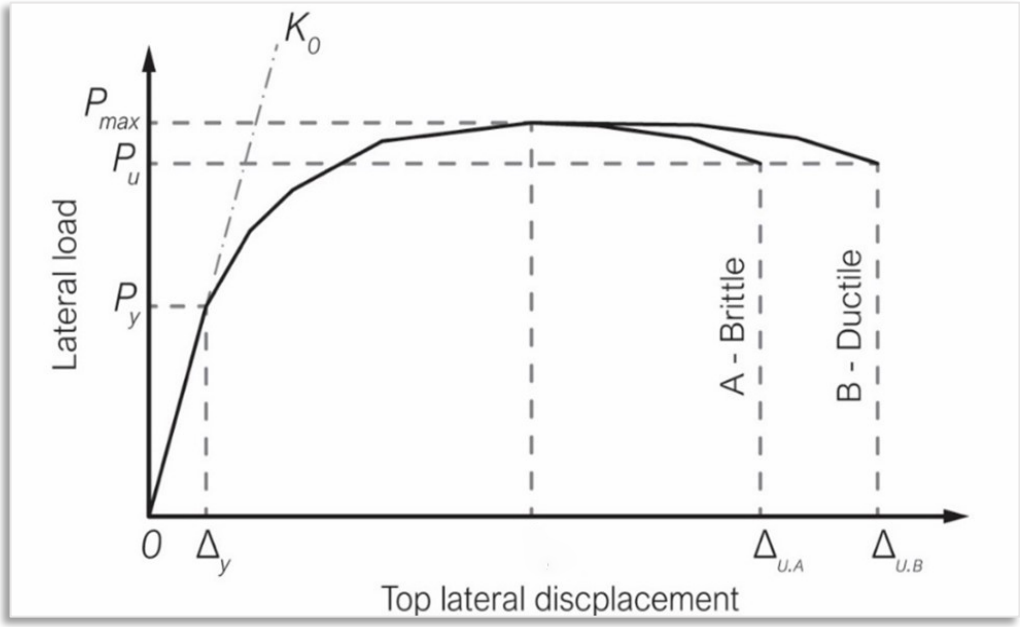

Figure 2.2: Definition of structural ductility[27]

The response amplitudes caused by seismic vibrations depend upon the energy dissipation of the structure. Structural ductility is beneficial for the structures in the event of overloading. In such situations, the structure will undergo large deformations and will not collapse. The building occupants can get sufficient warning signals for taking preventive measures, and their lives can be saved. Hence, strength and ductility play a vital role in the design of RC structures when subjected to large deformations beyond elastic limits.

2.3 DAMAGE QUANTIFICATION METHODS BASED ON NON-LINEAR BEHAVIOUR

The damage in the structural components can be represented by an index commonly known as the damage index (DI) or Index of Damage. It is a non-dimensional parameter commonly having values lying between 0 and 1. DI value of zero indicates no damage, whereas a value close to one represents the collapse of the structure. Numerous parameters are considered to evaluate the damage index of a structure, such as deformation, change of stiffness, energy loss and change of dynamic parameters[28]. Several damage indices are available in the literature. Among them, ductility ratio, inter-storey drift, slope ratio, flexural damage ratio, softening index, and Park and Ang damage index are the most commonly used damage indices. Some significant damage indices are discussed below.

2.3.1 Park and Ang Damage Index

Most structures subjected to seismic forces fail due to low ductility, strength, and stiffness deficiencies. Insufficient shear and confinement steel reinforcements lead to low ductility. It is important to assess the state of damage caused by seismic forces to safely use the building after an earthquake. The Park and Ang damage index model is the most acceptable DI, which incorporates both ductility and hysteretic energy and can be represented with equation-(2.1)

$$DI_{PARK} = \frac{\delta_{max}}{\delta_u} + \frac{\beta_2}{P_y \delta_u} \int dE \tag{2.1}$$

where δ_{max} is the maximum displacement experienced during an earthquake; δ_u is ultimate displacement capacity; P_y is yield strength; β_2 is a weighting factor for the effect of energy dissipated (E). $\int dE$ represents the hysteretic energy absorbed by the structural element. Determination of β_2 is typically very important for accurate prediction of damage index. A complete procedure has been provided by Park and Ang (1985) to evaluate β_2.

2.3.2 Stiffness damage index

The stiffness damage index (DI_k) is based on the relationship between the stiffness of

the undamaged and the damaged state of the structure[29] and has been expressed by the following equation:

$$DI_k = \frac{k_j - k_j^*}{k_j} = 1 - \frac{1}{v_j} \quad (2.2)$$

where k_j is the initial stiffness of the undamaged element, v_j is the stiffness ratio, and k_j^* is the initial stiffness of the damaged element of the j^{th} member. The superscript * is used to denote the damage state.

2.3.3 Displacement ductility

Refer the Figure 2.3 to understand the meaning of displacement ductility. The structural response curve has been idealised by the linearly elastic-perfectly plastic curve. According to Miranda et al. (1994)[30] , displacement ductility is the ratio of maximum displacement (δ_u) to the corresponding displacement at the onset of yielding (δ_y), with the equation-2.3.

$$\mu = \frac{\delta_u}{\delta_y} \quad (2.3)$$

2.3.4 Drift ratio

As per Brachmanni et al. (2004)[31], structural drift is expressed as the ratio between the displacement of the structure δ_m, at the target position m, and the storey height H and is given by the equation-2.4

$$Drift = \frac{\delta_m}{H} \quad (2.4)$$

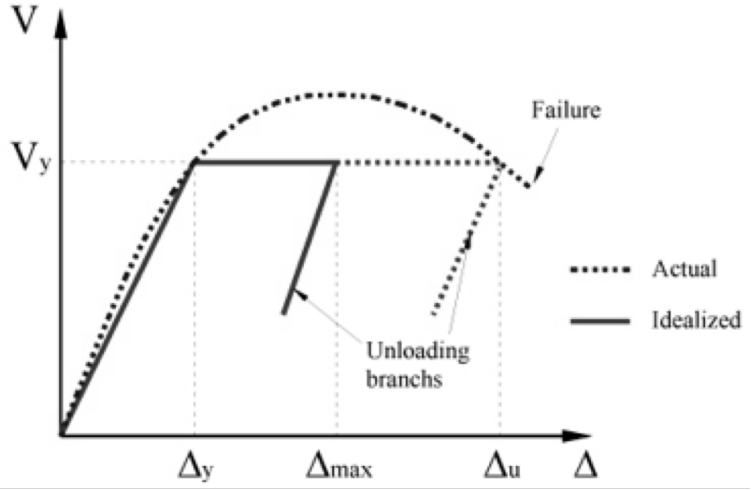

Figure 2.3: Actual and idealised structural response[32]

2.3.5 Stiffness degradation

The difference between initial stiffness and secant stiffness showed the post-yield behaviour of a component. The deterioration of stiffness as deterioration of the post-elastic stiffness versus the stretch stiffness (represented by $K_{deg}\%$) is calculated by using equation-2.5[33]. The rate of change in the stiffness after the elastic range is the measure of the inelastic performance of the component.

$$K_{deg}\% = \left[1 - \frac{K - K_y}{K_y}\right] \times 100 \tag{2.5}$$

where: K is the Stiffness of each cycle, kN/mm; K_y is the Yield stiffness, kN/mm

2.4 BEHAVIOUR OF BCJ UNDER MONOTONIC LOADING

The gravity loads are transferred to the foundation through beam-column connections in any moment-resisting RC frame. Thus, the behaviour of beam-column joints needs to be studied under monotonic loads. There can be several possible failure modes in beam-column joints, such as shear failure of beam and column, flexural failure of beam and columns; bond failure of reinforcement; and joint shear failure. Many numerical studies were discussed on BCJ under monotonic loading using different techniques discussed as followed.

Bakir et al. (2002)[34] have recommended new experimental correlations for exterior BCJ under monotonic loading and showed an increase in the shear capacity of the beam due to an increase in reinforcement ratios and joint transverse reinforcement. The authors have concluded that failure mode is shifted from beam failure to joint shear failure due to the provision of L bar detailing. The column axial load does not affect the ultimate shear capacity of BCJ.

Patil et al. (2013)[35] have investigated to compare the behaviour of exterior and corner BCJ under monotonic loading using the ANSYS finite element analysis by studying different parameters such as maximum principal stress, minimum principal stress, displacement, different boundary conditions, and stiffness variation, for comparative study.

Jinkoo et al. (2015)[36] have studied the capacity of a control RC BCJ and compared the

results with strengthened specimens tested and designed for gravity load and seismic loads. The authors have noticed that specimens designed for gravity loads failed by the failure of re-bars in the beams. In other specimens, the failure occurred after the maximum displacement capacity of specimens was reached. The specimens provided with unbonded strands showed the highest strength.

Tran et al. (2017)[37] have carried out experimental studies on exterior BCJ subjected to cyclic loading by considering the effect of three parameters, i.e. column axial stress level, concrete compressive strength, and the vertical and horizontal amount of shear reinforcement. The results were analysed by comparing the shear strength of the proposed model with analytical models and test results. This investigation discovered that the recommended model could efficiently forestall shear strength.

Mounika et al. (2018)[38] have studied the behaviour of exterior BCJ provided with reinforcement according to IS 456-2000 and confining reinforcement as per IS 13920-2016. The objective of the investigation was to satisfy the strong column and weak beam concepts subjected to monotonic load. The experimental studies were verified with finite element analysis using ANSYS. Different parameters were assessed both experimentally and analytically

Fei et al. (2019)[39] have researched reinforced concrete interior BCJ subjected to monotonic load. Compression and tension damage was considered in finite element models to calibrate test results regarding strains of longitudinal steel, load displacement and failure modes. The effect of the hoop reinforcement ratio in the joint core and the axial compression ratio on the responses of the joints was investigated. The results showed that the confinement mechanism also existed in the joint core, in addition to the truss and strut-and-tie mechanisms. Confinement in the joint core increased the yield load, decreased the beam's yield displacement, and improved joint ductility. The horizontal stirrups have little contribution to the joint performance.

2.5 SUMMARY

Based on the literature review, it has been observed that transverse reinforcement in the joint core increases the shear capacity. Joint stirrups have a noticeable influence on stiffness and ultimate capacity. The axial column force made the BCJ becomes more stiffer and less ductile when an axial force is applied to the column of BCJ. An increase in concrete strength increased the ultimate load and decreased the deformation capacity at the ultimate load. The increased column stirrups within the BCJ area increased ultimate load capacity.

2.6 BEHAVIOUR OF BCJ UNDER SEISMIC FORCES

2.6.1 General

Many experimental evaluations and theoretical studies have been carried out to examine the beam-column joints to find resistance against seismic forces. While analysing the RC multistorey buildings, the BCJs joints are generally assumed as rigid. The ductile detailing has been neglected in the older RC design codes, where attention is restricted to providing longitudinal reinforcement in the beam. Under gravity loads, these provisions may be acceptable. However, under seismic forces, many disastrous failures of RC structures have been noticed in past earthquakes. For example, the 1999 earthquakes in Turkey and Taiwan caused massive damage to buildings because of deficiencies in the design of BCJ. The severity of damage in RC frames is intensified by the high demand imposed by the connecting flexural members on the BCJ because they lack dissipating seismic energy. Improper provision of ductile reinforcement within the joint region may endanger the whole structure, even if individual structural elements such as beams and columns conform to the seismic design requirements. Reinforcing detailing/anchorage of bars and stirrups arrangements have a significant effect on the seismic behaviour of BCJ.

Providing seismic ductility to the structure is the prime motive behind every design philosophy. A mechanism of strong-column-weak beam behaviour is adopted so that failure should not occur in columns. The mechanism with such a feature is known as the column-yielding or storey mechanism. The occurrence of hinges in beams results in large horizontal

and vertical shear forces in the joint region.

The current concrete design Code in New Zealand[40] contains seismic provisions pertinent to beam-column joints, which are notably different from those adopted in the United States[41], [42]. The different design approaches and detailing requirements used in New Zealand and the United States have been discussed on various occasions[42, 43, 44, 45, 46]. Seismic Codes developed for European conditions [47, 48] include design provisions for beam-column joints with many similarities to those used in New Zealand[41]. Various research works on the response of BCJ under cyclic loads have been discussed in the following section.

2.6.2 Literature review based on seismic response

Park And Ang (1985)[14] have proposed a damage index for evaluating structural damage in reinforced concrete structures under earthquake ground motion. The damage index is based on the deformation response of the structure and energy dissipated during the cyclic loads. In seismically damaged structures, it is challenging to estimate the load response and hence the energy dissipated. Hence it is not easy to calculate the damage index for buildings suffering from earthquake motion.

Tsonos et al. (1992)[49] tested twenty full-scale specimens to specify the excursion of reinforced exterior beam-to-column connections. Experimental findings showed that oblique reinforcements crossed in the joint area are one of the most effective methods that could be employed to increase earthquake resistance in the outer joint area.

Pampanin et al. (2002)[50] have reported that improper reinforcement detailing can cause weak-column and strong-beam systems, which leads to the formation of soft-storey mechanisms. Thus, BCJ of RC frames designed with inadequate ductile detailing experience structural weaknesses resulting in brittle failure.

Fischer et al. (2003)[51] have investigated the effect of the ductile behaviour of ECC on the response of columns reinforced with steel and FRP subjected to cyclic loading. ECC is a type of FRCC that offers more durable and sustainable concrete infrastructure, which is cost-effective and easy to apply with conventional equipment. The presence of microfibres and the

absence of coarse aggregates act as secondary reinforcement, which bridges the cracks more effectively than traditional FRC and offers strain-hardening behaviour.

Said et al. (2004)[52] investigated the behaviour of BCJ reinforced using GFRP rebars and GFRP stirrups and compared the results with standard RC BCJ under quasi-static loading. The authors have concluded that BCJ reinforced with GFRP showed elastic behaviour with low plasticity. This resulted in lower energy dissipation and stiffness as compared to conventional RC BCJ.

Bazan et al. (2004)[53] have performed experiments on reinforced concrete (RC) elements under cyclic and monotonic displacements to examine Park and Ang damage index. It has been shown that the per cent of the variation in evaluating the new damage index at failure is appreciably smaller than that reported by Park et al. (1985). They also observed that although the displacement history can significantly affect the drift capacity of reinforced concrete specimens, the dissipated energy may not be a reliable measure to account for such an effect. A new damage index has been developed to estimate the drift ratio capacity of RC elements under cyclic loading.

Mukherjee et al. (2005)[54] have investigated the performance of RC BCJ under cyclic loading. The BCJ was cast with adequate and deficient bonds of reinforcements at the BCJ under cyclic loading. It was concluded that specimens strengthened with CFRPs had shown stiff behaviour than GFRP-strengthened specimens. Further, an increase in energy dissipation capacity was observed with the use of a small number of composites.

Wang et al. (2009)[55] have studied the performance of RC BCJ under cyclic loading. FRP sheets and strips were used in the joint region in different configurations. Fixed axial load was applied to the column, whereas displacement-controlled cyclic load was applied to the beam. The authors have compared the energy dissipation capacity of differently provided FRP configurations. The repairing was carried out using FRP, and their behaviour was compared with that of the control specimens.

Yuan et al. (2013)[56] studied the performance of reinforced concrete and ECC beam-column joints subjected to cyclic loading to verify the effect of concrete substitution with ECC in the BCJ zone. The replacement of concrete with ECC in the joint zone doesn't affect the brittle shear failure. However, it increased the load-carrying capacity and ductility of the BCJ specimens. It was also observed that there is an increase in the energy dissipation capacity because of the high ductility and shear strength of ECC material. Thus, the replacement of concrete with ECC in the BCJ increases the seismic resistance of BCJ specimens.

Qudah et al. (2014)[57] have studied the ECC-enhanced BCJ connections and compared their results with control samples to evaluate the benefits of using ECC. The load-displacement, cracking, and energy absorption capacity parameters were studied for comparison purposes. The results showed that ECC material could effectively enhance the joint energy absorption capacity, shear capacity, and cracking response. Thus, ECC can be successfully used to improve the seismic resistance of BCJ.

Muthuswamy et al. (2014)[58] have studied the ductile behaviour of HFRC used for the casting of beam-column joints. Two types of beam-column joints were cast. One uses conventional concrete, and another uses fibre-reinforced concrete. The specimens were tested under cyclic loading and studied load carrying capacity, load-deflection behaviour, ductility, energy absorption, and stiffness parameters. The experiment results of the BCJ provided with fibre-reinforced concrete were compared with the BCJ provided with conventional concrete. The BCJ with HFRC has 50% higher ductility and an 80% higher energy absorption capacity compared to conventional concrete. Thus, HFRC can be successfully used in BCJ to improve its seismic performance.

Ganesh et al. (2015)[59] have investigated the performance of hybrid fibres on the strength and behaviour of high-performance concrete BCJ subjected to cyclic load. BCJ was cast using a commonly used concrete mix of M25 in residential buildings. Crimped steel fibres and Glass fibres were used in hybrid forms. The test results showed that the volume fraction

of 0.75% for crimped steel fibres and 0.33% for glass fibres give the best results concerning energy dissipation capacity and stiffness degradation than the other combinations.

Cosgun et al. (2019)[60] have studied that the BCJ of substandard reinforced concrete buildings may fail to resist the design loads and deformations under severe seismic actions. The authors have further established the effectiveness of CFRP composites for repairing beam-column joints.

Wang et al. (2020)[61] have proposed a stiffness degradation index based on cycle load tests. The authors observed a relationship between the stiffness degradation index with the structural design criterion. They have performed tests under five performance levels. No damage $D_{k,k} < 0$, mild damage ($0 < D_{k,k} \leq 0.30$), moderate damage ($0.3 < D_{k,k} \leq 0.7$), severe damage ($0.7 < D_{k,k} \leq 0.9$), and destruction ($0.9 < D_{k,k} \leq 1$). It was observed that an increase in the transverse reinforcement ratio could notably reduce the stiffness damage, especially under conditions of low ductility. It was concluded that an increase in the transverse reinforcement and control of the ductility condition are effective methods for controlling the stiffness damage of RC members

2.6.3 Summary

Even though the structures have sufficient strength against lateral deformation, inadequate ductility is the main reason for a structural deficiency in the seismic performance of buildings designed for gravity loads. A weak-column and strong-beam system tends to develop a soft-storey mechanism at the global level. At the local level, inadequate strength of beam-column joint subassemblies may result in brittle failure of structural elements. Various deficiencies in the structure are related to:

- Inadequate confining reinforcement in the plastic region;
- Insufficient transverse reinforcement in the joint area;
- Inadequate column longitudinal reinforcement;
- Use of low-quality material, i.e., concrete and steel;

2.7 RETROFITTING STRATEGIES FOR REPAIR OF BCJ

The beam-column joint is a very vital structural member of any moment-resisting RC frame, especially under seismic forces. It is, therefore, desirable to check the structural integrity of BCJ samples under cyclic loads. Once the damages are observed in the structure, it is not economical to dismantle the whole or damaged parts. Hence to make the structural systems fit for use, the next task before the engineer is to retrofit them with the appropriate technique and material. Numerous research materials are available to repair the damaged parts depending on the type of structural elements and severity of the damage. FRP is one of the most popular materials used for retrofitting/repairing RC structures because they possess excellent properties, such as high tensile strength, high stiffness, corrosion resistance, and lightweight.

Enhancing the life of the structural systems is the main aim before selecting a retrofitting approach. The selection of the strengthening material is a significant factor affecting the successful strengthening technique of structures. The strengthening of existing members can be carried out by Fibre Reinforced Polymers (FRP) like Glass Fibre Reinforced Polymer (GFRP) and Carbon Fibre Reinforced Polymer (CFRP). In addition, steel or RC jacketing can also be done to strengthen the weaker structural elements. Nowadays, Engineering Cementitious Composites (ECC) are gaining popularity because of their ease of application and high-strength capabilities. The application of ECC has not been extensively studied by many researchers for beam-column joints. Mishra (1995)[62] found that the beam-column connections cast with engineering cementitious composites (ECC) poly-ethylene subjected to cyclic loading resulted in higher energy dissipation capacity. Yuan et al. (2013)[63] tested exterior beam-column joints provided with ECC–PVA (poly-vinyl-alcohol) in the joint zone. The results showed that ECC improved the seismic resistance and increased the peak load capacity and shear strength of BCJ. The presence of ECC and lateral steel hoops in the joint zone can prevent brittle shear failure in the joint area. Zhang et al. (2015) [64] investigated the beam-column joint connection provided with ECC. The authors have investigated that ECC material can be replaced with lateral steel hoops.

Given the above, the ECC material has been preferred in this research for repairing the damaged BCJ because of the following properties:

- ECC material is a very durable and sustainable concrete infrastructure that is cost-effective and can be constructed with conventional construction equipment.
- ECC has a high tensile strain capacity and compressive toughness compared to other traditional construction materials.
- It helps in reducing the crack size by evenly distributing the wide cracks into multiple tiny cracks on the tensile surface.
- It helps to improve the energy dissipation capacity.
- It can prevent brittle shear failure in the joint core of a beam-column connection.
- In jacketing, wrapping or reinforced polymer techniques, the polymer sheets cover the surface area. It is not possible to observe the crack pattern in laboratory experiments

CHAPTER-3. ACOUSTIC EMISSION MONITORING & REVIEW

3.1 GENERAL

Reinforced concrete is a complex material prepared by combining concrete and steel. These materials possess different mechanical properties, and it is tough to predict their behaviour. Out of many RC structures built worldwide, reinforced concrete structures deteriorate with age due to loading and environmental impacts. It isn't easy to ensure uniform quality and strength in every structural section during construction. Hence, there may be strength variation among various sectional elements compared to design parameters. If this variation is within the prescribed limit, the structure can be considered healthy and fit for use. But the variations beyond such limits may lead to severe damage to the structural elements, and there is a possibility of collapsing the entire structure.

Timely detection of damage in civil engineering structures is essential. Otherwise, it may create severe consequences for the safety of occupants. Many events may affect the strength of the structure. Among them, earthquakes are of prime importance. It should be ensured that the structures are safe to withstand forces caused by such natural disasters. The SHM will not only help in reducing catastrophic damages but will also be helpful for improvement in future designs. It is also essential for better management of the country's economy and the safety of human beings.

3.2 TECHNIQUES OF STRUCTURAL HEALTH MONITORING

Visual inspection by experienced personnel has been the favoured method of monitoring large structures such as bridges, multi-storey buildings etc. The visual inspection may not be successful in all situations; hence there is a need to follow other reliable approaches. Non-destructive testing techniques were introduced in the civil engineering field around the fourth decade of the twentieth century. The majority of these techniques have been standardised in ACI (1995)[65] based on the surface hardness of the concrete. The principal aim was to

determine fresh concrete's homogeneity and compressive strength to help the engineers remove the formworks. The challenges faced by engineers to detect and characterise hidden defects helped explore more tools for estimating the mechanical properties of materials.

Vibration-based monitoring techniques usually provide only the overall health of the whole structure. Fibre optics are mainly used to check strain and temperature variations which are based on the light wave's intensity, wavelength, and interference[65]. These can be used for a wide range of civil structures such as buildings, bridges, pipelines, tunnels and dams[66]. These are costlier and need highly trained professionals. Magnetic particle testing is an SHM technique wherein structures are subjected to a magnetic field and observed under ultra-violet light, making the cracks directly visible. It is undoubtedly economical to apply, but its application is restricted to magnetic materials only [67]. Eddy Currents Technique works on the principle that the presence of a flaw changes the eddy-current pattern. The main benefit of this technique is that the hardware required is not expensive and is simple to apply. This technique is limited to conductive materials. The ultrasonic Technique exhibits higher damage sensitivity than the global methods. Impact-echo is an NDT used for testing concrete and masonry structures to evaluate the extent of flaws and their location. This technique has limitations in detecting small-sized cracks.[68] The X-ray technique was initially used for medical diagnosis, but nowadays, it is being applied for structural non-destructive evaluation. Apart from these NDT techniques, Acoustic Emission (AE) has been recognised as a promising non-destructive technique to identify and quantify damage in RC structures. This research effort has chosen this technique to monitor the health of BCJ under cyclic load. Detailed historical background and other technical details have been discussed in the next section.

3.3 ACOUSTIC EMISSION TECHNIQUE

3.3.1 Introduction

Historically speaking, Acoustic Emission can be related to the period 6500 BC, during which potters were known to listen to audible sounds during their ceramics cooling to check

the flaws. Many tests referred to the audible emissions made by tin, iron, cadmium, and zinc in the late 19th century. Czochralski[69] witnessed one significant correlation between metals and acoustic emissions. The following 20 years further verified the work of Robert Anderson[70] during tensile testing of an aluminium alloy beyond its yield point. In the mid-1900s PhD thesis was presented by Joseph Kaiser[71] entitled "Results and Conclusions from Measurements of Sound in Metallic Materials under Tensile Stress". After that, Bradford Schofield[72] initiated the first research program in the US to look at the materials engineering applications of AE. Nowadays, Kaiser's research has been recognised as the commencement of modern-day acoustic emission testing. According to this investigation, the material under load emits acoustic waves when the primary load level exceeds the previous maximum value. The materials behave elastically up to a load value less than the previous maximum value during reloading. Thus, according to Kaiser's theory, little or no acoustic emission will be recorded before the previous maximum stress level is achieved. Damages caused by cyclic loads can be estimated using Kaiser Effect as discussed in section 6.2.5.

An AE event occurs as a consequence of crack propagation due to a change in pressure, load or temperature. AE event generates a transient elastic wave in the material. This elastic wave radiates in all directions, which, after propagating through the material, is detected by the piezoelectric sensors mounted on the surface of the structure. If the amplitude of the wave signal is higher than the threshold value, it is recorded by the AE data acquisition system and is known as AE hit. Many acoustic emission waveform parameters are recorded by the AE monitoring software. Frequently used AE parameters are shown in Figure 3.1.

Amplitude is the main damage detection parameter which gives the maximum voltage in a waveform and is measured in decibels (dB). The time taken by the wave from crossing the first threshold to the peak amplitude is known as Rise-Time. The number of pulses emitted between the first and last threshold crossing is known as Ring-down Count or simply Count. The period between the first and last threshold crossing is known as Duration, which is

measured in a microsecond. Apart from these, there are some important damage detection AE parameters such Rise-Angle (RA), average frequency (AF) and Ib-value. RA value is the ratio of Rise-Time and amplitude. Average Frequency (AF) is expressed as the ratio of AE counts to AE duration. RA Vs AF plots help to distinguish between tensile and shear cracks (JCMS-III:2015)[11]. It has been established that when the RA value is higher and the average frequency is low, the AE source is classified as a shear crack. On the other hand, low RA and high AF indicate tensile cracks.

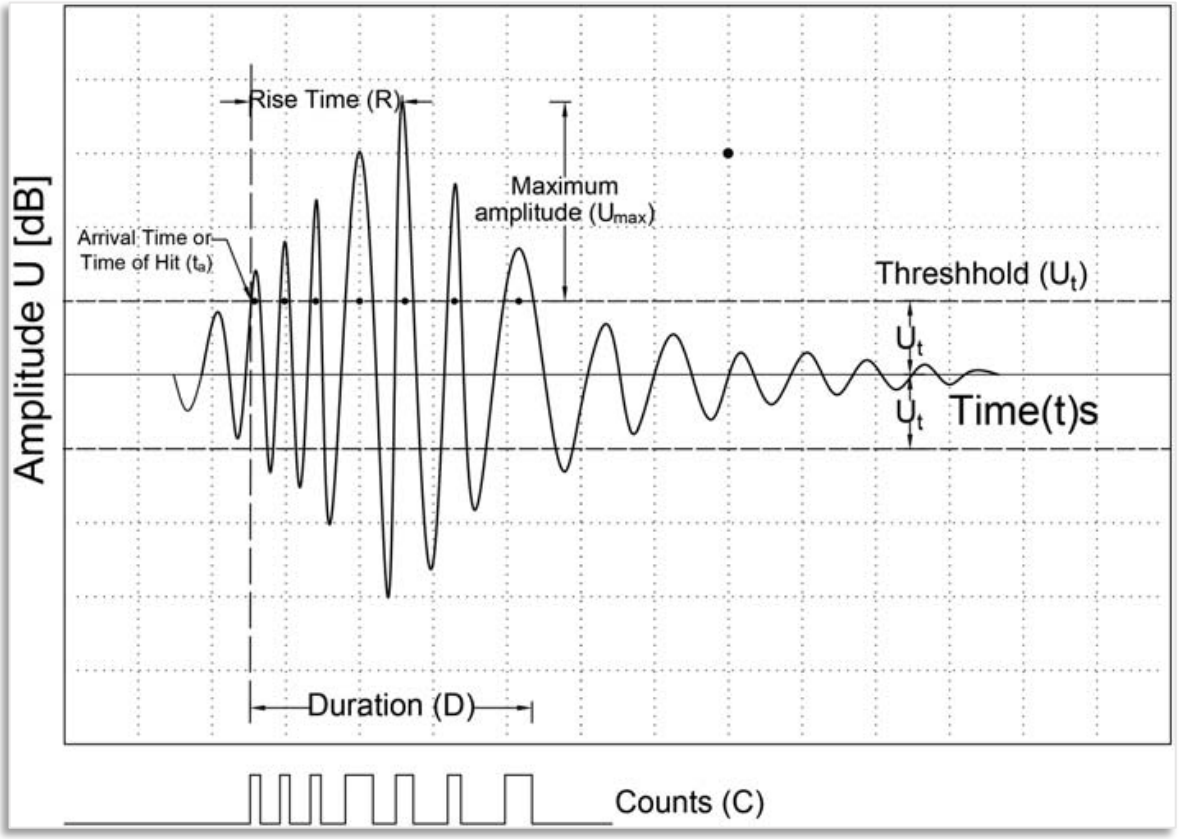

Figure 3.1: AE Parameters[73]

AE hit parameters are helpful for real-time monitoring to assess the damage occurring in the structures on the application of load[74]. Energy (also called PAC-Energy) is the integral of rectified voltage signal throughout AE hit. Its units are counts where 1 count equals 10 microvolts-sec. Hits recorded with low Energy indicate minor damage, while hits with high Energy represent major or severe damage. The AE Energy parameter helps estimate the quantum of damage in the structures. A sudden increase in the slope of cumulative energy Vs time plots indicates damage initiation. Signal Strength is another energy parameter defined as

the integral of the rectified voltage signal throughout the AE waveform packet. This feature is similar to PAC Energy, except that it is calculated over the entire AE signal dynamic range and is independent of gain. It provides reliable information regarding the damage assessment of the structure. The condition of RC structures, along with the initiation of cracks, can be predicted using Cumulative Signal Strength (CSS)[75].

The b-value is another AE parameter based on the Gutenberg-Richter[76] proposal developed in seismology to understand the relationship between the magnitude and frequency of earthquakes. The method is used in AE, primarily in the area of rock mechanics and concrete structures. In the AE technique, the b-value is usually calculated using the cumulative frequency-magnitude distribution obtained from AE cumulative hits Vs amplitude graph. A high b-value represents a stage of damage with micro-cracks. A low b-value represents macro-cracking in the structure. The b-value analysis is helpful to predict damage in RC beams subjected to cyclic loading[77]. The b-value has been defined in seismology based on a large number of observations over a long period. Thus, precise evaluation was possible. This is different from the AE application, where the main issue is to address the uncertainty of events to define the b-value. To resolve this, Shiotani et al (1994)[78] proposed an improved b-value, known as Ib-value, to evaluate failure in concrete and rocks. The Ib-value is calculated from the mean and standard deviation by using an amplitude distribution plot. Shiotani et al. (2000)[79] have successfully employed Ib-value to evaluate the fracture process in concrete.

The source locations are determined by the time required for the wave to travel through the material to the sensor. The wave velocity in concrete is not constant and is a difficult task to accurately calculate. When a wave propagates in all directions, its amplitude reduces by about 30% every time it doubles its distance in plate-like structures. In three-dimensional structures, the signal decay is approximately 50%. (RDSO, 2009[80]). This phenomenon of reduction in wave velocity is known as attenuation. Boundaries and discontinuities caused by cracks can cause attenuation due to scattering and diffraction. Various algorithms have been

developed to find out modified wave velocity to evaluate a more accurate source location[81].

To know the wave velocity and attenuation, Pencil Lead Break (PLB) test is performed before the main AE test in which a 2H pencil lead of 0.3 or 0.5 mm is passed through a cone-shaped Teflon shoe, designed to place the lead in contact with the surface of the material at an angle of 30°. Pencil-lead is broken by gently pressing against the material at predefined locations. The Signal produced by breaking the Lead is received by the AE sensors placed on the surface. The arrival times of the signals are recorded in the computer software. The wave velocity is then calculated by using the time difference between the two sensors. The test is performed by placing two sensors 200 mm apart. Four to five PLB tests are conducted at 50 mm distances on a line joining the sensors. The velocity is calculated by dividing the distance between the sensors by the difference in arrival time on the two sensors. The attenuation is also calculated using equation-3.1

$$Attenuation = \frac{\left[10\, log \frac{E_2}{E_1}\right]}{d} \tag{3.1}$$

Where E_1 & E_2 are energies recorded at sensors 1 & 2, respectively, and d is the distance between the two sensors. The average value of all the tests performed gives the wave velocity and attenuation. These values are used in the AE software for the main test.

3.3.2 Important terms

3.3.2.1 Attenuation

When an AE signal travels from the source or origin, its amplitude continues to reduce. This phenomenon is known as attenuation. The attenuation of the AE signal is a result of the geometric spreading of the wavefront, Internal friction, dissipation of wave into adjacent media, and dissipation of signal component. In plate-like structures, where the AE wave propagates in two-dimensional space, the AE signals are attenuated inversely to the square root of the propagation distance. The degree of attenuation can be defined with the equation (3.2).

$$Q = \frac{2\pi E}{\Delta E} \tag{3.2}$$

Where E is the energy of AE waves, ΔE is the attenuation value over a one-wavelength propagation distance (Ohtsu 1995[82]). The attenuation of AE signal amplitude can be evaluated by using the below equation.

$$U(f) = \exp\left(-\pi \frac{fD}{vQ}\right) \tag{3.3}$$

Where v is the AE wave velocity, D is the propagating distance, and f is the frequency. To take into account the attenuation effect, the values of attenuation are calculated using a pencil lead break test (explained later) before the start of the experiment on BCJ samples.

3.3.2.2 Background Noise

The background noise influences the accuracy and consistency of the testing results. To record a true AE signal, it is essential to filter the noise in the testing environments (Pollock 1989)[83]. The frequency of noise ranges from 100 kHz to 300 kHz. Filtering noise signals is important in AE testing. It is essential to apply noise filters in the acquisition and analysis of data by setting the frequency range.

3.3.2.3 Kaiser Effect

The idea of finding damage in structures subjected to repeated cyclic loads was first investigated by Dr Joseph Kaiser (1950)[84]. According to his investigation, the material under load emits acoustic waves when the primary load level exceeds the previous maximum value. The materials behave elastically up to a load value less than the previous maximum value during reloading. Thus, according to Kaiser's theory, little or no acoustic emission will be recorded before the previous maximum stress level is achieved. This is illustrated in Figure 3.2. AE events are recorded when a structure is loaded from A to B for the first time. On unloading from B to C, no AE events are recorded. Further, no AE event is recorded on reloading from C to D again. But when the load value exceeds D (i.e., higher than the previous maximum value at B), the AE events reappear. This phenomenon is known as Kaiser's effect. The validity of Kaiser's effect has been proven for homogeneous materials such as metals and

alloys. But some variations have been noticed in heterogeneous materials, such as rock concrete. Further studies have defined these deviations by a new theory known as the Felicity effect. In Figure 3.2, it can be seen that when the material is in the elastic stage of loading, the rate of AE activities is low, as can be seen from A to B in the forward load cycle. No activities are observed during unloading from B to C. While reloading from C to D, the AE activities are negligible, but the rate of AE activities starts to increase from D to E. Here D is a point where the load is higher than the previous cycle maximum value at B.

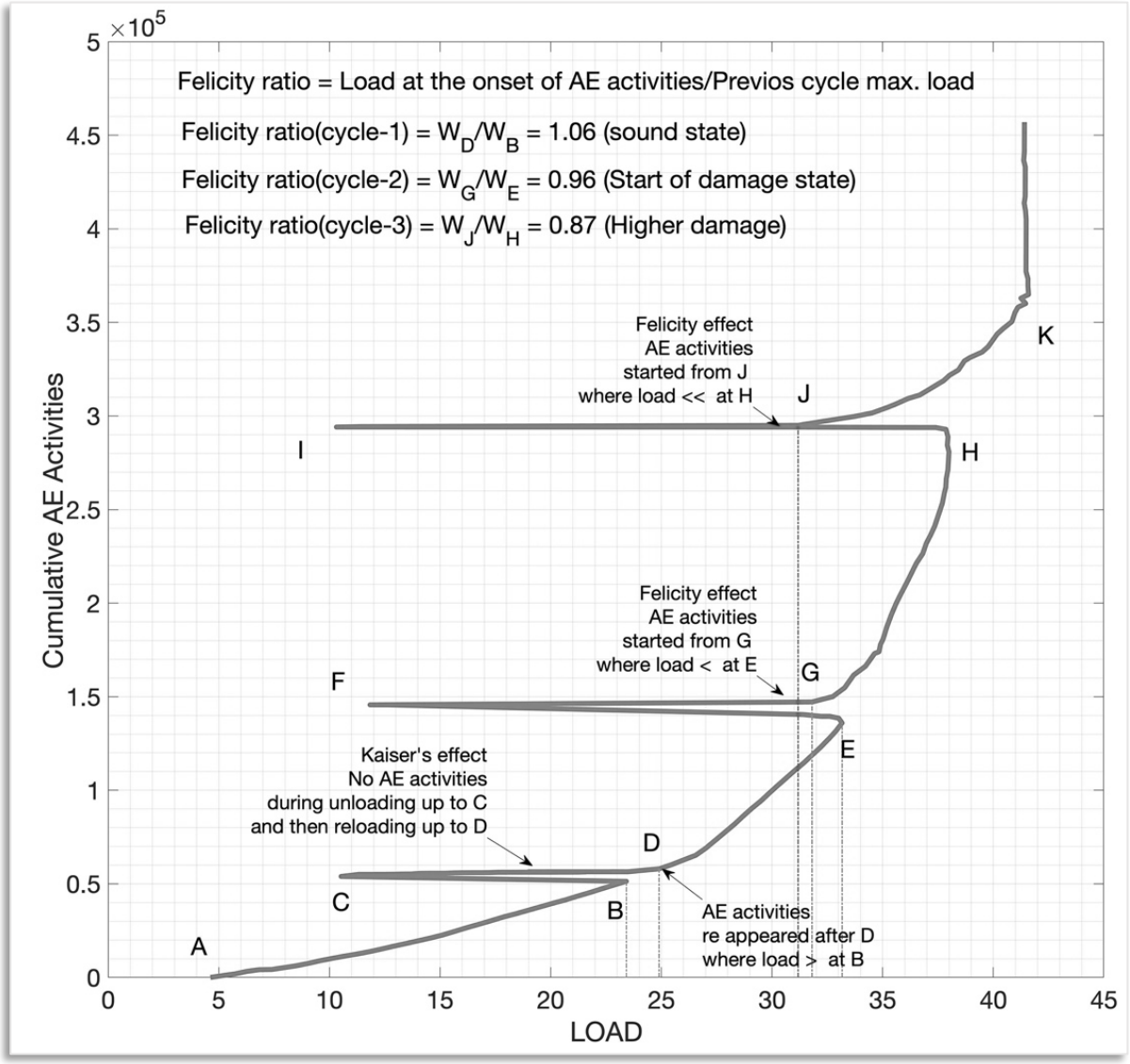

Figure 3.2: Kaiser and Felicity effects

At higher loads, the material tends to weaken and thus, emits acoustic waves shortly before the previous-cycle maximum load is reached as can be seen from G to H. Understanding the above effects helps us set the loading profiles to ensure sufficient generation of AE. Felicity

Ratio can be used to define the level of damage which is defined as the ratio of Load at the onset of AE activities to the previous maximum load value. Let the load at G be W_G and load at E be W_E then the Felicity ratio is given by the equation-(3.4):

$$Felicity\ ratio = \frac{W_G}{W_E} \tag{3.4}$$

A value of Felicity ratio less than one is an indication of the damage in the material. In stable conditions, the Felicity ratio >1 indicates no damage, as seen at point D. In cycle-2, FR is < 1, which indicates the start of damage from point G. The damage in the third cycle is even more because the Felicity ratio is lesser than in the second cycle.

3.3.3 Types of equipment used in AE monitoring

3.3.3.1 AE Sensors

Piezo-electric sensors are common in most AE testing (Figure 3.3). They are strong and more sensitive than other sensor techniques, e.g., capacitive, electro-dynamic, or laser-optical sensors[85]. In the testing of metal vessels, sensors comprising frequencies between 100 and 300 kHz are usually used. In this study, R6I sensors obtained from Physical Acoustic Corporation (PAC) have been used, which are suitable for testing concrete structures. They have an operating frequency in the range of 40-100 kHz.

Most of the sensors have a preamplifier and are attached to the objects using magnetic holding devices. The amplified AE signal is transmitted to the AE system via a signal cable. Usually, the 28Volt DC power supply for the pre-amplifiers is fed through a signal cable.

3.3.3.2 Couplant

The fluid/semisolid material placed between the sensor and material surface is known as a couplant which helps to transmit acoustic waves between two surfaces. Couplant should not be confused with bonding agents. Bonding agents (holders) help to hold the sensor to the surface physically. Usually, AE sensors are attached to the test object using magnetic holders (refer to Figure 3.4). Elastic ties, tapes, clamps, glue, etc., can also be used for convenience. A constant hold-down force must be ensured during the AE data acquisition process. Before

attaching a sensor, the material's surface is cleaned correctly, and a couplant is applied.

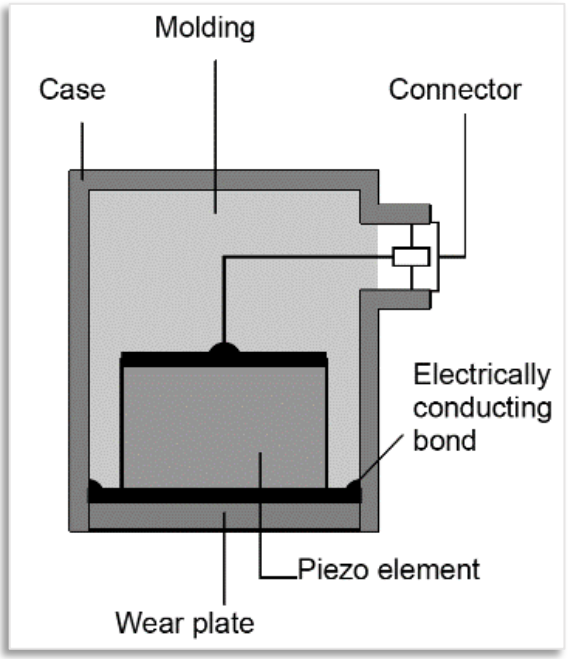

Figure 3.3: Basic setup of AE sensor[85]

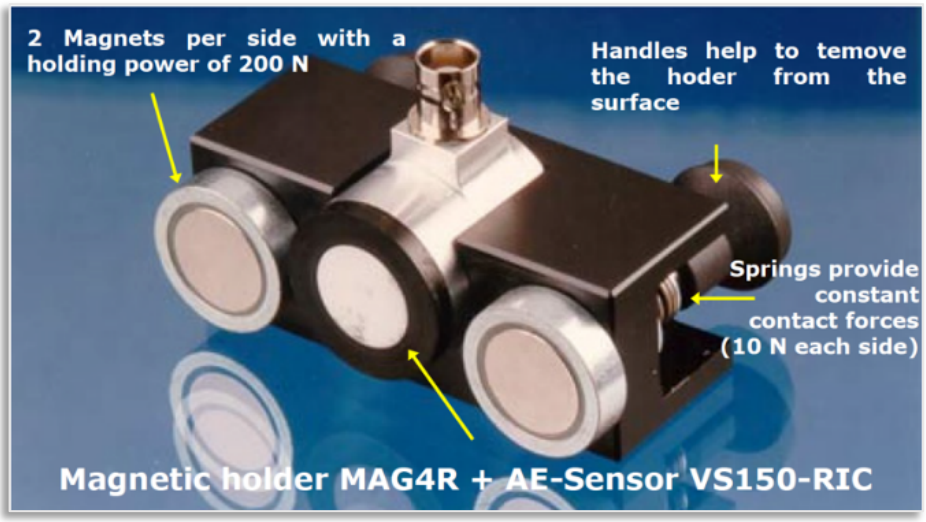

Figure 3.4: Magnetic holder[85]

3.3.3.3 Pre-Amplifiers

The primary objective of this device is to boost the signals and effectively filter and reject noise from areas outside the sensor operating range. There is the option of selecting 20, 40 or 60 dB gain on the preamplifiers. In most of the acoustic emission tests, the pre-amplifiers are set to a 40 dB value. (Figure 3.5).

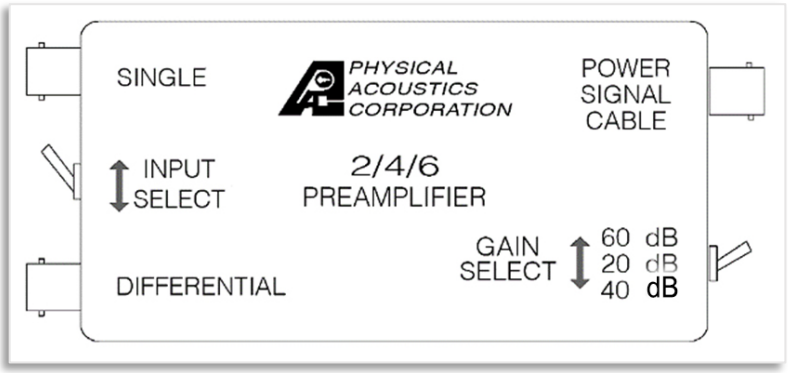

Figure 3.5: Pre-amplifier[86]

3.3.3.4 Frequency Filters

The frequency filters are used to eliminate unwanted frequency ranges, which are a source of the noise. Signals having frequencies below 20 kHz are not desirable to avoid local noise signal recording. A frequency filter of the range 20-100 kHz is used for composite materials such as RC structures. A frequency filter of the range 100-500 kHz is used for integrity testing of ceramics and metals. (Sandia report, 2013)[87]

3.3.3.5 Data acquisition system

AEwin data acquisition software developed by Physical Acoustic Corporation (PAC) has been used in this research work. These data acquisition systems use computers and appropriate software, provided with menu-driven parameter input and system control. All the signals received at the sensor end are acquired and stored in the acquisition system. These systems have inbuilt post-processing capabilities.

3.3.4 Analysis of AE Signals

The AE technique uses two approaches to detect deformations or damages in concrete structures. The first approach uses AE parameters for damage detection and is known as the Parametric Approach. The second approach is recording the AE signal directly and estimating the damage based on the signal behaviour Waveform analysis approach. In the parametric analysis, AE parameters are used. All modern-day data acquisition systems have provisions for collecting data in both forms. The AE parameters recorded are the hits, counts, Amplitude, Duration, Energy, Signal strength, Count, Average Frequency etc.

The post-processing of AE data is essential. The spreadsheets of Microsoft Excel are not sufficient to handle the huge data. MATLAB programming has been done to analyse the data for plotting graphs. Appendixes A, B and C have been provided for the post-processing of data.

3.4 LITERATURE REVIEW OF AE MONITORING

Labuz et al. (2001)[88] have performed three tests, i.e., diametric compression, flexural, and indentation on quasi-brittle materials. The authors have concluded that the AE technique helps observe the damage, throughout the entire volume, at various stages of loading.

Shigeishi et al. (2001)[89] have investigated the health monitoring of ancient masonry and RC arch bridges. The AE technique was applied, and feasibility was proved in inspecting crack growth in the bridges.

Leszek et al. (2002)[90] have reported the applicability of the AE technique in monitoring realistic RC, prestressed concrete and concrete-steel bridges. The testing observed that it is possible to compare AE parameters with other physical parameters such as the width of cracks, deflection and strain. The analysis of these values gave a complete view of procedures occurring in tested elements and allowed the use of the AE method for in situ structure testing.

Chen et al. (2004)[91] investigated the influence of notch depth and fibre content using AE signal parameters in an RC beam subjected to a three-point bending test. It was observed that with the increase of notch depth, the peak of AE signals was deferred, and the amplitude of the AE signals was reduced.

Farid et al. (2004) [92], **Grosse (2006)** [93] **and Ohno et al. (2010)**[94] have applied the AE technique to classify the types of cracking. The crack classification methods were introduced by analysing AE parameters such as hits, count, duration time, amplitude, energy, and rise time. RA value and average frequency parameters were employed to differentiate between tensile and shear cracks. The AE results were analysed using parameter-based and signal-based methods. It was observed that the parameter-based methods adopt all AE signals; however, the signal-based methods only analyse AE events.

Carpinteri et al. (2007)[95] have applied acoustic emission techniques to identify flaws in RC structures and masonry buildings. Using this technique, a specific procedure has been presented for monitoring crack propagation and damage assessment. The method was useful to assess the amount of energy released during crack propagation. A procedure has been proposed to forecast the damage evolution and the time to structural collapse.

Xu (2008)[96] has demonstrated that AE is a wave generated from dislocations and microcracking in a stressed material which is detected by using AE sensors. These sensors convert the mechanical waves into electric signals that can be monitored and measured to determine the characteristics of the test object. The amount of acoustic energy depends mainly on the size of the deformation and speed. It was further observed that AE activities are sensitive to both elastic and brittle materials.

Climent et al. (2008)[97] have used the AE technique for measuring fatigue damage in reinforced concrete exterior BCJ under seismic loading in the laboratory. Specimens located in the lower and upper stories of the building have been considered for comparison reasons. A significant increase in the AE activity has been noticed in both specimens at the start of the yielding of the longitudinal beam reinforcement. Next, using the AE Ib-value analysis, it was observed that the macroscopical fractures occurred mainly during loading and were located in the vicinity of the BCJ. They have also observed an association between the plastic strain energy and the AE energy until a sudden drop in strength determines the failure of the specimen. This correlation allows us to propose a tentative formula to predict damage intensity and the occurrence of failure.

Carpinteri et al. (2013)[98] have conducted tests to examine the association between energy absorbed/released and AE energy in brittle materials. The energy absorbed per unit area was computed. This parameter was compared to the elastic energy accumulated in the body at the end of the elastic stage to define a structural brittleness index. Load Vs displacement response has been obtained up to failure under different conditions. All the tests were monitored using the AE methodology. Post-analysis of AE data was carried out to find a connection with the energy released and to single out the different failure mechanisms.

Abdelrahman et al. (2014)[99] have performed cyclic load testing on pre-cracked and differently corroded prestressed specimens using AET to evaluate damage using the DI. A correlation was observed between the calculated DI values and the observed amount of damage. Based on these observations, a modified index of damage (MID) was proposed to detect yielding points for cracked and uncracked specimens.

Ma et al. (2017)[100] have demonstrated that effectiveness of AE hits in analysing the crack process of a strengthened column by using a b-values parameter. This parameter can replicate the variation in the size of concrete crack growth. The variation of AE energy and hysteretic energy was analysed, and it was observed that these parameters have a definite correlation.

Sagasta et al. (2018)[101] investigated damage evaluation of RC structures subjected to cyclic loads using the AE technique. They presented that the b-value represents a better parameter of the AE signals rather than peak amplitude. An association has been observed between the energy dissipated and the AE energy. They conducted experiments on two exterior and interior BCJs which were instrumented with AE sensors. The energy b-value along the loading process conveys the evolution of the severe damage near the beam-column joint connections. Thus, AE techniques showed promising results which can be used for structural health monitoring.

Zeng et al. (2020)[102] have investigated that structural behaviour and crack development show a good correlation with acoustic emission activities. Load Ratio and Calm Ratio parameters can be used to examine the damage severity limits. The b-value analysis can be employed as an indicator for the initiation and propagation of damage. The variation in the b-value can identify the crack process in the prestressed concrete beam.

Zhang et al. (2020)[103] investigated corroded RC beam-column joints under cyclic loading using the AE technique to study their damage features. The authors observed that the AE technique could be used as an effective tool for monitoring and assessing the damage to corroded reinforced concrete structures. They have further analysed AE hits and amplitude parameters to investigate the crack development process and the possible damage pattern. The

variation of the cracks due to lateral loading was also examined using b-value analysis. The acoustic emission intensity analysis exposed a good association between the peak value of the history index and the drift ratio for corroded joints. The cumulative AE energy and cumulative hysteretic energy also showed a good correlation which helped to predict the damage level for corroded joints.

Prem et al. (2021)[104] have observed that acoustic emission parameters have a strong relationship with the nature of failure processes in the RC beams. The authors have demonstrated that the AE technique can be effectively employed for crack monitoring and damage characterisation in RC beams.

3.5 CLOSURE

The literature review shows that the AE technique is the most effective non-destructive technique that helps monitor active defects. The source of the origin of acoustic emissions can be detected by employing multiple sensors on the surface of the structure, which can be measured in real-time. It is possible to differentiate between actual damage-associated signals and background noise by analysing the signals in detail. Apart from these advantages, acoustic emission monitoring has some disadvantages too. Acoustic emission waves are generated from local irreversible changes in materials. Most materials display the unique Kaiser effect; thus, a generalised loading profile cannot be used to test the integrity of any structure. Reinforced concrete materials tend to attenuate acoustic signals faster than metals. It is tough to examine the damage progression in brittle materials using the AE technique. In reinforced concrete structures, the AE wave velocity is also a major issue for accurately predicting the location of the damage. Many sensors are required to monitor the health of big structures like bridges and multistorey buildings. The placement of sensors on them is a major and critical issue in AE monitoring.

CHAPTER-4. EXPERIMENTAL PROGRAM & METHODOLOGY

4.1 GENERAL

Most damage indices are based on load-displacement parameters obtained from non-linear behaviour. In acoustic emission testing, the available indices are based on the AE parameter alone, such as AE energy. However, in addition to AE energy, displacement and dissipation energy response also contribute to damage quantification. Thus, it is proposed in this research work to study the displacement and AE energy responses to develop a damage index to achieve the aims and objectives as explained in chapter 1. To evaluate the results experimentally, a 1:2 scaled model of reinforced concrete samples representing an exterior BCJ of a multistorey structure has been subjected to cyclic loading. A reverse cyclic load has been applied on the free end of the beam using a hydraulic jack. The samples were instrumented with load cells to measure applied loads. Two linear variable differential transformers (LVDT) were attached to measure displacement response. The samples were instrumented with surface-mounted AE sensors and AE data acquisition set up to record AE parameters during loading and unloading. The samples were loaded until the collapse. The damaged BCJ samples were further repaired using Engineering Cementitious Composites (ECC). This chapter discusses in detail the various materials used in casting BCJ samples, the casting procedure, and the adopted experimental setup for testing and strengthening systems employed for repairing the damaged BCJ.

4.2 MATERIAL PROPERTIES AND TESTING

The Beam-Column Joint samples were cast in the present study in the Structural concrete laboratory of the civil engineering department at Thapar Institute of Engineering and Technology. The materials used for casting BCJ and their further repairing consist of concrete, steel reinforcement, Engineering Cementitious Composites (ECC) etc. Relevant tests have been conducted following Indian Standard (IS) codes of practice to determine the physical

properties of the materials as per IS-8112, 1989; IS-1489 (Part-I), 1976; IS-383, 1970. The material properties and relevant tests to conform to the material properties have been presented in the following sub-sections.

4.2.1 Cement

Ordinary Portland Cement (OPC) conforming to IS codes: OPC 43 grade - IS 8112-1989[105] or OPC 53 grade - IS 12269–1987[106] are often used in laboratory testing. In this study, 7.6a 43-grade cement having minimum strength of 43 N/mm^2 at 28 days has been used to cast BCJ samples. Laboratory tests have been conducted to confirm the properties of cement. The standard consistency of the cement has been worked out to be 31.2%. The specific gravity of cement was found to be 3.14 g/cc. The initial setting time calculated has been recorded as 47 minutes and the final setting time as 460 minutes. The standard value of the fineness of cement should be less than 10 %. The test results indicate that the cement used has an acceptable value of fineness, having a fineness of 8.22%. The calculated 7 days' compressive strength has been worked out to be 34 Mpa, and that of 28 days has been worked out to be 46 Mpa.

4.2.2 Aggregates

Aggregates are inert materials such as sand or gravel, which, together with water and Portland cement, are an integral part of concrete. Using the appropriate aggregates possessing desired properties is essential to get concrete of desired strength. The aggregates account for 60 to 75 % of the concrete volume and strongly affect the properties and economy concrete mix. The aggregates are of two types, i.e., fine and coarse. The term **fineness modulus** is used to define the fineness of aggregates.

The fineness modulus of fine aggregates is calculated by dividing the cumulative sum of fine aggregates retained on sieves up to 150-micron size by 100. For RC structures, fine aggregates with fineness modulus in the range of 2.0 to 4.0 are generally used. The higher the FM coarser the sand. The FM of the sand used in the casting of BCJ samples was found to be

2.8, which indicates that the sand used is coarser. Water absorption capacity is important for designing a concrete mix. IS code 2386 (Part 3) 1983 is followed for finding water absorption of aggregates. The permitted value of water absorption varies from 0.1 to 2 %. The experimentally tested value of water absorption was 1.46. The specific gravity parameter is useful to check the strength of aggregates. The permitted value of specific gravity as per the Indian standard is 2.5 to 3. The specific gravity of aggregates worked out with the help of Pycnometer bottles was found to be 2.7.

The CA grading limits have been provided in IS 383-1970-Table 2, clauses 4.1 and 4.2. The grading is essential to get cohesive and dense concrete. The CA can have round, angular, or irregular shapes. The round aggregates possess the lowest surface area and will have the lowest water demand. Crushed aggregates of a maximum size of 20 mm have been used in this work to prepare the BCJ sample. Grading of CA is carried out by performing a sieve analysis. The average value of FM of CA has been calculated as 7.6. The coarse aggregates used in this study consist of surface dried and free from any silt with a specific gravity of 2.56 and water absorption of 1.9%.

4.2.3 Concrete

Concrete is an essential material used in most civil engineering structures. The versatility of moulding concrete into any shape and size with locally available materials with ease and economy has made it the second-largest consumed material on earth. It is composed of cement, fine aggregates (sand) and coarse aggregates mixed with water which hardens with time. The strength of concrete primarily depends on the proportions of these four constituents. IS 456:2000[107] has provided different grades of concrete depending upon the characteristic compressive strength of concrete, e.g., the M30 grade of concrete possesses 28 days characteristic compressive strength of 30 N/mm^2 when tested on a 150 mm cube. IS 10262: 2009[108] guidelines have been followed to proportion the concrete mix to get the M30 concrete mix.

4.2.4 Reinforcement

High-strength deformed reinforcing steel rebars have been used for casting beam-column joints. Steel reinforcement plays an important role in any RC structure so that the two materials act together in resisting forces. As per IS 432 (part-1)[109] , plain bars are designated as Fe-250. They have a yield stress of 250 N/mm^2 . Bars conforming to IS 1786:2008[110] have high yield strength. These are designated as Fe415, Fe415D, Fe500, Fe500D, Fe550, Fe550D, and Fe600, where the letter 'D' indicates that it is more ductile. Longitudinal bars of 10 mm dia and shear stirrups of 6 mm dia bars have been used in this study to cast beam-column joint samples. The properties of bars used as per test results have been shown in the table below.

Table 4.1: Tensile strength of steel bars

Size of reinforcement bars	Yield strength (MPa)	Ultimate strength (MPa)
10 mm dia bars	493	573
6 mm dia bars	507	614

4.3 SPECIMEN DETAILS

Two types of specimens were cast. Type-1 specimens of beam-column joints were cast with steel reinforcement detailing as per IS:456-2000 without ductile detailing named SP1, and Type-2 specimens were cast as per IS 13920-2016 with ductile detailing named SP2. The reinforcement details are shown in Figure 4.1. In the present study, the cross-section of the beam and column has been kept at 200 $mm \times 150$ mm. The concrete mix has been designed for characteristic compressive strength f_{ck} = 35 N/mm^2 as per IS 10262-2009 guidelines using locally available materials for casting the BCJ. The concrete mix ratio calculated is 1: 1.20: 2.32 by weight of Cement: Sand: Coarse-Aggregates with a water-cement ratio of 0.36. All these ingredients used in making concrete were mixed thoroughly to cast BCJ samples. Two types of samples were cast, first designed without ductile detailing and another with ductile detailing as per reinforcement details shown in Figure 4.1. The mix design for both samples has been kept the same. At the time of casting BCJ samples, 9 cubes of size $150mm \times 150mm \times 150mm$ were cast to determine 7 days, 14 days and 28 days

compressive strength. The 7 days, 14 days and 28 days compressive strength of the cubes has been worked out to be 19.1, 26 and 37 N/mm^2 respectively. The above-mentioned experimental work for casting the samples and testing the cubes has been shown in Figure 4.2.

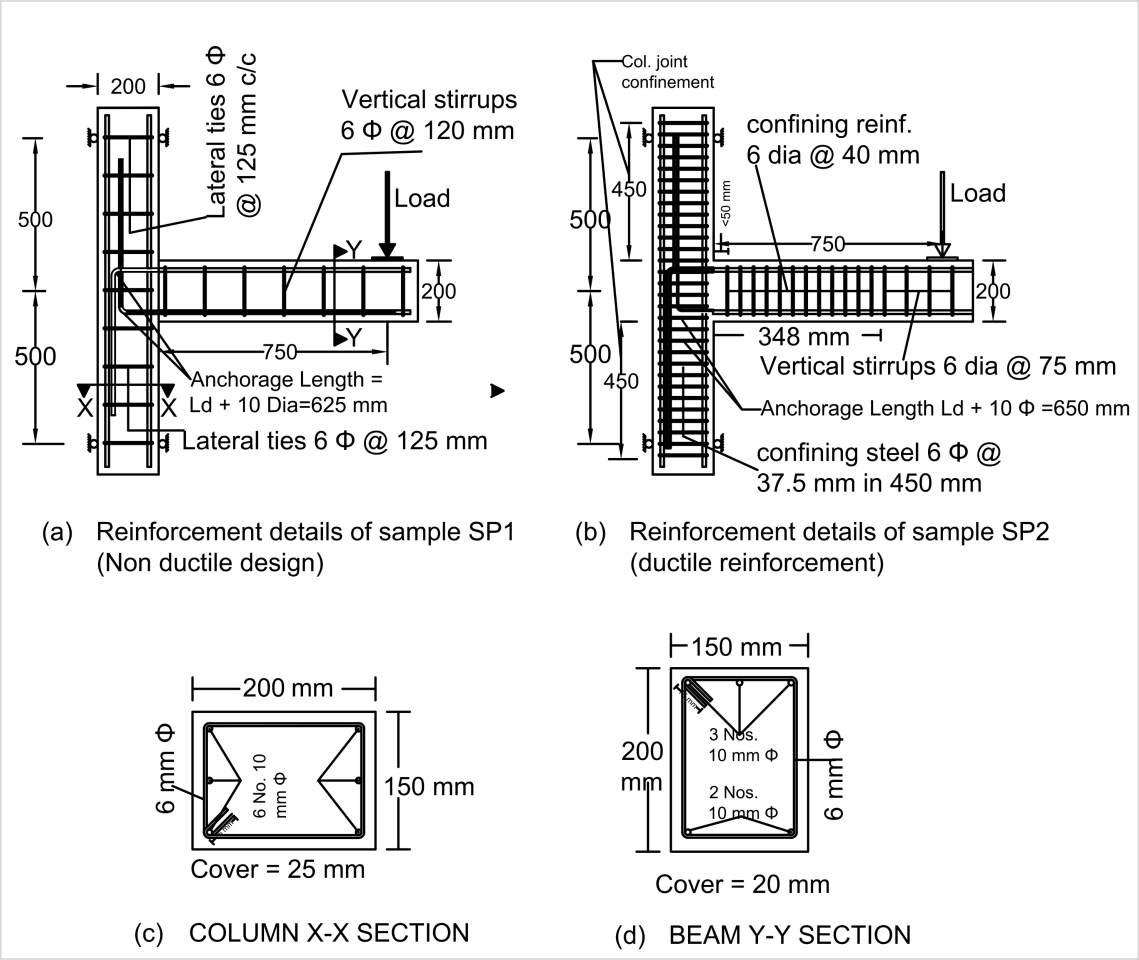

Figure 4.1: Reinforced details of BCJ. (a) Sample SP1, (b) Sample SP2

The longitudinal reinforcement in both samples is the same. The beam has been provided with three bars of 10 mm diameter on one face and two bars of 10 mm diameter on another face, whereas the column has been provided with three bars of 10 mm diameter on both faces (Figure 4.1). Thus, the area of tensile reinforcement in the forward cycle is higher than compression reinforcement. When the load cycle reverses, the tensile face in the forward cycle becomes compression, and the compression face becomes a tensile face. Since flexural resistance primarily depends on tensile reinforcement, the BCJ has different bending resistance in forward and reverse loadings.

Figure 4.2: Casting of BCJ(a-f)

4.4 NOMENCLATURE FOR BCJ SAMPLES

The specimens have been designated differently for monotonic and cyclic load tests performed for control and retrofitted samples. The BCJ reinforced without ductile reinforcement is designated SP1, and BCJ reinforced with ductile reinforcement is designated SP2. The BCJ sample SP1 and SP2 tested under monotonic loads has been maned as SPM1 and SPM2 respectively. The letter M is replaced with C, representing BCJ samples tested under

cyclic loading such as SPC1, SPC2 etc. Letter R has been added when damaged BCJ samples SPC1 and SPC2 are repaired, e.g., SPCR1 represent the BCJ sample repaired with ECC and tested under cyclic loading. Figure 4.3 and Table 4.2 may be referred to for detailed policy about the nomenclature of BCJ samples.

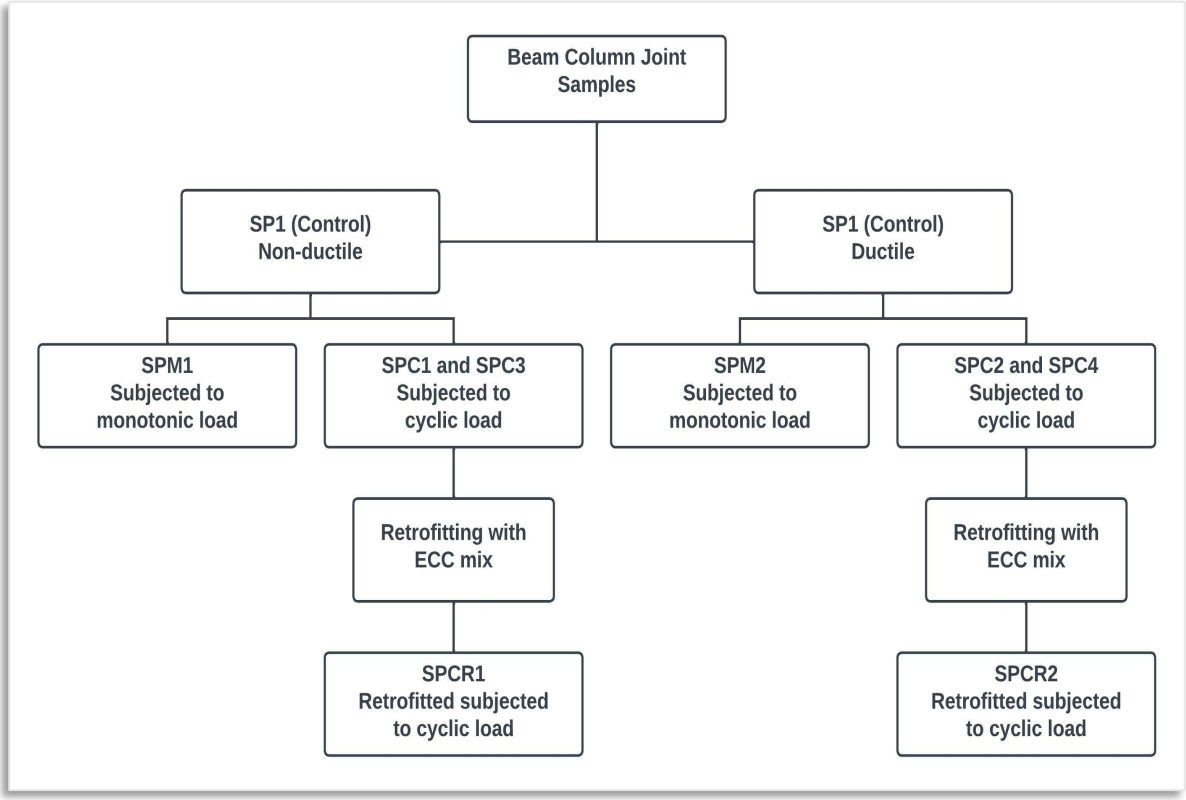

Figure 4.3: Nomenclature for BCJ samples

Table 4.2: Nomenclature of BCJ samples

Sr No	Specimen	Detail
1	SP1	BCJ samples reinforced without ductile detailing
2	SP2	BCJ samples reinforced with ductile detailing
3	SPM1	Sample SP1 tested under monotonic loads before retrofitting
4	SPM2	Sample SP2 tested under monotonic loads before retrofitting
5	SPC1, SPC3	Sample SP1 tested under cyclic loads before retrofitting
6	SPC2, SPC4	Sample SP2 tested under cyclic loads before retrofitting
7	SPCR1	Damaged sample SPC1 repaired with ECC under cyclic loads
8	SPCR2	Damaged sample SPC2 repaired with ECC under cyclic loads

4.5 FLEXURAL TEST SET-UP

The experimental setup for flexural loading and testing is shown in a schematic diagram (Figure 4.4). The column ends are clamped with rigidly fixed girders at a distance of 500 mm from the centre to provide hinged support. It is free to rotate along Z-axis and restricted for translational movement in the Y-direction. The details of the loading mechanism have been presented in Figure 4.4. The beam's free end demands translational movement along Y-axis and rotational movement along Z-axis. A swivel mechanism has been attached to the double-acting hydraulic jack to get a force component in a direction parallel to the column axis so that the direction of force applied on the beam does not change with the deflection of the beam. It will also help release any rotational moment on the beam's free end caused by the rotation of the beam axis. In real structures, every column has been subjected to a permanent axial compressive force caused by gravity loads. Thus, to represent a real model, a compressive force has been induced in the column of BCJ.

Keeping in mind a stress limit of 0.1 to $0.5f_{ck}$, as recommended by Paulay et al. (1992)[111] and $0.8f_{ck}$ in IS-13920[112], a fixed axial force of 90 kN has been applied to the column with the help of a hydraulic jack. During the application of axial force, the hydraulic jack attached to the beam should be free so that un-noticed stresses are not developed in the sample due to the movement of the column with axial force. The value of axial force is recorded with a load cell placed between the jack and column end. Another end of the column is restrained for axial displacement with the help of an anchor block adequately welded to the supporting girder assembly. A load cell is placed between the hydraulic jack and swivel head to monitor the forces applied to the beam.

A square grid of horizontal and vertical lines has been made with a lead pencil on all the sides of the BCJ sample, as shown in Figure 4.5 (b). This is helpful in measuring the location of cracks, the width of cracks and strains developing on the surface of the BCJ sample. The cyclic displacement-controlled force is applied on the beam's free end. It is controlled with

the pressure and release valves provided in the servo-controlled compressor. It is measured by using linear variable differential transformer (LVDT) devices. These devices convert linear displacement into an electrical signal through the principle of mutual induction.

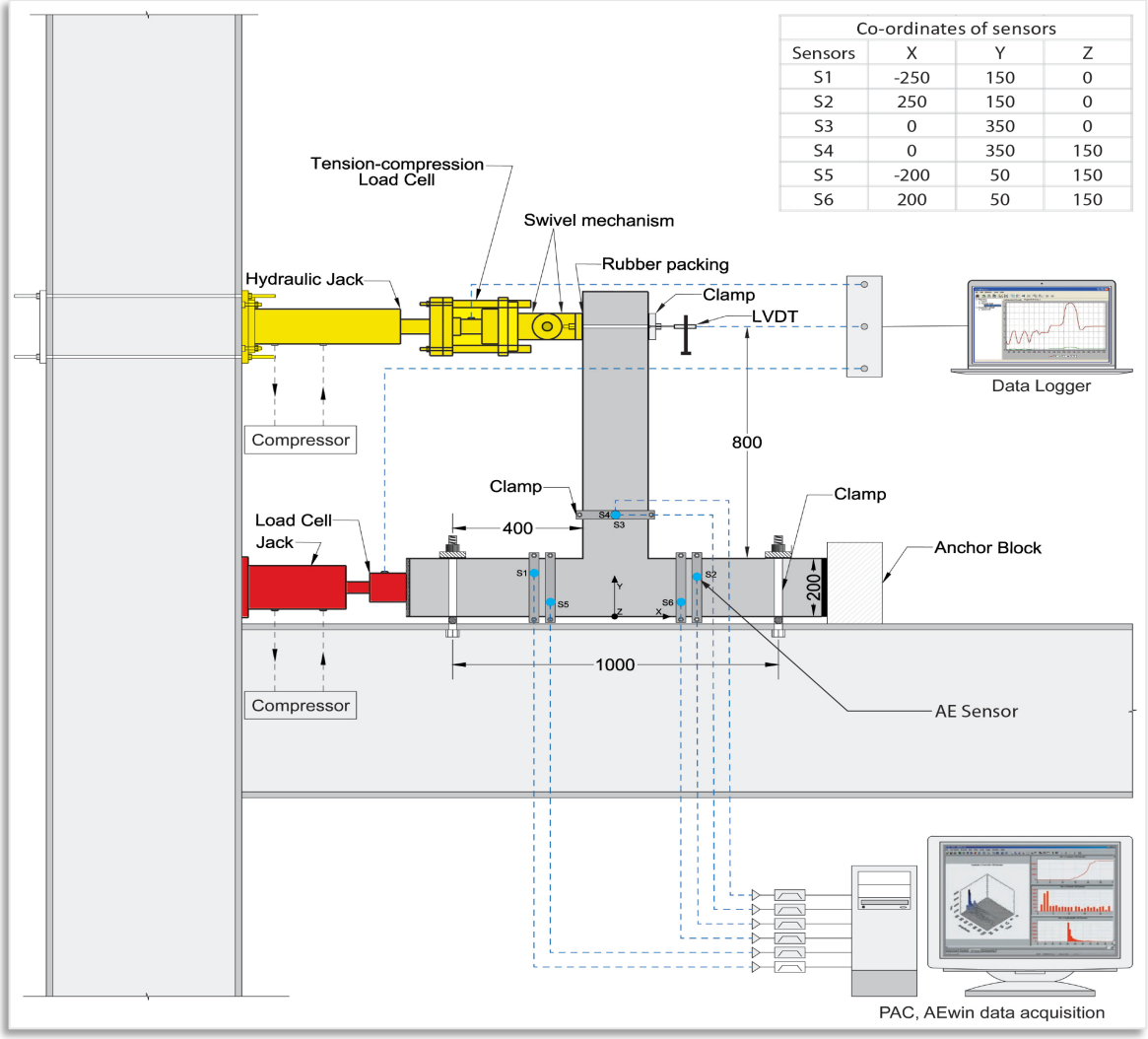

Figure 4.4: Experimental setup for BCJ testing

Data logger software has been used to monitor and record displacement data. Two LVDTs have been installed on the beam, close to the applied force, to monitor the displacements during loading and unloading. The load and displacement data are monitored carefully on the computer screen, as shown in Figure 4.5 (c). The experiment should be put on hold when the displacement approaches the maximum limit of LVDT. In case the experiment is required to be performed beyond the LVDT maximum limit, the LVDT should be reset to the minimum value, and the data recorded thereafter should be adjusted manually by adding the difference between the maximum recorded value at the time of hold and the minimum value

on LVDT after reset, to all the displacement values recorded after reset. Both the BCJ samples have been loaded till failure to study damage parameters.

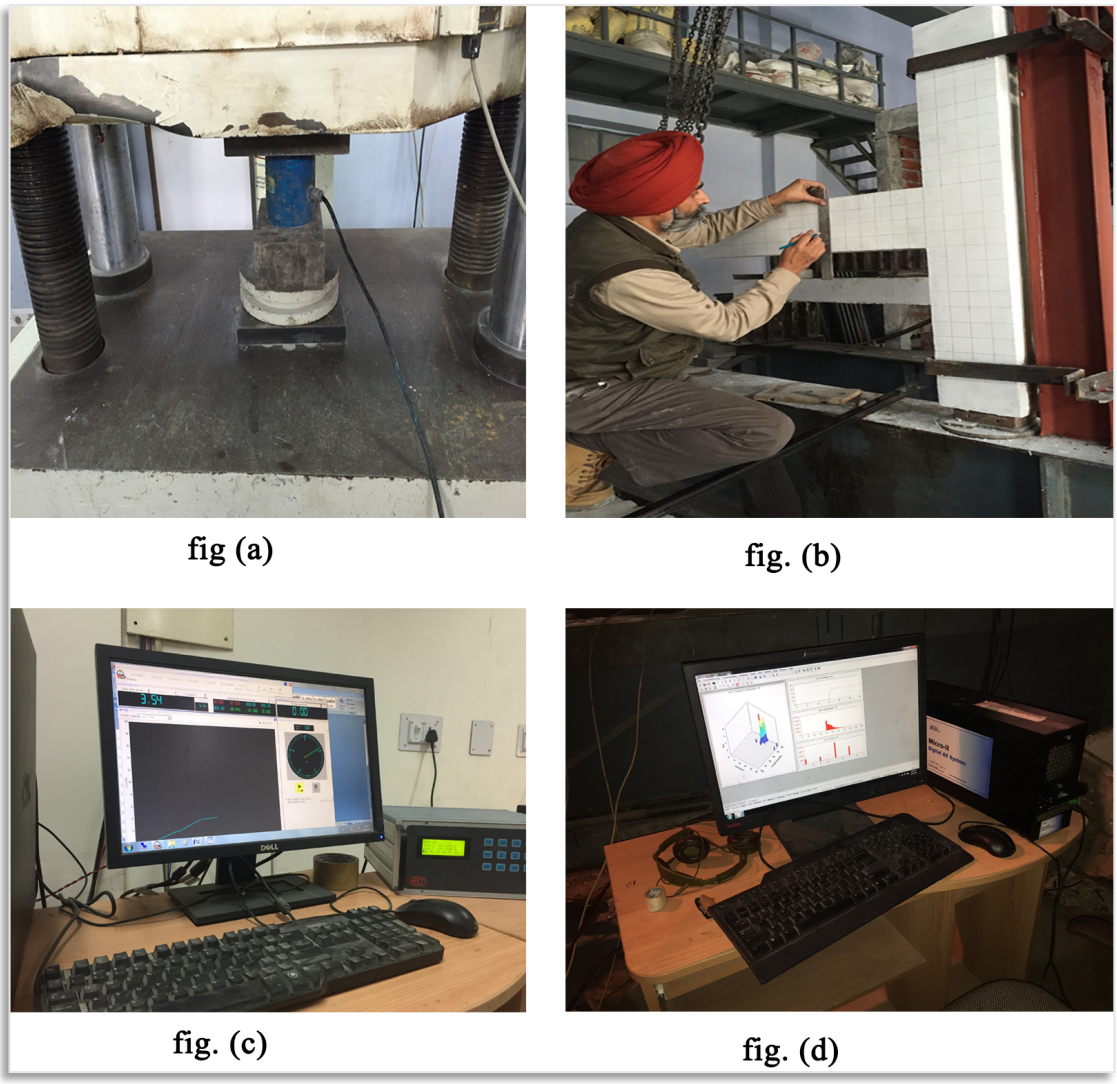

fig (a) fig. (b)

fig. (c) fig. (d)

Figure 4.5: Methodology of AE Testing

4.6 EXPERIMENTAL SETUP FOR AE MONITORING

Six number AE sensors (of type R6α as recommended by PAC[86] for monitoring damage in concrete, with a resonant frequency of 60 kHz and 40 dB preamplifier gain), have been installed in the proximity of the beam-column joint (Figure 4.4) and attached to 8-Channel AEwin Data acquisition software. The placement of sensors is essential to detect all the AE signals. The surface of the BCJ sample is adequately cleaned with fine sandpaper. After applying grease couplant on the cleaned surface, sensors are gently placed on the couplant and tightened with a clamp to hold them securely. All the sensors have been carefully connected to Data acquisition software for monitoring AE activities. Initially, Pencil Lead Break (PLB) tests

were performed as per the procedure laid down by Hsu[55] to know attenuation and wave velocity.

Higher noise level is one of the major problems of acoustic emission (AE) testing that affects the results. The signals that have crossed a pre-defined threshold level are recorded to overcome this problem. Care should be taken to select the threshold level because setting a very high value for the threshold may prevent potentially important signals from being recorded, and setting the threshold very low may cause the background noise to cross the threshold and result in a large amount of unwanted data being recorded. A threshold value equal to 40 dB has been set up in the AE data acquisition system to filter out unwanted AE data.

Before starting the experiment, special care has been taken that no unwanted noise exists in the vicinity of the test specimens. On application of load on the beam, the formation of cracks is carefully monitored, and the observed cracks are marked on the sample during the loading and unloading cycle. Acoustic emission data being acquired is monitored simultaneously from AE graphs plotted by AEwin software. Further, it is also essential that specific AE parameters need to be set before starting the data test, as shown in Table 4.3.

The threshold value setting is done in the AEwin data acquisition software, which is a standard hardware setup which is required to record signals having an amplitude higher than the threshold and also to filter background noise. HDT, PDT, and HLT are the timing parameters of the AE signal. The PDT parameter helps to measure the rise time. The HDT parameter is used to determine when the hit has ended. The HLT setting enables the discarding of spurious signal decay measurements. A pre-decided value of all the above parameters is set in data acquisition software, as shown in Table 4.3. The AE parameters can be monitored on the AE data acquisition system screen, as shown in Figure 4.5 (d).

Table 4.3: Instrument settings

Parameter	Value to be set
Acquisition Threshold	40 dB
Hit definition time (HDT)	400 µs
Peak definition time (PDT)	200 µs
Hit Lockout time (HLT)	200 µs

4.7 LOADING PROFILE

Two types of loading profiles have been used. Type-1 loading profile consists of a monotonic load applied on the free end of the BCJ beam. The tests under monotonic load are performed to assess the ultimate displacement capacity, yield load, yield displacement and ultimate acoustic energy capacity of BCJ samples. The BCJ samples tested under monotonic loads have been designated as SPM1 and SPM2. The second loading profile consists of cyclic load which is applied on the free end of the beam for samples SPC1, SPC2, SPC3 and SPC4. The displacement-controlled cyclic loads are applied until the failure of BCJ. The LVDT and load cells automatically record the displacement and load data. The AE parameters are recorded by data acquisition software connected through AE sensors placed on BCJ samples. The damaged samples were repaired with Engineering Cementitious Composites (ECC) mix and tested under cyclic loading.

4.8 STRENGTHENING OF DAMAGED BCJ USING ECC

Engineered Cementitious Composite (ECC) is a material reinforced uniformly with short fibres having a volume fraction lower than 2-3% and features like tensile hardening and multiple cracking[113]. It possesses ultimate tensile strain from 3 to 8%, which is about 300-800 times more than ordinary fibre-reinforced concrete[114]. The high crack control property of ECC has made it a favourable material in RC structures for repair and retrofitting because it helps to spread tiny cracks on the tensile surfaces. This research work presents an experimental

investigation of the structural performance of ECC-repaired RC BCJ subjected to cyclic loading. The control BCJ tested under cyclic loading up to the collapse stage has been repaired by removing the loose/crushed concrete and replacing it with ECC. The following components of composite strengthening resin are used these days:

4.8.1 Crack injector

Crack Injector (MasterInject® 1315) is a low-viscosity epoxy resin consisting of a crack injection resin system based on trimethyl-hexane-1,6-diamine. It possesses a long life designed to seal cracks in the concrete and restore its structural integrity. It can quickly be injected into fine cracks to bond between damaged joints. It can restore the structural integrity of concrete due to the high strength of the concrete joint. The crack injector consists of two parts: resin and hardener and aggregates. The properties of the crack injector are given in Table 4.4.

4.8.2 Epoxy aggregate

Epoxy aggregates (MBrace) are 100% solid epoxy resin material. This epoxy aggregates mix consists of resin, hardener, and aggregate. The composition contains free silica (quartz), which is available in natural mineral deposits of rock or sand and gravel. It has been used to fill and seal cavities on the damaged BCJ.

4.8.3 Epoxy 2200

Epoxy 2200 (M Brace) is the adhesive used to bond concrete with bisphenol-A epoxy (epi-chlorohydrin) resin. It is highly viscous. Epoxy resin can repair in the presence of moisture up to a temperature of 2°C when applied to sound concrete. The Primer gives the M Brace composite strengthening system high tensile bond strength. For obtaining effective results, the workplace must be well-ventilated. The primer should not be used if the ambient temperature is below 5°C. Only the amount of primer used within its useful life should be mixed. The mixed primer should be pasted with a roller brush. If necessary, a second layer can be applied if the surface is very permeable.

Table 4.4 Physical properties of Epoxies

Properties of Epoxy	Crack injector 1315	Epoxy 2200
Viscosity	Low	High
Compressive strength 1 day 7 days	 65 MPa 70 MPa	 40 MPa 65 MPa
Flexural strength (7days)	55 MPa	20 MPa
Tensile strength	18 MPa	10 MPa
Bond strength	>2.5 MPa (conc. failure)	>2.0 MPa (conc. failure)
Pot life	50 min. (at 25°C) 30 min. (at 40°C)	50 min. (25°C) 30 min. (40°C)

4.8.4 Engineering Cementitious composite (ECC)

The ECC composite mix has been prepared by mixing various ingredients, as shown in Table 4.5. The mix is used to replace the damaged concrete in BCJ after testing samples SPC1 and SPC2. The procedure for repairing BCH samples has been elaborated in the subsequent section.

Table 4.5: ECC Mix Proportion and Properties of material

ECC Mix Ratio	
Cement: Sand: Fly Ash: Silica Fumes	1: 0.5: 0.2: 0.1
Water Cement Ratio	0.45
Plasticizer (SP-1) (percentage of cement content by weight)	0.75%
Polypropylene Fibres	2.5%
Properties of Fly ash	
Colour	Whitish Grey
Bulk Density	1490 kg/m^3
Specific gravity	2.3

Properties of Silica Fume	
Colour	Dark Grey
Specific gravity	2.25
Mean grain size (μm)	0.15
Bulk Density	2.25 mg/m^3
Properties of Poly Propylene fibres and Admixture SP-1	
Colour	Dark brown liquid
Specific gravity	1.160 at 25°C
Chloride content	chloride-free
Freezing point	0°c

4.9 RETROFITTING PROCEDURE

The control BCJ has been tested until failure under cyclic load. Massive damage occurred at the beam-column joint junction due to wide-open cracks and spalling of concrete. To restore its lost strength, the damaged BCJ has been repaired with ECC. A strengthening scheme used by various researchers such as Etman et al. 2019)[115] and Singh et al. (2020)[116], has been followed to repair the BCJ samples. No fibre-reinforced polymer sheets have been used to strengthen the beam-column joint. The performance of only ECC has been investigated in this research. The concrete cover, along with any loose concrete mass near the BCJ junction, has been removed completely with the chipping hammer as shown in Figure 4.7. The exposed surface of the steel reinforcement has been cleaned thoroughly using a steel wire brush. The surface of removed concrete near the edges has been kept curved to avoid any stress concentration, as shown in Figure 4.7 for samples SPCR1 and SPCR2, respectively.

The reinforcing bars were straightened with a light hammer. An air blower was used to remove loose dust particles. Epoxy aggregate (M Brace) has been used to seal the wide-open cracks and level the irregular surfaces before epoxy injection. The micro-cracks have been filled with Crack Injector 1315 (M Brace). Epoxy 2200 has been applied thoroughly on the

concrete surface to have a better bond. The BCJ sample was placed inside the steel mould shuttering. ECC mix, prepared as per mix proportions shown in Table 4.5, has been filled into the space.

A light vibrator has been applied to fill the gaps uniformly and allow the air to escape. Spatula has been used to level the top surface and remove the extra material to maintain the shape and size of the retrofitted sample with control BCJ sample SPC1. Proper shuttering has also been used to maintain the shape and size of the sample. The ECC strengthening of BCJ has been illustrated in Figure 4.6. After 24 hours of casting, the samples were removed from the mould and cured for 28 days by covering the specimen with several layers of sponge and spraying the sponges daily with water. These retrofitted BCJ samples are now ready for testing in the laboratory as per a procedure similar to control samples.

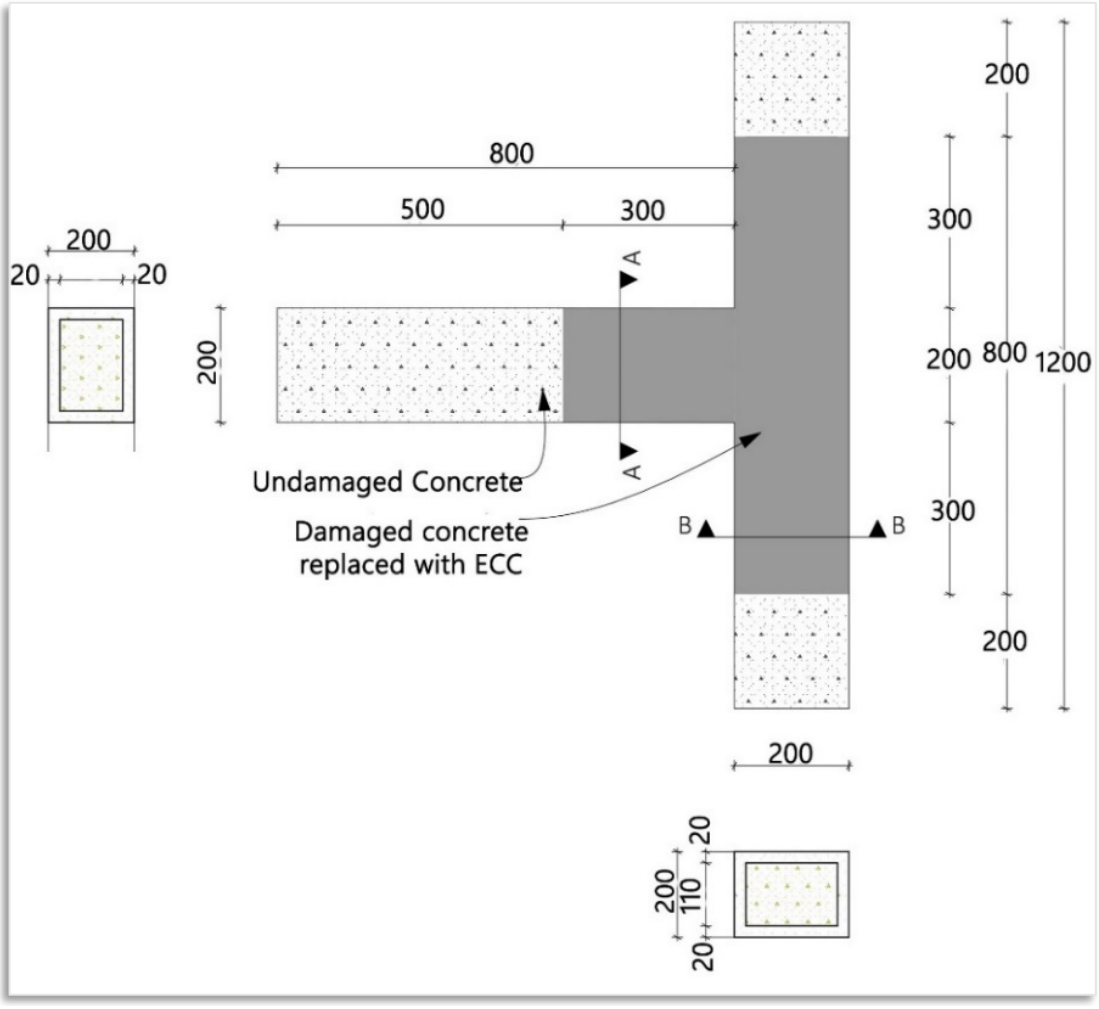

Figure 4.6: Schematic diagram for retrofitting BCJ with ECC

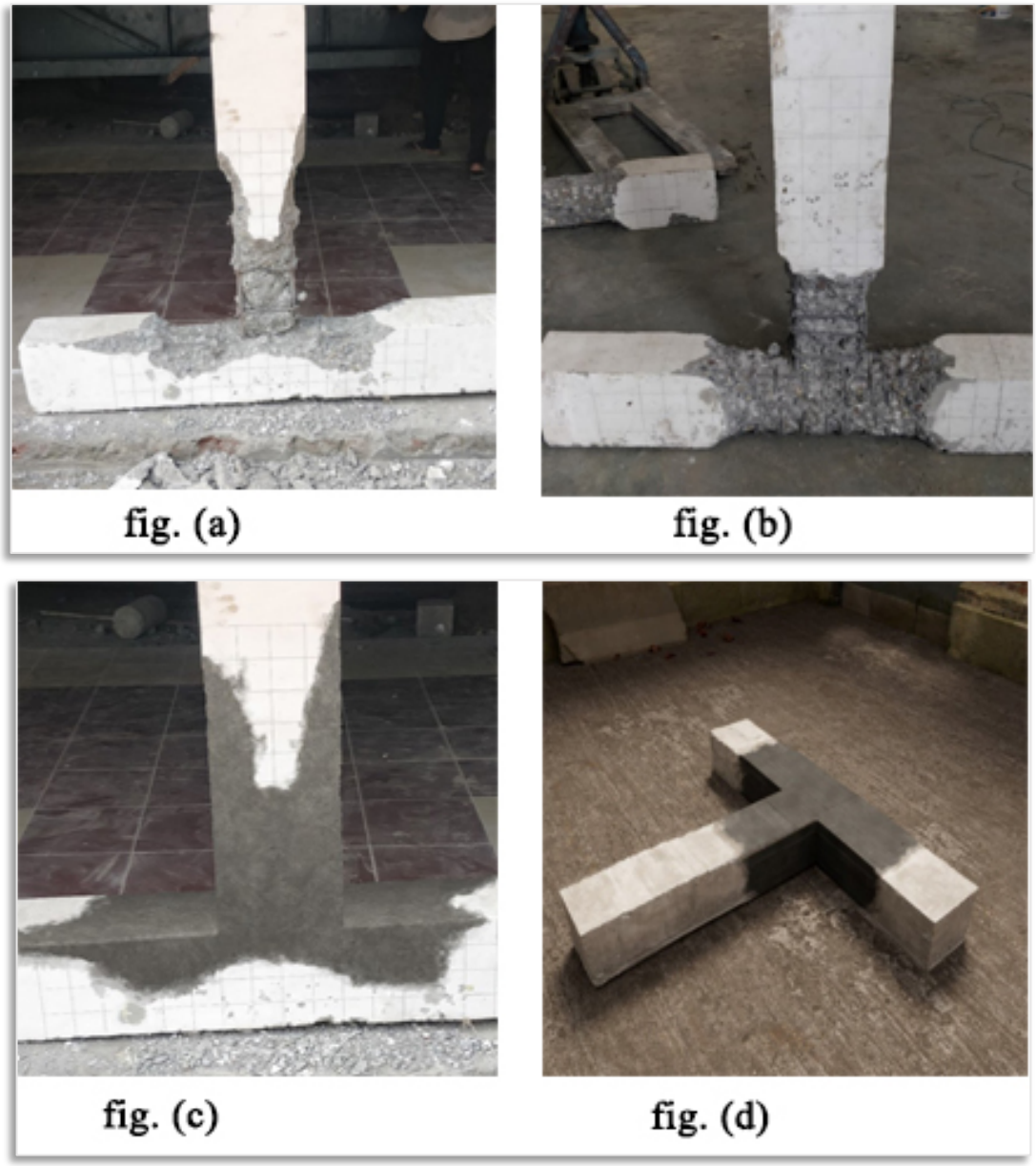

Figure 4.7: Repairing of BCJ

4.10 CLOSING REMARKS

This chapter highlights the experimental program and methodology used to test Beam-Column Joint samples reinforced with and without ductile detailing. The properties of various materials used in casting the control BCJ samples, i.e., cement, concrete, fine aggregates, coarse aggregates, and reinforcing bars, have been discussed in detail. A concrete mix comprising of M35 grade has been designed having a mix ratio of 1:1.2:2.32 with a water-cement ratio of 0.36. Details of the BCJ sample and its casting procedure have also been discussed. The 7 days, 14 days and 28 days compressive strength of the cubes has been worked out to be 19.1, 26 and 37 N/mm^2, respectively.

The methodology consists of testing the BCJ under monotonic and cyclic loads for control and repaired BCJ samples. Testing under monotonic loads is required to evaluate the ultimate load, and deformation capacities of BCJ reinforced with and without ductile detailing. The cyclic load test has been performed to know the seismic behaviour of BCJ. The energy dissipation for all the load cycles has been worked out from the load-deformation curves by calculating the area enclosed inside the hysteresis loop. The BCJ samples have also been instrumented with AE sensors to record acoustic emission parameters. The damaged samples have been repaired using ECC, and the repaired samples have again been tested under cyclic load to know the performance of ECC material.

CHAPTER-5. PERFORMANCE OF BEAM-COLUMN JOINTS

5.1 GENERAL

The reverse cyclic load imposed by seismic forces leads to large inelastic deformations in the beam-column joints of RC-framed structures. The performance of BCJ can be significantly affected in case the BCJ are not designed and detailed adequately. The limited space available in the BCJ region requires more attention from the design engineers. In the design of framed structures, it is assumed that BCJ is strong enough to sustain seismic forces and transfer these forces from one structural element to another. The assumption regarding the rigidity of BCJ fails to consider the effect of high shear forces developed within the BCJ.[117] The behaviour of BCJ has already been discussed in detail in chapter-2.

The present study has been undertaken to compare the behaviour of exterior BCJ under cyclic loading reinforced without ductile detailing, designed as per IS 456, 2000, and BCJ reinforced with ductile detailing, reinforced as per IS 13920. The damaged BCJ samples have been repaired using ECC and tested again to compare the change in the behaviour of the control BCJ. To monitor the damage in BCJ samples, the following experiments and data analysis have been performed:

- Tests of control BCJ samples (detailed with and without ductile reinforcements) have been performed under monotonic load. The acoustic emission and load-deflection data has been analysed to get the ultimate displacement capacity of BCJ. The corresponding values of ultimate dissipation energy and ultimate acoustic energy values have also been obtained from the results of this testing.
- Tests of the control BCJ sample subjected to cyclic load have been performed, and acoustic emission and load-deformation data has been collected to assess damage in BCJ and find out the damage index of the control BCJ sample.

- The damaged BCJ samples tested under cyclic loads have been retrofitted using ECC material.
- Tests of retrofitted samples have been performed under cyclic loads to assess the damage and determine the damage index of the retrofitted BCJ sample.
- Test result data has been analysed, and comparative analysis has been performed between controlled and retrofitted BCJ samples.

5.2 BEHAVIOUR OF CONTROL BCJ UNDER MONOTONIC LOADS

The sample SPM1 represents BCJ reinforced according to IS-456 without ductile detailing, whereas the sample SPM2 is detailed with ductile reinforcement designed as per IS-13920. Both of these samples have been tested under monotonic loading. The purpose of these tests is to find the ultimate load and displacement capacity of these two samples. The AE data, load data and displacement data have been obtained.

5.2.1 Visual observations

The majority of the cracks at the BCJ junction are flexural, as shown in Figure 5.1. Since the load is applied in one direction, the cracks' width is less compared to the test performed under cyclic loads. The crushing and spalling of concrete have also not been observed.

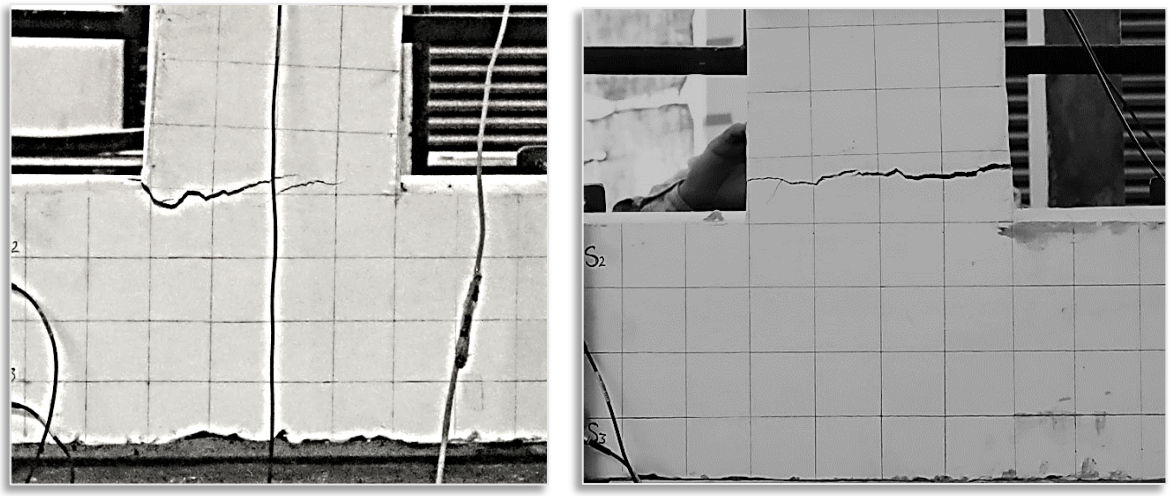

(a) Sample SPM1 **(b) Sample SPM2**

Figure 5.1: Crack formation in BCJ under monotonic load

5.2.2 Load deflection behaviour

The primary purpose of this test is to get the yield and ultimate capacities of BCJ. Load Vs deflection plots for the test, conducted under monotonic load, have been presented in Figures 5.3 and 5.4 for SPM1 and SPM2, respectively. The ultimate displacement (δ_u) has been estimated from a bi-linear curve assuming equivalent elastic-perfectly plastic response[118]. The following two conditions should be satisfied for calculating (δu) using a bi-linear curve:

- The sum of the area under this curve should be zero, i.e., $\sum \boldsymbol{A_i} = \mathbf{0}$. Areas A_1 and A_3 are positive as they fall inside the load-deflection envelope and areas A_2 and A_4 are taken as negative being lying outside the envelope and
- The absolute sum of the areas enclosed between these curves should be minimum, i.e., $\sum |\boldsymbol{A_i}| = \boldsymbol{minimum}$. (See Figure 5.2).

Based upon the above criteria, the load-deflection plot has been divided into sectors by drawing straight lines OP1, P1P2 and P2P3. P3 is a point on the load-deflection curve corresponding to a load value of $0.8P_{max}$. Where, P_{max} is the maximum load experienced by the sample under the monotonic load. P1 and P2 points are chosen such that the areas A_1, A_2, A_3 and A_4 satisfy the above-mentioned two criteria. The abscissa of point P1 represents yield deflection, and the abscissa of point P2 represents ultimate deflection. The ordinate of P1 or P2 represents the ultimate load of the sample. Applying this procedure in Figure 5.3, the yield displacement (δ_y), ultimate displacement (δ_u), and ultimate load (P_u) values for SPM1 have been obtained as 2.1 mm, 11.5 mm and 19.5 kN, respectively. Similarly, δ_y, δ_u and P_u values for SPM2 are 3 mm, 35.3 mm, and 25 kN, respectively as shown in Figure 5.4.

5.2.3 AE monitoring of BCJ under monotonic loading

Various AE parameters such as AE hits, Rise time, average frequency, energy, signal strength etc., were recorded during the test. Only the AE energy parameter has been discussed here for calculating the ultimate energy capacity of the beam-column joints. For this purpose,

the cumulative AE energy Vs deflection graph has been plotted for SPM1 and SPM2 as presented in Figures 5.5 and 5.6. The ultimate cumulative energy (E_u) value of 3.138×10^6 and 1.233×10^7 mVolts.sec for SPM1 and SPM2, respectively, have been obtained from these graphs corresponding to the ultimate deflection value. Further, these values have been used to evaluate the damage index.

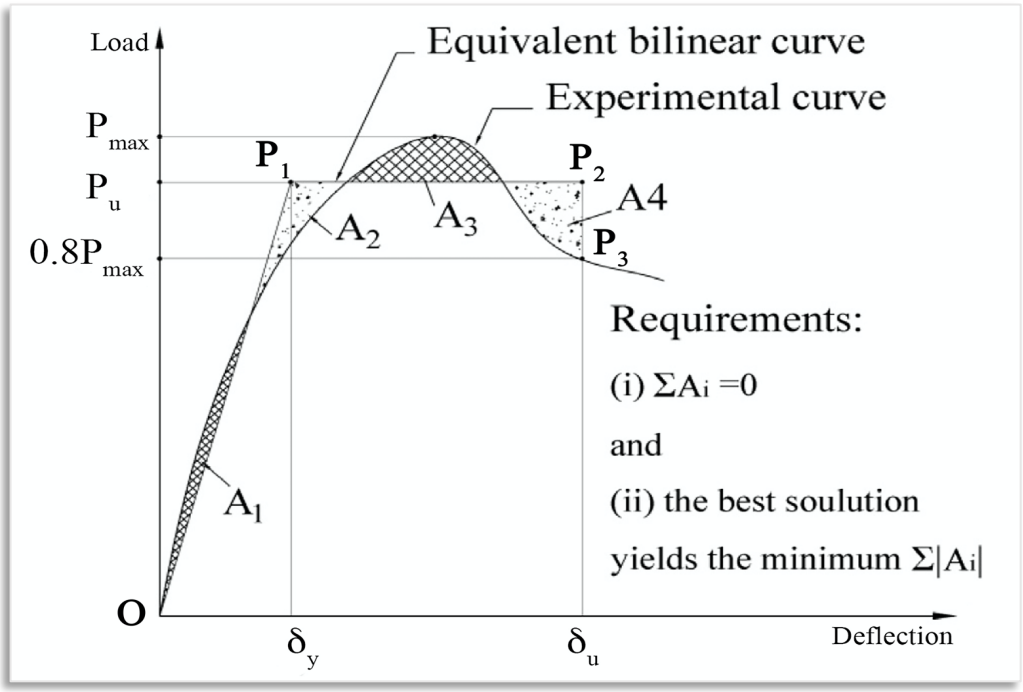

Figure 5.2: Bilinear curve for evaluation of ultimate displacement

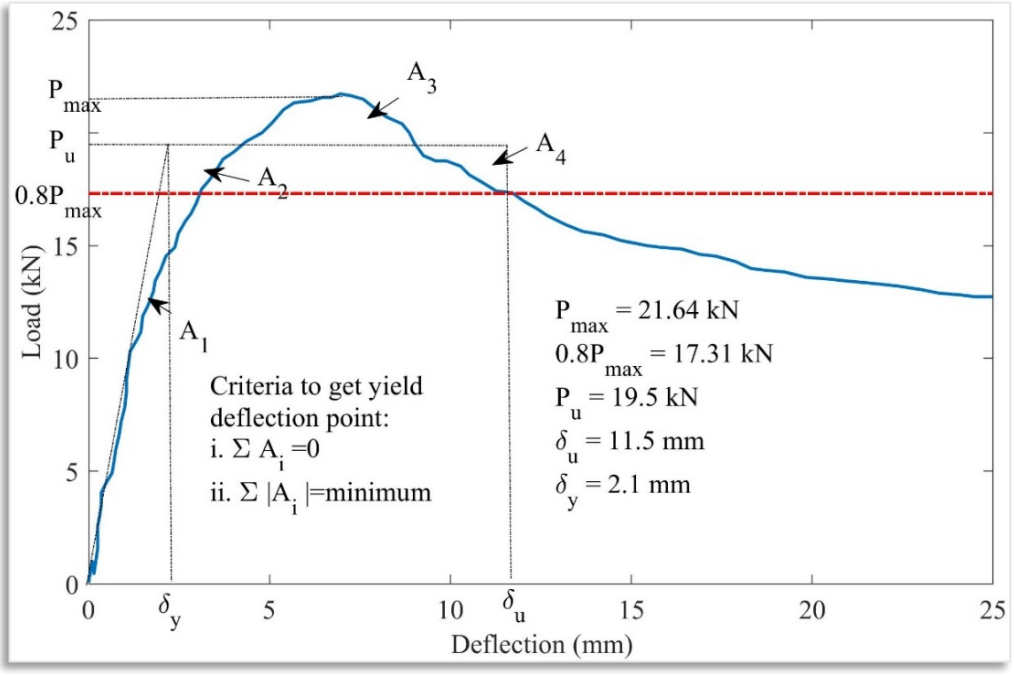

Figure 5.3: Load deflection of sample SPM1 under monotonic load

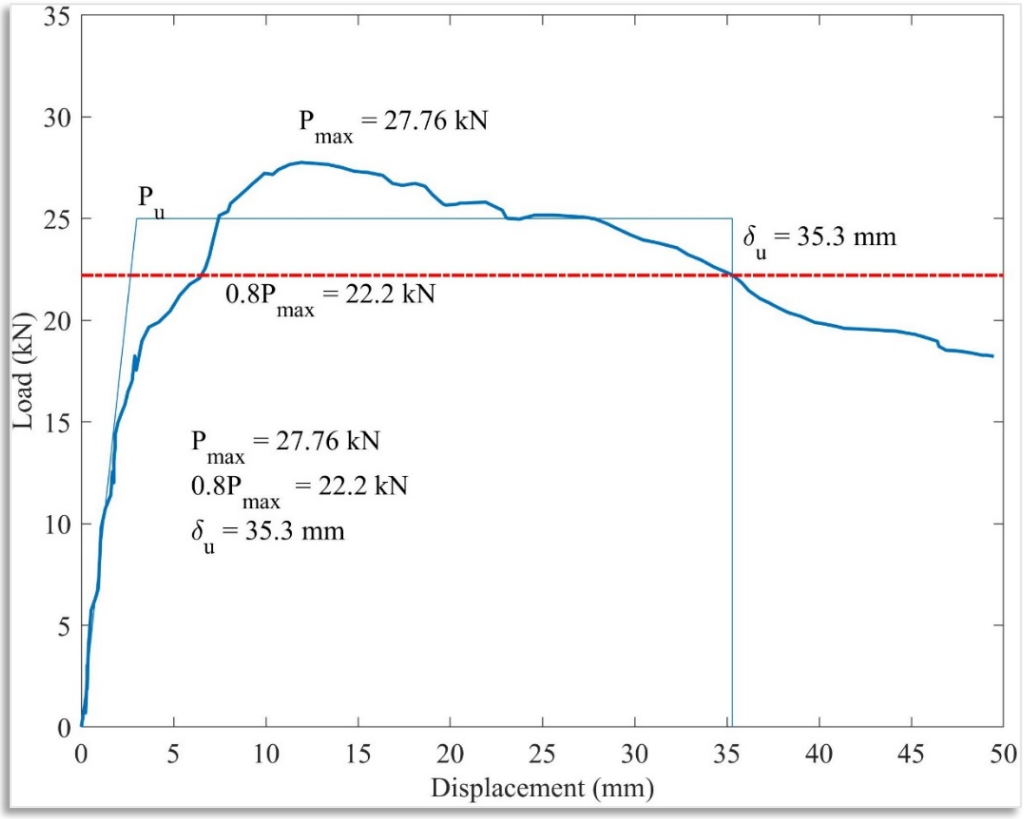

Figure 5.4: Load deflection of sample SPM2 under monotonic load

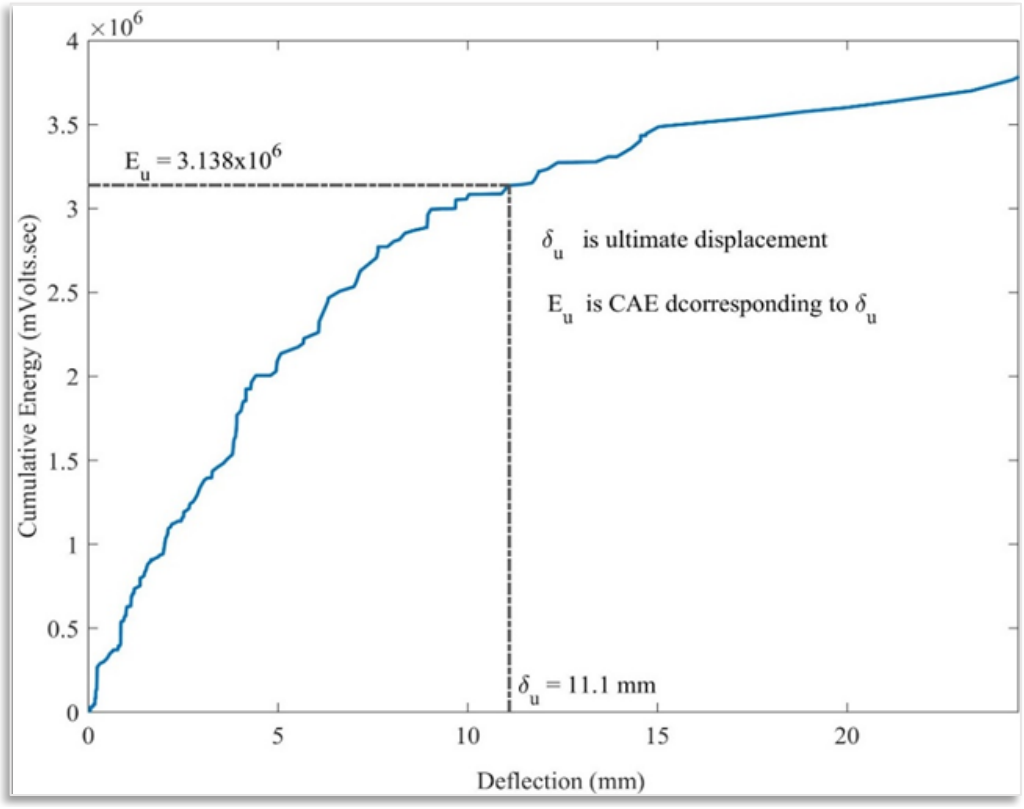

Figure 5.5: AE energy Vs Deflection of SPM1

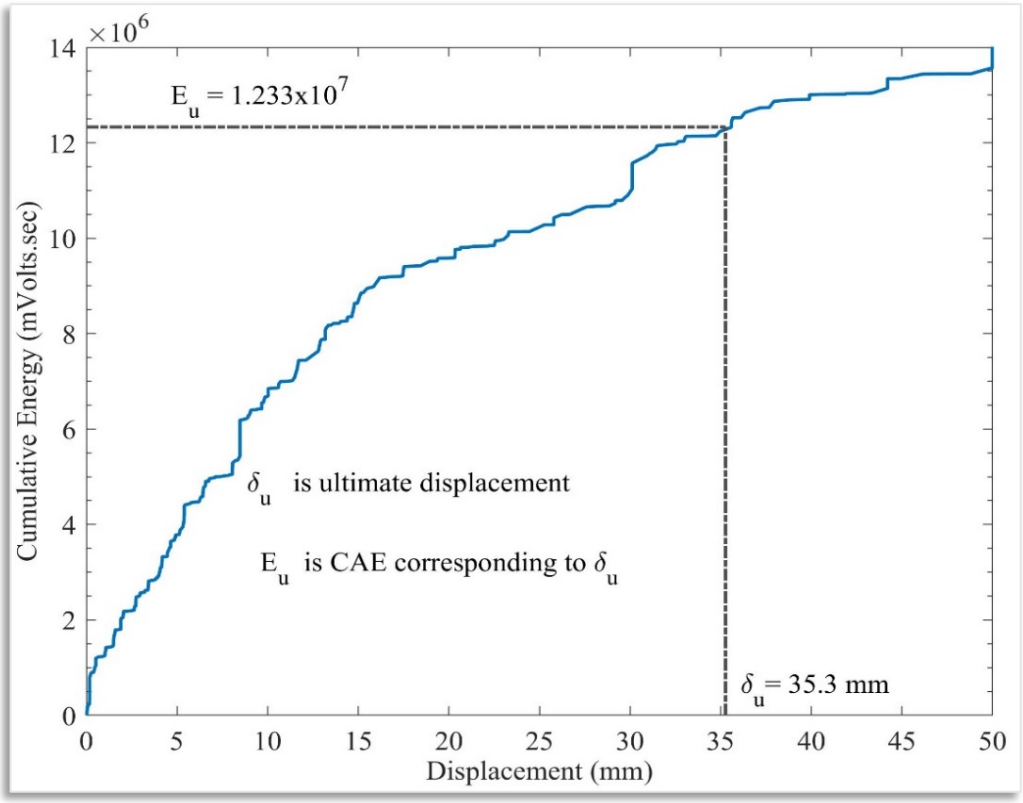

Figure 5.6: AE energy Vs Deflection of SPM2

5.3 BEHAVIOUR OF CONTROL BCJ UNDER CYCLIC LOADING:

5.3.1 Visual observations

Displacement-controlled cyclic tests have been performed on the BCJ samples. Flexural cracks at the beam-column junction and shear cracks in the beam have been observed in SPC1 and SPC2 for all the cycles. The formation of wide-open cracks near the BCJ junction has been observed due to the flexural failure, crushing and cracking of concrete (Figure 5.7 and 5.8). The spalling of concrete is visible near the damage stage during the fifth and sixth cycles.

5.3.2 Load deflection behaviour

Load Vs deflection response has been presented in Figures 5.9 and 5.10 for BCJ SPC1 and SPC2, respectively. The yield and ultimate values of displacement parameters obtained from the monotonic load test have been used to analyse test results from the cyclic load. The maximum displacement of 25 mm in the forward cycle and about 22 mm in the reverse cycle has been observed in SPC1. In contrast, a maximum displacement of 50 mm in the forward

cycle and 43 mm in the reverse direction has been observed in SPC2. This reflects that SPC2 is more ductile than SPC1. The maximum load of 21.64 kN in the forward direction and 18.1 kN in the reverse direction has been observed for BCJ sample SPC1. Maximum values of displacement and load are higher in the forward cycle than in the reverse cycle because there is a difference in longitudinal reinforcement on the top and bottom face of the BCJ beam resulting in a higher moment of resistance of the beam in the forward than reverse load direction. Thus, an increase in the percentage of longitudinal tensile steel improves ductility and increases ultimate load-carrying capacities. Based on ultimate displacement values and the yield loads of SPC1, the first two cycles belong to the elastic zone. The third cycle passes from the elastic to the plastic zone, i.e., this cycle falls in the elastoplastic zone. All the cycles beyond 3rd load cycle belong to the plastic zone.

Similarly, in SPC2, Cycle-1 is in the elastic zone, Cycle-2 is in the elastic-plastic zone, and cycles-3, 4 and 5 fall in the plastic zone. The observed peak load value in SPC2 is 25.2 kN, about 3.7 kN higher than the SPC1. Thus, ductile reinforcement increases the peak load-carrying capacity of BCJ.

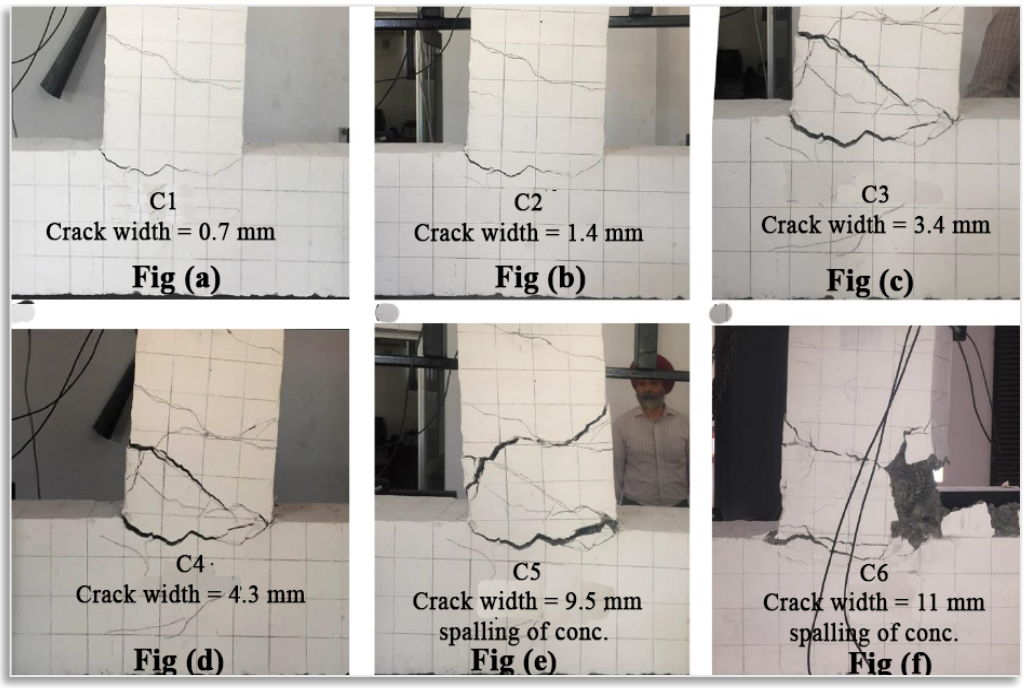

Figure 5.7: Formation of cracks in BCJ sample SPC1

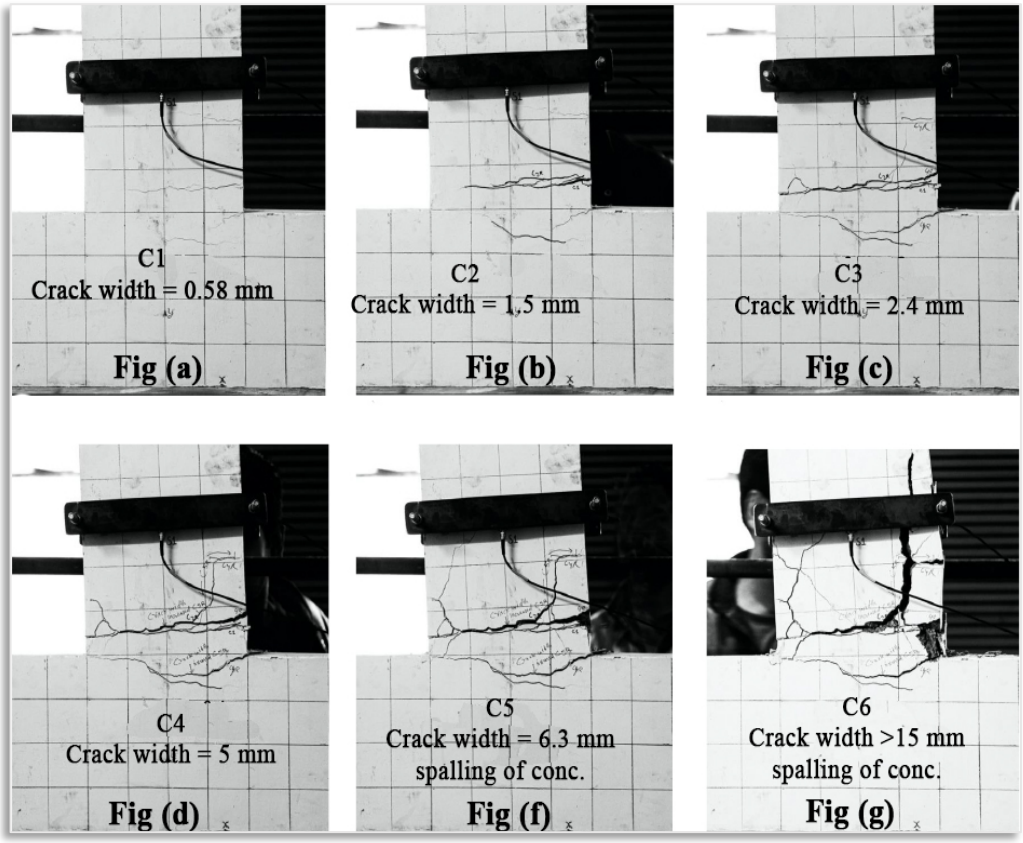

Figure 5.8: Formation of cracks in BCJ sample SPC2

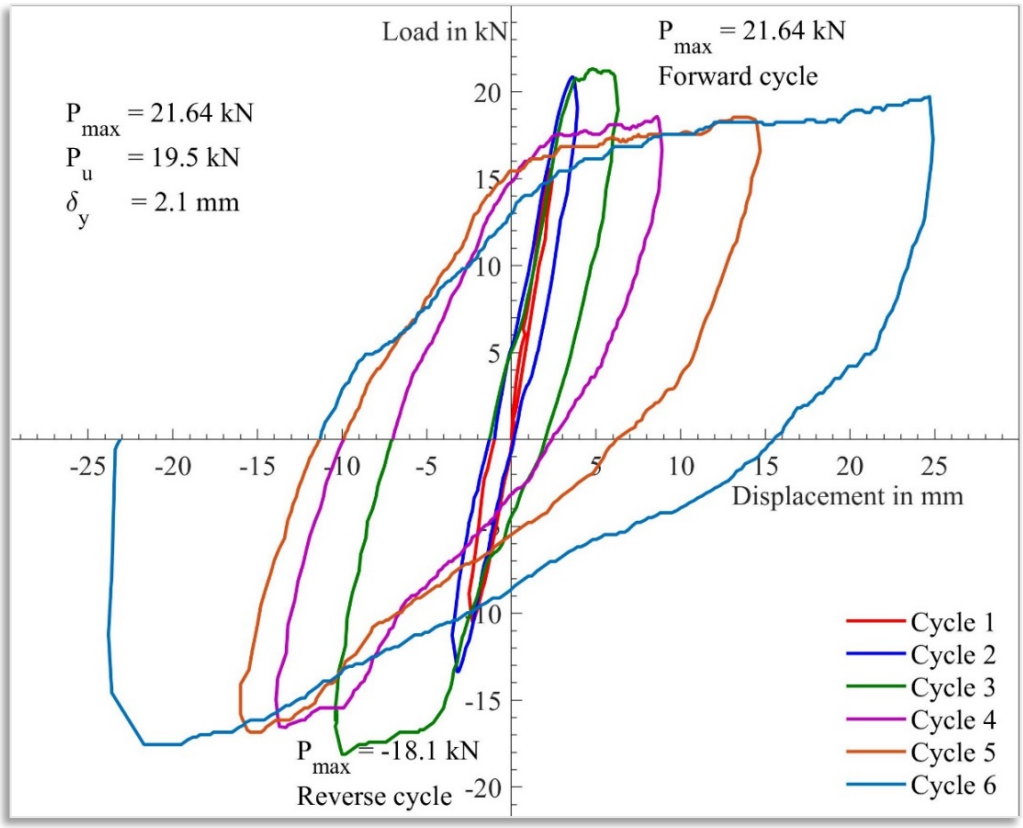

Figure 5.9: Load deflection plot of sample SPC1

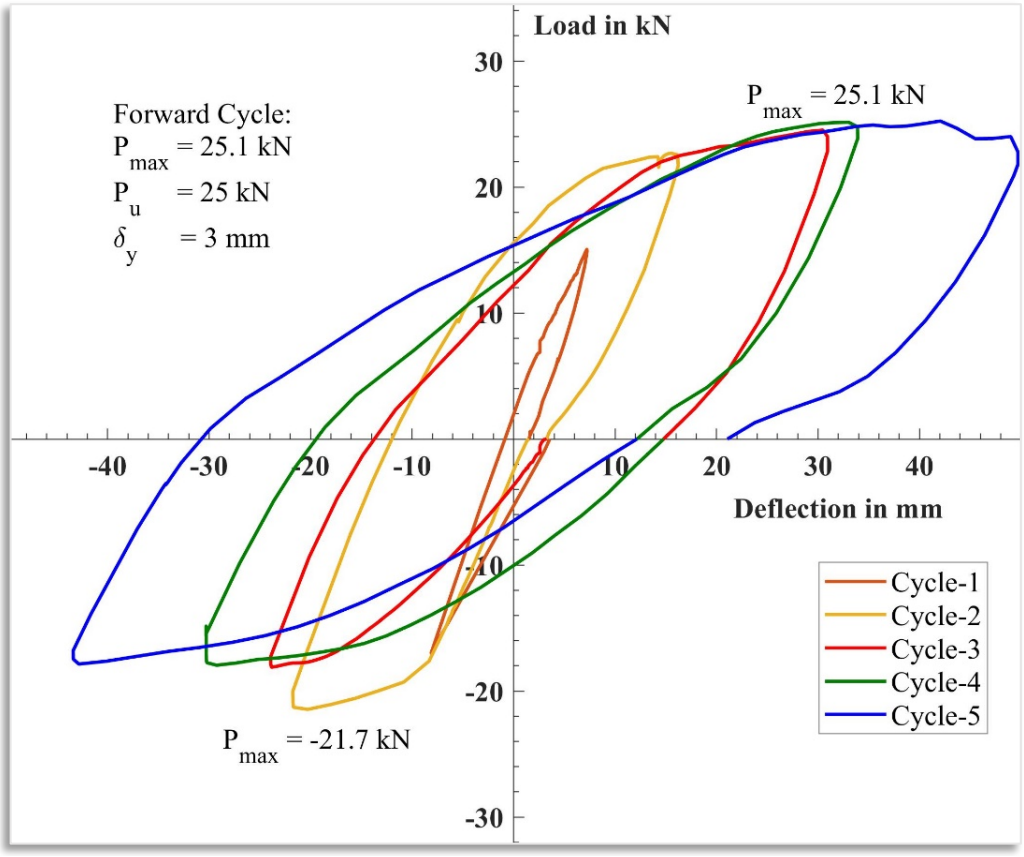

Figure 5.10: Load deflection plot of sample SPC2

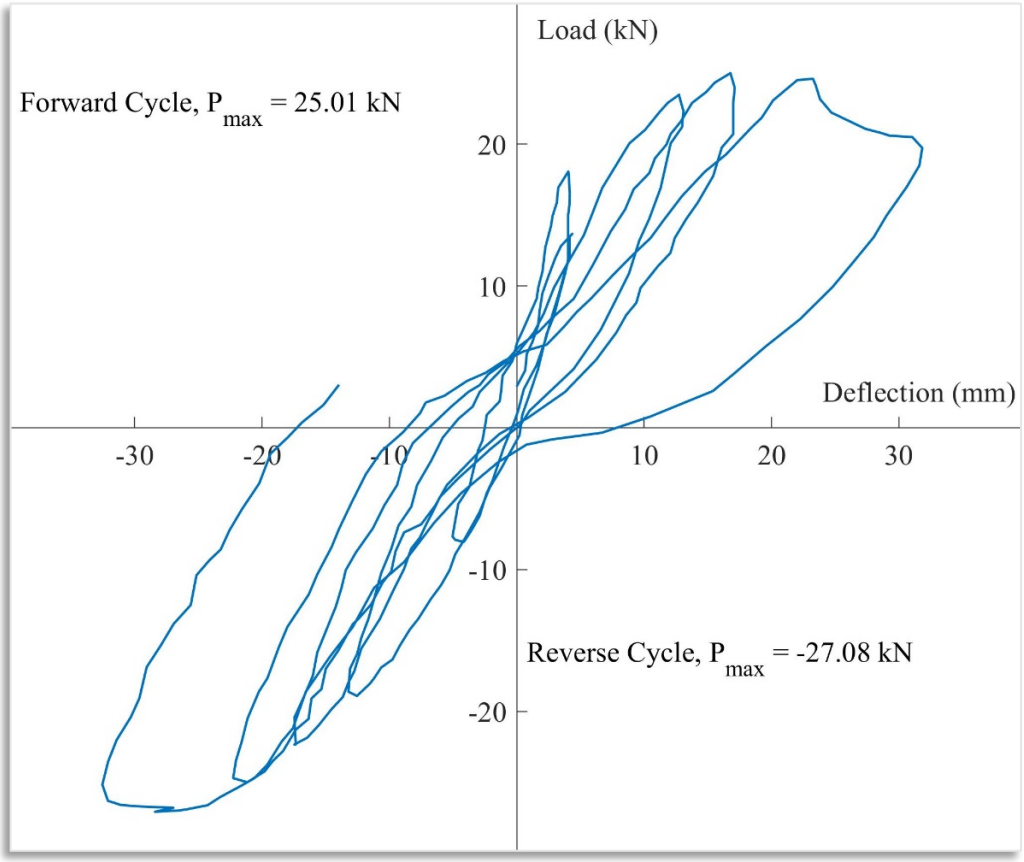

Figure 5.11: Load Deflection SPC3

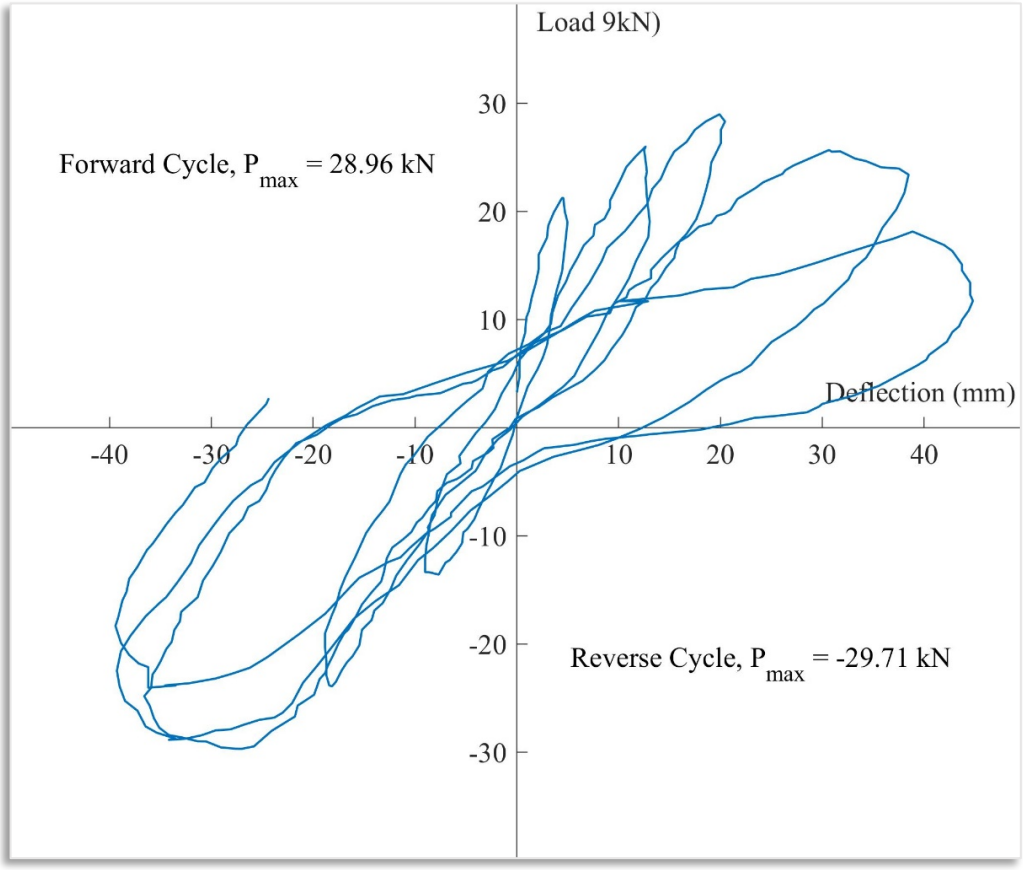

Figure 5.12: Load Deflection for SPC4

BCJ samples SPC3 and SPC4 have also been tested under cyclic load. The load, deflection and AE data have been recorded. The load Vs deflection response has been presented in Figures 5.11 and 5.12. In BCJ sample SPC3 the maximum displacement has been recorded as 32 mm, whereas in SPC4, the value recorded is 45 mm in the forward direction. These values recorded in the reverse direction are 33 mm and 40 mm, respectively, for SPC3 and SPC4. The maximum load values in the forward direction for SPC3 and SPC4 are 24 kN and 28 kN. These values in the reverse direction are 27 kN and 30 kN, respectively. From graphs of SPC1 and SPC3, it is observed that the behaviour of these non-ductile BCJ samples is identical. In SPC3, Cycle-1 and 2 belong to the elastic zone, Cycle-3 to the elastoplastic zone and Cycle-4 and 5 to the plastic zone. In SPC4, Cycle-1 is in the elastic zone, Cycles-2 and 3 are in the elastoplastic zone, and Cycles 4 and 5 are in the plastic zone.

5.3.3 Derived parameters from load-deflection

5.3.3.1 Energy Dissipated

The cyclic behaviour of structural members can be expressed with three parameters: strength, deformability and energy dissipation capacity per cycle. The RC members show complex cyclic behaviour with stiffness degradation. Hence strength and deformability are better parameters to assess the cyclic behaviour of RC members. The RC members dissipate energy by experiencing inelastic behaviour under cyclic loading. The energy dissipated for a particular load cycle has been obtained from the area enclosed by the load-deflection curve inside a hysteresis loop. Since RC members are composed of concrete and reinforcing steel, their energy dissipated can be defined by the sum of the energy dissipated by concrete and reinforcing steel. Because of the brittle nature of concrete, its contribution to the energy dissipated is considerably less than reinforcing steel. Due to this, the energy dissipated after the initial cracking of concrete is approximately equivalent to the energy dissipated by flexural reinforcing bars alone. However, it should be noted that concrete dissipates considerable energy for the member subjected to excessively high axial compressive load because a large volume of concrete contributes to resisting the axial load. A MATLAB programme has been used to evaluate the area inside the hysteresis loop corresponding to each load cycle. The values obtained have been presented graphically in Figure 5.13 for SPC1 and SPC2.

The average energy dissipated by SPC2 is about 4.5 times higher than SPC1. Thus, BCJ designed and detailed with ductile reinforcements is 4-5 times more ductile than samples not considered for ductile detailing. Thus, ductile reinforcement detailing improves the structural performance under cyclic loads. Similarly, energy dissipated has been worked out for SPC3 and SPC4 as shown in Figure 5.14. The energy dissipated in ductile sample SPC4 is about 3 to 4 times more than the non-ductile sample SPC3.

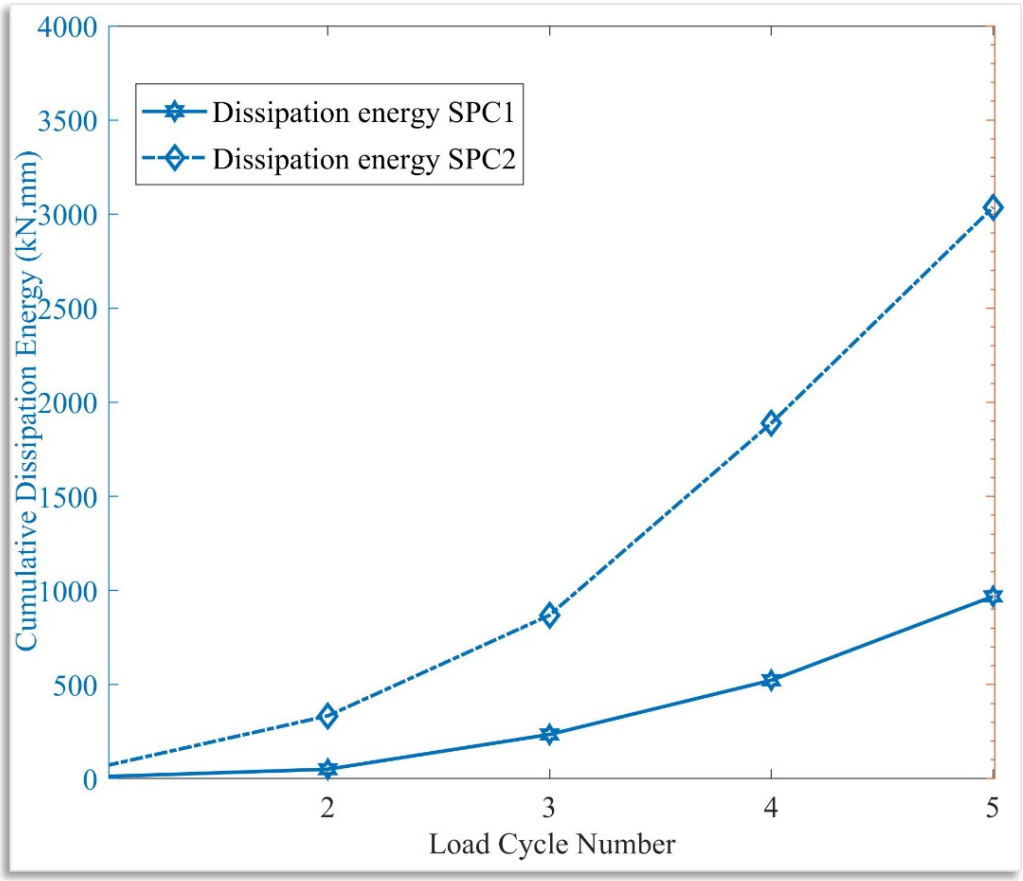

Figure 5.13: Cyclic variation of Energy dissipated of SPC1 and SPC2

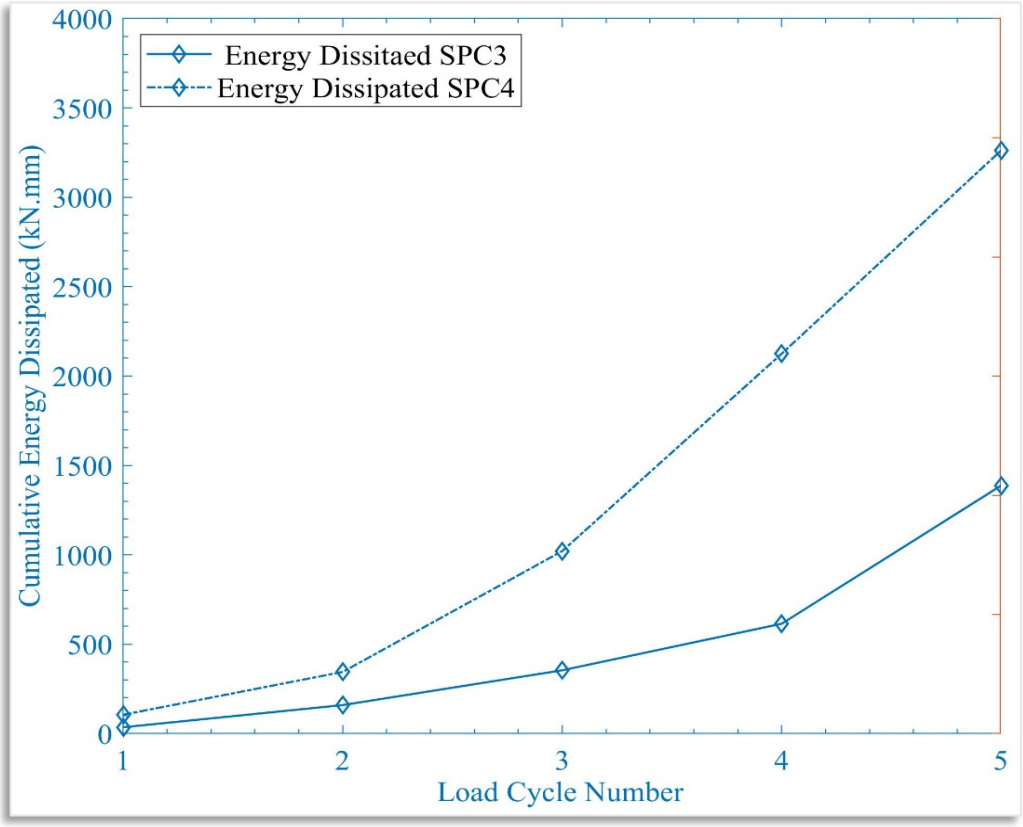

Figure 5.14: Cyclic variation of Energy dissipated of SPC3 and SPC4

5.3.3.2 Stiffness factor (SF)

Stiffness has been worked out from the load-deflection plot, presented in Figures 5.15 and 5.16 for BCJ samples SPC1 and SPC2, respectively. This can be obtained by drawing a tangent on the curve at a point corresponding to a load value of $0.8P_{max}$, where $P_{max}$is the maximum load of a particular cycle. The slope of the tangent represents the Stiffness Factor (SF) of that cycle[119]. The results of SF have been presented in Figures 5.15 and 5.16 for samples SPC1 and SPC2, respectively.

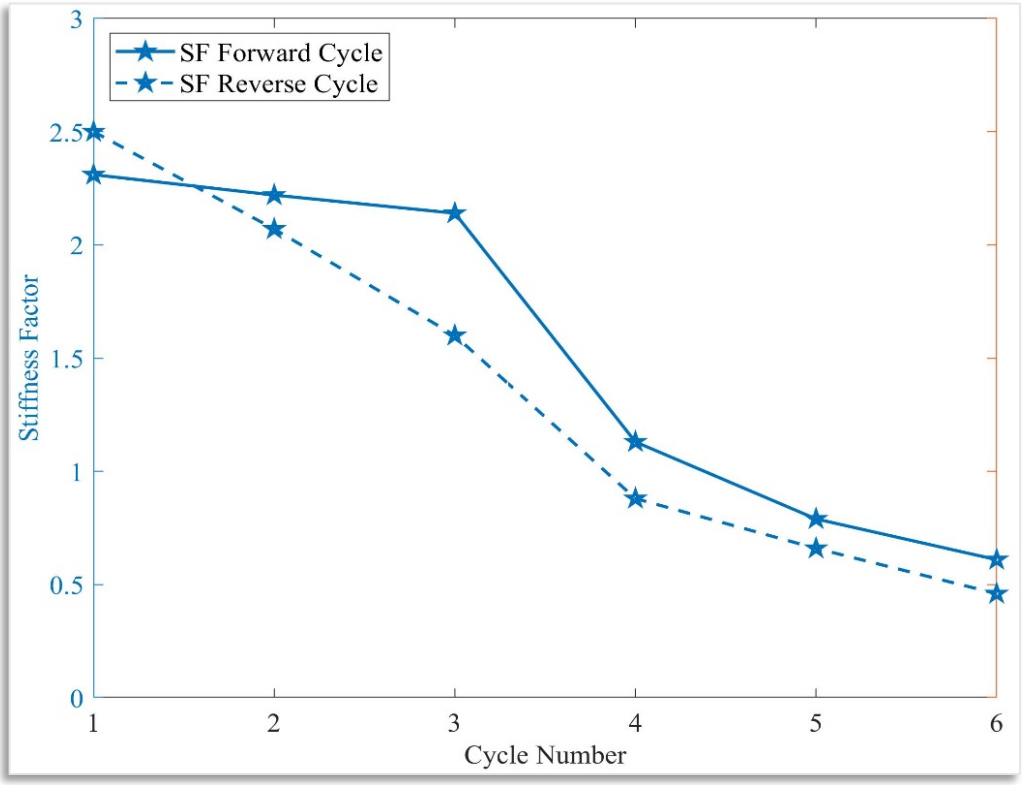

Figure 5.15: Stiffness factors SPC1

From these figures, it is observed that the sample SPC1 is slightly stiffer in the forward direction than in the reverse direction within the elastic limit up to the third cycle. The rate of stiffness degradation in non-ductile BCJ sample SPC1 is lesser initially up to the third cycle and increases after that. However, in sample SPC2, the rate of stiffness degradation is higher up to the third cycle and reduces after reaching failure. There is apparent stiffness degrading after the third load cycle in SPC1. In sample SPC2, there is sharp stiffness degradation up to the third load cycle. The rate of stiffness degradation reduces after the third load cycle because of the contribution of confining steel after the concrete failure. The confining steel in SPC2

contributes to reducing stiffness degradation at higher load cycles. Further, longitudinal steel contributes to reducing stiffness degradation.

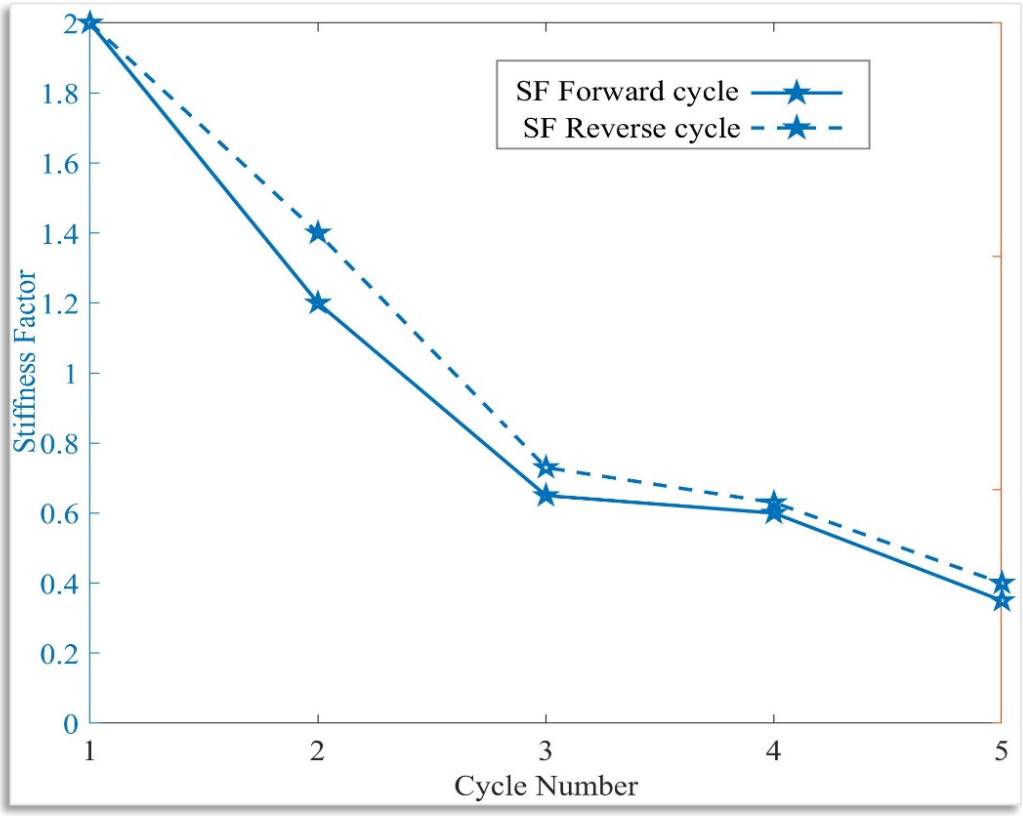

Figure 5.16: Stiffness factors SPC2

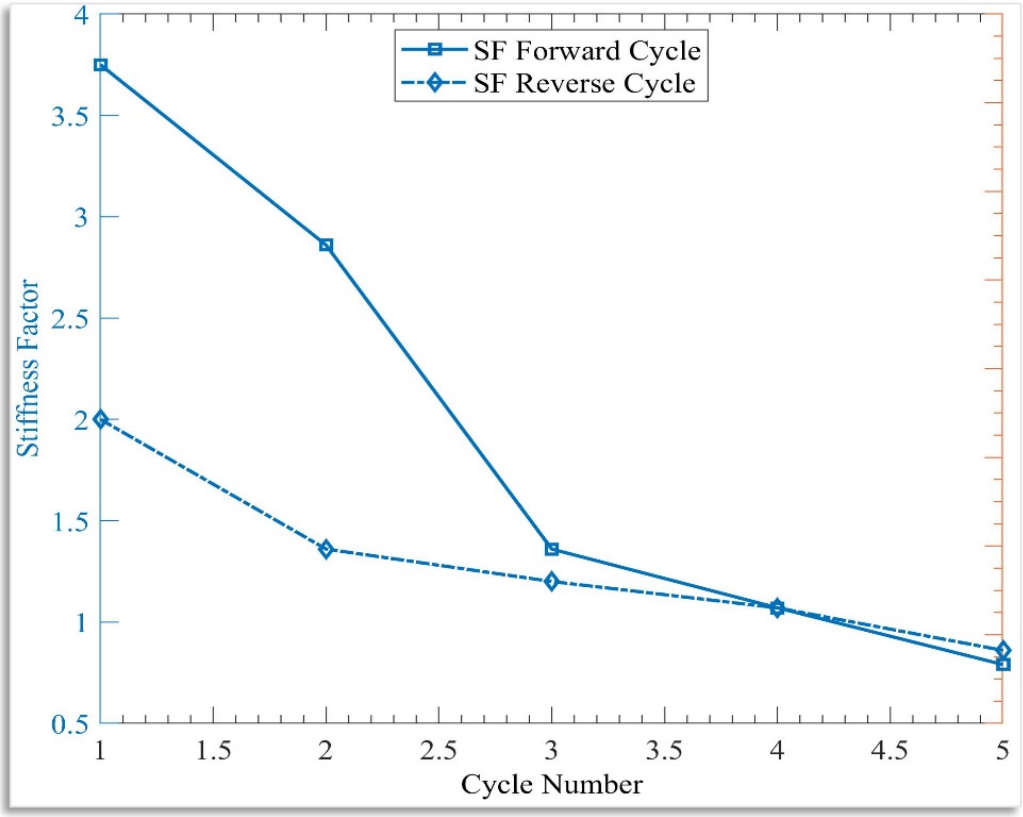

Figure 5.17: Stiffness factors SPC3

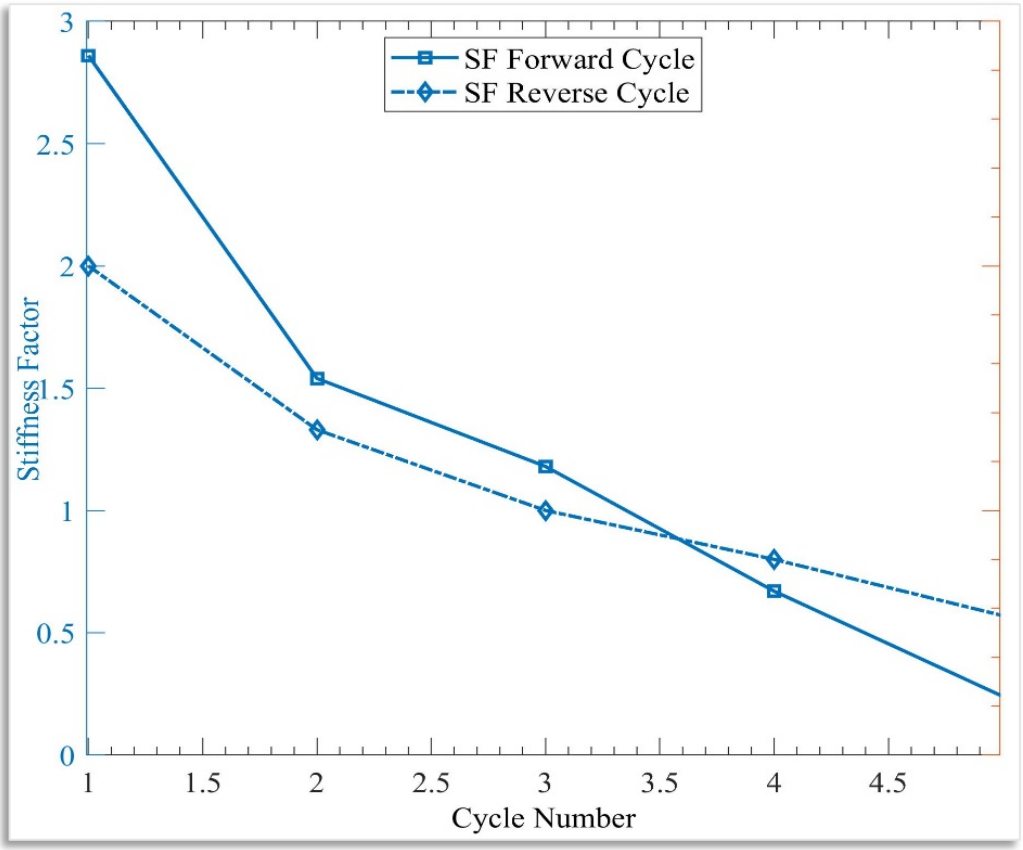

Figure 5.18: Stiffness factors SPC4

Similarly, the stiffness factors for SPC3 and SPC4 have been plotted as shown in Figures 5.17 and 5.18, respectively. The trend of stiffness degradation in SPC3 and SPC4 is similar to SPC1 and SPC2. In the non-ductile sample SPC3, there is sharp stiffness degradation up to the third load cycle, and after that, the rate of stiffness degradation reduces. In the ductile sample SPC4, there is almost constant degradation in the stiffness factor.

5.3.3.3 Ductility Factor (DF)

The ductility factor (DF) is computed as the ratio of maximum deflection to yield deflection. The values obtained for samples SPC1, SPC2, SPC3 and SPC4 have been presented graphically in Figures 5.19 to 5.22. It has been noticed that when the load is increased beyond the elastic limit, the maximum load-carrying capacity of the joint reduces and the ductility of the structure plays an essential role in sustaining the load without total collapse. Cracks continued to appear at increasing loads with a DF of 0.6. The BCJ SPC1 cracked extensively after the third cycle when DF was more than 2.4. The BCJ specimens started exhibiting lower

load-carrying capacity at DF equal to 3.5, as is apparent in subsequent load cycles. The decline of the load-carrying capacity of the BCJ could be attributed to the reduction in friction contribution of coarse aggregate.

The longitudinal reinforcement of SPC2 is the same as in SPC1. However, additional confining reinforcement is provided, as shown in Figure 4.1. As observed from the load-deformation plots (Figures 5.9 and 5.10), the ultimate load capacity of SPC2 is higher than SPC1. Sample SPC2 has a maximum load-carrying capacity of 25.1 kN and has not collapsed at a deflection of 50 mm in the forward cycle. In the reverse direction, the SPC2 can resist a force of 21.7 kN up to a deflection of 42.4 mm, whereas the SPC1 can resist 18.1 kN force at a maximum deflection of 24 mm. Thus, it can be concluded that in SPC2, there is a considerable amount of strength enhancement with improved ductility.

From the theoretical evaluation of ultimate deflection (calculated using monotonic load tests on SPM1 and SPM2), the samples SPC1 and SPC2 can resist deformations up to 11.5 mm and 35.3 mm, respectively. However, in the cyclic load tests performed on SPC1 and SPC2, the samples can withstand constant loads of about 18 kN for SPC1 and about 25 kN for SPC2 at deformation much beyond ultimate values due to the formation of plastic hinge in the beam. The ultimate displacement parameter has been used to define the failure of BCJ. Based upon this criterion, the samples SPC1 and SPC2 may be considered fully damaged during the fourth cycle. The ductility factor (DF) of BCJ increases after each cycle in both samples. The value of DF is higher in sample SPC2 than in sample SPC1. This indicates that BCJ SPC2 is more ductile and can perform better under seismic forces. The sample SPC2 also has a higher load-carrying capacity than the non-ductile sample SPC1. Thus, it is concluded that the BCJ members provided with ductile detailing exhibit better ductility after failure to protect the structure from total collapse and provide higher load-carrying capacity.

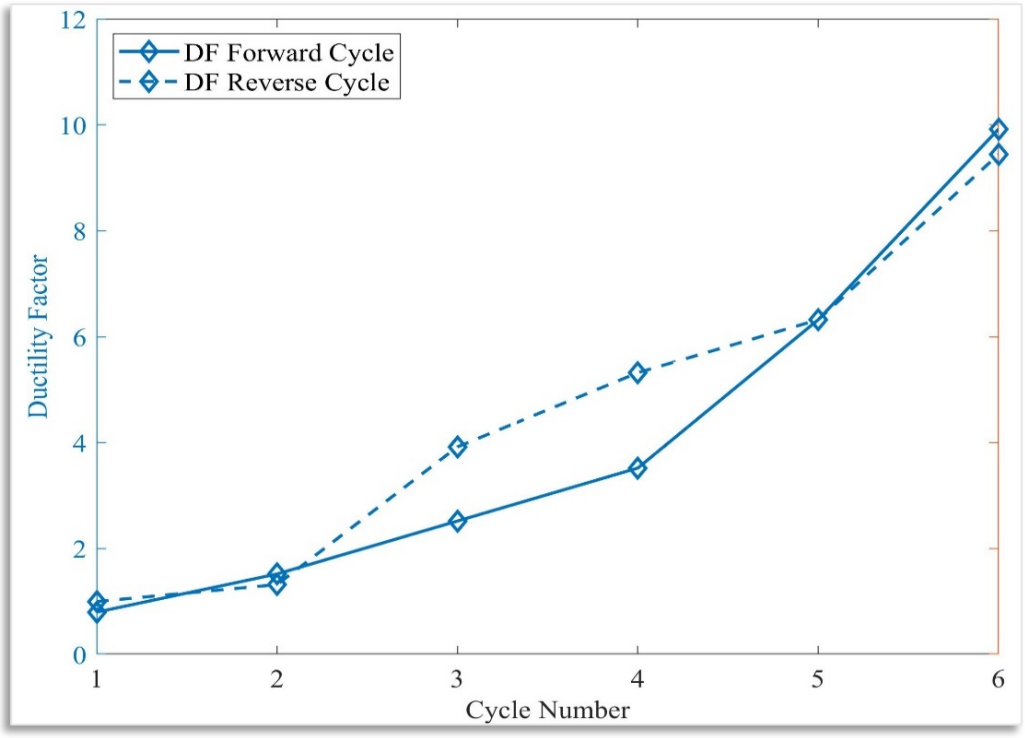

Figure 5.19: Ductility Factor SPC1

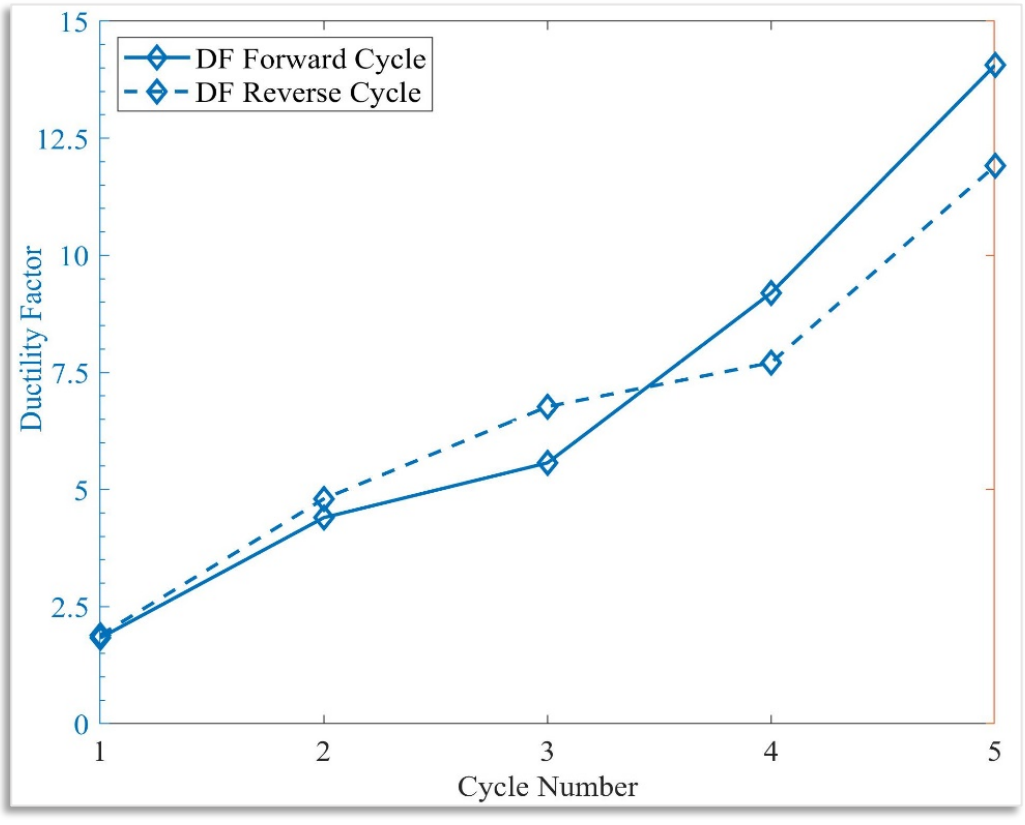

Figure 5.20: Ductility Factor SPC2

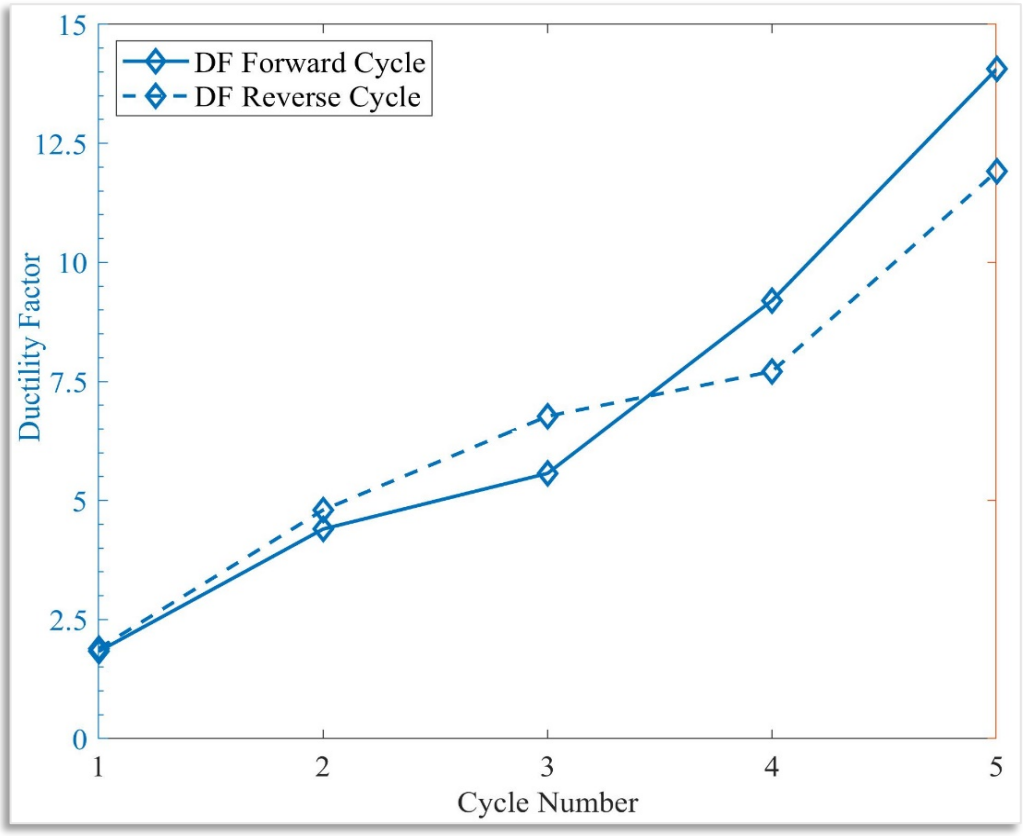

Figure 5.21: Ductility Factor SPC3

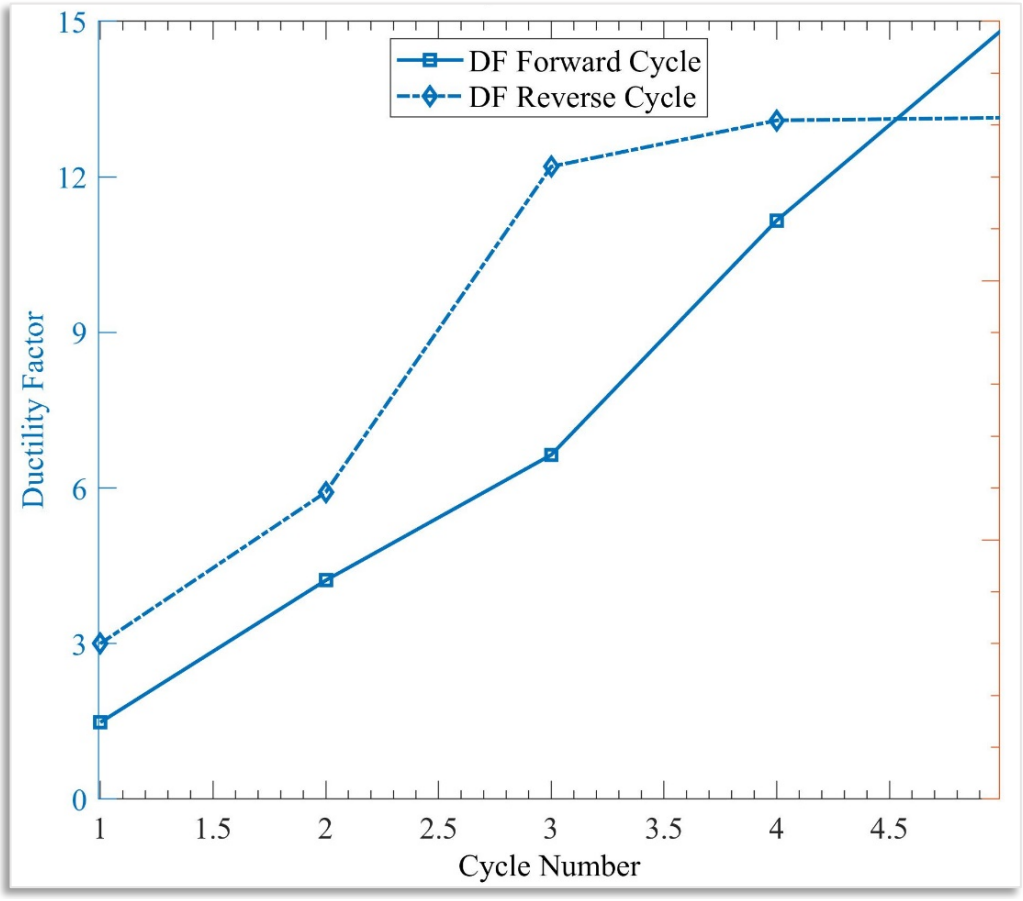

Figure 5.22: Ductility Factor SPC4

5.4 AE MONITORING OF BCJ UNDER CYCLIC LOADING

5.4.1 AE Event Mapping

AE X-Y plots provide real-time visualisation of the initiation and progression of cracks inside concrete. These graphs mark the location of each event as it occurs, as shown in Figure 5.23 (a) and (b) for BCJ samples SPC1 and SPC2.

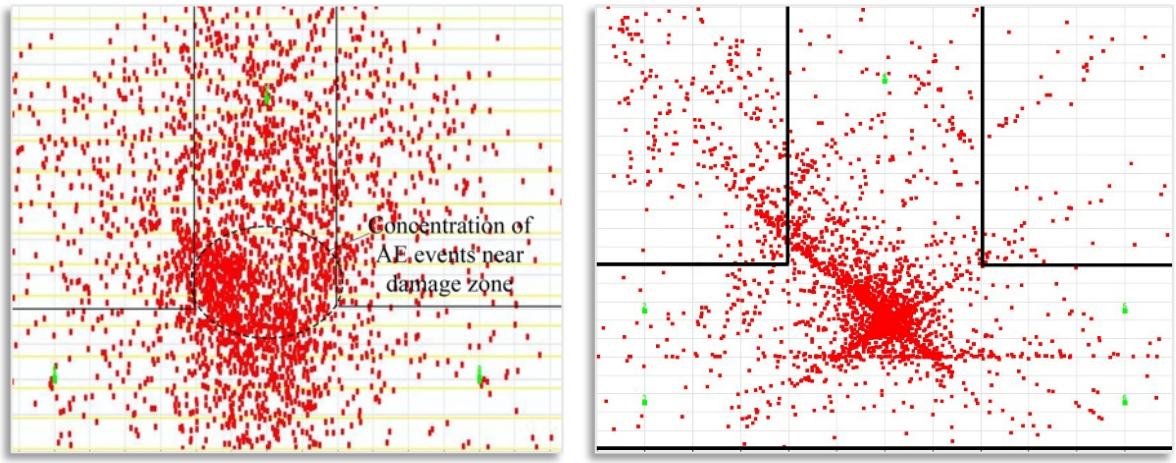

(a) **(b)**

Figure 5.23: AE Event Map of (a) SPC1 and (b) SPC2

The AEwin data acquisition software, developed by Physical Acoustic Corporation (PAC)[120], can record the initiation and propagation of cracks inside concrete in the BCJ that are still not visible to the naked eye. Every dot on the AE Event Map represents an AE event. Some dots are observed outside the boundaries of the BCJ sample. The main reason for this deviation is that the AE event coordinates are calculated using the arrival time of the AE wave. The arrival time further depends on the wave velocity. Since wave velocity cannot be predicted accurately in RC structures, there will always be a deviation in calculating the location coordinates of damage occurrence. The discontinuities caused by cracks on the path of waves travelling from the source to sensors interfere with the wave velocity. It is essential to mention here that the AE event map showing the concentration of AE events representing the damaged zone closely maps with the cracked specimens. However, the concentration of AE events gives an idea of the damage that occurred in the structure. Hence, the AE event map gives a pictorial representation of acoustic events occurring inside concrete due to microcracking much before it is visible to the naked eye and serves as an effective NDT tool for effectively picking up

damage initiation and its progression. It can serve as a real-time effective NDT damage mapping tool of BCJ.

5.4.2 AE hits and AE Energy

Variation of cumulative AE hits and AE energy with time has been presented graphically in Figures 5.24 and 5.25 for SPC1 and SPC2, respectively, with per cent cumulative hits and cumulative energy on the left y-axis and time on the x-axis. To study the effect of load variation, Time Vs Load has been plotted with a load scale on the right y-axis. A consistent rise in the slope of cumulative AE hits indicates significant AE activity. The horizontal parts of the graph indicate that no or very few cracking events occurred during that period. Many AE hits are observed even before the appearance of visible cracks at small loads. Up to A, the structure is in the elastic stage, during which the AE hits increase slowly and consistently up to a load of 16.3 kN. From A to B, very few hits are recorded during unloading. From B to C, the load starts increasing in the reverse direction, and AE hits also begin to grow faster. The AE hits recorded in the second loading cycle are less than in the fourth cycle because the BCJ is in the elastic stage up to the third cycle. The elastoplastic stage appears after the third cycle, and concrete starts to deteriorate faster, resulting in a sudden burst of AE hits. Many AE hits are observed during load reversal, as seen at I and J, which may be due to frictional resistance between cracked faces trying to occupy the original position. The horizontal part of the graph during the unloading and load-holding stages indicates fewer AE hits and points towards no or minor damage during this period. Very few hits are recorded from C to D because the structure has already been loaded up to this load value in the previous cycle, and no further cracking occurs. This phenomenon has been studied by Kaiser and is helpful for damage detection by observing the number of AE hits appearing during the loading phase. From D to E, the load value increases beyond the previous cycle's maximum load, causing an increase in AE hits. A sudden jump in the AE hits indicates macro-cracking in concrete, as seen near E and F. During this phase, the micro-cracks coalesce to form macro-cracks.

The trend of variation of cumulative AE energy is also almost similar to that of AE hits;

however, it has been observed that during the elastic stage, the rate of AE energy is comparatively less than the rate of AE hits (near A). This is because hits appearing during this stage have lesser energy. The trend is reversed in the plastic stage near E1 and F1, where more prominent knees of AE energy are seen than knees due to AE hits. Horizontal parts of curves or curves with mild slopes during loading or unloading phases, having a load value less than the maximum load of the previous cycle (shown by line AB, CD, EF etc.), is known as Kaiser's Effect (discussed in detail in section 3.3.2). Hence, the energy parameter gives an idea about the magnitude of damage. The use of cumulative AE hits and AE energy can better represent cracking initiation, progression, and quantum of damage in concrete in the BCJ. Comparing AE Energy variations of SPC1 and SPC2 from Figures 5.24 and 5.25, it has been observed that the sample SPC2 has a smooth release of energy in each loading cycle. In contrast, there is a sudden increase in energy in the third cycle of the SPC1 sample. This is because the energy absorption capacity of this sample SPC2 is higher than SPC1. Hence, AE Energy is a valuable parameter for studying and observing ductile behaviour and damage level in RC structures.

Similarly, cumulative Hits and Energy data have been plotted for SPC3 and SPC4, as shown in Figures 5.26 and 5.27, respectively. The trend of variation in cumulative hits and cumulative energy has also been observed in SPC2 & SPC4, as in the case of SPC1 and SPC2. Whenever there is a load increment, there is a rise in the slope of cumulative hits and cumulative Energy lines. Within the elastic limit, the energy rate is less than the elastoplastic stage. Thus, these plots can serve to observe the changes in the RC structures caused by load variations and can be very helpful in monitoring the health of RC structures. Kaiser described that material under load emits acoustic waves only after a primary load level is exceeded. During reloading, these materials behave elastically before the previous maximum load is reached. Thus, according to the theory developed by Kaiser, little or no acoustic emission hits/energy should be recorded before the previous maximum stress level is achieved.

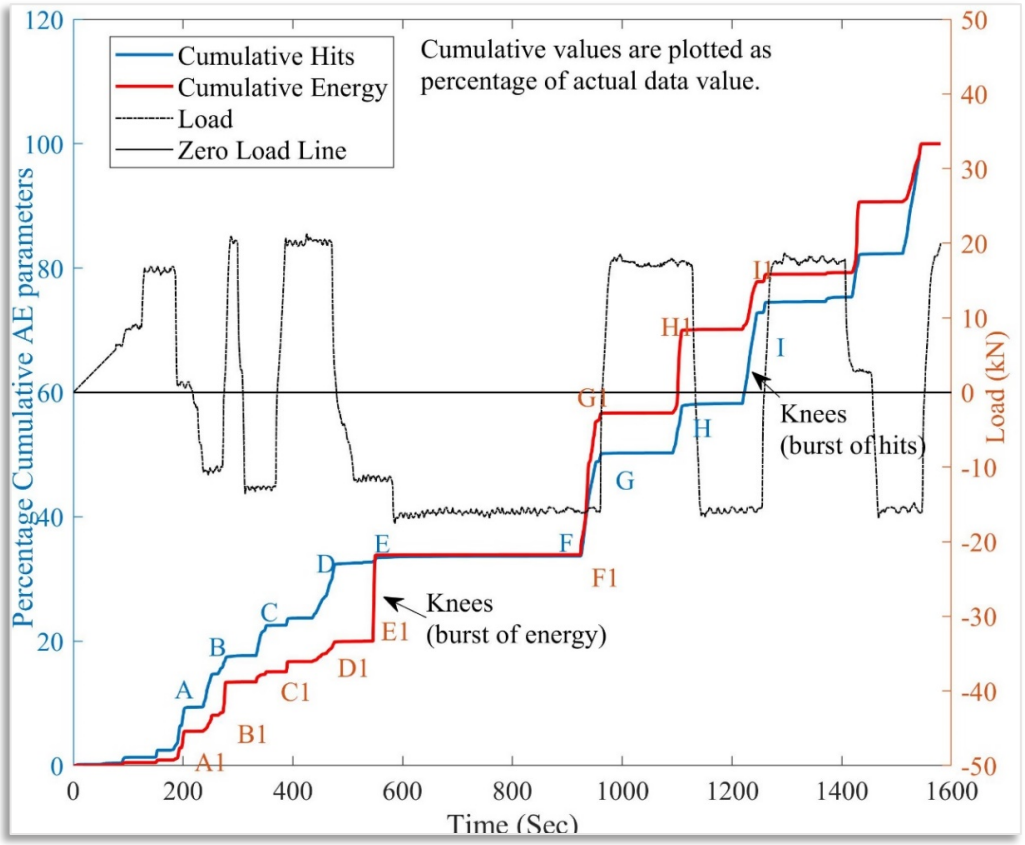

Figure 5.24: Cumulative AE energy, Hits and Load for SPC1

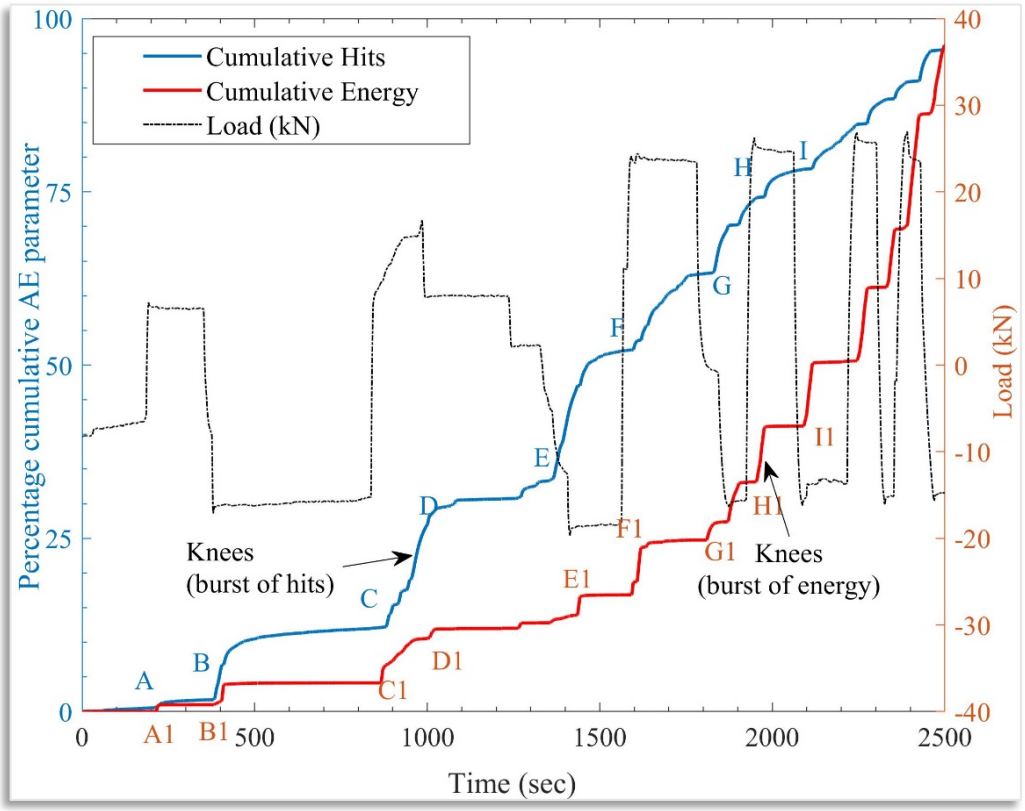

Figure 5.25: Cumulative AE energy, Hits and Load for SPC2

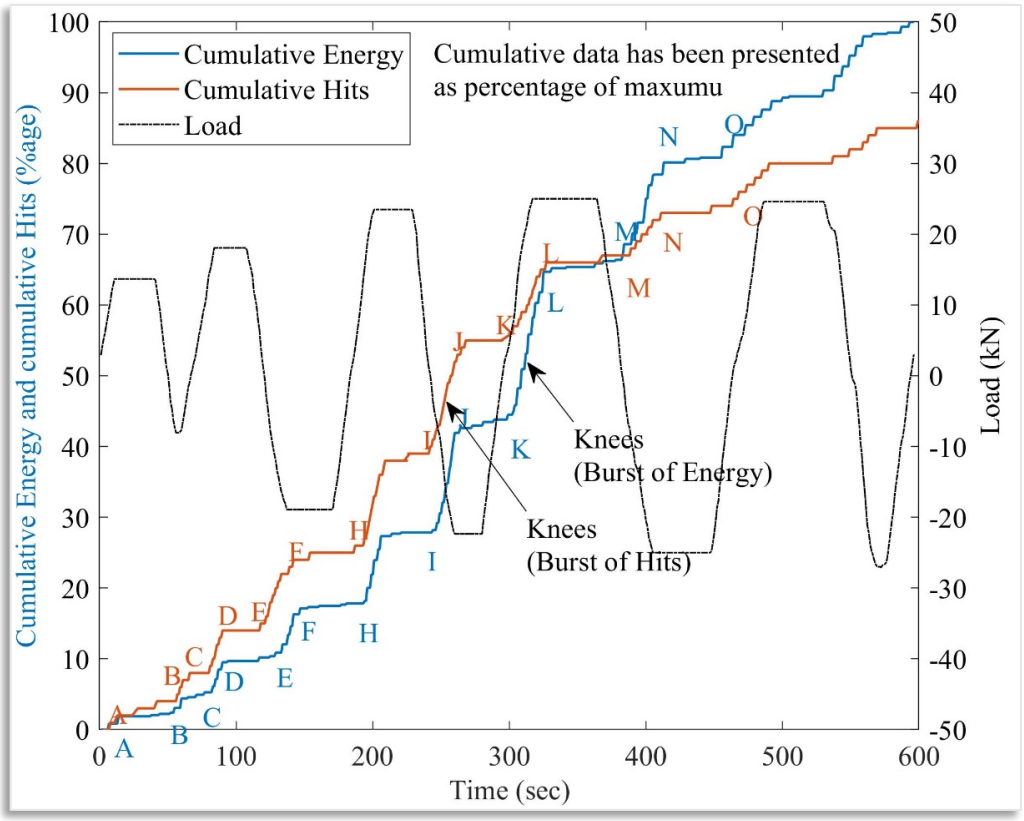

Figure 5.26: Cumulative AE energy, Hits and Load for SPC3

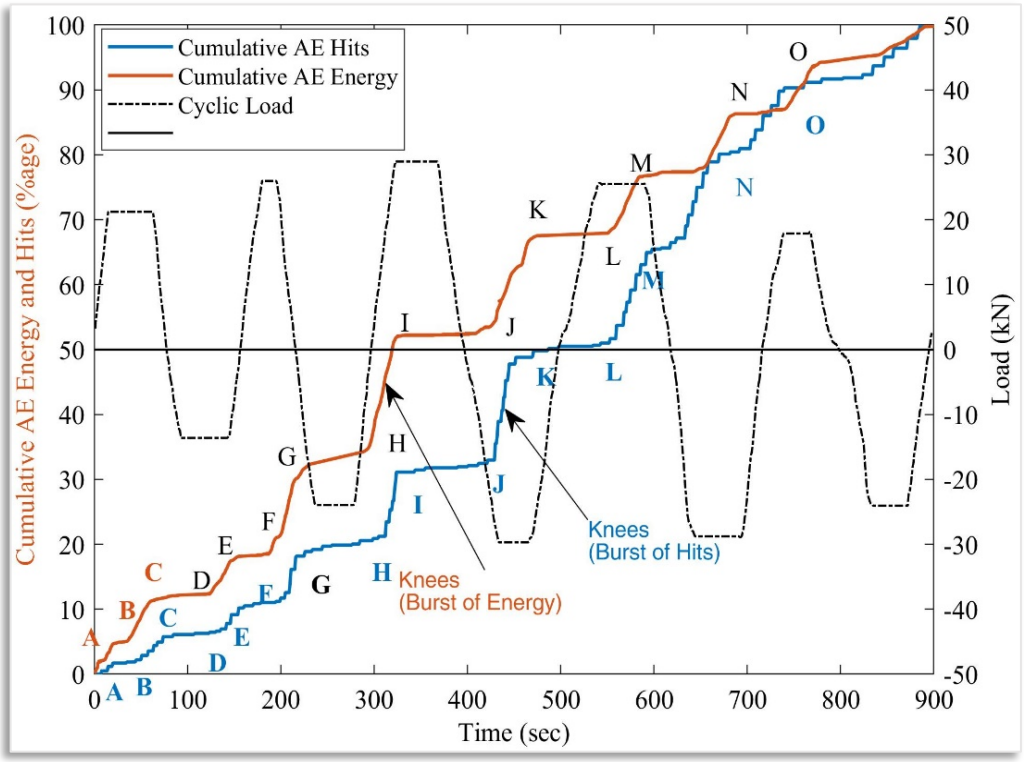

Figure 5.27: Cumulative AE energy, Hits and Load for SPC4

The Load Vs cumulative energy graph has been plotted as presented in Figure 5.28 to verify Kaiser's effect using the AE energy parameter. In the first load cycle, the slope of the curve is mild from O to A because the load is below the yield value, and the structure is within the elastic stage. There is negligible energy while unloading the BCJ from A to B, and the slope of lines A-B is almost zero. From B to C, the BCJ is loaded in the reverse direction. There is a constant rise in the slope of line B-C, indicating that the energy is increasing with an increase in load. When the reverse direction load is reduced, there is no release of energy as seen from C to D. From D onwards, the load is higher than the previous cycle's maximum load value (i.e., at A). From D to E, there is an increase in the slope of the line indicating the release of energy. Thus, Kaiser's effect, which was first studied by Kaiser with cumulative Hits Data is also equally valid for the AE energy parameter. From E to G', the BCJ is unloaded in the forward direction and reloaded in the reverse direction. During this phase, there is again a minimal amount of energy. But it is observed that the slope of line G′G starts to rise from a load value that is less than the previous cycle maximum value (i.e., load at G' is less than load at C). This effect is known as the conjugate of Kaiser's effect. Kaiser defined the Felicity ratio as the ratio of load at G' to the load at C. The Felicity ratio of less than one indicates damage to the structure.

Thus, it can be concluded that the BCJ started to deteriorate in the second reverse load cycle after reaching the load value at G'. Similarly, in the third forward cycle, the slope of the line started to increase before reaching the previous cycle's maximum load, as seen at point H. In the subsequent load cycles, the slope of the line started to increase much before the previous cycle's maximum load. This indicates severe damage to the BCJ.

Similarly, the Kaiser's effect has been observed in BCJ samples SPC2, SPC3 and SPC4,

as can be seen in Figures 5.29, 5.30 and 5.31, respectively. It is difficult to distinguish between ductile and non-ductile samples' behaviour from these graphs because ductility depends on displacement parameters. However, it is observed that there is a higher release of energy in the case of ductile samples than in non-ductile samples. The Cumulative Acoustic Energy (CAE) corresponding to each cycle has been obtained from these Load Vs Cumulative Energy plots. The total AE energy recorded in SPC2 is about two times more than in SPC1 and about 1.7 times more in SPC4 than in SPC3.

The AE energy depends upon the amplitude and duration of the acoustic wave received by AE sensors. The greater the damage, the higher will be the amplitude and duration of the waveform. Thus, AE energy is a direct indication of the intensity of the damage. The cycle-wise variation of CAE has been further presented in Figure 5.32 for SPC1 and SPC2. From this graph, it is seen that the average CAE of SPC2 is about three times more than that of SPC1. This is due to the provision of ductile reinforcement in SPC2. Similarly, the variation of AE energy and Energy dissipated in each load cycle has been plotted for SPC3 and SPC4 in Figure 5.33. It is observed that Energy dissipated and AE energy are closely associated with each other. The average energy dissipated by SPC4 is about three times that of SPC3. The average AE energy recorded by AE tests for SPC4 is about 2.7 times that of SPC3. Thus, there is a trend of higher AE energy and Energy dissipated in ductile samples than in non-ductile samples. A uniform variation is observed. This resulted in the idea of finding a relationship between AE energy and energy dissipated. A detailed discussion has been done to find this relationship in the following section.

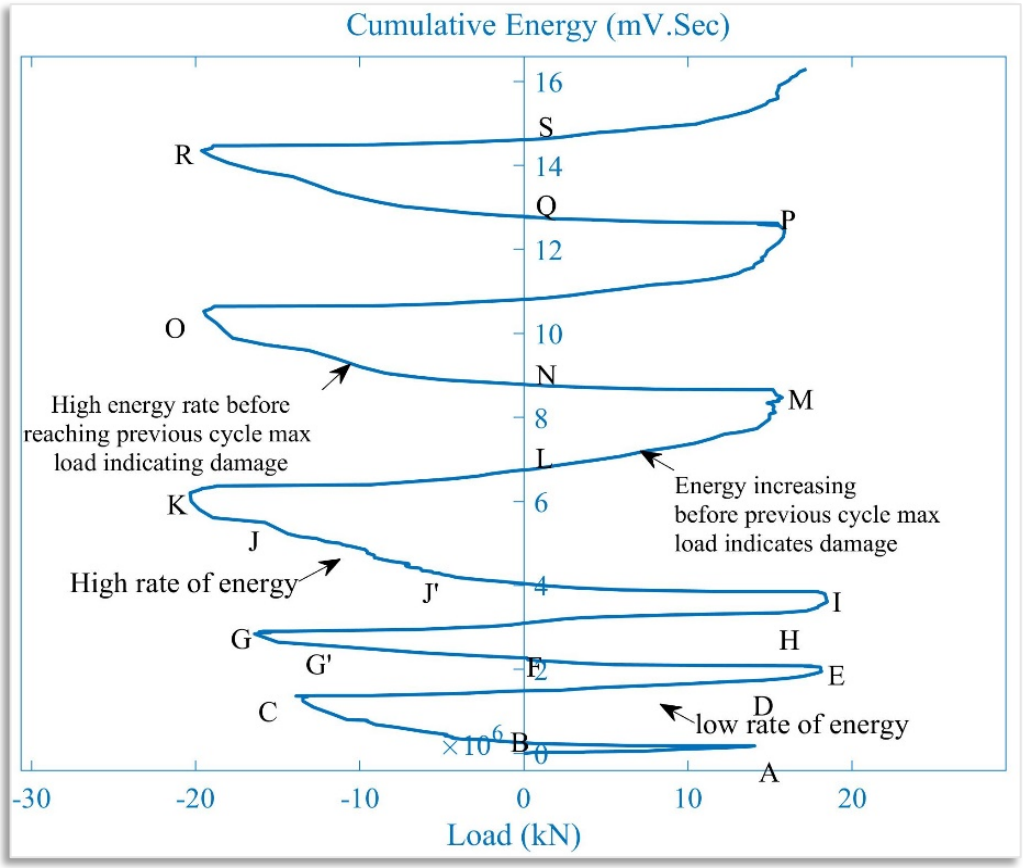

Figure 5.28: Load Vs cumulative AE energy for sample SPC1

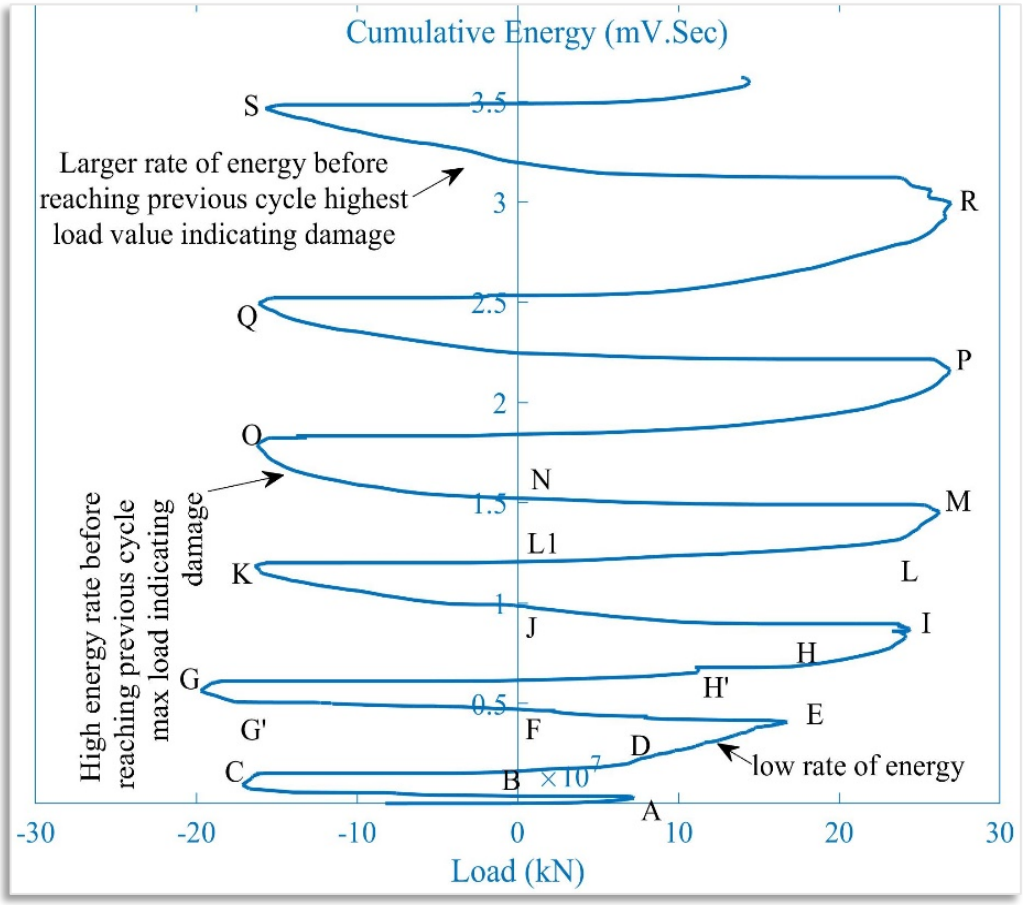

Figure 5.29: Load Vs cumulative AE energy for sample SPC2

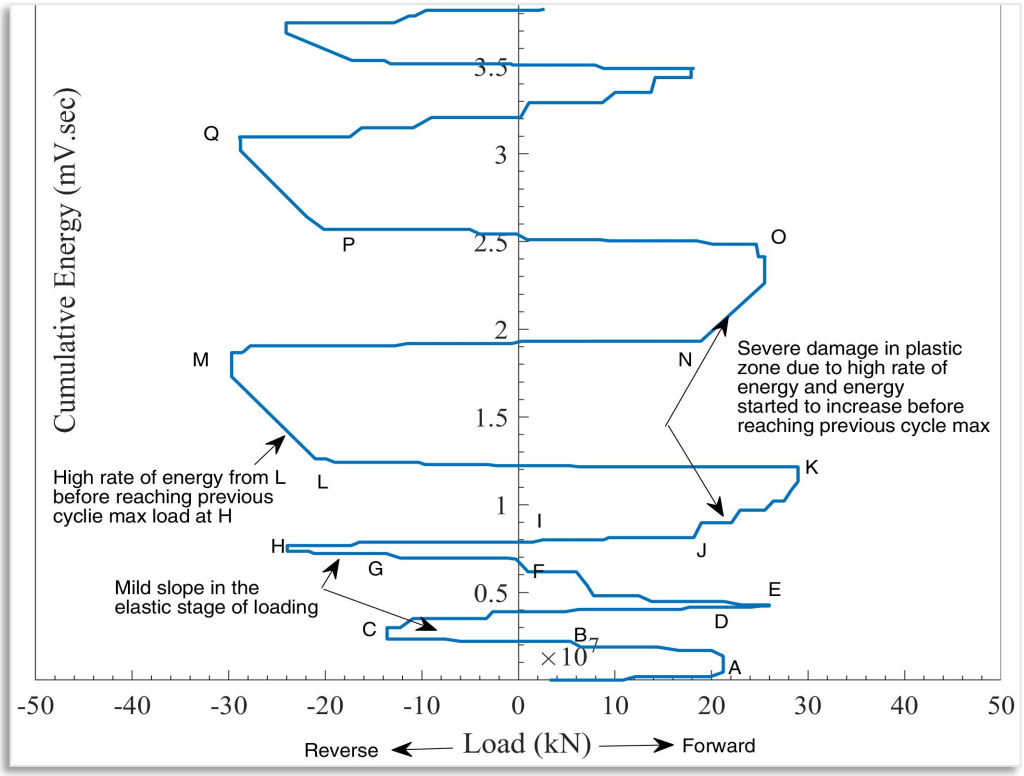

Figure 5.30: Load Vs Cumulative Energy SPC3

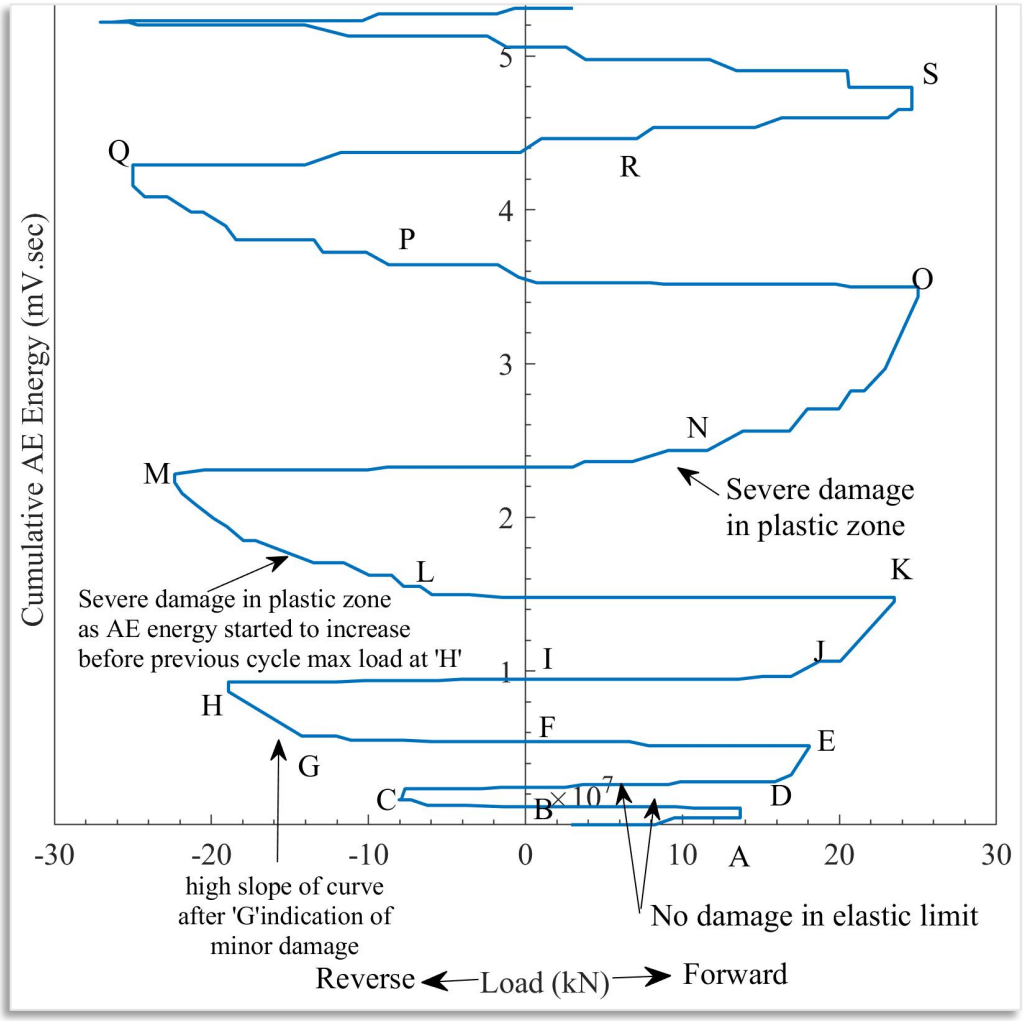

Figure 5.31: Load Vs Cumulative Energy SPC4

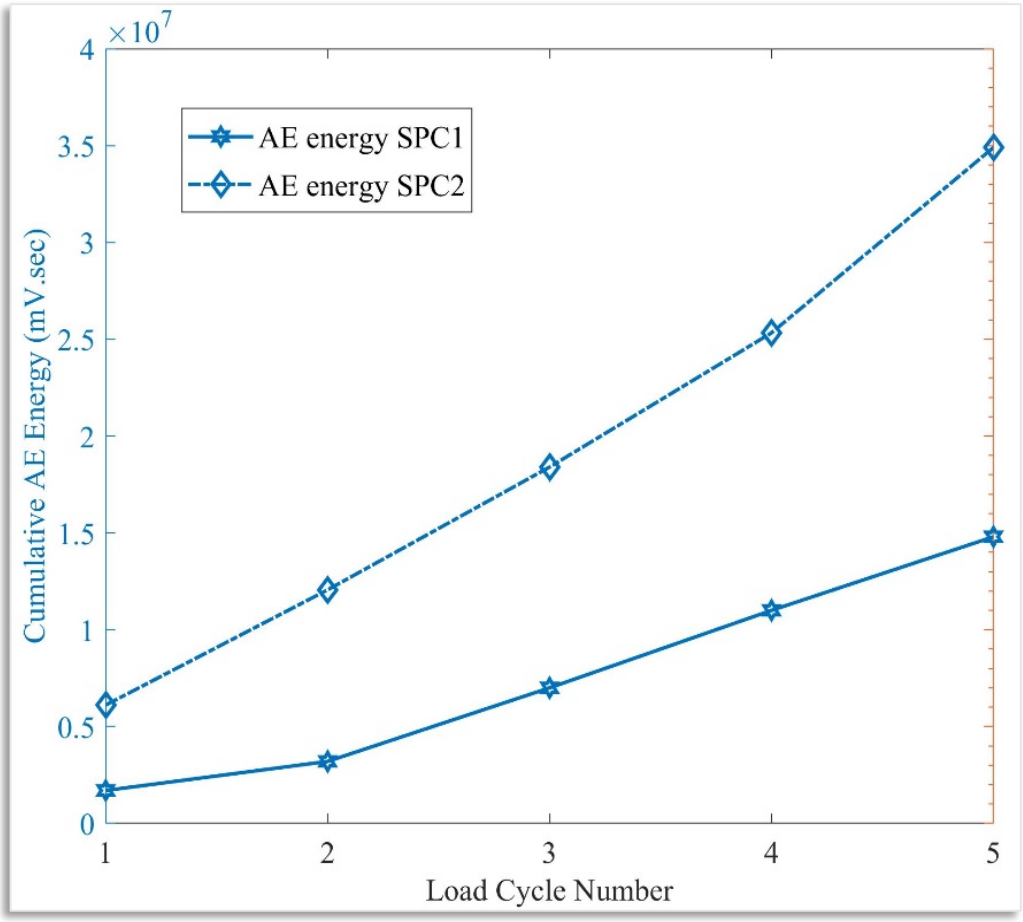

Figure 5.32: Cyclic variation of AE energy of SPC1 and SPC2

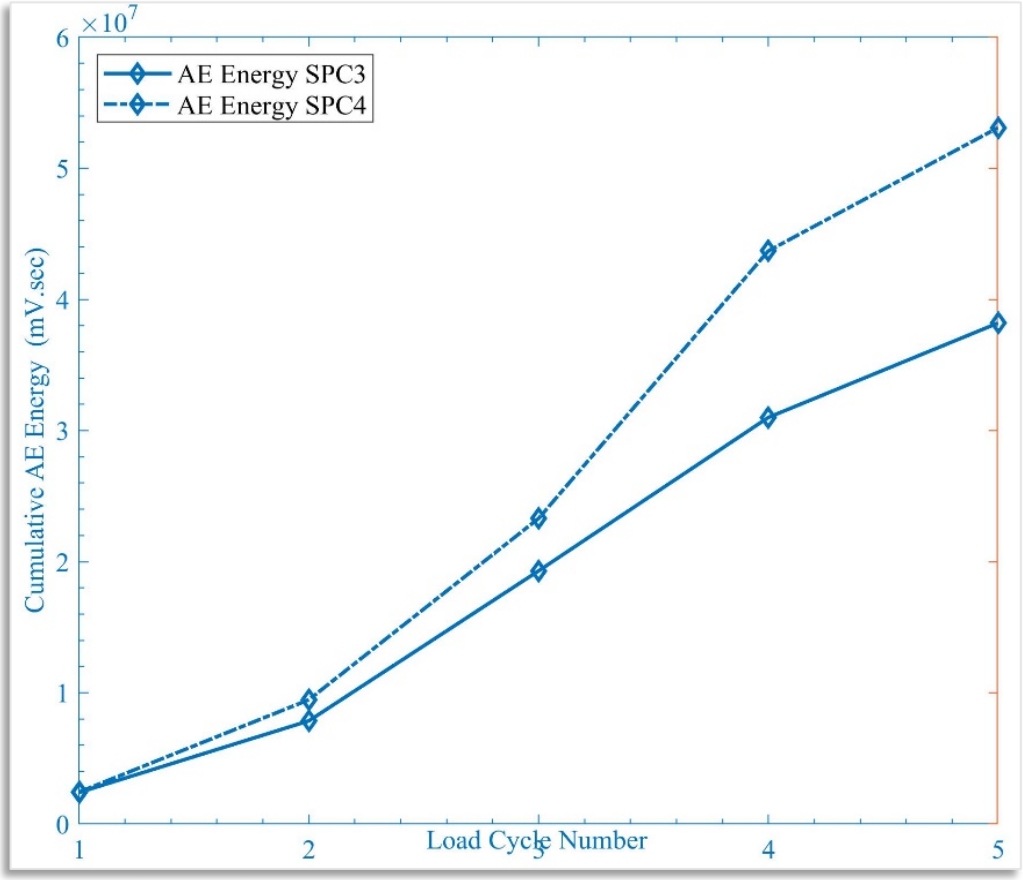

Figure 5.33: Cyclic variation of AE Energy of SPC3 and SPC4

5.4.3 Relationship between Energy dissipated and acoustic energy:

To express the relationship between the Energy-dissipated (ED) for each load cycle and Cumulated Acoustic Energy, a graph between these two parameters has been plotted and presented in Figures 5.34 and 5.35. The cumulative AE energy is very closely related to cumulative energy dissipated. The variation between these two energies is nearly linear; however, using mathematical models more accurate relationship can be obtained with the help of computer software. A mathematical model has been developed using MATLAB functions. From this modelling, a quadratic relationship between AE energy and energy dissipated has been established, as shown by equations- 5.1and 5.2for BCJ SPC1 and SPC2, respectively.

$$\text{For SPC1, } E_{ED} = 2 \times 10^{-10 \times} {E_{AE}}^2 + 7.7 \times 10^{-5} \times E_{AE} + 2.8 \quad 5.1$$

$$\text{For SPC2, } E_{ED} = 23 \times 10^{-10} {E_{AE}}^2 + 24 \times 10^{-5} \times E_{AE} - 82 \quad 5.2$$

Where, E_{ED} is the cumulative energy dissipated, E_{AE} is the cumulative AE energy. Similarly, data from BCJ samples SPC3 and SPC4 have been graphically presented in Figures 5.34 and 5.35, respectively.

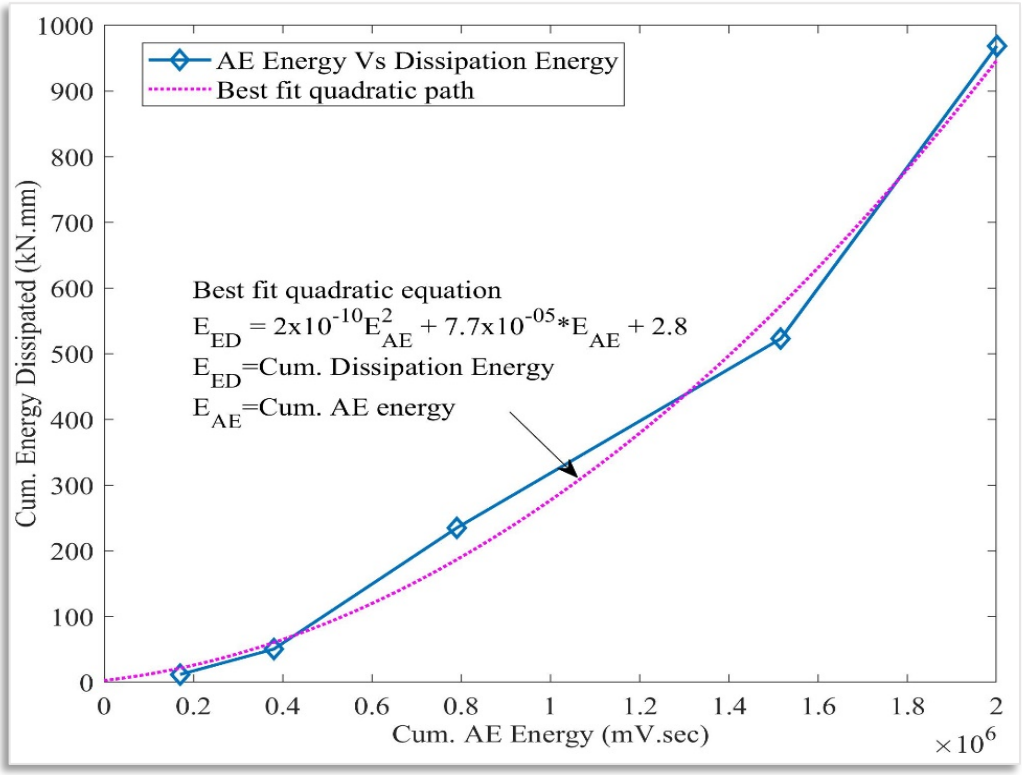

Figure 5.34: AE energy Vs Energy dissipated for SPC1

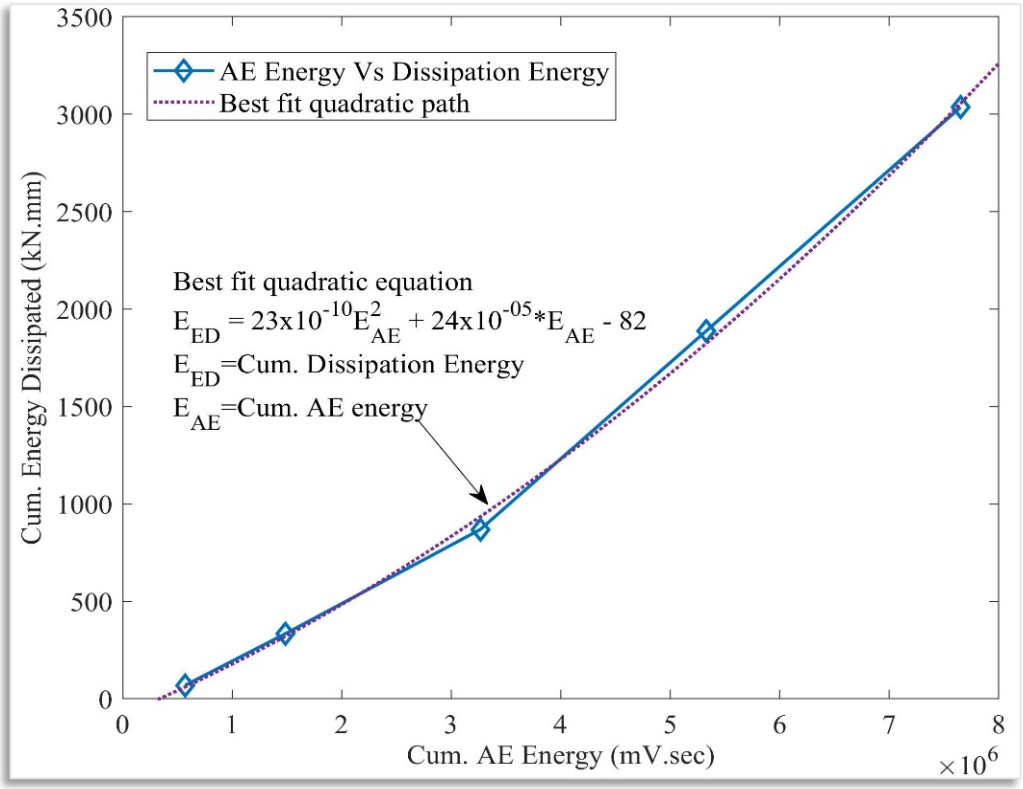

Figure 5.35: AE energy Vs Energy dissipated for SPC2

The data has been further analysed using MATLAB tools to develop a mathematical model for finding a relationship between AE energy and Energy dissipated. The equations developed have been shown by equations 5.3 and 5.4 for specimens SPC3 and SPC4, respectively.

$$\text{For SPC3, } E_{ED} = 1.22 \times 10^{-12\times} E_{AE}{}^2 - 1.645 \times 10^{-5} \times E_{AE} + 137.3 \quad 5.3$$

$$\text{For SPC4, } E_{ED} = 7.609 \times 10^{-13} E_{AE}{}^2 + 1.724 \times 10^{-5} \times E_{AE} + 99.89 \quad 5.4$$

These relations can be beneficial for monitoring the health of structures subjected to seismic forces because it is tough to accurately predict the acoustic energy that a structure will release under a specific load or displacement after an earthquake. This is because AE energy depends upon several parameters such as steel reinforcement, concrete mix design, the cross-sectional area of RC member, rate of loading, etc. We need to test samples of the same cross-section, same reinforcement, and mix design to estimate accurately. Once an accurate equation is developed, it can be used to find damage from available damage index models such as Park and Ang models. Carpinteri et al.[98] have also reported similar results in compression testing on concrete and rocks, wherein the authors have concluded that the number of AE events is

proportional to the released energy that is evaluated as the difference between the elastic strain energy at peak load and the energy absorbed by crushing.

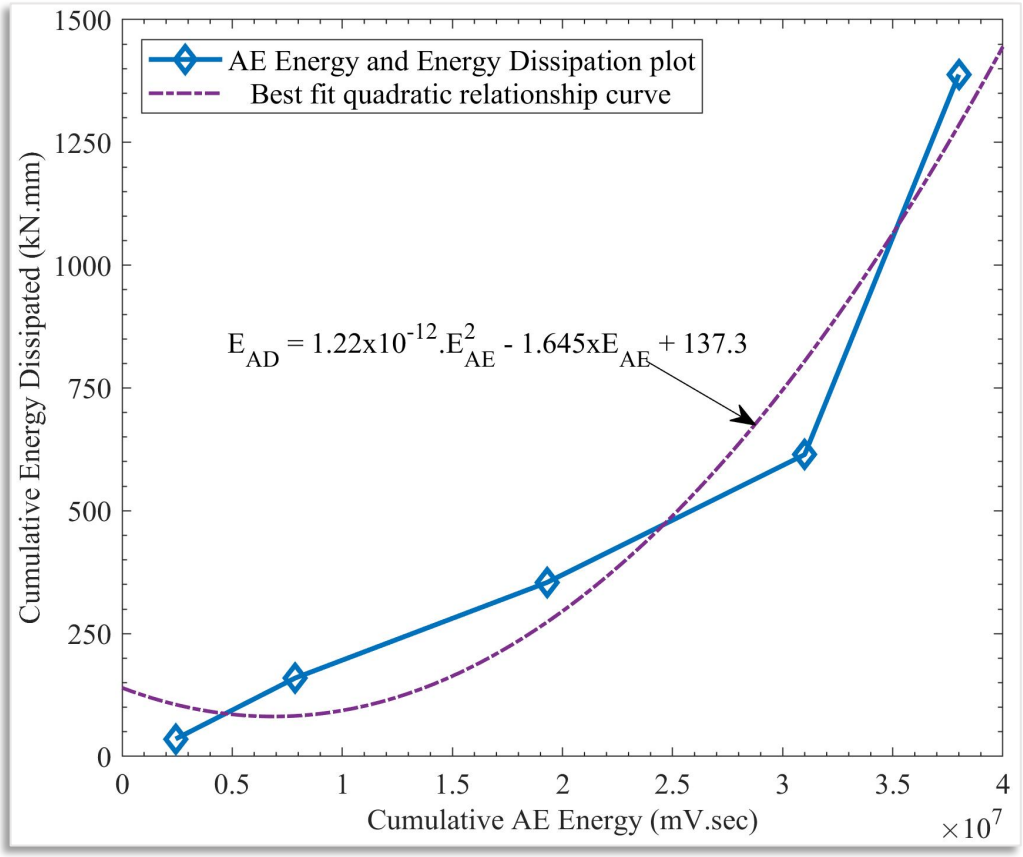

Figure 5.36: AE energy Vs Energy dissipated for SPC3

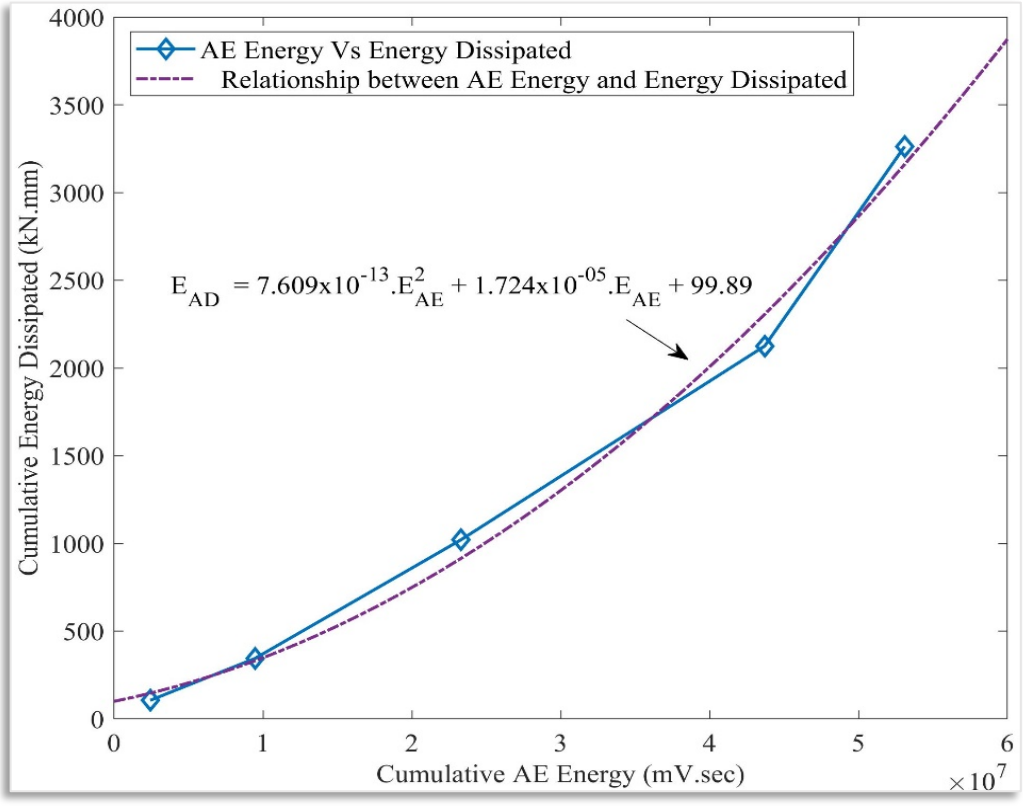

Figure 5.37: AE energy Vs Energy dissipated for SPC4

5.4.4 Crack classification

Average Frequency (AF) and the Rise-Angle (RA) value parameter can be used to distinguish between different modes of cracks, as shown in Figure 5.38. The Average Frequency is derived using AE counts and duration data. The RA value is the Rise Time divided by the maximum amplitude of the AE signal. These two parameters help to analyse crack classification. As per Ohno et al.[94], it is challenging to determine distinctive RA and the AF for each crack type. The slope of the dotted line (K) helps to distinguish between shear and tensile cracks. RA Vs AF value lying above the dotted line belongs to a tensile crack, whereas any value lying below this line represents a shear crack. The slope of this dotted line varies and depends upon the type of material, the geometry of the specimen and the loading profile. As a guideline, refers to Table 5.1 for deciding the slope of the diagonal line obtained on concrete-based specimens under four-point-bending tests by various researchers. The slope of this diagonal line needs to be fixed from the user's experience. However, this estimation may limit the usefulness of this method for classifying cracks in specific modes. In this research, the slope of the line dividing the tensile and shear hits has been kept as 1:10 as suggested by the RILEM Technical committee (2010)[121]. From the FA vs RA graphs, the percentage of AE Hits corresponding to shear and tensile crack occurrences can be separated. A conclusion can be drawn from the percentage difference of whether the damage is caused by shear failure or tensile failure.

The acoustic emission parameters such as peak amplitude, duration, frequency, and counts have been used to calculate RA and AF values for every AE Hit. A MATLAB programme has been developed to derive these parameters (refer to Annexure-A). The calculated values have been further plotted, as shown in Figure 5.39 and 5.40. From these plots, it is observed that in the first two cycles, when the BC joint is subjected to load within the elastic range, most of the damage initiated is due to tensile cracking inside the concrete. As the load increases, some shear cracks begin to appear. Thus, the nature of initial cracks is tensile, but with a further increase in load/deflection, there has been some damage due to an increase

in shear stress. Since the BC joint is strong enough to resist shear, most of the damage falls in the tensile zone.

The shear crack noises are produced because of rubbing due to translation caused by the development of macro cracking during load cycles-three onwards. Cracking initiation is in the form of tensile cracks, which later coalesce together in the actual crack pattern. The majority of damages in both the BCJ samples are attributable to tensile cracks. The data of RA Vs AF indicates that there is about 6.8 times increase in Hits due to Tensile cracks and 3.3 times increase in Hits due to Shear cracks in SPC2. The test results indicate that tensile cracks govern overall failure. However, during the fourth load cycle in SPC1 and SPC2, there is a percentage increase in hits due to shear cracks. This indicates an increase in shear damage in the beam at higher loads near the collapse stage. When the BCJ is deformed beyond a value corresponding to yield load, the crushing of concrete begins resulting in shear cracks due to the rubbing action of concrete. Although it is difficult to quantify damage using these graphs, the engineers can assess whether the failure is due to shear cracks or tensile cracks.

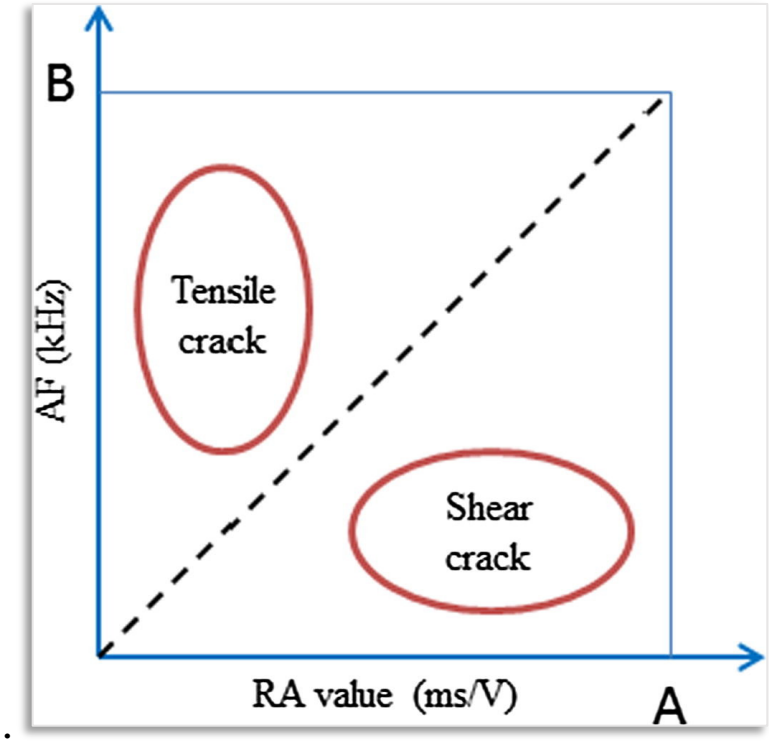

Figure 5.38: Variation of RA and AF in concrete[122]

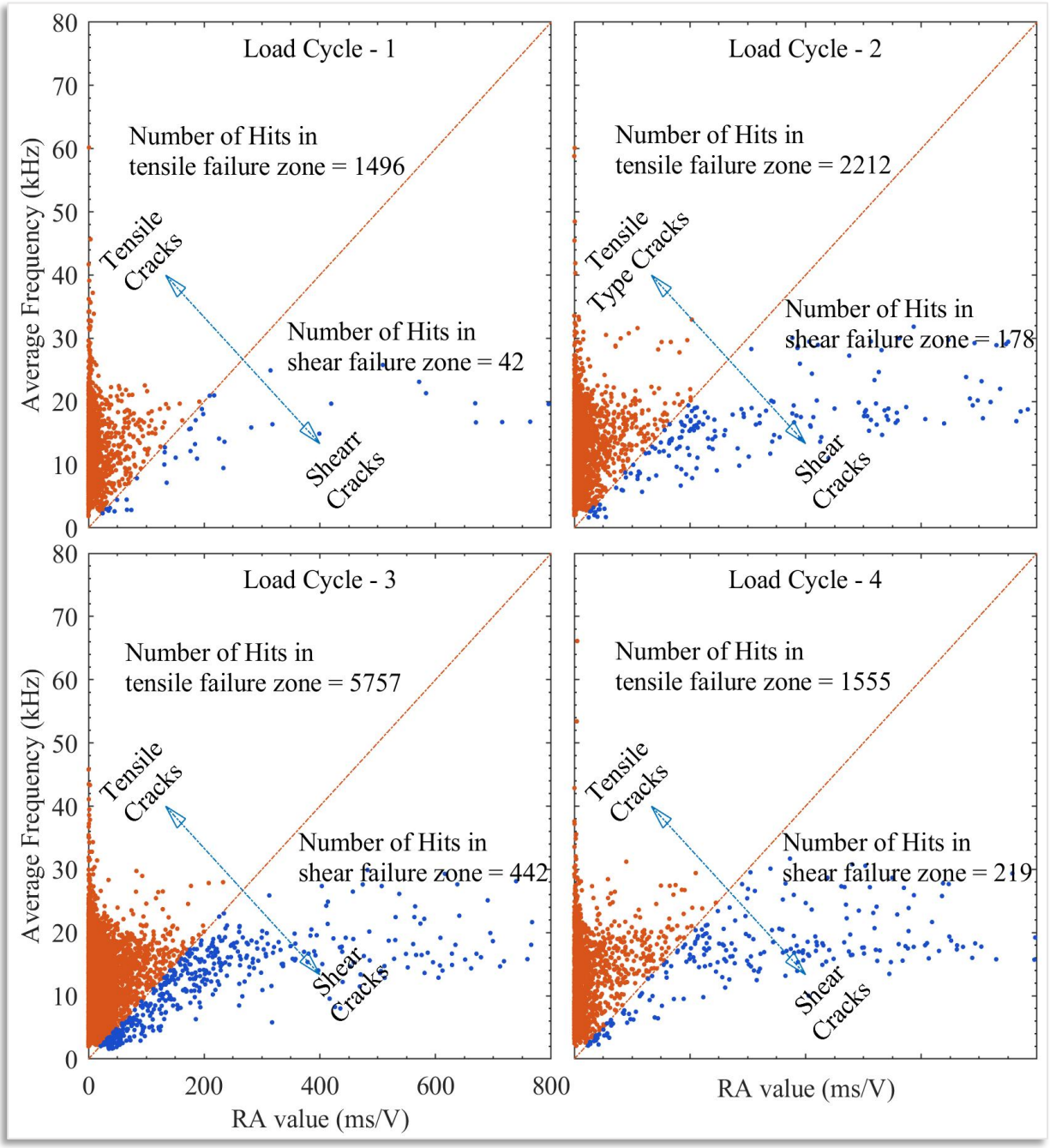

Figure 5.39: RAVs AF for SPC1

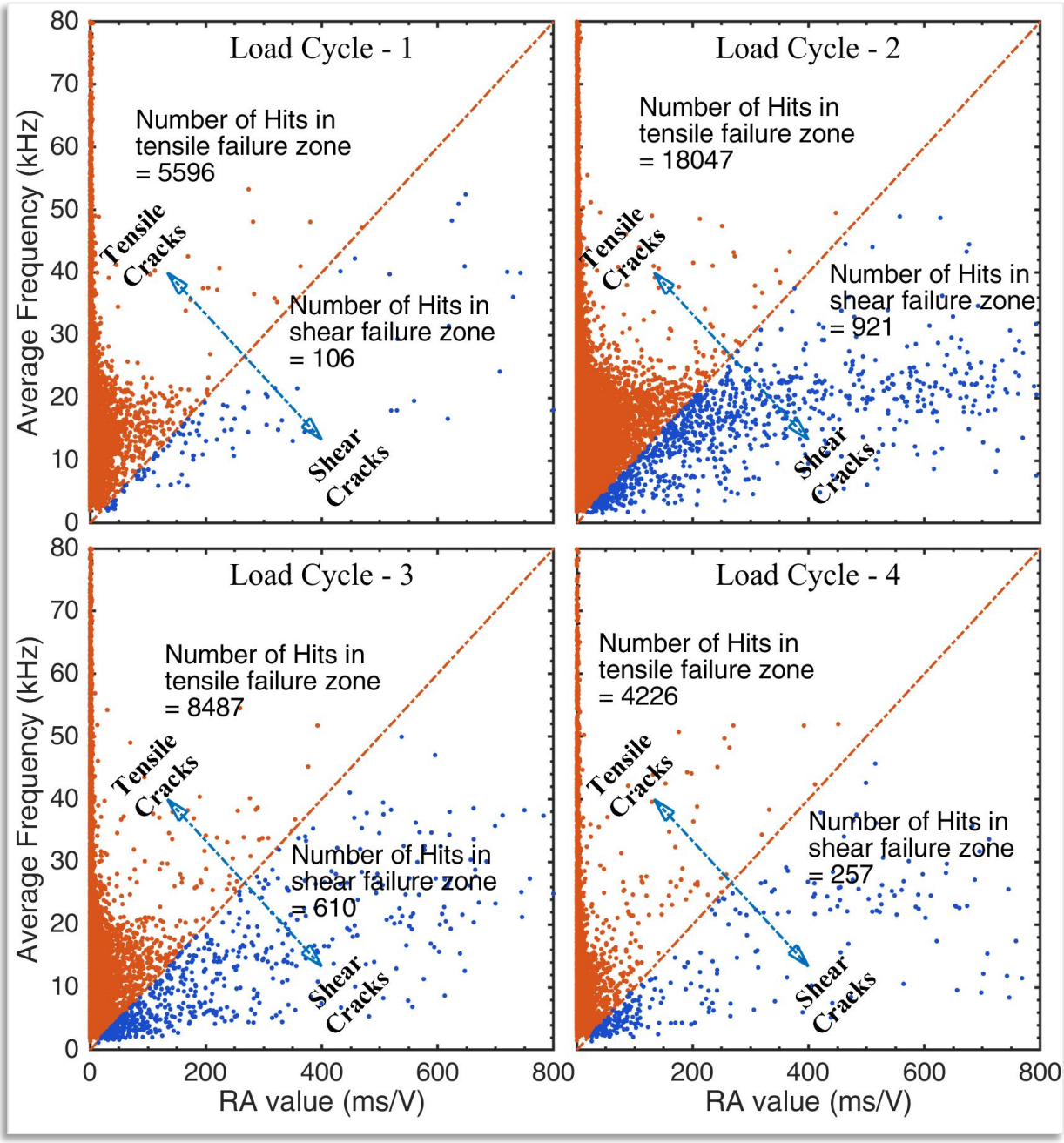

Figure 5.40: RAVs AF for SPC2

Table 5.1: K values on concrete-based specimens under bending tests.

Authors	Type of specimen	Dimensions (mm)	Loading type	RA (ms/V)	AF (kHz)	K (ms/V/kHz)
Soulioti et al.[123]	Steel Fibre concrete specimen	100 × 100 × 400	Monotonic	6	65	0.09
Calabrese et al.[124]	Plain concrete specimen.	140 × 140 × 500	Cyclic	7	350	0.02
Aggelis[30]	Plain concrete specimen.	100 × 100 × 400	Monotonic	15	550	0.027
Shahidan et al.[125]	Reinforced concrete specimen.	150 × 250 × 1900	Cyclic	150	150	1
Aldahdooh et al.[126]	Reinforced concrete specimen.	1500 mm in length	Monotonic	5	400	0.0125
Shahidan et al.[127]	Reinforced concrete specimen	150 × 250 × 1900	Cyclic	200	160	1.25
			Monotonic	40	40	1
Behnia et al.[128]	RC, SFRC, PFRC beam specimen	200 × 250 × 2500	Cyclic	5×10^{-3}	400	12.5×10^{-6}
Prem et al.[129]	Reinforced concrete specimen.	100 × 200 × 1500	Monotonic	200	200	1

5.4.5 b-value analysis

b-value analysis, used in the acoustic emission technique, is based on the Gutenberg-Richter (GR) relationship developed for estimating the frequency of occurrence of earthquakes. The GR law states that earthquake magnitudes are distributed exponentially by the equation-5.5

$$\log_{10} N = a - bM_L \quad (5.5)$$

Where N is the number of events with a magnitude in the range of $M_L \pm \Delta M$, b is the scaling parameter, and a is a constant. Estimating the b value is crucial for finding the probability of earthquake occurrence. Generally, the b value is very close to 1. The above principle has been

applied to the AE technique to study the "Amplitude Distribution" of acoustic emission waves generated during cracking. From equation-5.5, the b-value is the negative gradient of the log-linear AE frequency/magnitude plot, and hence it represents the slope of the amplitude distribution. In the AE technique, the GR formula can be modified as

$$\log_{10} N = a - b' A_{dB} \tag{5.6}$$

Where A_{dB} is the peak amplitude of AE events expressed in decibels.

$$A_{dB} = 10 \log_{10} A_{max}^2 = 20 \log_{10} A_{max} \tag{5.7}$$

Comparing the above equations, the b-value obtained with this relationship should be multiplied by a factor of 20 to be comparable with seismology[130]. Although the analysis of the b-value is well-known in rock mechanics and seismology, very little work has been done on RC structures. In the work of Sammonds et al. (1994)[131] on damage evolution in rock, the trend of the b-value over time is plotted. The decrease in b-value leads directly to dynamic failure immediately following the minimum b-value. An 'improved' Ib-value was proposed and applied to the evaluation of slope failure by Shiotani et al. (1994). The Ib-value was defined by the following equation:

$$Ib = \frac{\log N(\mu - \alpha_1 \sigma) - \log N(\mu - \alpha_2 \sigma)}{(\alpha_1 + \alpha_2)\sigma} \tag{5.8}$$

Where σ =standard deviation; μ =mean value of the magnitude distribution; α_1=coefficient related to the smaller amplitude: and α_2 = coefficient related to fracture level.

The use of the improved Ib-value was later on applied by Shiotani et al. (2000)[132] to evaluate the fracture process in concrete. They have shown that the Ib-value analysis was successful in evaluating the fracture process of concrete specimens. The conventional b-value analysis was applied to the data recorded on a reinforced concrete beam and assuming $b = b' \times 20$.

The amplitude distribution of acoustic emission signals through b-value analysis can act as a suitable damage quantification tool for reinforced structures. However, damage

quantification using the acoustic emission technique is one of the biggest challenges because the mechanism of AE generation, its wave propagation and the recording of signals can differ depending on many factors such as environmental conditions, shape and size of the structure sensor selection.

Many AE signals having smaller amplitudes are generated with the initiation of micro-cracks, and AE signals of larger amplitudes are generated on the appearance of macro-cracks (Kurz et al. (2006)). The low Ib-value represents unstable crack growth due to a large number of high-amplitude AE hits (Rao et al. (2005)). As the load increases, the fracture process moves from micro to macro cracking, and AE signals of larger amplitude are generated at higher loads. As a result, the Ib-value decreases. In this work, it is observed that the Ib-value is dependent on loading levels and is sensitive to crack growth in RC beam-column joint specimens. Thus, the Ib-value is a powerful index to examine the levels of damage in BCJ.

The evaluation of the Ib-value is a tedious procedure. A frequency distribution graph is drawn as shown in Figure 5.41 which has been used to find the Ib-value. The Ib-value for this particular group has been worked out using equation-5.9

$$Ib = 20 * \frac{\mathrm{logN1} - \mathrm{logN2}}{\mathrm{a2} - \mathrm{a1}} \tag{5.9}$$

The manual calculations are complicated and time-consuming. However, a mathematical tool using MATLAB programming helped to handle the huge AE data. The average time of group and Ib-value data is obtained from this MATLAB programme (Appendix B:) which has been used to plot Time Vs Ib-value graphs as shown in Figures 5.42 and 5.43 for BCJ samples SPC1 and SPC2, respectively. From the graphs, it is observed that there are sharp variations in Ib-value when the load is increased. However, it has been observed that Ib-values increase sharply due to the formation of a large number of new micro-cracks. From these graphs, the damage can be identified by noticing the concentration of red dots belonging to severe damage. However, it is not possible to quantify the damage. To verify the level of damage concerning Ib-values, the hit data has been separated for different Ib-value indexes in

each quarter cycle of loading. The cumulated value of these Hits has been plotted for all the Samples (see Figures 5.44 and 5.45 for SPC1 and SPC2). The majority of the Hits belong to the Moderate Damage Level (having Ib-value 1 to 2). From these graphs, it is observed that SPC1 has more damage after the second loading cycle, whereas in SPC2, there is severe damage after the first loading cycle. In SPC2 there is about two-times increase in Hits having Ib-Value <1 and about 3.1 times increase in Hits falling in the Ib-value of moderate damage.

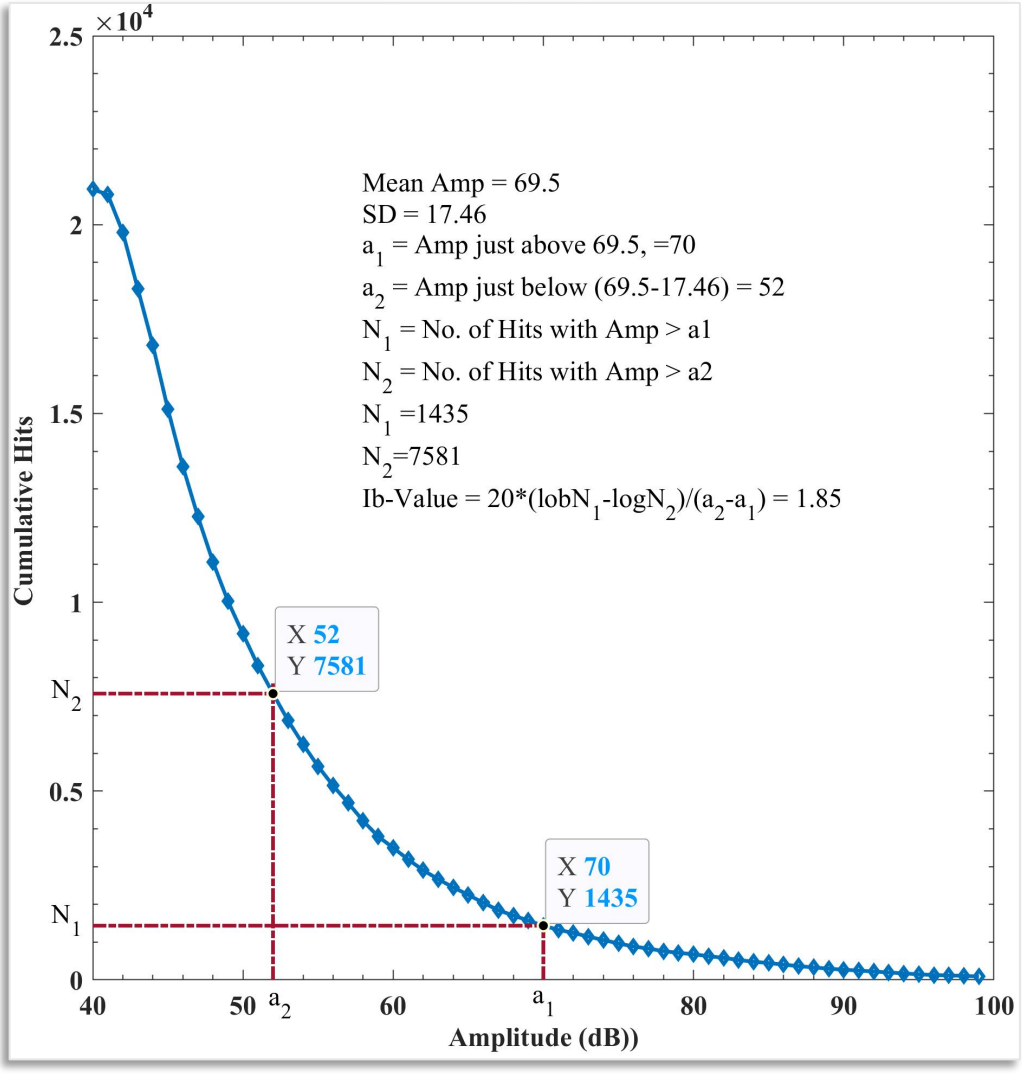

Figure 5.41: A Typical Frequency Distribution to find Ib-value

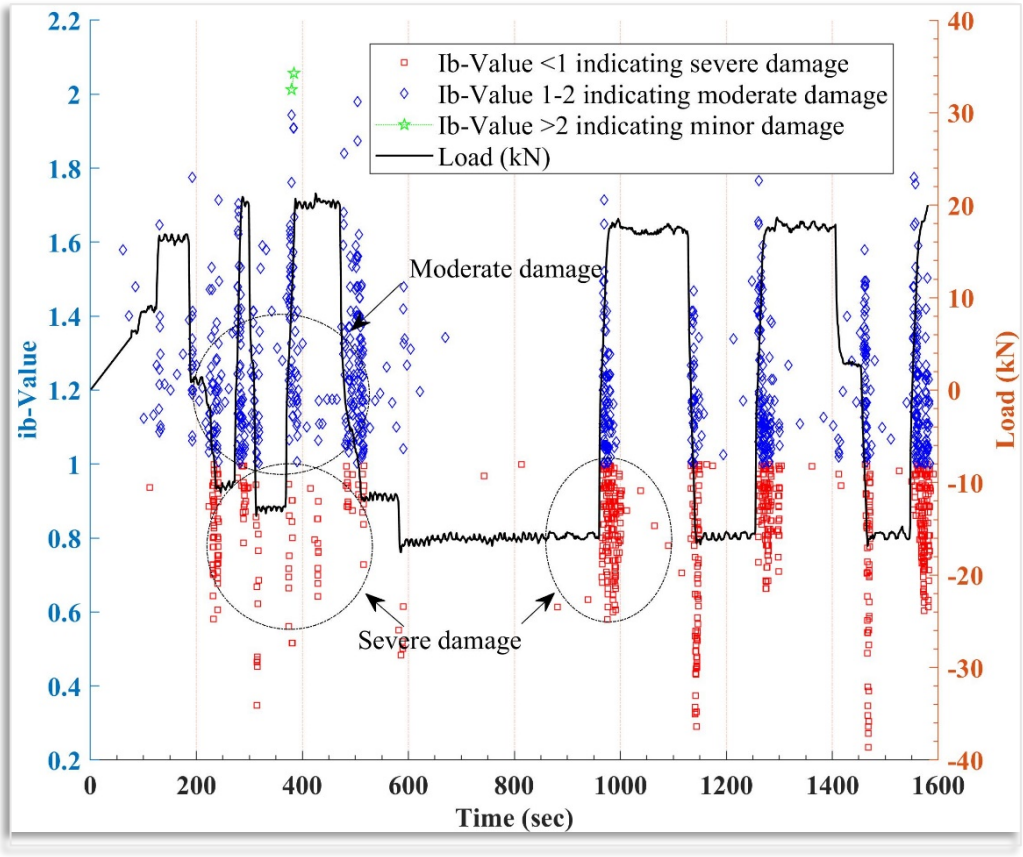

Figure 5.42: Ib-Value Vs Time BCJ sample SPC1

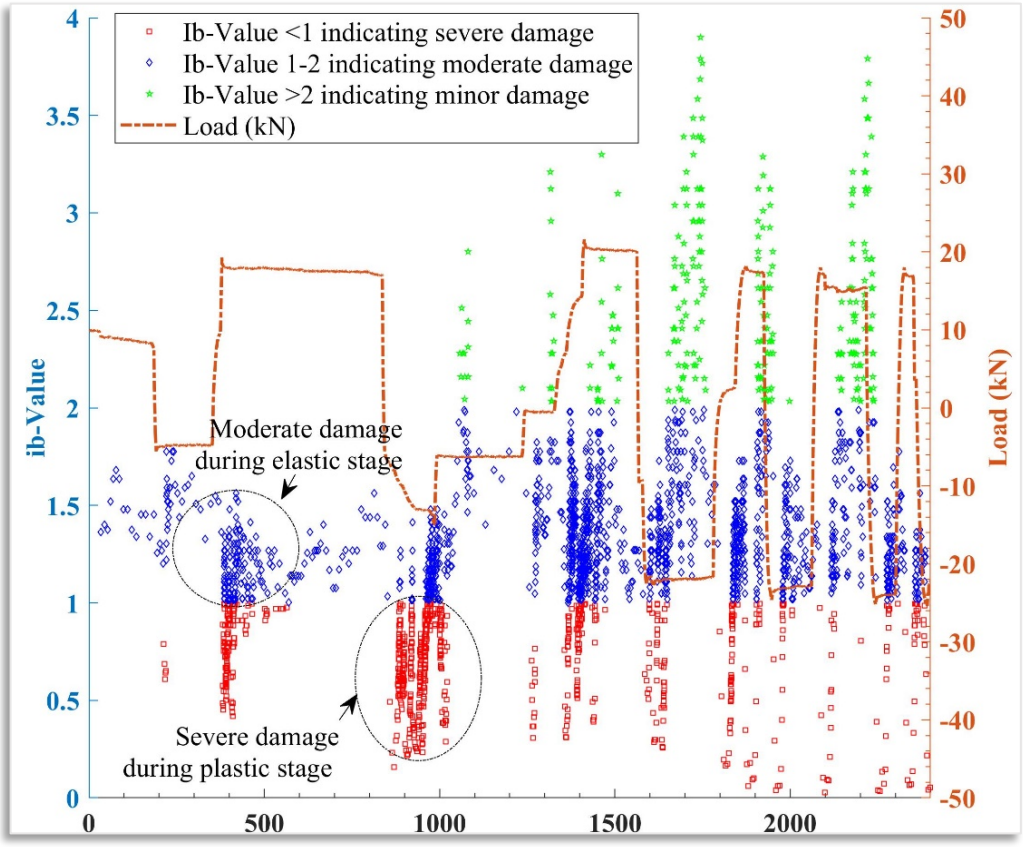

Figure 5.43: Ib-Value Vs Time BCJ sample SPC2

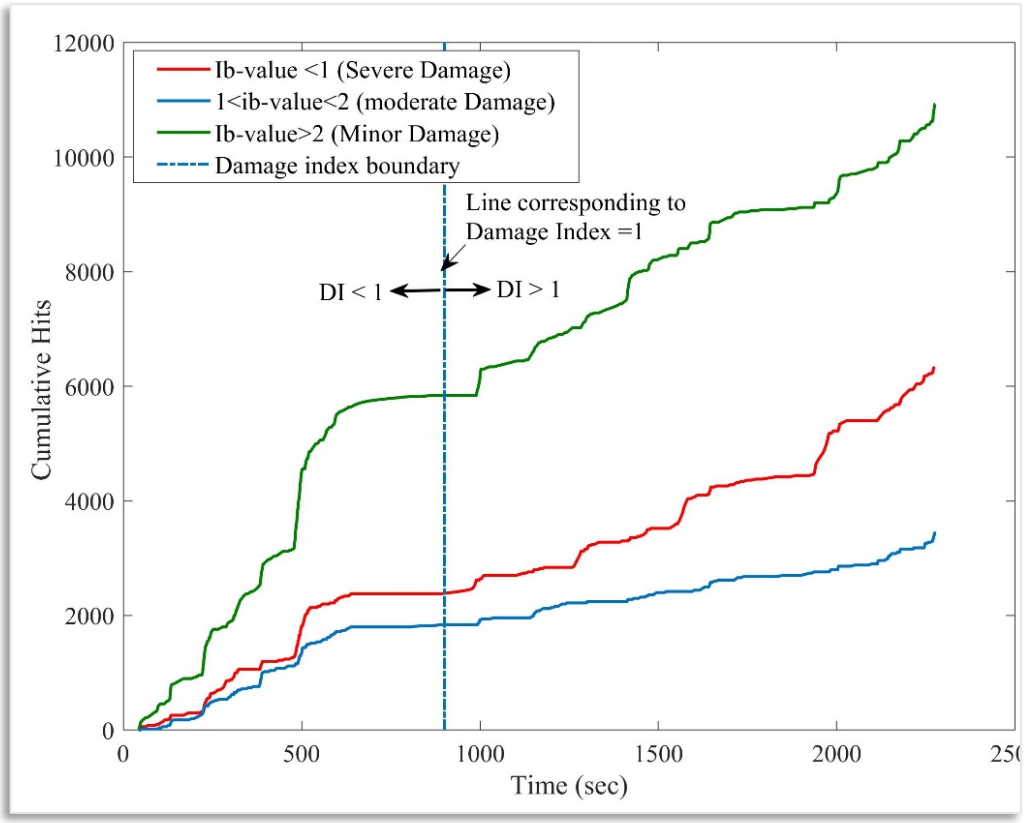

Figure 5.44: Hits for different levels of damage as per Ib-Value SPC1

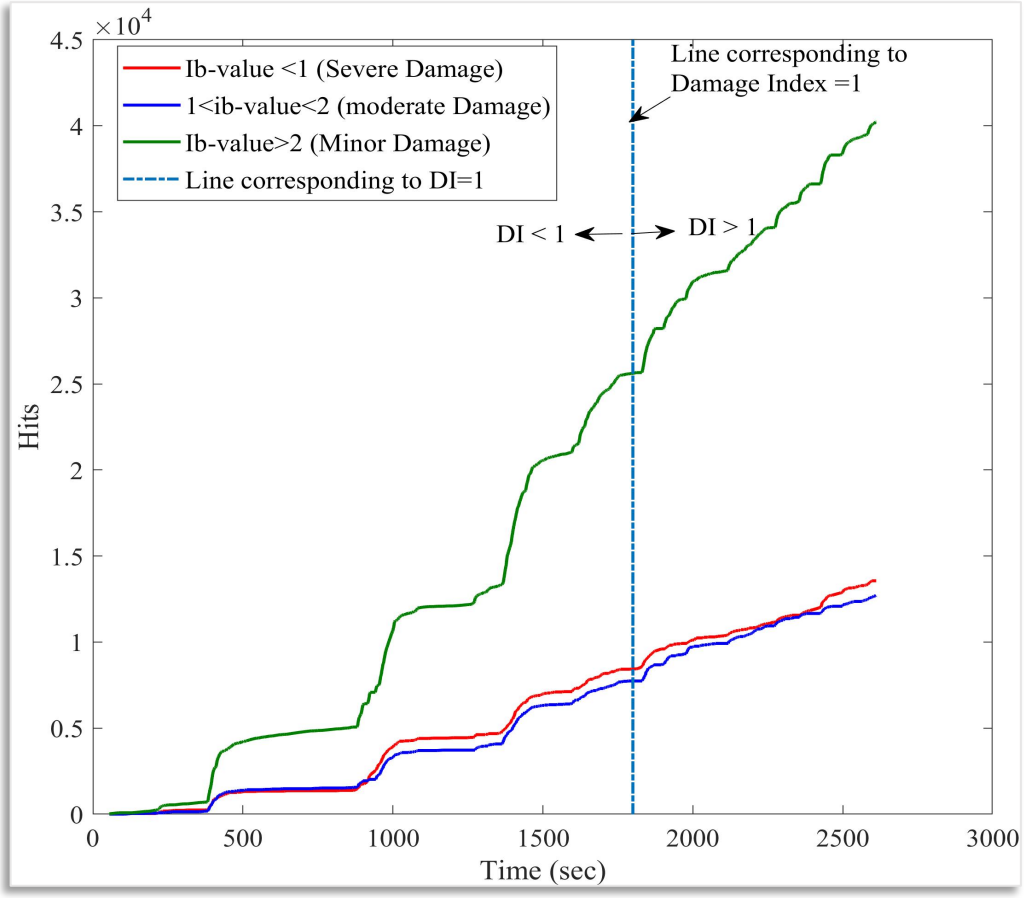

Figure 5.45: Hits for different levels of damage as per Ib-Value SPC2

5.5 BEHAVIOUR OF RETROFITTED BCJ UNDER CYCLIC LOADS

The concrete samples SPC1 and SPC2 have been damaged due to cyclic load; however, the steel reinforcement is intact, but the steel has lost resistance due to several deformation cycles. This research aims to retrofit the damaged BCJ samples with Engineered Cementitious Composite (ECC). The damaged concrete has been removed, and Epoxy 2200 jointer has been applied to the exposed concrete surface for a better bond between old and new concrete. The broken concrete removed has then been replaced with ECC. The retrofitted samples SPCR1 and SPCR2 have been tested using the AE technique similar to SPC1 and SPC2. The formation of cracks in the retrofitted samples has been shown in Figures 5.46 and 5.47 for samples SPCR1 and SPCR2, respectively. The load Vs deflection plots of retrofitted samples have been shown in Figures 5.48 and 5.49. The cumulative AE energy parameter Vs load has been plotted in Figures 5.59 and 5.60.

5.5.1 Visual observations

The crack width of the specimen has been measured at the end of each load cycle. It has been observed that the crack width of the retrofitted sample is lesser than the control BCJ samples. A crack width of 11 mm in SPC1 and 15 mm in SPC2 has been observed. The crack widths of retrofitted BCJ samples SPR1, and SPR2 have been observed as 4.5 mm and 5 mm. Thus, crack width in BCJ samples retrofitted using ECC reduces by 35-40%. This is because when ECC is applied in an RC structure, more tiny cracks spread over the tensile surface due to the bridging effect of fibres, whereas fewer wider cracks form in an ordinary RC member as can be seen from Figures 5.46 and 5.47 for SPRC1 and SPRC2, respectively.

5.5.2 Load deflection behaviour

The yield and ultimate values of displacement parameters obtained from the monotonic load test have been used to analyse test results from the cyclic load. Load Vs deflection

response of retrofitted BCJ has been presented in Figures 5.48 and 5.49 for SPCR1 and SPCR2, respectively. Maximum displacements of 29 mm in the forward cycle and about 36 mm in the reverse cycle have been observed in SPCR1. In contrast, maximum displacements of 42 mm in the forward cycle and 43 mm in the reverse direction have been observed in SPCR2. This reflects that SPCR2 is more ductile than SPCR1. The maximum load of 24 kN in the forward direction and 19.5 kN in the reverse direction has been observed for BCJ sample SPCR1.

Figure 5.46: Crack formation of BCJ sample SPRC1

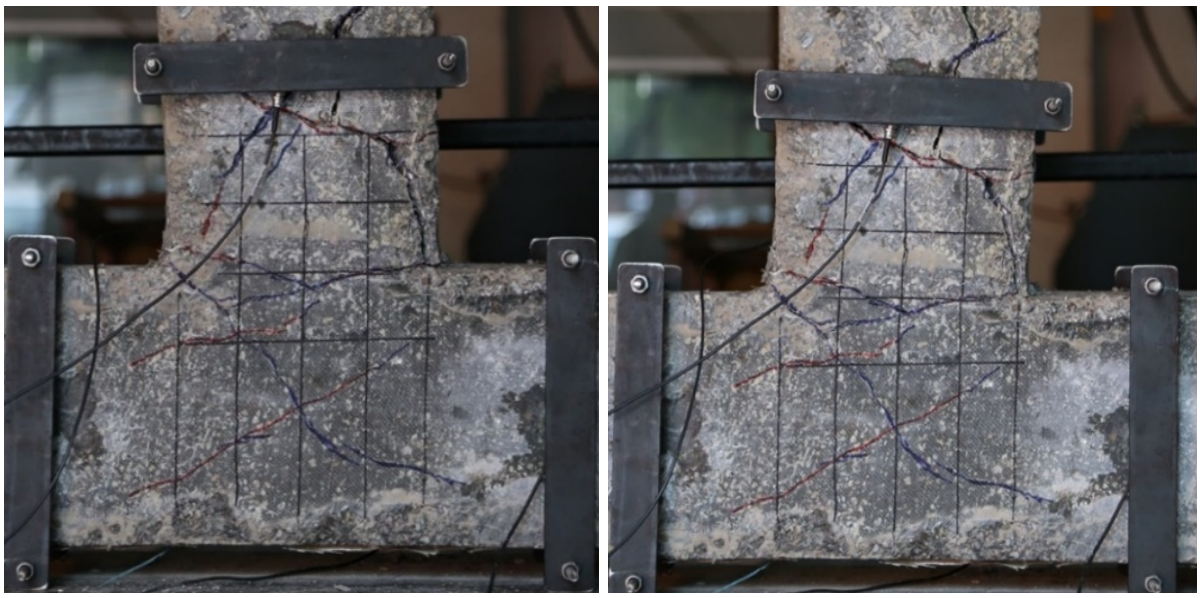

Figure 5.47: Crack formation of BCJ sample SPCR2

Maximum values of displacement and load are higher in the forward cycle than in the reverse cycle because there is a difference in longitudinal reinforcement on the top and bottom face of the BCJ beam resulting in a higher moment of resistance of the beam in the forward than reverse load direction. The maximum displacement achieved by the retrofitted samples is higher than the ultimate displacement design capacity. Similarly, the maximum load achieved without failure is higher than the ultimate load-carrying capacity of BCJ SPC1. Similarly, the maximum load of 27 kN in the forward direction and 20 kN in the reverse direction has been observed for BCJ sample SPCR2. The maximum displacement of the retrofitted samples SPCR2 is also higher than the ultimate design load capacity. Thus, it can be concluded that the ECC retrofitted non-ductile samples have achieved desired load and displacement capacities.

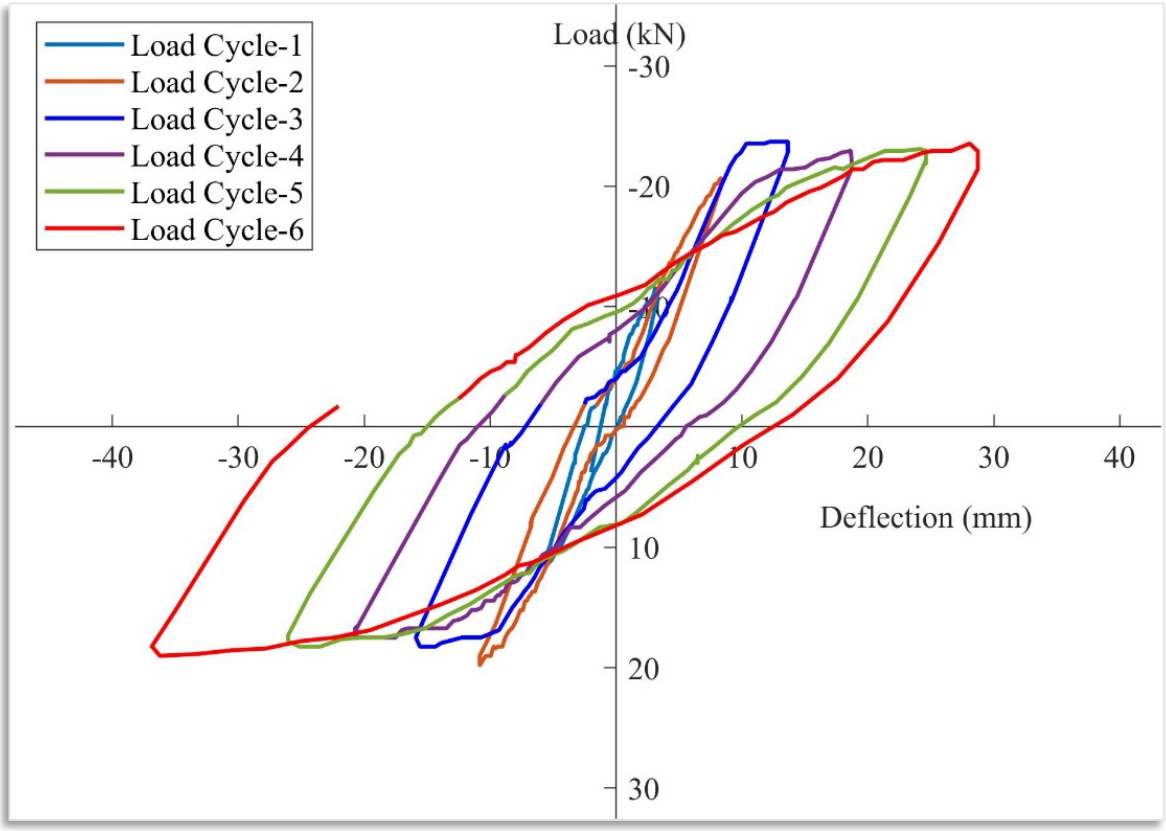

Figure 5.48: Load Vs Deflection of SPCR1

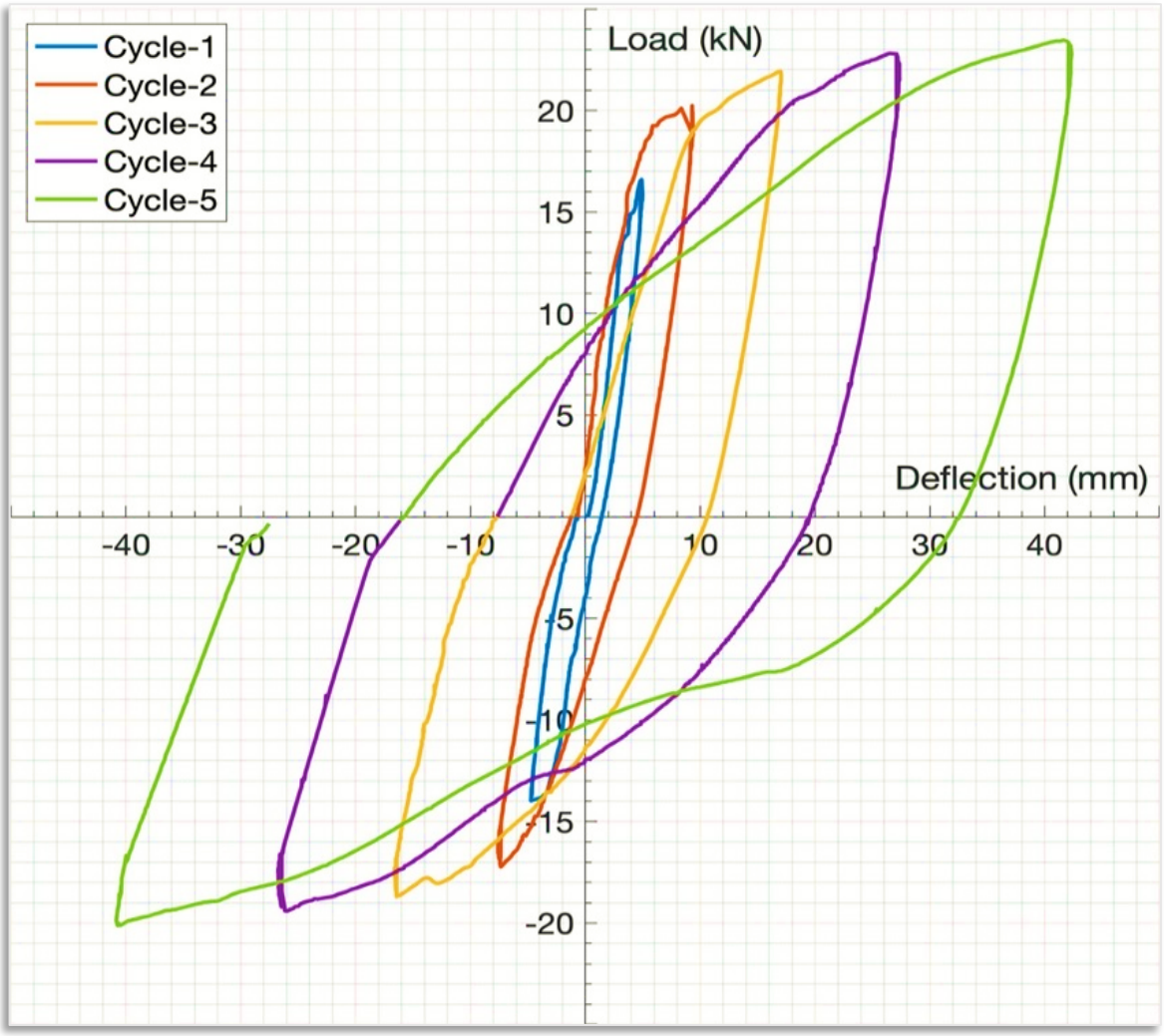

Figure 5.49: Load Vs Deflection plot of SPCR2

5.5.2.1 Energy Dissipated

The energy dissipated capacity of the structure under cyclic loads is required to precisely know the cyclic behaviour of RC members. The complete procedure has already been explained in section 5.3.3.1. The values obtained have been graphically shown in Figure 5.50. As in the case of control samples, there is a close relationship between Energy dissipated and AE energy. Thus, AE energy parameter can be utilised in place of energy dissipated if a mathematical functional relationship is obtained between these two parameters. The formation of the equation shall be discussed in detail in the coming sections.

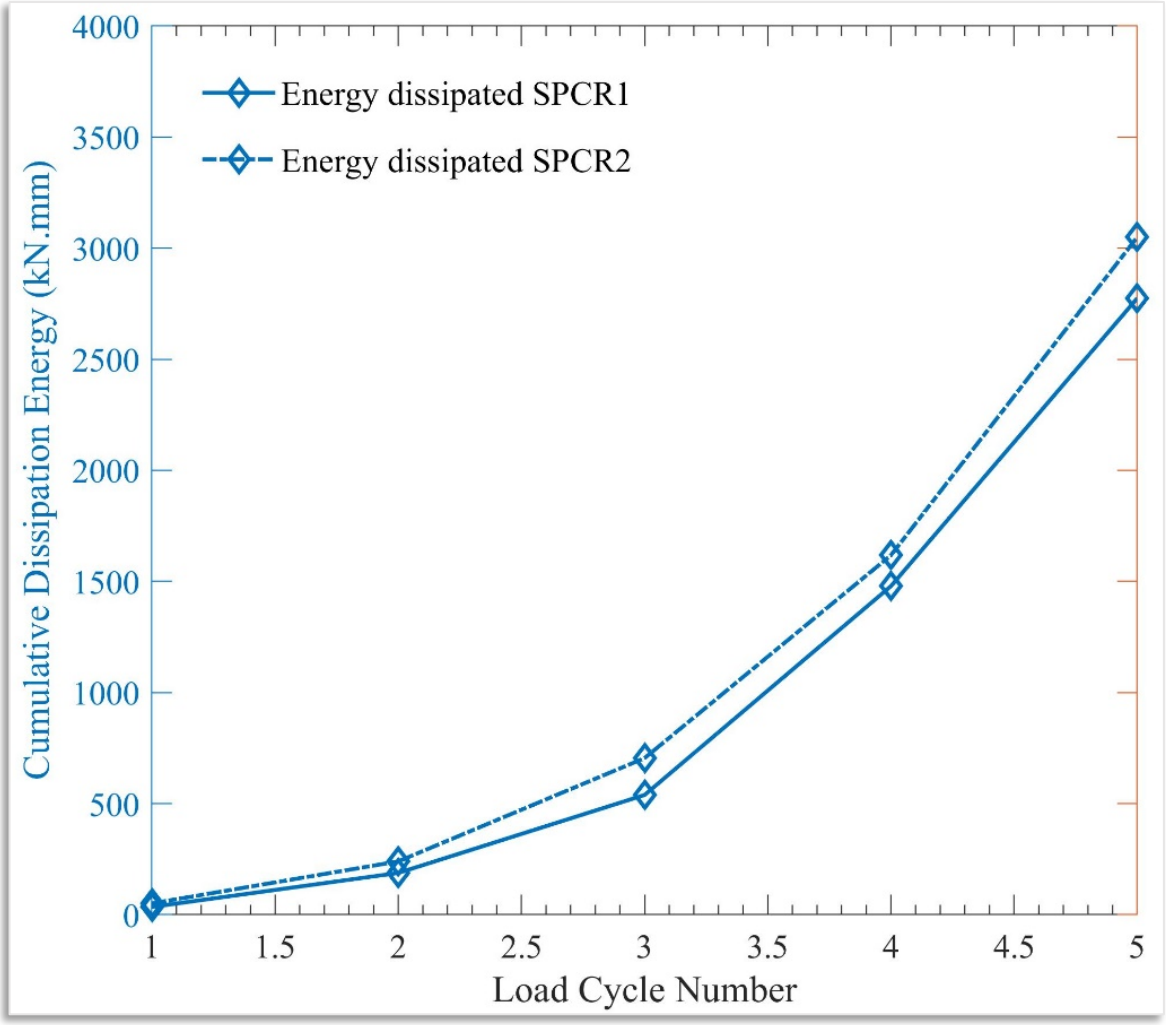

Figure 5.50: Energy Dissipated for SPCR1 and SPCR2

5.5.3 Derived parameters from load deflection for retrofitted samples

5.5.3.1 Stiffness factor (SF)

Stiffness has been worked out from the load-deflection plot, presented in Figures 5.48 and 5.49 for BCJ samples SPCR1 and SPCR2, respectively. The complete procedure has already been explained under section 5.3.3.2. The values of SF have been graphically shown in Figures 5.51 and 5.52. The trend of variation of stiffness degradation is similar to that of control BCJ samples. Thus, it can be said that ECC retrofitted samples behaved close to control samples from a stiffness resistance point of view.

5.5.3.2 Ductility Factor (DF)

The ductility factor (DF) is computed as the ratio of maximum deflection to yield deflection. The complete procedure has already been explained under section 5.3.3.3. The values obtained for samples SPCR1 and SPCR2 have been presented graphically in Figures 5.53 and 5.54, respectively. The trend of variation of ductility factors is similar to control BCJ samples. Thus, it can be said that ECC retrofitted samples behaved close to control samples from a ductility point of view.

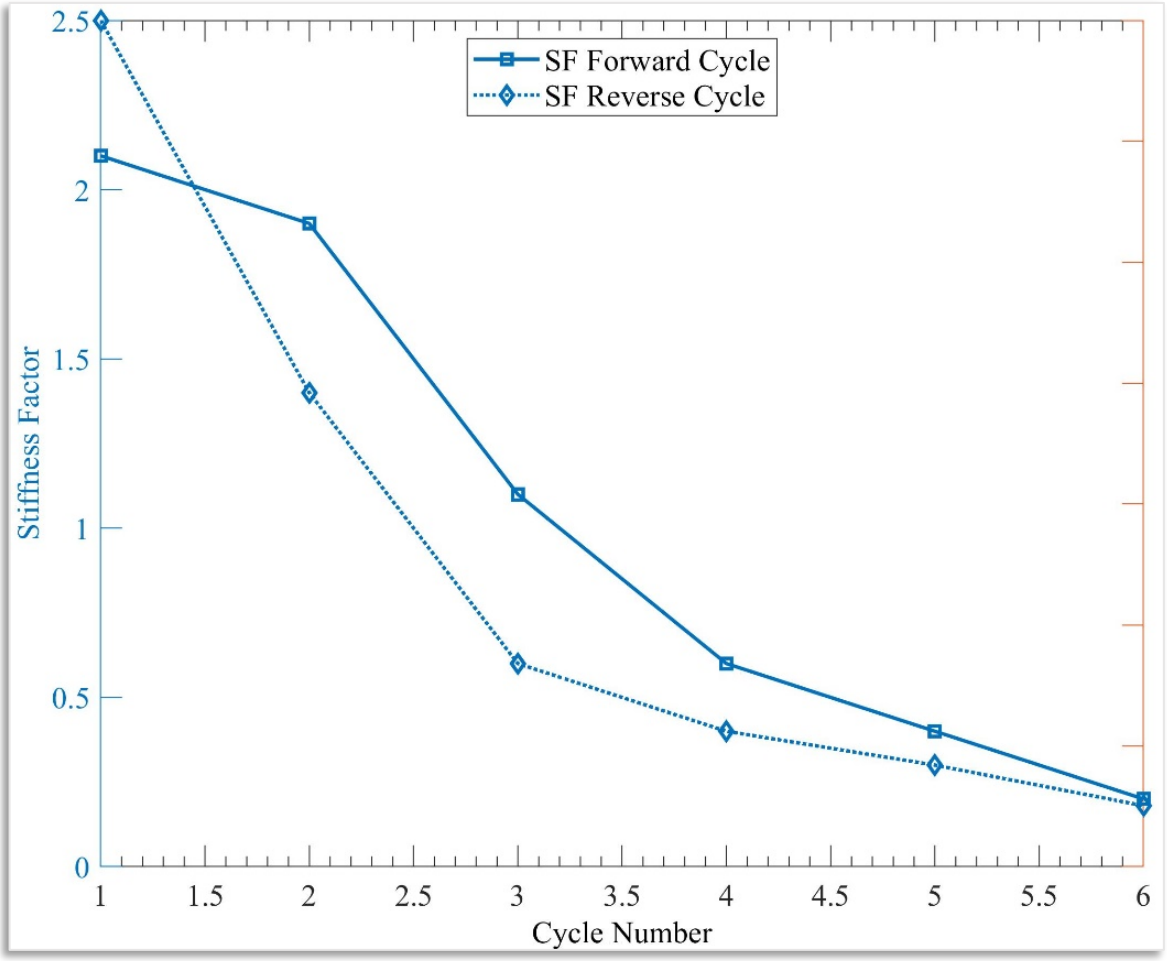

Figure 5.51: Stiffness factors for SPCR1

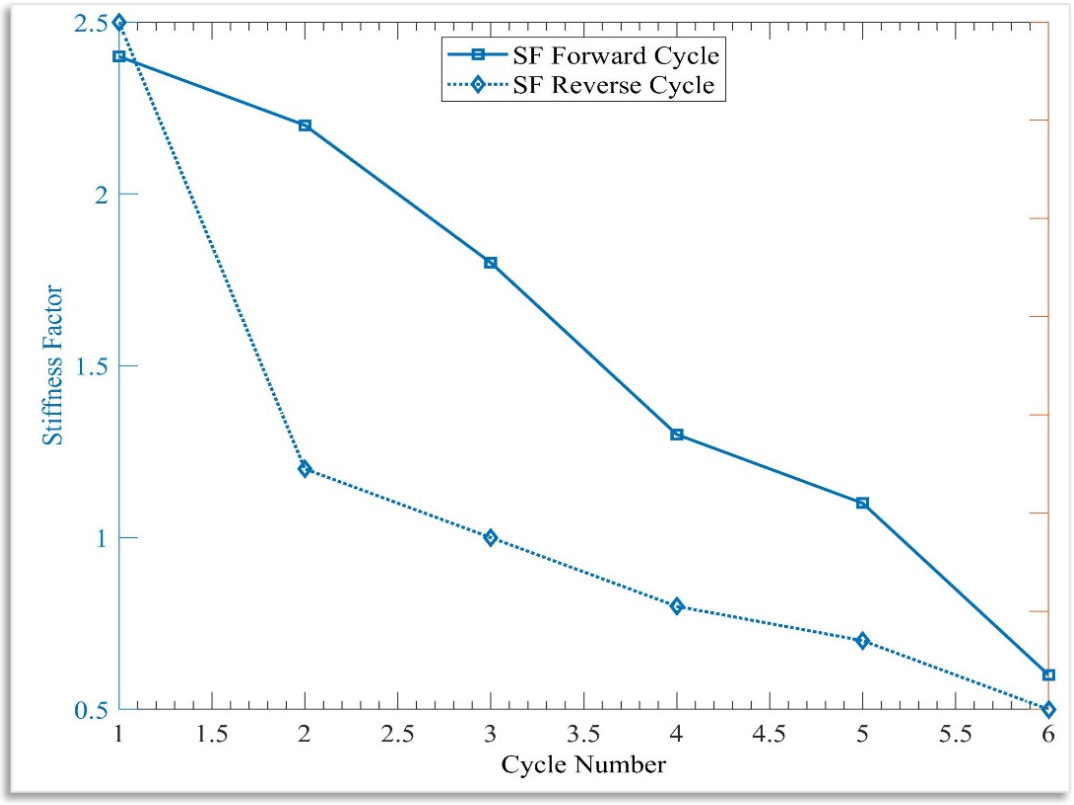

Figure 5.52: Stiffness Factors for SPCR2

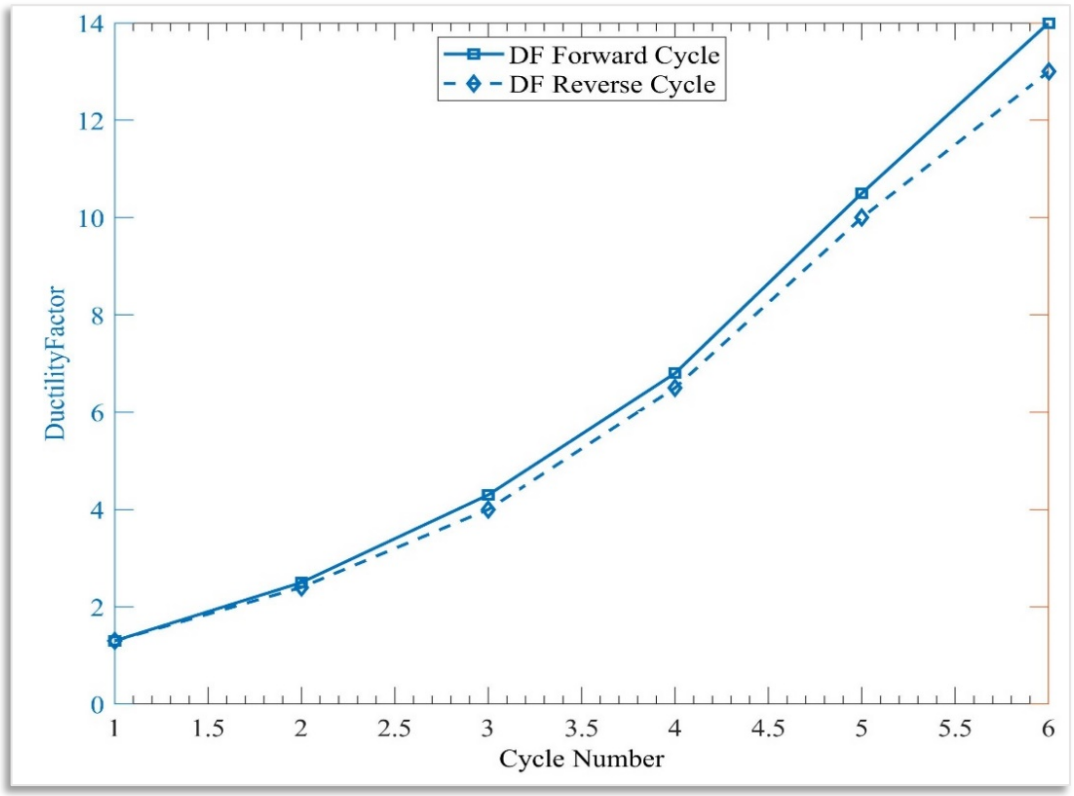

Figure 5.53: Ductility Factor SPCR1

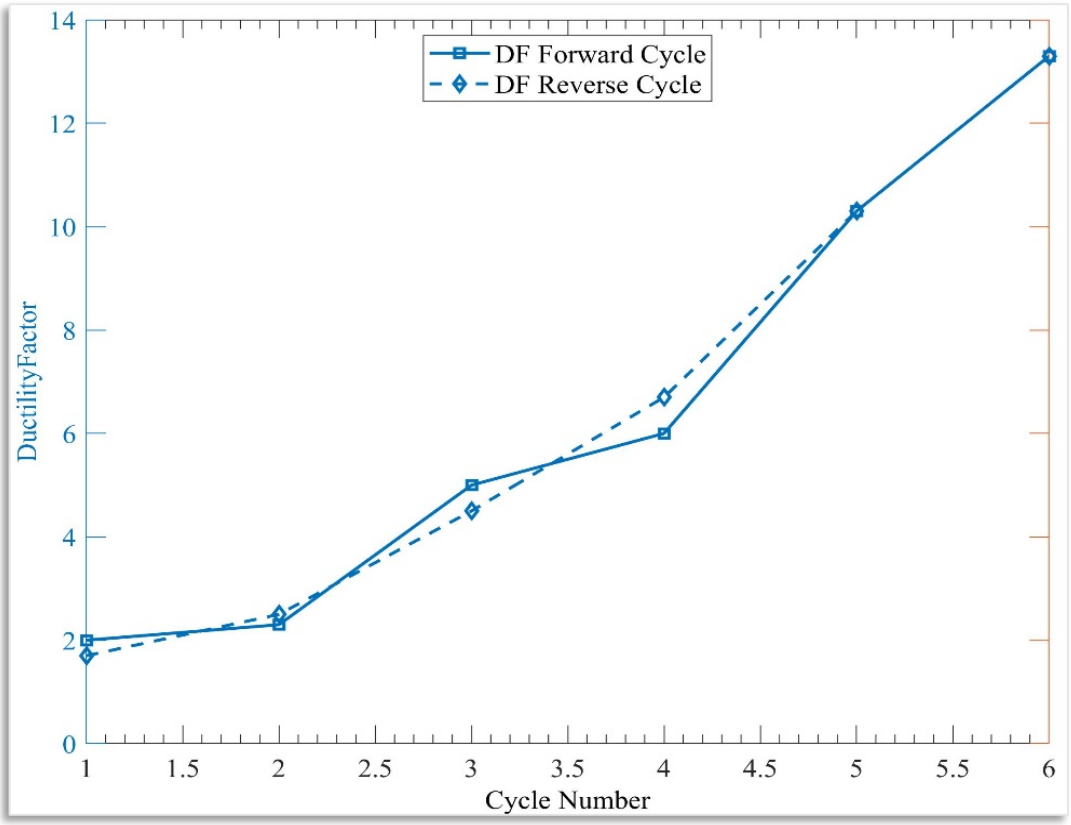

Figure 5.54: Ductility Factor SPCR2

5.5.4 AE Monitoring of retrofitted samples

5.5.4.1 AE Event Mapping

As in the case of control BCJ samples, most of the events fall within the sample area. However, some dots fall outside the area because of variations in wave velocity. As explained in section 5.4.1, more research is required to predict the source location accurately.

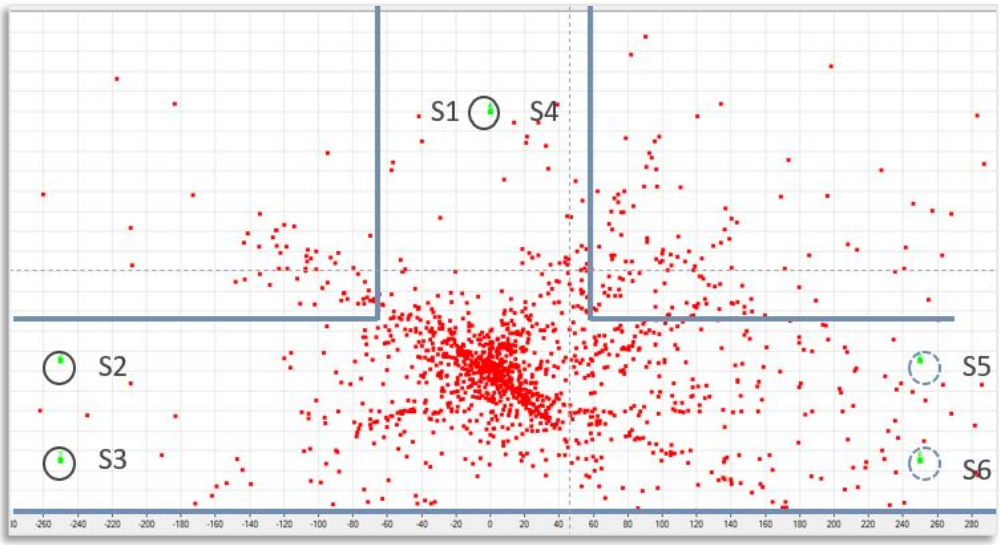

Figure 5.55: AE Hit MAP for SPCR1

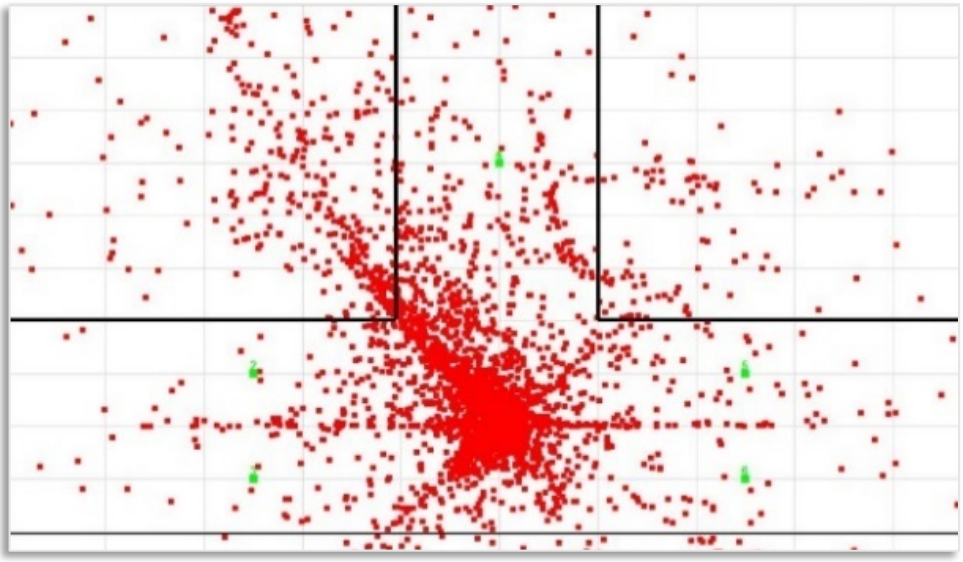

Figure 5.56: AE Hit MAP for SPCR2

5.5.4.2 AE hits and AE Energy

Variation of cumulative AE hits and AE energy with time has been presented graphically in Figures 5.57 and 5.58 for SPC1 and SPC2, respectively, with per cent cumulative hits and cumulative energy on the left y-axis and time on the x-axis. As explained in section 5.4.2 sharp rise in the cumulative Energy and Hits graphs indicates damage. There is a clear correspondence between load variation and cumulative energy. Thus, cumulative energy graphs can be used to predict damage in the samples. Variations of cumulative AE energy with load can be seen in Figures 5.59 and 5.60 for SPCR1 and SPCR2, respectively. The AE energy cumulated at the end of the fifth cycle is about 6×10^6 mV. sec SPCR1 and about 12×10^6 mV. sec in SPCR2. The AE energy for control samples was about 4×10^7 mV. sec in SPC1 and about 5.3×10^7 mV. sec in SPC2. Thus, in retrofitted samples, the AE energy is less as compared to control samples.

Thus, damages occurring in retrofitted samples are less as compared to control samples. Thus, it can be concluded that, from an AE energy point of view, ECC material can be successfully used to retrofit BCJ samples to restore their strength. The variation of AE energy at the end of each cycle has been demonstrated in Figure 5.61. It can be seen that the AE energy of ductile sample SPCR2 retrofitted with ECC is 2 to 3 times more than the non-ductile retrofitted sample SPCR1. Thus, it can be concluded that ductile-designed samples developed higher AE energy than non-ductile samples.

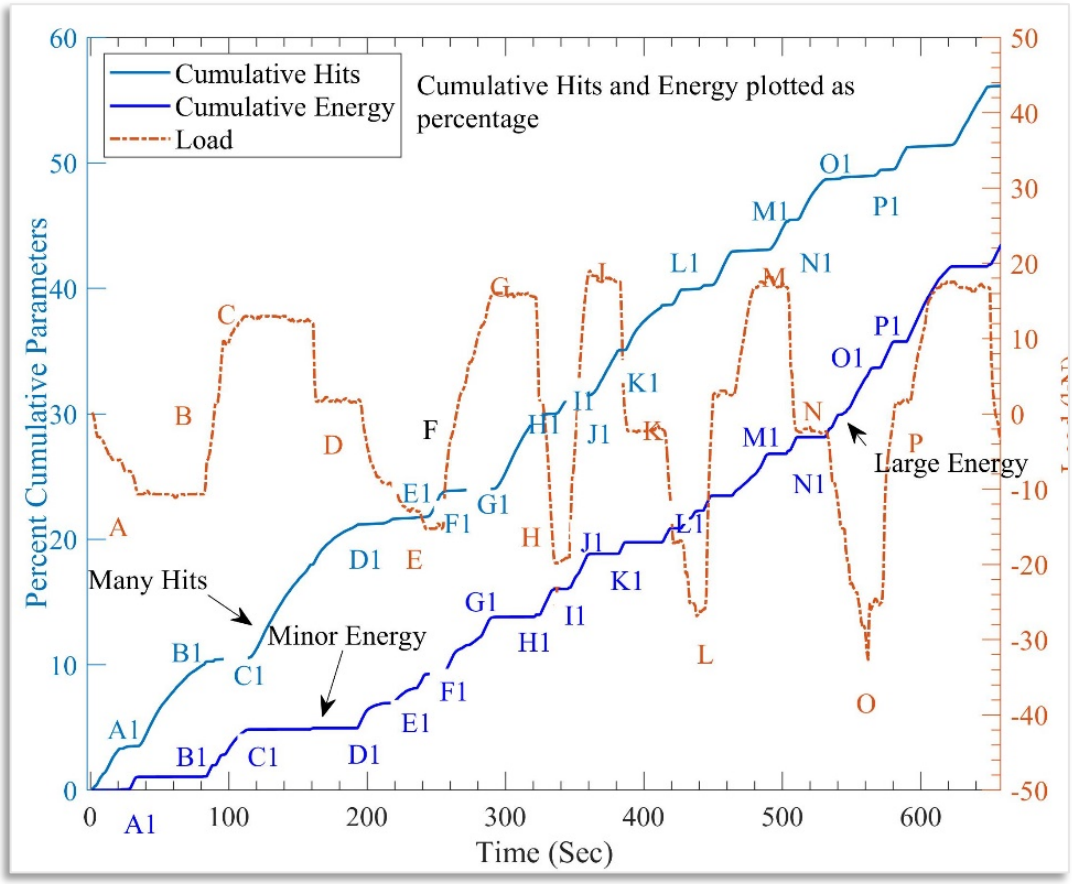

Figure 5.57: Cumulative Energy and AE Hits for SPCR1

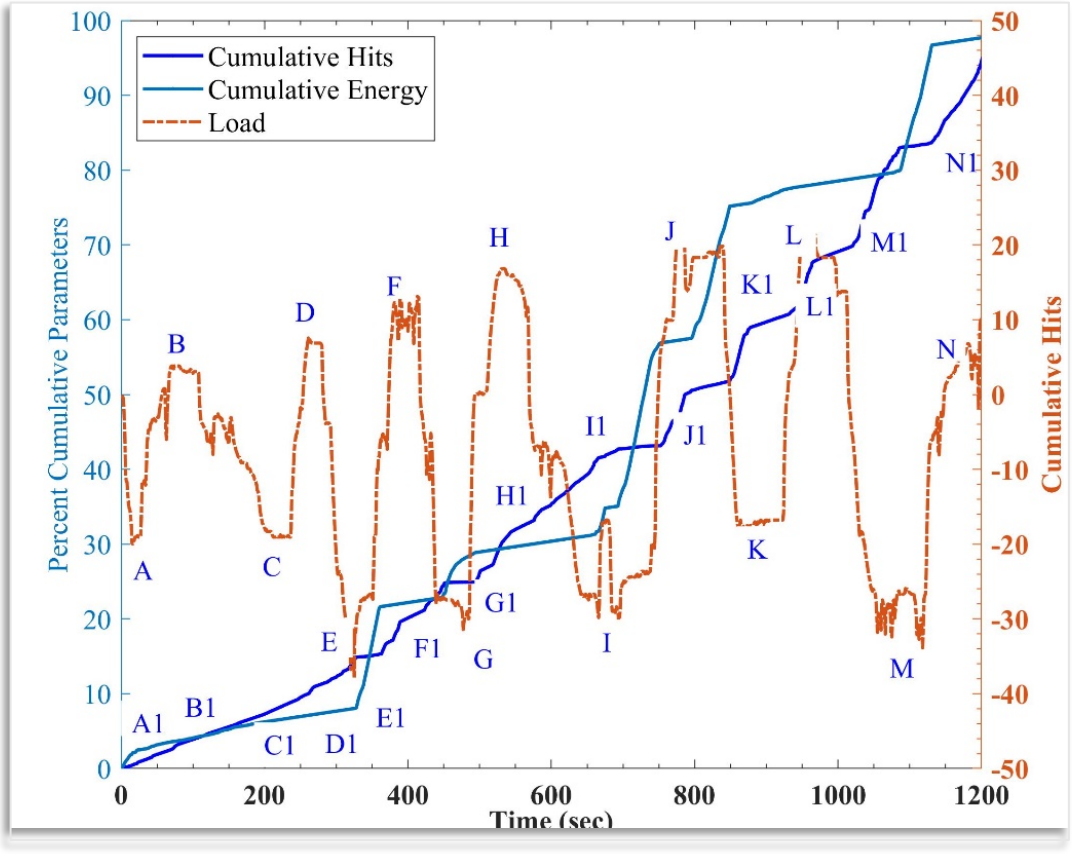

Figure 5.58: Cumulative AE Energy and Hits for SPCR2

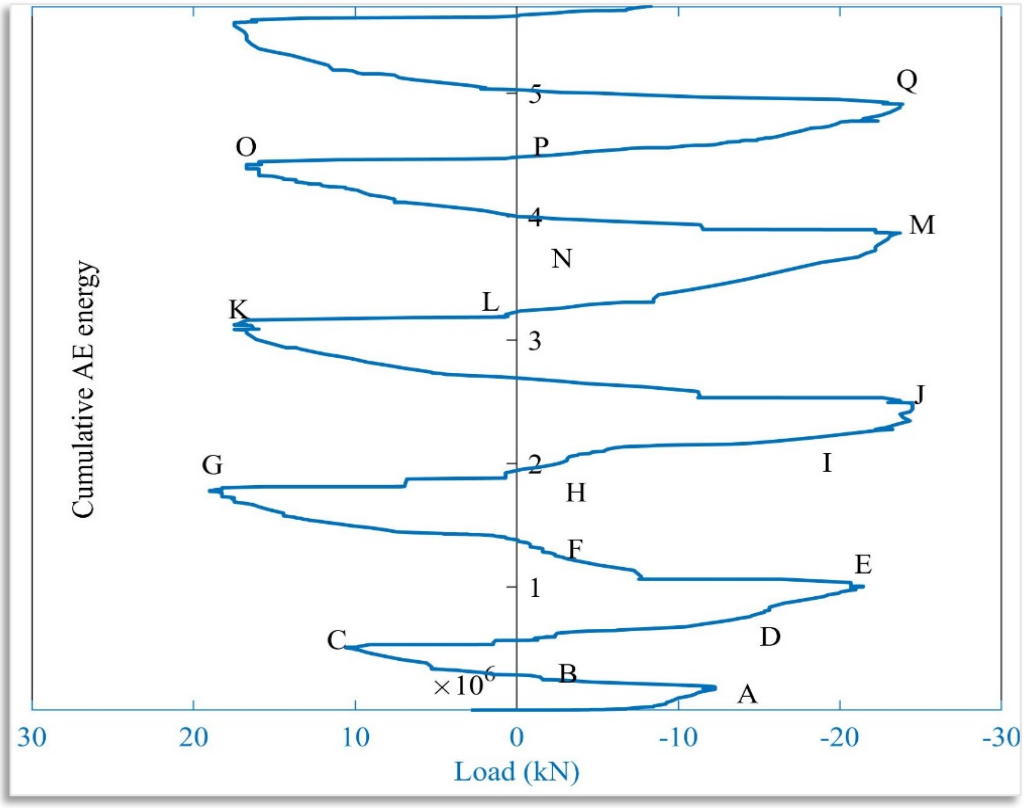

Figure 5.59: Load Vs cumulative Energy of SPCR1

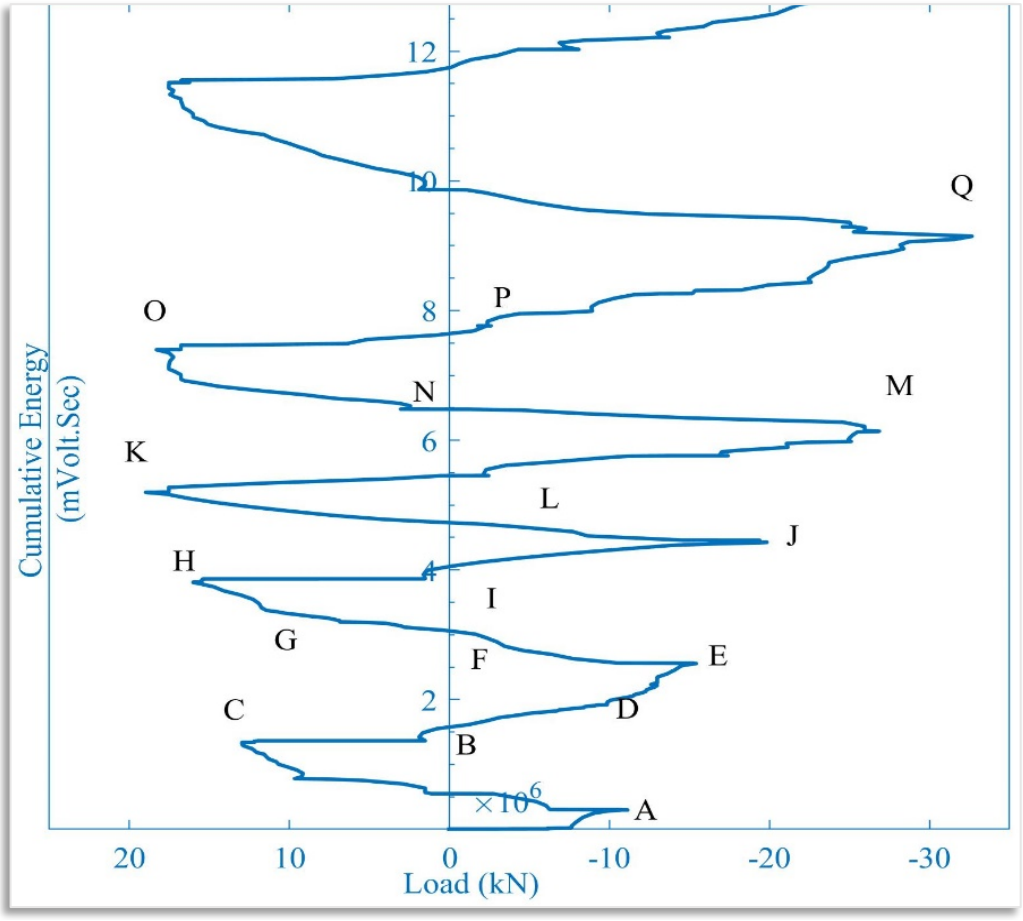

Figure 5.60: Load Vs cumulative Energy of SPCR2

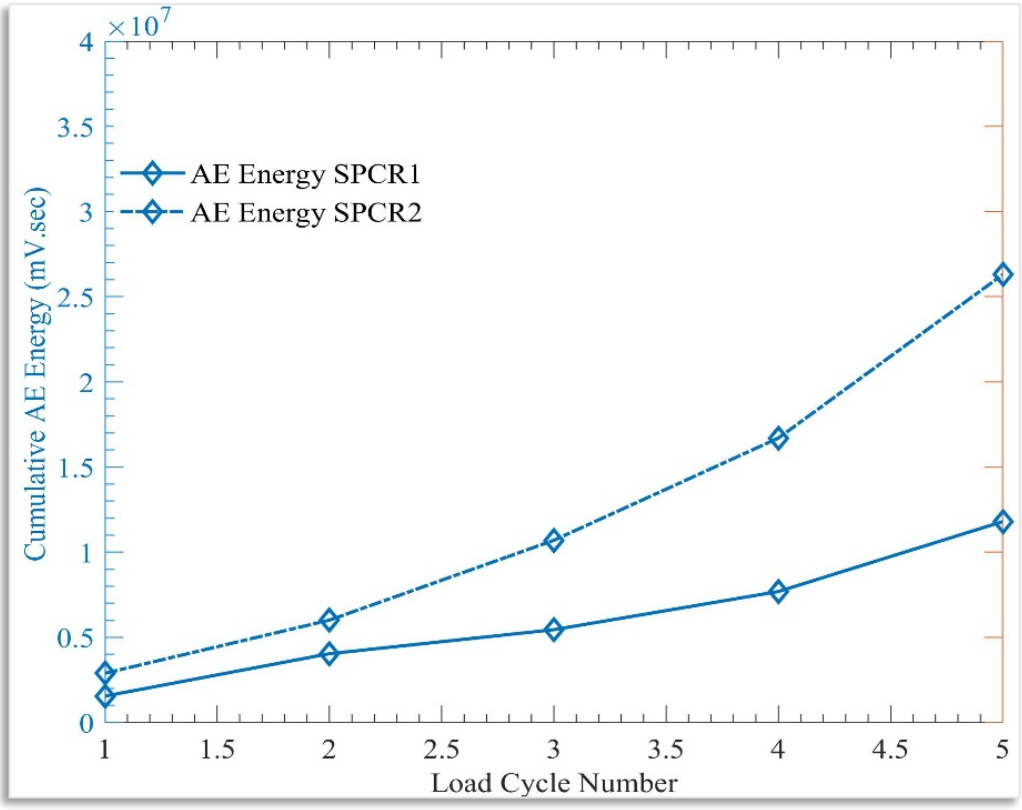

Figure 5.61: Cumulative AE energy for SPCR1 and SPCR2

5.5.4.3 Relationship between Energy dissipated and acoustic energy:

To express the relationship between the Energy-dissipated (ED) for each load cycle and Cumulated Acoustic Energy, a graph between these two parameters has been plotted and presented in Figures 5.62 and 5.63 for BCJ samples SPCR1 and SPCR2, respectively. The complete procedure has already been explained in detail under section 5.4.3. The resulting equations developed are shown below:

$$For\ SPCR1, E_{ED} = 2.086 \times 10^{-12\times} {E_{AE}}^2 + 7.008 \times 10^{-5} \times E_{AE} - 215.9 \quad (5.10)$$

$$For\ SPCR2, E_{ED} = 1.619 \times 10^{-11} {E_{AE}}^2 + 6.515 \times 10^{-5} \times E_{AE} - 194.5 \quad (5.11)$$

There is a visible variation between the relations obtained for control and retrofitted samples. This is because the two energy variables depend upon many factors such as steel reinforcement, concrete grade, type and method of loading, rate of loading, etc. Thus, to get a more accurate and matching relationship, more experimentation is required by keeping these variables into account.

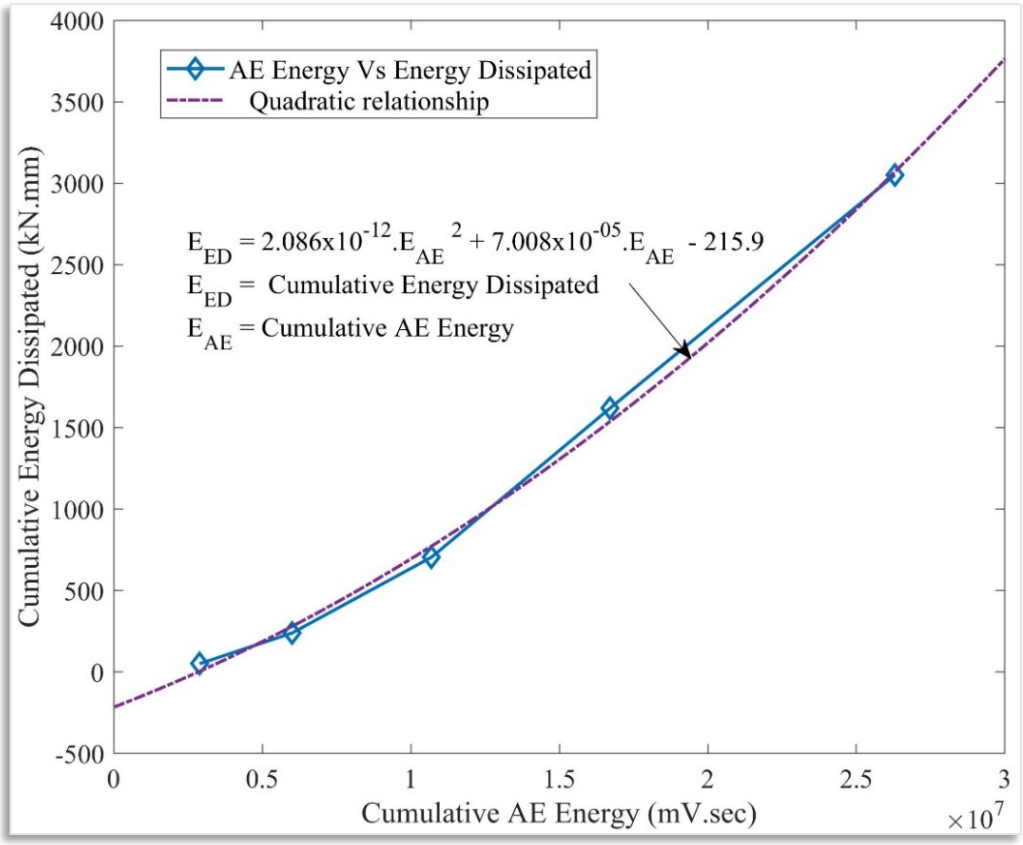

Figure 5.62: AE Energy Vs Energy Dissipated SPCR1

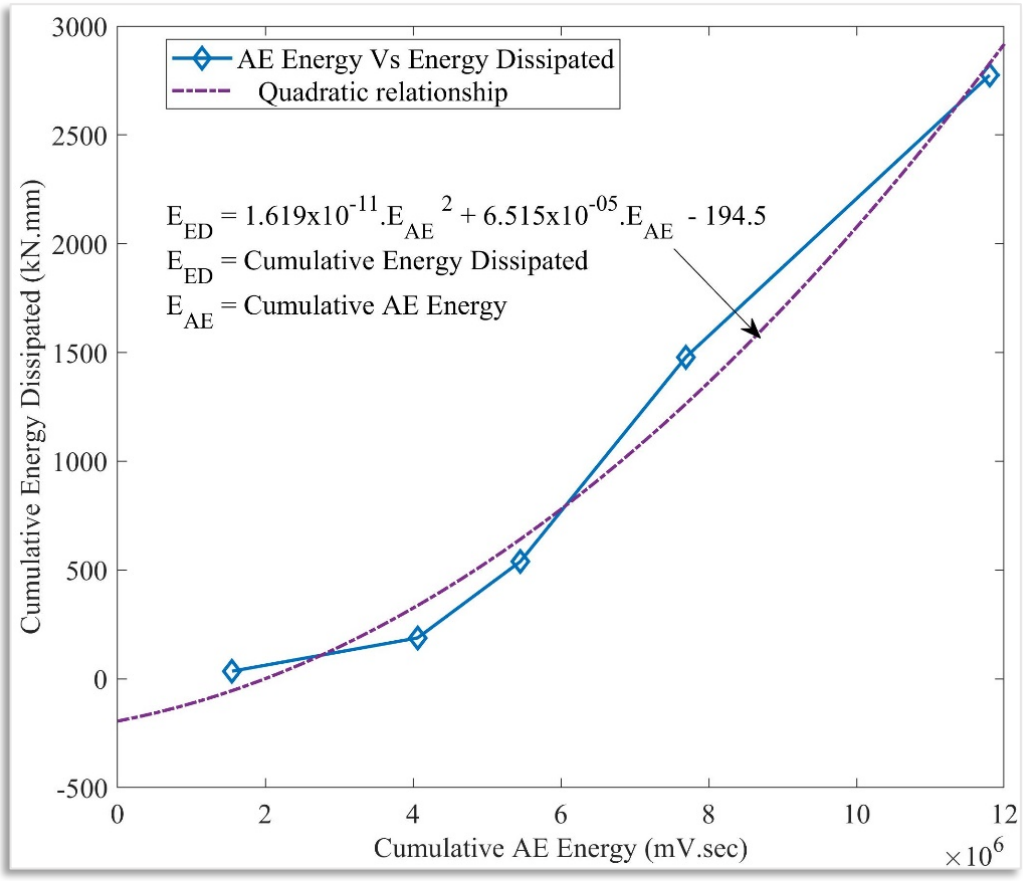

Figure 5.63: AE Energy Vs Energy Dissipated SPCR2

5.5.4.4 Crack classification of retrofitted samples

As discussed in detail under section 5.3.4.4, the RA and AF values are used to classify the cracking mode into the tensile and shear cracks. The AE data has been used to evaluate RA and AF with the help of MATLAB programming. The RA Vs AF graphs have been plotted as shown in Figures 5.64 and 5.65 for samples SPCR1 and SPCR2, respectively. For comparison purposes, refer to the Figures 5.39 and 5.40 plotted for control samples SPC1 and SPC2, respectively. In control samples, the percentage of shear cracks is lesser as compared to retrofitted samples. This indicates that in ECC retrofitted samples mixed types of failure modes are noticed, whereas, in control samples, failure is dominated by tensile mode. Thus, ECC material can be used to improve the tensile capacity of BCJ.

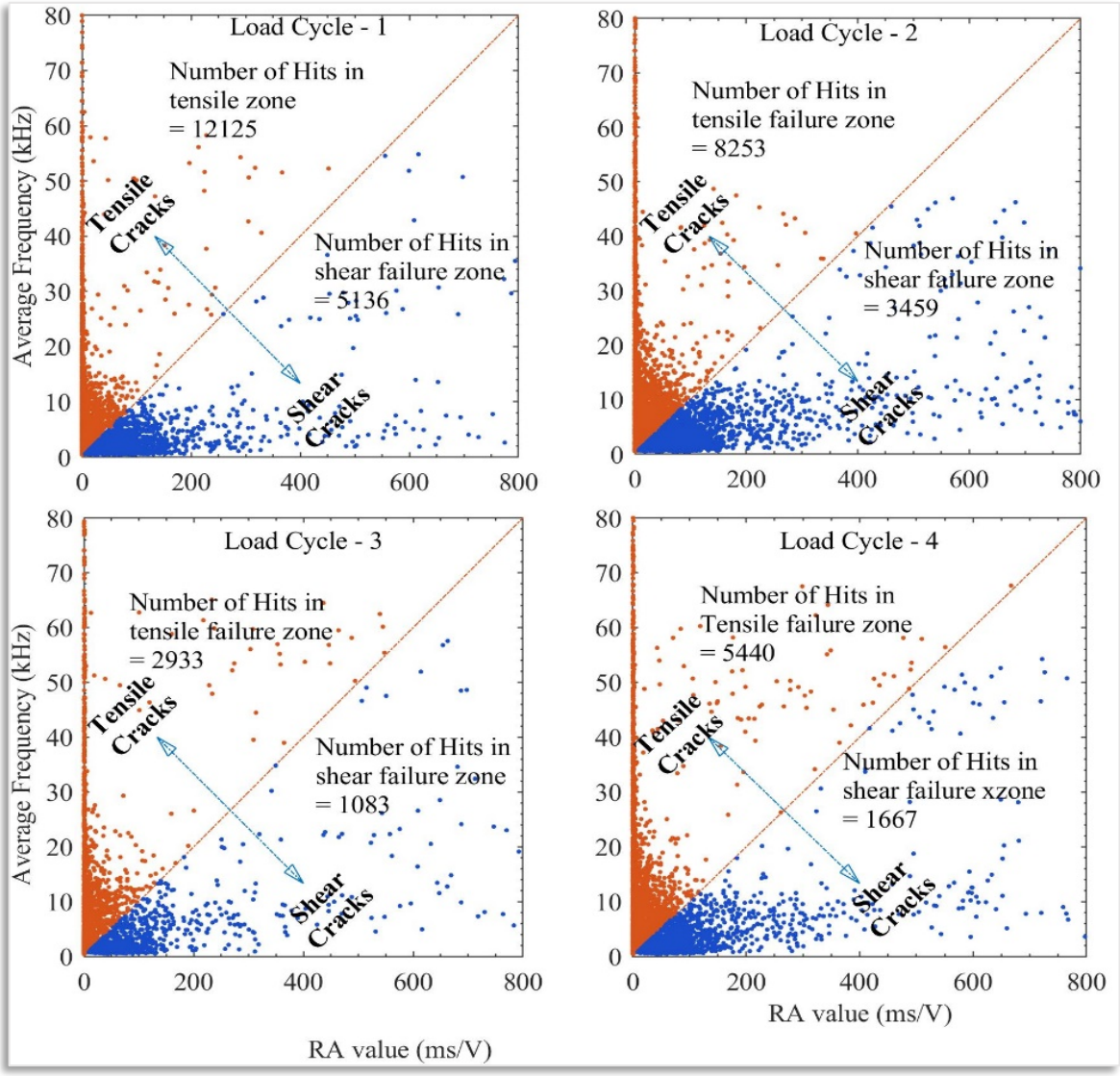

Figure 5.64: RA Vs AF for retrofitted samples SPCR1

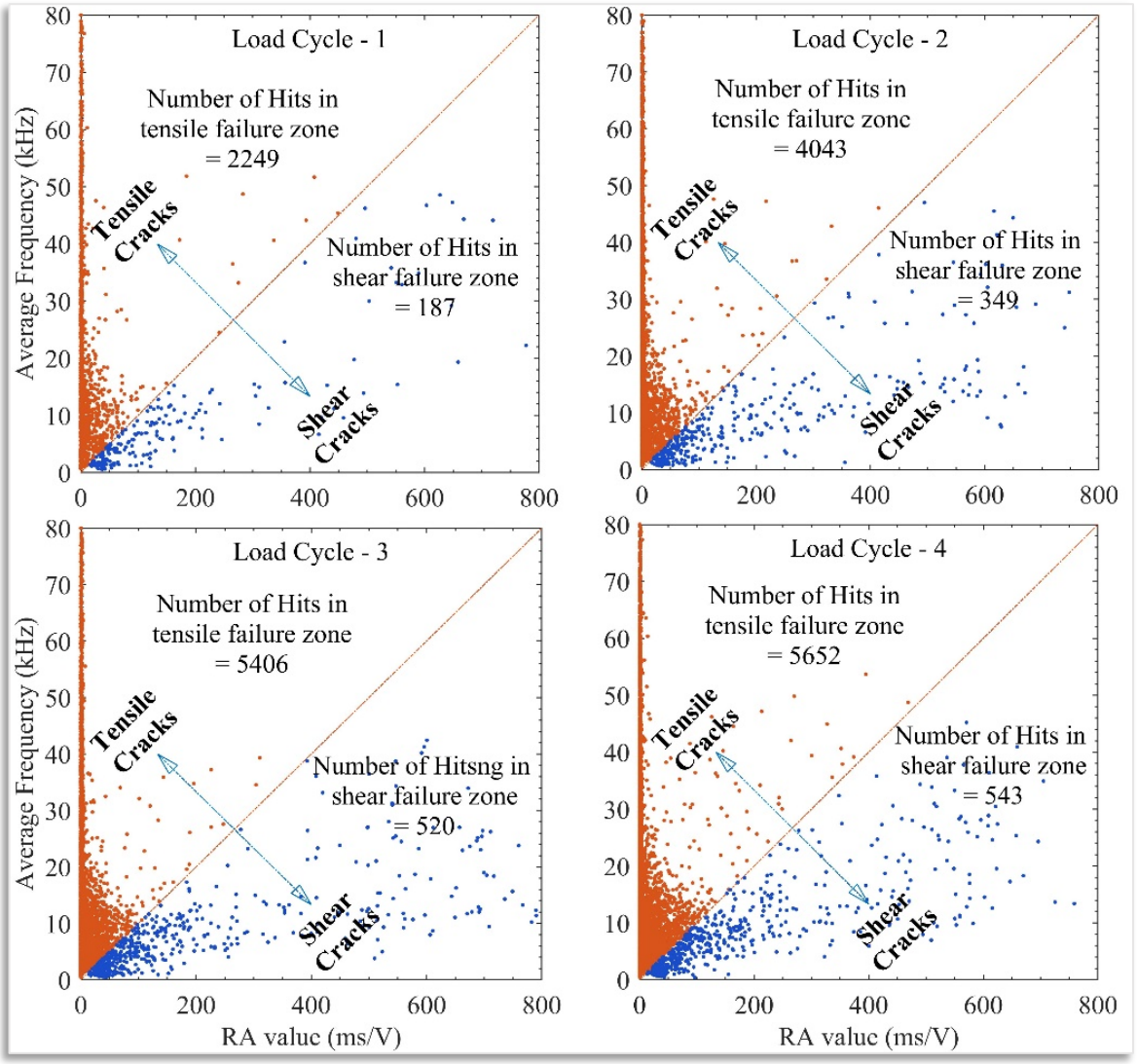

Figure 5.65: Ra Vs FA Retrofitted sample SPCR2

5.5.4.5 b-Value analysis of retrofitted samples

As already discussed in detail under section 5.4.5, the Ib-Value analysis has been carried out using AE hit data with the help of MATLAB programming. The loading time Vs Ib-Value graph has been plotted for SPR1 and SPR2, as shown in Figures 5.66 and 5.67. Lesser hits with severe damage have been observed during the first load cycle because the structure is in the elastic stage. During the elastoplastic stage concentration of hits having severe to moderate damage has been observed. The hit data has been separated for different Ib-value indexes in each quarter cycle of loading to verify the level of damage concerning Ib-values. The cumulated value of these Hits has been plotted for all the Samples, as shown in Figures 5.68 and 5.69 for SPCR1 and SPCR2, respectively. For sample SPCR1, the majority of the Hits belong to the minor Damage Level (Ib-value > 2), whereas in SPCR2, the majority of hits belong to severe damage having Ib-Value <1. In the control samples SPC1 and SPC2 (refer to Figures 5.44 and 5.45), the

majority of hits belong to minor damage in both samples.

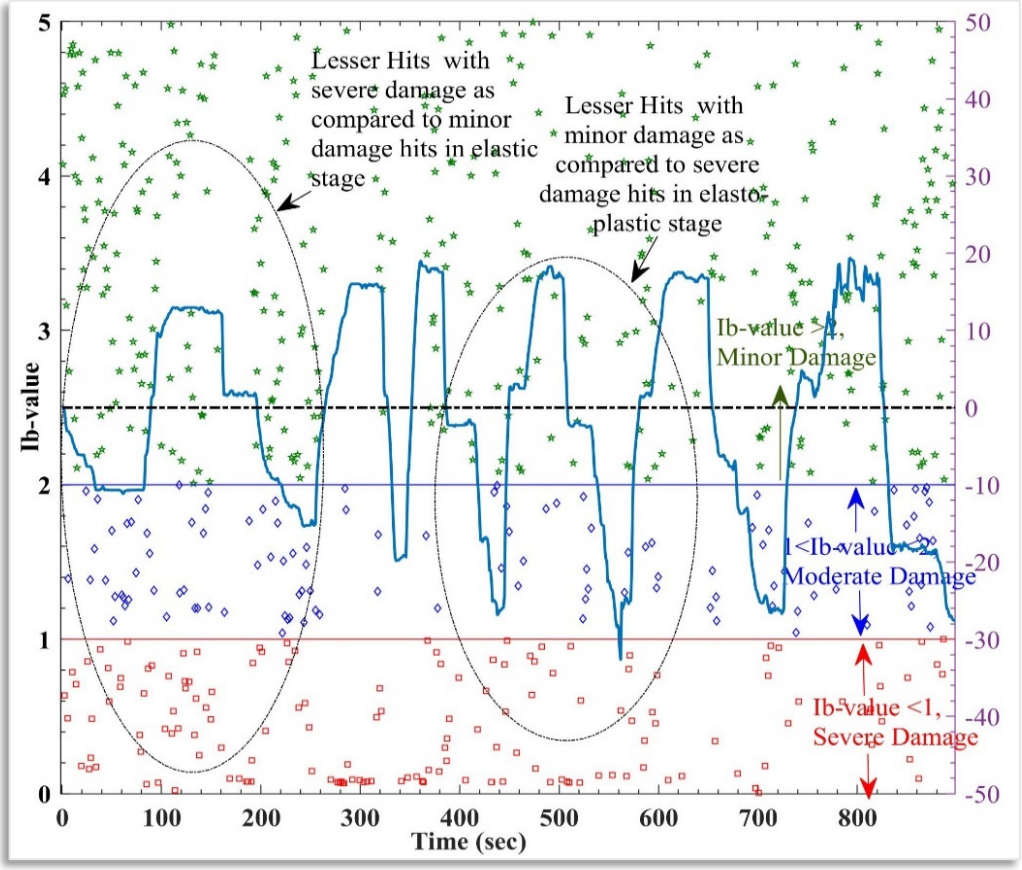

Figure 5.66: Ib-value retrofitted sample SPCR1

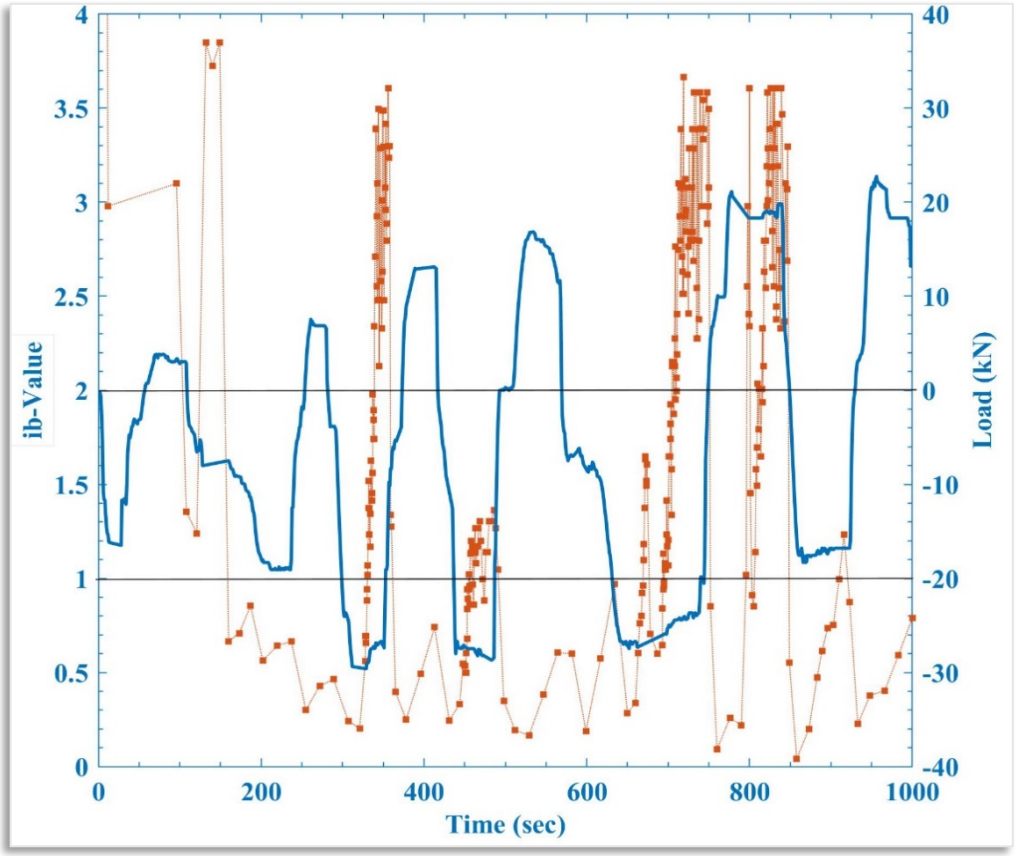

Figure 5.67: Ib-value analysis SPCR2

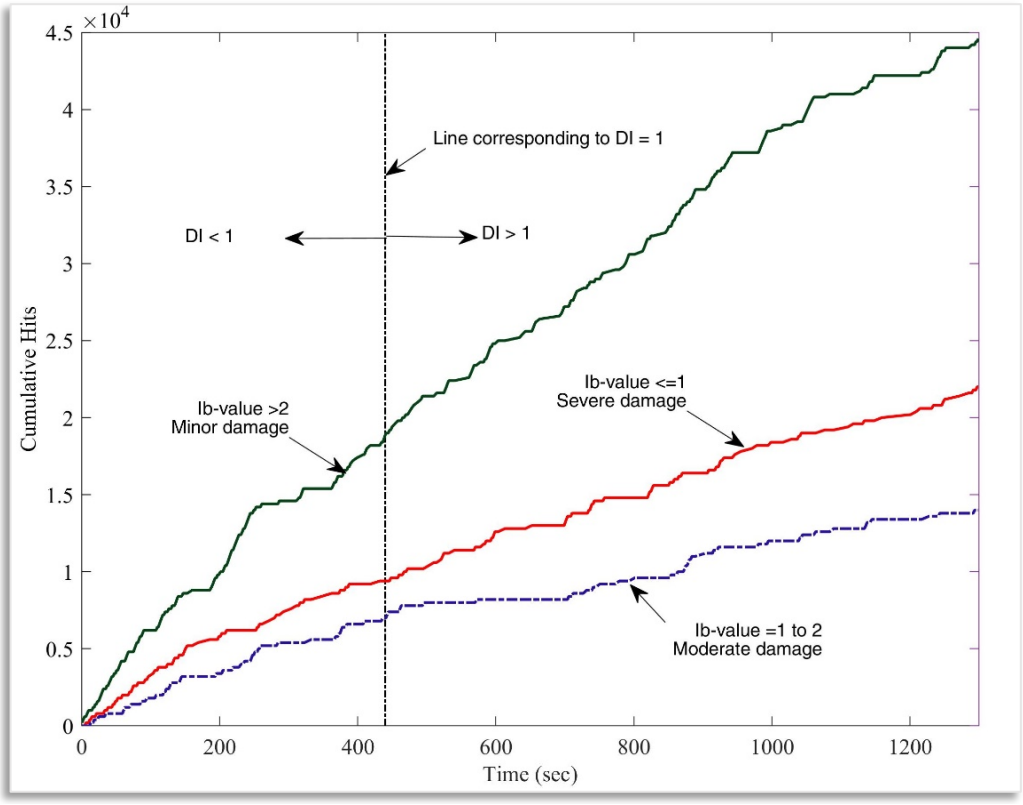

Figure 5.68: Ib-values based hits for SPCR1

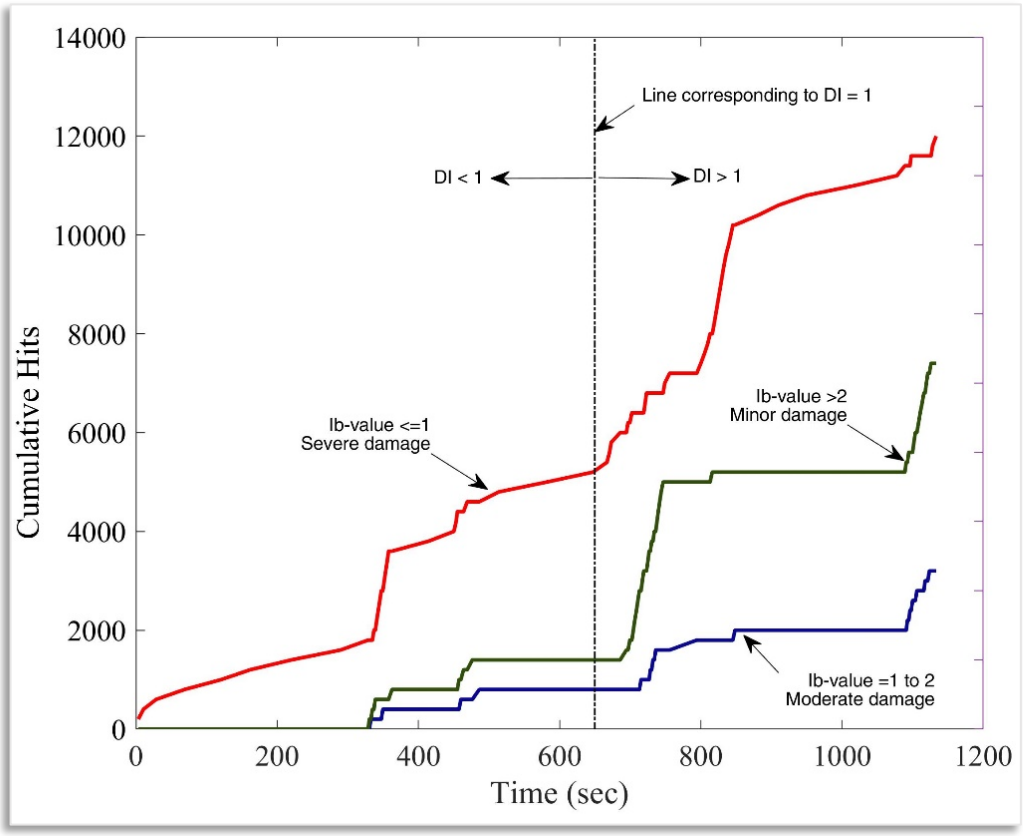

Figure 5.69: Ib-values based hits for SPCR2

Table 5.2: Comparison of control and retrofitted samples from load-deformation

Sr.	Parameter	Ductility	Control BCJ	Retrofitted BCJ	Variations
1	Ultimate Load	Non-ductile	19.5 kN	19.8 kN	+0.3 kN
	Ultimate Load	Ductile	25 kN	19.5 kN	-4.5 kN
2	Ultimate Deflection	Non-ductile	11.5 mm	16.5 mm	+5mm
	Ultimate Deflection	Ductile	35.3 mm	28.8 mm	-6.5mm
3	Energy Dissipated up to DI=1	Non-ductile	523 kN.mm	510 kNmm	≈ same
		Ductile	1888 kN.mm	723 kNmm	≈ 0.4 times

Table 5.3: Comparison of control and retrofitted samples from load-deformation

Sr.	Parameter	Ductility	Control BCJ	Retrofitted BCJ	Variations
1	Tensile Hits up to DI=1	Non-ductile	7100	23300	≈ 3 times
		Ductile	40800	11700	≈ 0.3 times
2	Shear Hits up to DI=1	Non-ductile	3200	9680	≈ 3 times
		Ductile	7600	1600	≈ 0.2 times
3	Hits for severe damage (Ib-value <1) up to DI=1	Non-ductile	2380 (17%)	9340 (11.5%)	-6.5%
		Ductile	8520 (13%)	4700 (20%)	+7%
4	Ultimate AE Energy	Non-ductile	3.13 x106	1.275 x107	≈ 4 times
		Ductile	12.33 x106	4 x107	≈ 3.2 times

5.6 SUMMARY

The analysed data obtained from all the tests for ductile and non-ductile BCJ samples before and after retrofitting has been tabulated in Tables 5.2 and 5.3 to compare the result. Overall, ductile BCJ (SPC2) has better ductility, higher load-carrying capacity, and higher

ultimate displacement values than non-ductile BCJ (SPC1). Thus, SPC2 has better seismic performance than SPC. After repairing the BCJ using ECC, restoring the properties as per design requirements is possible. Hence, ECC can be successfully utilised as a retrofitting material for RC BCJ.

CHAPTER-6. DAMAGE QUANTIFICATION USING AE TECHNIQUE

6.1 GENERAL

The damages in RC structures are often associated with the under-performance of the structural systems. It is essential to localise such damages, followed by remedial measures for the proper functioning of the structural system during its design life. The acoustic emission technique is an effective non-destructive technique employed for damage localisation. This chapter describes the theoretical methods, currently in practice, for damage quantification based on acoustic emission parameters.

When the specimen is subjected to internal or external stress, strain energy is released. The strain energy spreads within the material in the form of an elastic wave known as an AE signal. It has been described in detail in chapter 3 that AE signals are generated by the localized internal energy released during damage to the sample. The analysis of the AE signals permits the cracks to be characterized and the material condition to be assessed. In civil engineering structures, the defects like generation of cracks, yielding of concrete and steel, failure of bonds, fibre failure etc., generate AE waves. Therefore, the AE technique can be utilised to locate the damage occurrence and know the type and extent of such structural damage.

Data recorded from the AE sensors may be used in localizing the damage, which is one of the most important criteria for detecting damage and its classification. The researchers carried out various studies concerning AE source localisation. Once the source is localised, it is essential to estimate the extent of damage to be analysed based on AE data. This chapter describes various research efforts for damage quantification based on acoustic emission data. Based on this research, appropriate methods have been employed for the damage quantification of beam-column joint samples. A new damage model, named Novel Damage Index, has also been developed in this study. Different damage states have been proposed for assessing the condition of the structure based on a novel damage index.

6.2 DAMAGE QUANTIFICATION METHODS

6.2.1 Intensity charts

Ledeczi et al. (2009)[133] proposed an intensity chart to classify AE activities into inactive, active and critically active categories. The developed chart is shown in Figure 6.1. where the vertical axis represents intensity, and the horizontal axis represents the activity of AE. The activities are recognised as critically active if the events are consistently found at peak load. These are active if events are random over the load spectrum. And lastly, inactive if no significant events are found. The average amplitude value of less than 50 dB falls in the low-intensity region. In the case of intense events, the average amplitude value lies between 50-75 dB, and in critically intense events, the average amplitude is more than 75 dB.

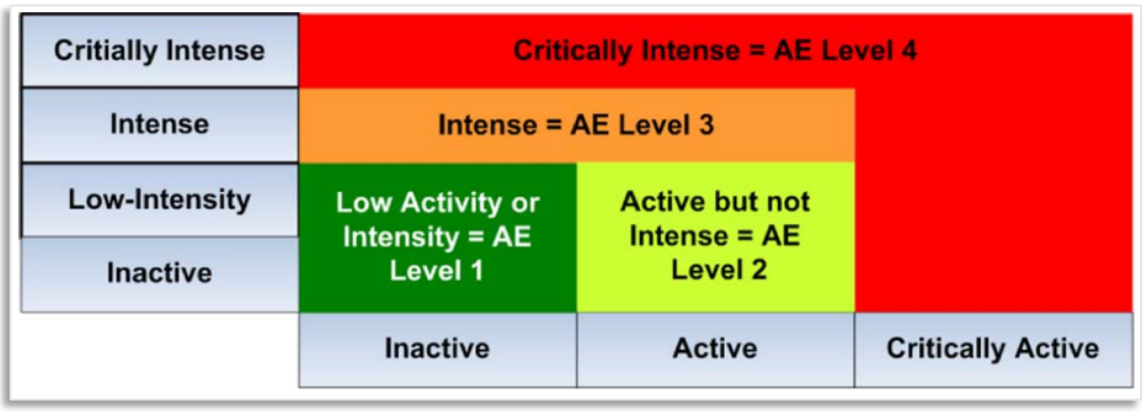

Figure 6.1: Classification of AE based on activity and intensity (Ledeczi et al.)

6.2.2 Acoustic emission count rate analysis

Behnia et al. (2014)[134] have investigated AE activity depending on the loading type and configuration. They have quantified fracture development in concrete beams by AE count rate analysis. Most of the AE activities are due to micro-cracking before the initiation of visible cracks. More AE activities were noticed due to the formation of macrocracks into the material. Further, the severity of damage in the materials increased AE activities. Gong et al. (1992)[135] have proposed a new parameter N' (Acoustic Emission Count Rate) to express AE activities expressed by equation-6.1.

$$N' = \mathrm{A}(\Delta \mathrm{K})^{n} \tag{6.1}$$

Where K is the stress intensity factor; A and n are experimental constants. The equation is

closely related to the Paris Law of fatigue crack propagation by the equation:

$$\frac{da}{d\eta} = \mathrm{C}(\Delta \mathrm{K})^m \tag{6.2}$$

Where $\frac{da}{d\eta}$ represents crack growth rate, C and m are experimental constants. The relationships among the crack safety index, crack growth rate, count rate, and ΔK for the steel bridge have been graphically represented in Figure 6.2. As seen in the figure, the stress intensity factor ranges from 0 to more than 50 and the respective five different levels of crack. Table 6.1 can also be referred to wherein Gong at el. have shown crack safety index worked out for steel bridges.

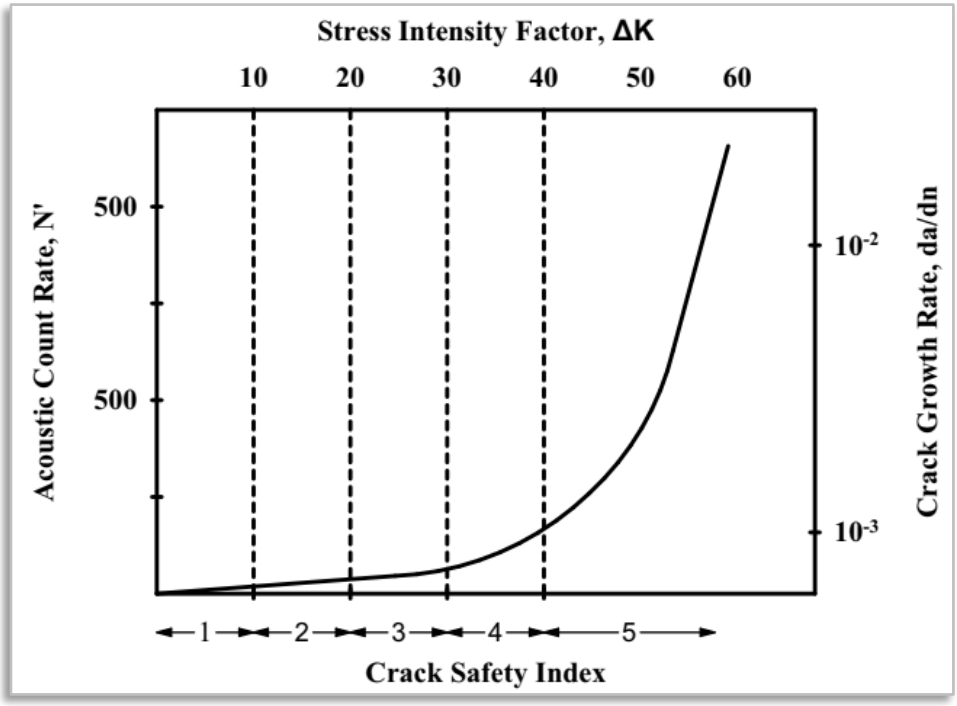

Figure 6.2: Crack safety index for steel bridge (Gong et. al)

Table 6.1: Crack safety index for steel bridge (Gong et. al)

Range of ΔK	Crack safety Index	Crack description
0<ΔK<10	1	Minor defect
10<ΔK<20	2	Slow crack growth
20<ΔK<30	3	Requires repair
30<ΔK<40	4	Dangerous
40<ΔK	5	Imminent failure

6.2.3 NDIS damage Index

Non-destructive Inspection (NDIS) method has been proposed by the Japanese Society for damage identification based on load ratio and calm ratio. The Load Ratio is defined as the ratio of load at the onset of AE activity to the previous cycle maximum load. Calm Ratio is the ratio of number of cumulative AE activities during the unloading process to the total AE activity during the last loading cycle up to the maximum. An assessment chart has been recommended by the NDIS-2421[136] which is based on these two parameters, as shown in Figure 6.3. The graph is divided into four zones of damage. Based on preliminary tests predefined classification limits need to be worked out as shown by dotted lines[137].

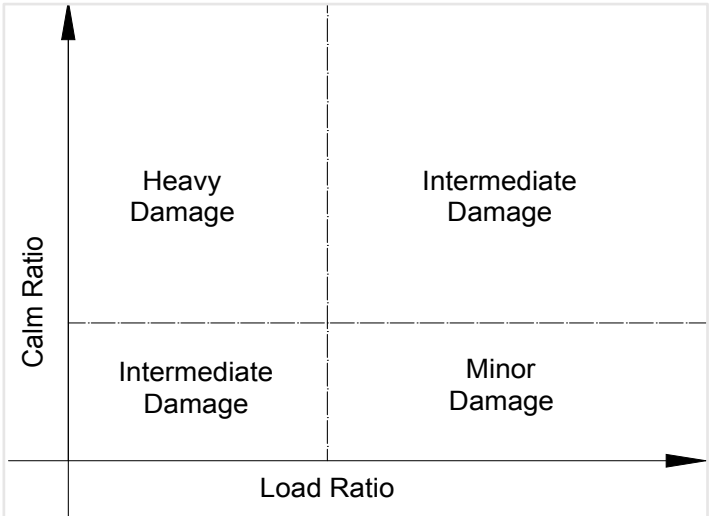

Figure 6.3: Damage Assessment as per NDIS

6.2.4 Colombo Damage index

This damage index is based on a study by Cox et al. (1993)[138] on the microcrack formation in rock and is represented by the equation:

$$D = \sum 10^{cm} \tag{6.3}$$

Where m = seismic magnitude; and c was assigned a value of 3 because the instrument acts as an accelerometer. The equation applies to a seismic response. The AE waveform also behaves similarly to the seismic waveform. Hence, the term 'm' can be replaced with AE amplitude. But since AE amplitude is measured in dB, the term 'm' should be replaced with AE-amplitude/20. Thus, the equation can be modified for AE amplitude as shown in Equation-(6.4).

$$D = \sum 10^{\frac{3A_{dB}}{20}} \quad (6.4)$$

where A_{dB} is AE hit amplitude in dB. As per Colombo's investigation, the parameter is descriptive of damage and has been related to the volume of the cracks, i.e., to a change of porosity in the concrete.

6.2.5 Damage Index Based on Kaiser Effect

The Kaiser effect has been discussed in detail under section-3.3.2.3. According to Kaiser's theory, little or no acoustic emission will be recorded before the previous maximum stress level is achieved. When BCJ is tested under cyclic loads, damage can be observed by observing AE activities after each load cycle and damage levels can be estimated by using the Felicity ratio which is the ratio of load at the onset of AE activities to the previous cycle maximum load. A value of Felicity ratio less than one is an indication of the damage in the material. In stable conditions, the Felicity ratio >1 indicates no damage, as seen at point D, where FR is more than 1. In cycle-2, FR is < 1, which indicates the start of damage. The damage in the third cycle is even more because the Felicity ratio is lesser than in the second cycle.

6.2.6 Acoustic emission signal strength analysis

The AE signal strength can be expressed as a function of the AE amplitude and duration of the AE signal. It provides reliable information regarding damage assessment. The AE hits are often influenced by loading configuration. Therefore, cumulative signal strength (CSS) offers a better parameter for damage evaluation in AET. CSS increases with the micro-crack formation during initial loading at a slower rate. Its value increases at a higher rate when the loading enters the elastoplastic stage. The rate of increase continues at an even higher rate until the collapse stage. The higher the rate of AE signal strength, the more damage to the material[139].

6.2.7 Intensity Index based on Historic and Severity indices

Intensity indices quantify damage based on the AE signal strength parameter. This analysis is a statistical approach. At a particular time, the historic index is the ratio of the

average signal strength of recent hits to the average signal strength of all the hits until that time. It is represented by the equation-(6.5)

$$H(I) = \frac{N}{N-K}\left(\frac{\sum_{i+K+1}^{N} S_{oi}}{\sum_{i=1}^{N} S_{oi}}\right) \quad (6.5)$$

Gostautas et al. (2005)[140] have demonstrated that the severity index represents the average value of the most significant signal strength of a certain number of events. The number of such events depends on the material type, as shown in Table 6.2. It is calculated by using the equation-(6.6)

$$S_r = \frac{1}{J}\left(\sum_{i=1}^{J} S_{oi}\right) \quad (6.6)$$

Where H(I) is the historic index at time t, N = number of hits up to and including time t, S_{oi} = signal strength of the i^{th} event. K and J are empirically derived constants based on material type values for metal depending on N and are given by Nair et al. (2010)[141]

Table 6.2 Values of K and J are related to N

For Concrete[142, 143]		**For Metals**[143]	
N < = 50	K = 0	N < 15	K = 0
51< N < 200	K = N – 30	16< N <75	K = N – 15
201 < N < 500	K = 0.85 N	76 < N < 1000	K = 0.8 N
N >= 50	K = N-75	N > 1000	K = N-200
N < 50	J = 0	N < 10	J = 0
N > 50	J = 50	N > 10	J = 10

Signal strength data collected by each sensor can be used to evaluate these indices. The $H(I)$ Vs S_r charts help identify different levels of damage, as shown in Figure 6.4. Insignificant acoustic emission activities are seen in Zone A representing the sound state of the structure. No, follow up required during such activities. AE activities falling in Zone B is an indication of minor damage. Such damage is caused by minor surface cracks. Zone C belongs to intermediate damage where the proper evaluation of the structural state is required. Zone D is a follow-up zone, representing substantial damage requiring further inspection. Finally, Zone

E represents an area of major damage. This requires instant closure and frequent follow-up inspections of the structure.

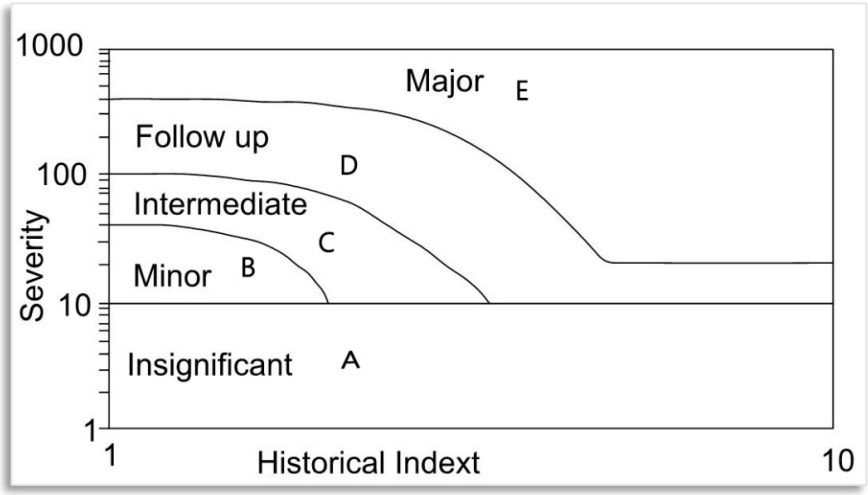

Figure 6.4: Typical intensity chart for FRP material[142]

6.2.8 Park and Ang damage Model

The Park and Ang model for evaluating damage index has been explained in detail under section 2.3.1. Various other damage index models are available in the literature, such as the Stiffness damage index of the global frame presented by Ghobarah et al. (1999)[144] based on stiffness response and the damage index presented by Dipasquale et al. (1989)[145] based on fundamental period. The Damage index proposed by Park and Ang is a better representative of damage because it takes into account displacement, load response and energy dissipated by the structure. The Park and Ang model has been considered in this research to find out the damage index. The Park-Ang Model has a drawback in evaluating DI for seismically damaged structures because it is very difficult to evaluate load response after the occurrence of an earthquake. To fill this gap, AE energy has been used instead of hysteric energy.

6.2.9 Closure remarks

From the literature review, it has been observed that the acoustic emission technique has the potential to be employed for the damage quantification and health monitoring of RC structures. The Kaiser's effect and Felicity ratio provide good tools for quantifying damage when loaded higher than the previous loads. Intensity charts can be used to measure AE

activities. AE count-rate analysis can be used to quantify fracture development. Load ratio and Calm-ratio can be helpful for damage identification. A statistical approach can be used to find Historic Index and Severity Index to quantify damage based on signal strength parameters. b-value analysis can be used for severity assessment based on the amplitude of AE waves. In this research, the damage in BCJs has been quantified with the Felicity ratio, Park and Ang Model and Novel Damage index.

6.3 DAMAGE IN CONTROL BCJ USING AE PARAMETERS

6.3.1 Kaiser's effect and Felicity ratio

The Kaiser and Felicity effects have already been discussed in detail under section-3.3.2.3. The Felicity ratio parameter can be used to observe the damage stage in cyclic load tests. Whenever the cumulative energy starts to increase before reaching the previous cycle's maximum load, the damage is supposed to have started. Refer to Figure 5.28, showing the variation of cumulative AE energy with a change in load. The felicity ratio (FR) at the end of the second load cycle in the forward direction is calculated as the ratio of the load at D to the load at A. For the second reverse cycle, the FR =load at G'/load at C. The FR values have been shown in Tables 6.3 to 6.10 for samples SPC1, SPC2, SPC3 and SPC4 worked out for forward and reverse load cycles. SPC1 has severe damage in the third load cycle. The fact can be cross-verified from the load-deformation plot because, in the fourth load cycle, the peak load capacity of SPC1 has reduced from 21.4 kN to 17.5 kN. In the reverse load direction also, the sample suffered severe damage in the fourth cycle. In SPC2, The FR value is nearly one in the fourth cycle. The BCJ suffered severe damage in the fifth load cycle. This can be verified from the load-deflection plot in Figure 5.10 because the displacement in the fifth load cycle exceeded the ultimate value.

A similar trend has been observed for BCJ samples SPC3 and SPC4, as can be seen in Tables 6.7 to 6.10. Thus, it can be concluded that the acoustic emission-based FR parameter can be used to identify damage in RC BCJs when subjected to cyclic loads.

Table 6.3: Felicity Ratio for SPC1 in the forward direction

Cycle No.	Load at the onset of AE activities W1	Previous cycle max load W2	Felicity Ratio	Damage severity
1-2	14.48	13.99	1.04	No damage
2-3	17.22	18.13	0.95	Damage initiation
3-4	7.4	18.5	0.4	Severely damaged
4-5	After the fourth forward cycle, the displacement has exceeded ultimate values; hence FR can't be used for damage detection			

Table 6.4: Felicity Ratio for SPC1 in Reverse direction

1-2	14.6	13.3	1.1	No damage
2-3	8.6	16.4	0.53	Severe damage
3-4	8.4	20.33	0.41	Severe damage
4-5	After the fourth reverse cycle, the displacement has exceeded ultimate values; hence FR can't be used for damage detection			

Table 6.5: Felicity Ratio for SPC2 in Forwar direction

1-2	7.1	6.9	1.03	No damage
2-3	17.2	16.8	1.02	No damage
3-4	23.7	24.4	0.97	Initiation of damage
4-5	15.6	26.5	0.38	Severe damage
5-6	From the fifth forward cycle, the displacement has exceeded ultimate values; hence FR can't be used for damage detection			

Table 6.6: Felicity Ratio for SPC2 in Reverse direction

1-2	14	8.1	1.73	No damage
2-3	17.56	17.13	1.16	No damage
3-4	5.4	19.73	0.27	Severe damage
4-5	From the fourth reverse cycle, the displacement has exceeded ultimate values; hence FR can't be used for damage detection			

Table 6.7: Felicity Ratio for SPC3 in Forward direction

1-2	15.9	13.7	1.16	No damage
2-3	16.9	18	0.94	Initiation of damage
3-4	23.4	11.6	2	Severe damage
4-5	From the fourth forward cycle, the displacement has exceeded ultimate values; hence FR can't be used for damage detection			

Table 6.8: Felicity Ratio for SPC3 in Reverse direction

1-2	11.1	8.05	1.14	No damage
2-3	5.95	18.9	0.3	Severe damage
3-4	From the Third reverse cycle, the displacement has exceeded ultimate values; hence FR can't be used for damage detection			

Table 6.9: Felicity Ratio for SPC4 in Forwarding direction

1-2	15.9	21.22	1.16	No damage
2-3	16.9	18	0.94	Initiation of damage
3-4	23.4	11.6	2	Severe damage
4-5	From the fourth forward cycle, the displacement has exceeded ultimate values; hence FR can't be used for damage detection			

Table 6.10: Felicity Ratio for SPC4 in Reverse direction

1-2	21.97	8.05	1.04	No damage
2-3	25.52	25.98	0.98	Initiation of damage
3-4	10.25	28.96	0.35	Severe damage
4-5	From the Third reverse cycle, the displacement has exceeded ultimate values; hence FR can't be used for damage detection			

6.3.2 Novel Damage Index based on AE energy

Due to the limitation of estimating energy dissipated, a new Damage Index model has been proposed in this research wherein Cumulative Acoustic Energy (CAE) and displacement parameters are used to quantify damage in a seismically damaged structure using equation-(6.7)

$$DI_{AE} = \frac{\delta_i}{\delta_u} + \beta_1 \frac{\sum E_i}{E_u} \tag{6.7}$$

where: δ_i is the maximum displacement response of the structure of i^{th} load cycle; $\sum E_i$ is the total AE energy cumulated at the end of the i^{th} cycle; δ_u is ultimate displacement capacity (It has been worked out as per procedure laid down in Park and Ang (1985) from BCJ under monotonic loading as shown in Figures 5.3 and 5.4; E_u is total AE energy corresponding to ultimate displacement value in monotonic load test; β_1 is the experimentally calculated value corresponding to unit damage index (at collapse using equation-6.8 wherein are the values of deflection and AE energy at the collapse stage

The estimation of the collapse stage is a major issue in laboratory tests. The ultimate displacement capacities for SPC1 and SPC2 have been obtained. The BCJ samples SPC1 and SPC2, tested under cyclic loads, continued to deform beyond these ultimate capacities at almost constant peak loads after the third load cycle because of the formation of a plastic hinge in the beam. Thus, the ultimate displacement parameter has been used to define a failure point. The BCJ are assumed to be collapsed when the displacement experienced by them increases the ultimate value. Based on this criterion, both samples collapsed after the fourth cycle. The damage index value corresponding to ultimate deformation is taken as unity. For the DI_{AE} a value equal to one, the unknown parameter is calculated using equation-6.8. Further, DI_{AE} at the end of each cycle has been evaluated from this equation. The complete DI_{AE} prediction procedure has been presented in a flowchart, as shown in Figure 6.5.

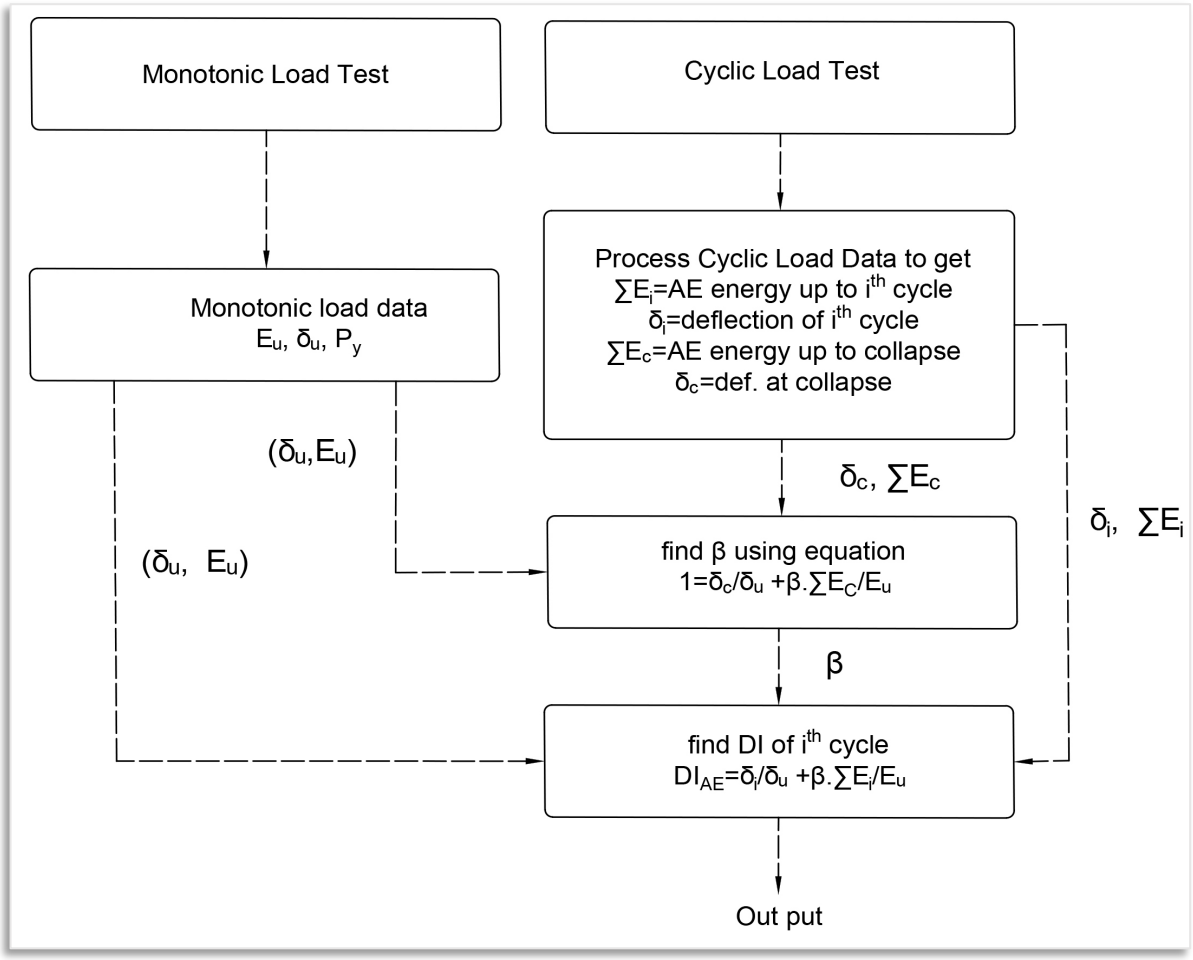

Figure 6.5: Flow chart for damage index prediction procedure

The Damage Index based on energy dissipated presented by Park and Ang (1985) has also been worked out using equation-6.9 for comparing results with the damage index based on AE energy developed in this research work.

$$DI_{PARK} = \frac{\delta_{max}}{\delta_u} + \frac{\beta_2}{P_y \delta_u} \int dE \tag{6.8}$$

where δ_{max} is the maximum displacement experienced during an earthquake; δ_u is ultimate displacement capacity; P_y is yield strength; β_2 is a weighting factor for the effect of energy dissipated (E). The complete set of calculated results has been tabulated in Table-1 and Table-2. The damage indices worked out using equations 6.8 and 6.9 have been plotted to compare results graphically in Figure 6.6 and Figure 6.7. Similarly, damage indices have been worked out for samples SPC3 and SPC4, as shown in Figure 6.8 and Figure 6.9, respectively. The damage indices have been tabulated in Tables **6.13** and 6.14 for SPC3 and SPC4, respectively. From all the results, it is clear that the damage indices worked out using AE data

are very close to the damage index model of Park and Ang. Thus, it can be concluded that the AE energy can be successfully used to predict the damage state of RC beam-column joints.

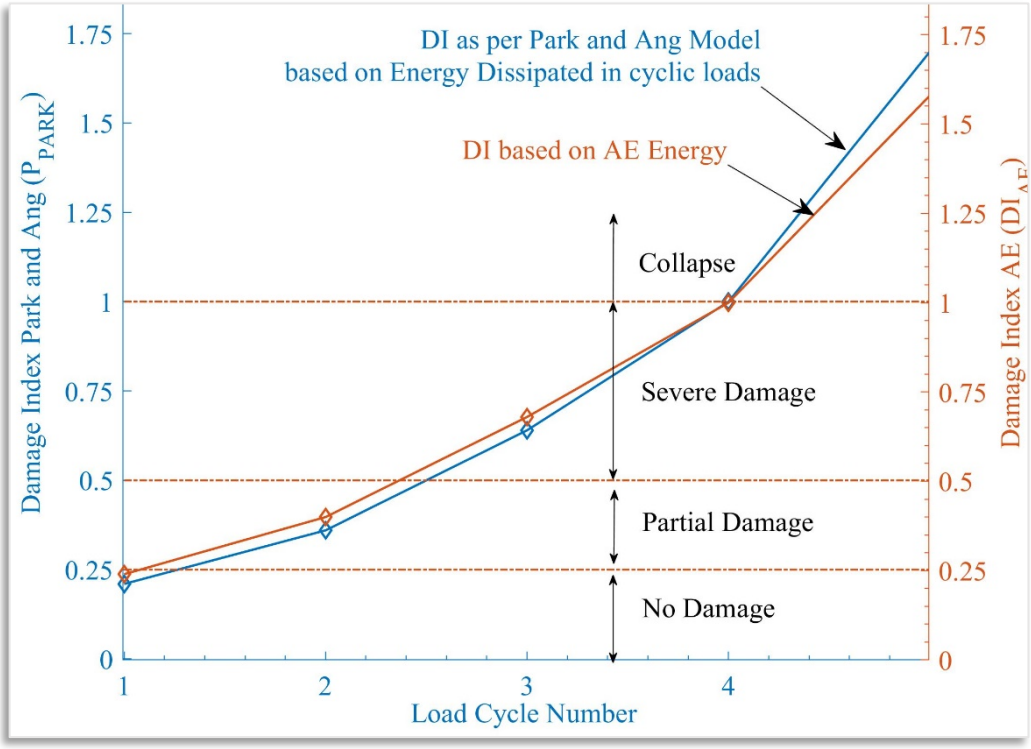

Figure 6.6: Damage index for sample SPC1

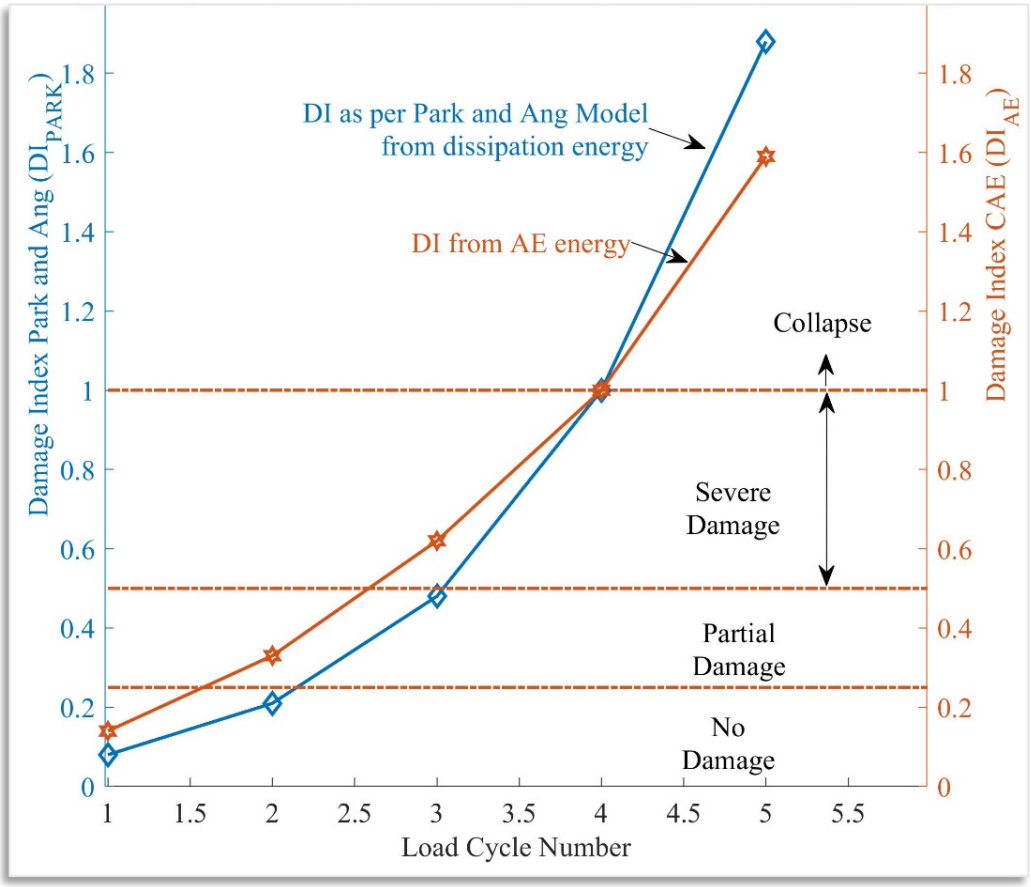

Figure 6.7: Damage index for sample SPC2

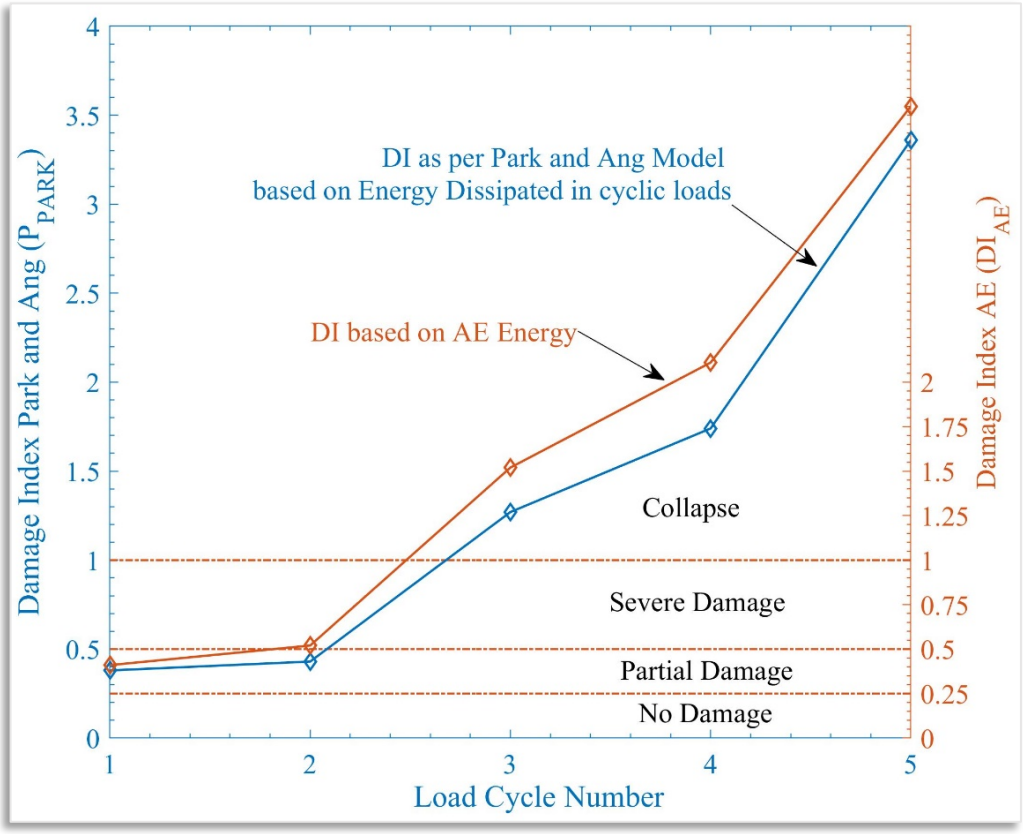

Figure 6.8: Damage Index for sample SPC3

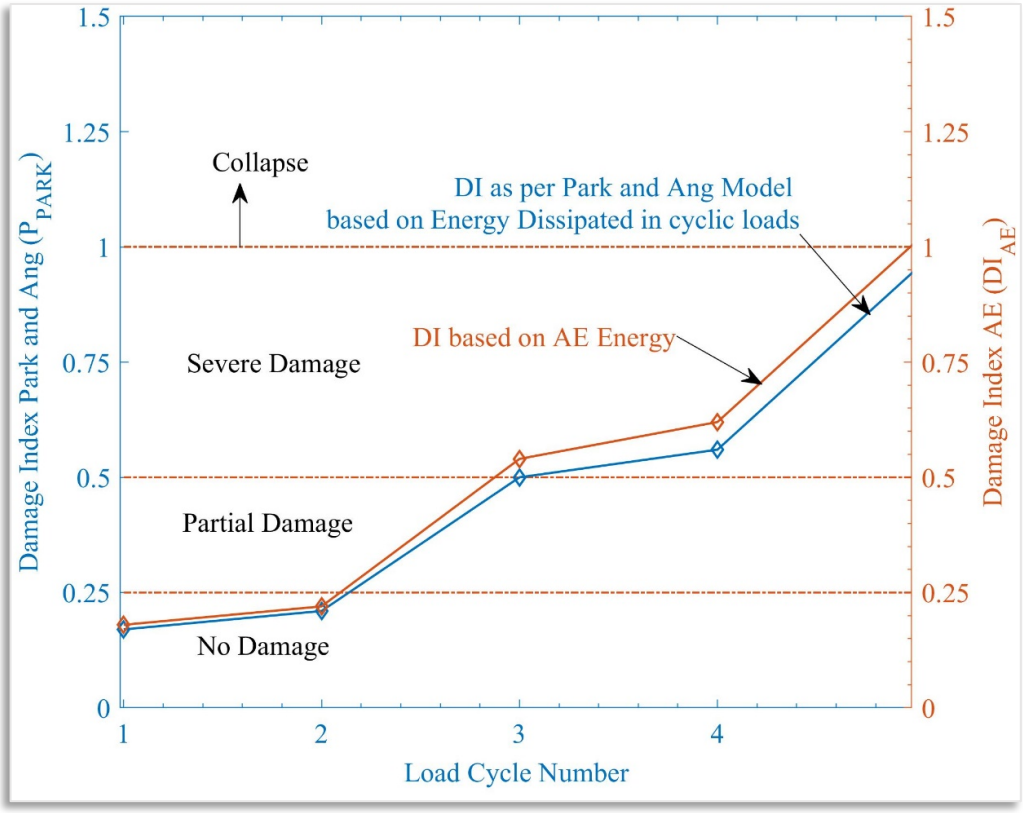

Figure 6.9: Damage Index for Sample SPC4

Table 6.11: Damage index for SPC1

P_u = 19.5 kN, $E_u = 3.138 \times 10^6$, mV.sec, δ_u= 11.5 mm					
Cycle No.	**Dissipation energy (kN.mm)**	**AE energy (mV.sec)**	**Max. cycle def (mm)**	**Damage Index**	
				DI_{PARK}	DI_{AE}
1	11.80	1700000	2.4	0.21	0.24
2	50.45	3200000	3.9	0.36	0.40
3	235.00	7000000	6.2	0.64	0.68
4	523.00	11000000	8.9	1.00	1.00
5	968.60	14800000	14.7	1.70	1.58

Table 6.12: Damage Index for SPC2:

P_u = 25 kN, $E_u = 1.233 \times 10^7$, mV.sec, δ_u= 35.3 mm					
1	69.37	6110000	7.20	0.21	0.21
2	333.94	12060000	16.22	0.48	0.47
3	868.92	18400000	30.93	0.91	0.91
4	1888.80	25330000	33.90	1.00	1.03
5	3035.60	34900000	49.70	1.46	1.52

Table 6.13: Damage Index for SPC3

P_u = 19.5 kN, $E_u = 3.138 \times 10^6$, mV.sec, δ_u= 11.5 mm					
1	35	2.40E+06	4.15	0.38	0.41
2	124	7.86E+06	4.15	0.43	0.52
3	195	1.93E+07	12.87	1.27	1.52
4	260	3.10E+07	17	1.74	2.11
5	773	3.82E+07	31.84	3.55	3.10

Table 6.14: Damage Index of SPC4

$P_u = 25$ kN, $E_u = 1.233 \times 10^7$, mV. sec, $\delta_u = 35.3$ mm					
1	105.65	2.43E+06	6	0.17	0.18
2	345.01	9.47E+06	7	0.21	0.22
3	1020.87	2.33E+07	17	0.50	0.54
4	2125.12	4.37E+07	18	0.56	0.62
5	3262.51	5.31E+07	31	0.95	1.01

6.4 DAMAGE IN REPAIRED BCJ SAMPLES USING AE PARAMETERS

6.4.1 Damage quantification using Kaiser's effect

The Felicity ratio (FR) has been worked out for retrofitted samples by the procedure as carried out for the control BCJ sample in section 6.3.1, as can be seen in Tables 6.15 to 6.18 for BCJ sample SPCR1 and SPCR2. It can be seen from the tables that sample SPCR1 suffered severe damage in the fourth cycle, whereas sample SPCR2 was severely damaged during the third cycle. The FR indicates that the sample SPCR1 suffered severe damage in the third cycle and SPCR2 in the fourth cycle, which can be verified from load-deformation plots wherein it is clear that SPCR1 exceeded ultimate displacement in the third cycle and SPCR2 crossed ultimate deformation in the fourth cycle. The FR indicates that ECC retrofitted gained desired strength parameters. Thus, ECC can be successfully used to strengthen the BCJ.

Table 6.15: Felicity Ratio for SPCR1 in the forward direction

Cycle No.	Load at the onset of AE activities W1	Previous cycle max load W2	Felicity Ratio FR=W1/W2	Damage severity
1-2	14	12	1.42	No damage
2-3	15	16	0.94	Partial Damage
3-4	8	21	0.33	severe damage
4-5	6	26	0.23	Severe damaged
5-6	After the 5th forward cycle, the displacement has exceeded ultimate values; hence FR can't be used for damage detection			

Table 6.16: Felicity Ratio for SPCR1 in Reverse direction

1-2	15	12	1.25	Initiation of damage
2-3	15	18	0.83	Partial damage
3-4	10	18	0.55	Severe damage
4-5	After the 4th reverse cycle, the displacement has exceeded ultimate values; hence FR can't be used for damage detection			

Table 6.17: Felicity Ratio for SPCR2 in the forward direction

1-2	14	12	1.42	No damage
2-3	20	21	0.95	Partial damage
3-4	8	24	0.33	Severe damaged
4-5	After the fourth forward cycle, the displacement has exceeded ultimate values; hence FR can't be used for damage detection			

Table 6.18: Felicity Ratio for SPCR2 in Reverse direction

1-2	12.5	12	1.04	No damage
2-3	25	26	0.96	Initiation of damage
3-4	14	15.5	0.90	Minor damage
4-5	8	17	0.47	Severe damage
5-6	After the fourth reverse cycle, the displacement has exceeded ultimate values; hence FR can't be used for damage detection			

6.4.2 Damage quantification using AE Energy

The cumulative dissipation and AE energy variation have been shown in Figure 5.50. As described in section 0, the novel damage indices have been worked out for retrofitted samples also. In addition to this, damage indices have also been calculated as per Park and Ang damage model for SPCR1 and SPCR2 to verify the results for the proposed Damage Index. The complete data obtained has been tabulated in Tables 6.19 and 6.20 for samples SPCR1 and SPCR2, respectively and further graphically shown in Figures 6.10 and 6.11.

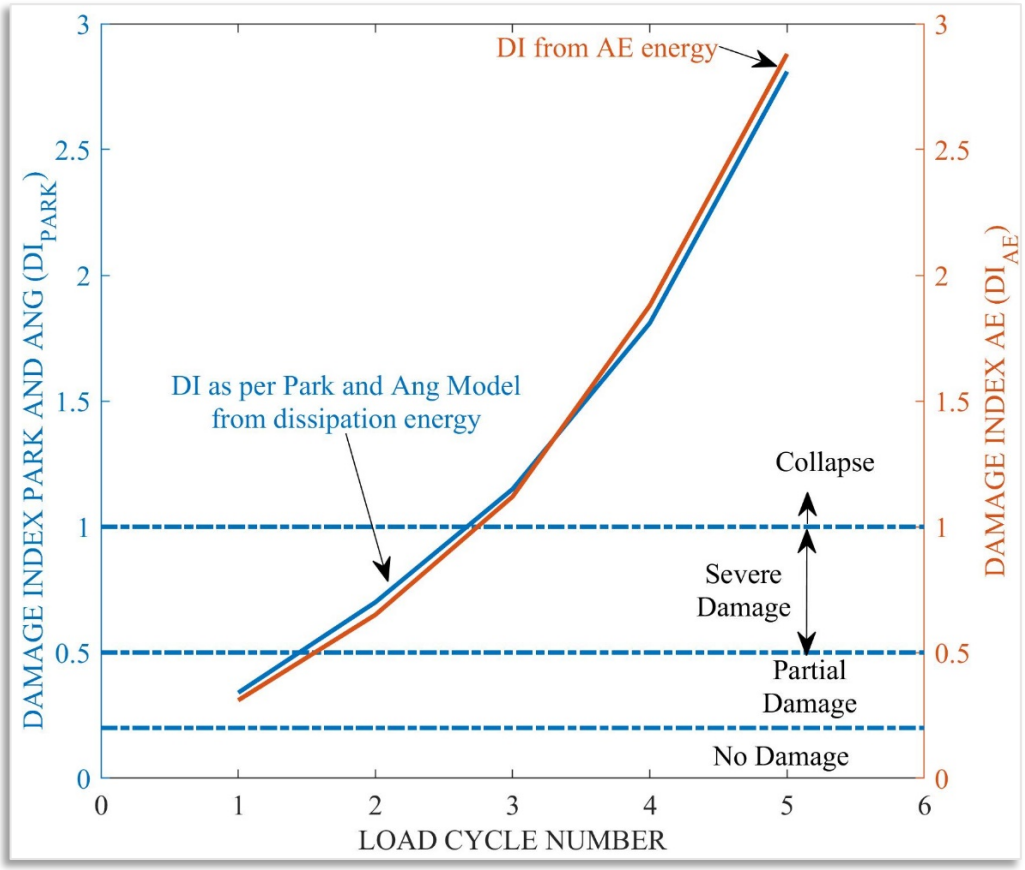

Figure 6.10: Damage Index Retrofitted samples SPCR1

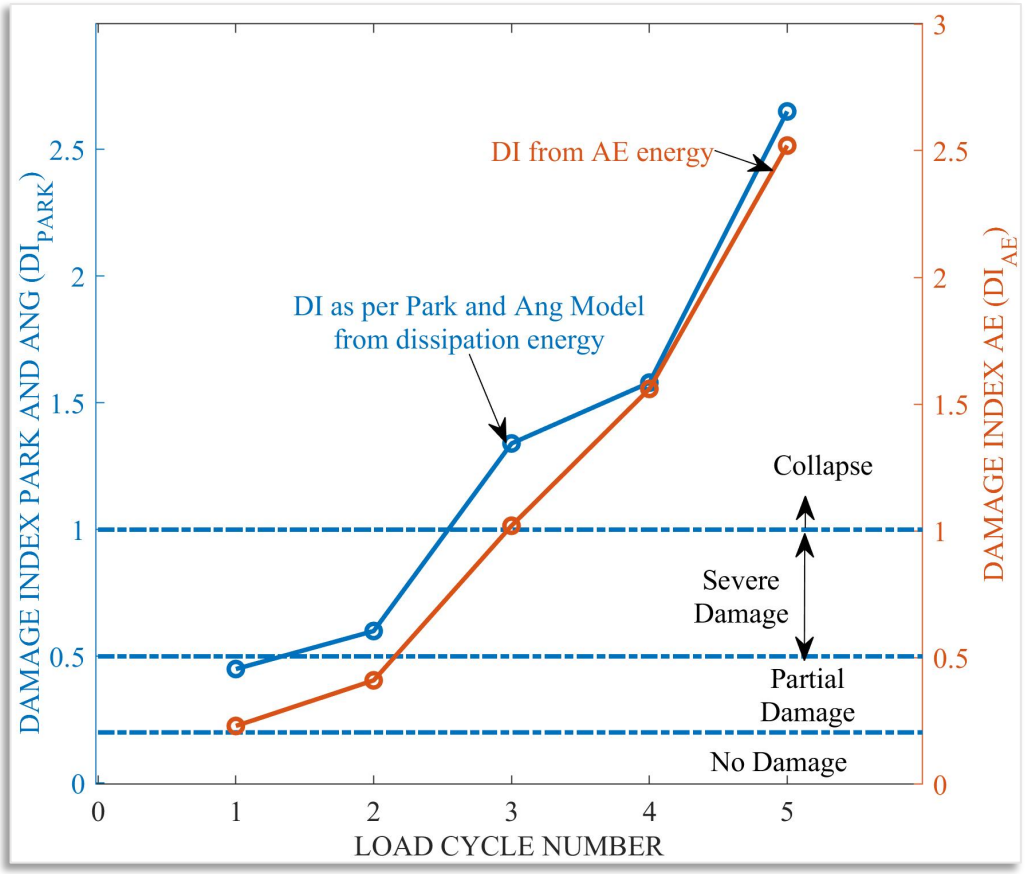

Figure 6.11: Damage Index Retrofitted sample SPCR2

Table 6.19: Damage Index of retrofitted sample SPCR1

Cycle No.	Dissipation energy (kN.mm)	AE energy (mV.sec)	Max. cycle def (mm)	Damage Index	
				DI_{PARK}	DI_{AE}
1	35	1.55E+06	5	0.34	0.31
2	188	4.06E+06	10	0.70	0.64
3	539	5.45E+06	17	1.15	1.12
4	1479	7.69E+06	27	1.81	1.89
5	2775	1.18E+07	42	2.81	3.01

Table 6.20: Damage Index of retrofitted sample SPCR2

Cycle No.	Dissipation energy (kN.mm)	AE energy (mV.sec)	Max. cycle def. (mm)	Damage Index	
				DI_{PARK}	DI_{AE}
1	51	2.89E+06	6	0.45	0.20
2	240	6.01E+06	7	0.60	0.35
3	705	1.07E+07	17	1.34	0.94
4	1618	1.67E+07	18	1.58	1.56
5	3050	2.63E+07	31	2.65	2.85

6.5 COMPARATIVE ANALYSIS OF CONTROL AND REPAIRED BCJ

A comparison of control and retrofitted samples reveals that the overall maximum load-carrying capacity of retrofitted sample SPR1 slightly improved compared to SPC1 and reduced somewhat in sample SPR2 compared to SPC2. However, the maximum load-carrying capacity of both retrofitted samples SPR1 and SPR2 is higher than the design load capacities. There is a reduction in energy dissipated in both samples, which may be due to the lower contribution of steel bars that have already experienced strain beyond yield values. It is due to the strain hardening property that steel bars undergo during plastic deformation. The steel bars do not

retain their original shape and size during unloading. In retrofitted samples, the steel bars have already experienced strains beyond yield values and have a lesser contribution to behave in a ductile manner. Thus, the energy dissipated in retrofitted samples is less than in control samples. This phenomenon has been verified from the test results of control and retrofitted BCJ samples. The BCJ SPC1 has 1324 kNmm cumulative dissipation energy at the end of the fifth cycle, whereas the retrofitted sample SPR1 has witnessed a dissipation energy of 1240 kNmm.

Similarly, dissipation energy at the end of the fifth cycle in SPC2 and SPCR2 has been observed to be 3060 and 2878 kNmm, respectively. Thus, there is a slight reduction in the energy dissipated in the retrofitted sample. A similar trend has been observed in the AE energy values. The AE energy at the end of the fifth cycle for SPC1 and SPCR1 has been observed to be 1.46×10^7 mV.sec and 5.63×10^6 mV.sec whereas, for samples SPC2 and SPCR2, the values have been observed to be 3.49×10^7mV.sec and 1.17×10^7 mV.sec, respectively. A decrease in energy dissipated indicates a reduction in the structure's ductility to perform under seismic forces. A reduction in AE energy with an increase in displacement suggests that the contribution of steel to resist higher displacements is lesser. Thus, both AE energy and dissipation energy parameters can be used to observe the damage levels in RC beam-column joints.

6.6 NEW DAMAGE STATES

Assessment of damage states is also important to allow engineers to evaluate the post-earthquake status of buildings and categorise the damage. A new procedure for identifying damage states has been proposed based on DI_{AE}, followed by visual observations, crack widths and Felicity Ratio. The damage state ‘D1’ has been defined based on invisible cracks in the samples. The value of the damage Index in this state is less than 0.2. The structure is sound without any noticeable damage.

The second damage state (D2) corresponds to a DI_{AE} a value between 0.2 and 0.5. Hair cracks less than 0.5 mm wide start to appear, indicating partial damage, but the structure has

not lost its capacity. Only minor surface treatments are desirable for this damage state.

The third damage state (D3) belongs to DI_{AE} value lying between 0.5 and 0.75. The cracks of width 0.5 to 2 mm start appearing, exposing the steel reinforcement and causing minor damage to the structure, requiring treatment of cracks to protect the steel reinforcement from weathering effects.

The fourth damage state (D4) has been categorised for DI_{AE} value lying between 0.75 and 0.85. Wide-open cracks of width 2-3 mm start to appear, and steel reinforcement is exposed. Structures falling under this damage state need immediate repair of structural elements. Expert engineering opinion and a safety certificate are desired to put the building back into use.

The damage state D5 has been categorised based on DI_{AE} values varying from 0.85 to 1. This damage state indicates major damage having wide open cracks exposing steel reinforcement followed by spalling concrete. However, the confining core is intact, and there is no crushing of concrete. Major repair and/or strengthening of structural elements is desired. The opinion of a health monitoring expert is desirable to decide whether the structure is repairable or not.

Damage state D6, having a DI_{AE} value of more than one is an indicator of the collapse of the structure. Wide-open cracks of width more than 5 mm are observed, followed by spalling of concrete, crushing of confined core and buckling or breakage of steel bars. In this case, the special opinion of structural engineers is desired to decide the reusability of the structure.

All these damage states have been briefly described in tabular form below in Table 6.21. Based upon this damage index, three different stages, namely minor damage ($DI_{AE} < 0.5$), moderate damage ($0.5 < DI_{AE}E < 0.75$) and major damage ($DI_{AE} > 0.75$) can be defined.

It is pointed out that these damage states are specific to the beam-column joint of the size mentioned in Section-4.3 . Change in the dimensions of the specimen changes the crack pattern and size of the cracks. Further, these observations are based on 5-6 load cycles. In order

to refine these damage states, it is proposed to conduct cyclic load tests having controlled displacement parameters by increasing the number of cycles at least up to the ultimate displacement capacity.

Table 6.21: New Damage states Proposed in this research

DI_{AE} Range	Damage State	Description of damage
< 0.2	D1	No visible cracks indicate no damage;
0.2 to 0.5	D2	Hair cracks < 0.5 mm indicate partial damage requiring surface treatments only;
0.5 to 0.75	D3	A Crack width range from 0.5 to 2 mm indicates minor damage requiring treatment of cracks;
0.75 to 0.85	D4	A crack width range from 2 to 3 mm indicates severe damage requiring major repair of structural elements;
0.85 to 1	D5	Crack width > 3 mm followed by spalling of cover concrete indicates very severe damage requiring major repair and/or strengthening of structural elements;
> 1	D6	Crack width > 5 mm followed by spalling of concrete, crushing of confined core and buckling or breakage of steel bars indicates the total collapse of the structural elements and needs special attention of the structural engineers to decide about the reusability of the structure.

CHAPTER-7. CONCLUSIONS

7.1 GENERAL

The present study has been undertaken to monitor the health of Beam-Column Joints (BCJ) subjected to cyclic loading using the Acoustic Emission Technique (AET). Further, the behaviour of BCJ retrofitted with Engineering Cementitious Composites (ECC) when subjected to similar cyclic loading has also been done and compared with control BCJ. A novel damage index (NDI) has been developed to quantify damage in the BCJ before and after ECC repair. The acoustic Emission Technique has shown promising results for the localisation and quantification of damage in BCJ. It is possible to classify cracks into tensile and shear cracks using various AE parameters. Further, the use of ECC as a retrofitting material has shown promising results in restoring the strength and ductility of the damaged BCJ well supported by AE parameters. The main conclusions derived from this study are summarised in the following section.

7.2 LOAD-DEFORMATION CHARACTERISTICS OF BCJ

- BCJ samples were tested under monotonic loads to find the ultimate displacement capacity. The results indicate that the ultimate displacement capacity of the ductile BCJ sample is about three times more than the non-ductile BCJ sample.
- Spalling of concrete and wide-open cracks have been observed in BCJ subjected to cyclic loads. The damage in the case of non-ductile BCJ samples has occurred at much lower displacements as compared to ductile samples.
- The maximum displacement near failure in ductile BCJ samples is about 1.5 to 2 times higher than in the non-ductile BCJ sample. This indicates that ductile BCJ samples have higher ductility than non-ductile BCJ samples.
- BCJ with ductile detailing exhibits higher peak-load carrying capacity than non-ductile BCJ samples because ductile samples are provided with a higher reinforcement percentage.

- The Energy Dissipation in ductile BCJ samples is about 3 to 4 times more than in the non-ductile BCJ sample, as calculated from the area enclosed inside the hysteresis loop of BCJ subjected to cyclic loading. Thus, ductile reinforcement helps to improve the ductility of BCJ.
- The ductile detailing in BCJ helps reduce stiffness degradation when deformed beyond ultimate load-carrying capacities.
- The ductility factor is a useful parameter to check the ductile behaviour of BCJ samples. The ductility factor of the ductile BCJ sample is about three more than the non-ductile BCJ sample.

7.3 MONITORING OF BCJ USING ACOUSTIC EMISSION TECHNIQUE

- AE X-Y plots give a pictorial representation of AE events occurring in BCJ when subjected to increasing cyclic loading. The concentration of AE events gives an idea about the location as well as the severity of damage in the BCJ.
- The BCJ members designed for ductility have witnessed about seven times more AE hits corresponding to tensile cracks and about three times more AE hits corresponding to shear cracks than BCJ designed without ductile detailing.
- From the cumulative AE hits and AE energy graphs, it has been observed that the rate of AE hits is higher than the rate of AE energy in the elastic stage of loading, where the damage is almost negligible. This trend of variation of the rate of AE hits and rate of AE energy reverses in the plastic stage of loading, wherein the majority of damage occurs. This indicates that AE hit is a qualitative measuring tool of damage, whereas AE energy serves both qualitative and quantitative tools to relate damage in BCJ. Hence, acoustic energy is a better parameter to quantify damage than AE hits.
- The variation of the energy dissipation curve closely matches the AE energy curve for various stages of damage of BCJ subjected to cyclic loading. A relationship has been developed between these two parameters using MATLAB mathematical tool. Thus, the

energy dissipation can be estimated by using AE energy obtained from AE testing.

- The AE energy is defined as the integral of the rectified voltage signal over the AE hit or waveform duration. In the ductile BCJ sample, AE energy is about two times more than in the non-ductile BCJ sample. Thus, AE energy can serve as a useful tool to check the ductility of BCJ.
- The Ib-value analysis, which is based on Gutenberg-Richter law, helps identify different stages of damage in the structures and assess the presence of macro cracks. An Ib-value less than one indicates the occurrence of severe damage and a value from one to two shows intermediate damage. An Ib-value of more than two is an indication of minor damage. BCJ members designed for ductility produced about two times more AE hits corresponding to severe damage than a non-ductile sample and about three times more hits corresponding to moderate damage.

7.4 DAMAGE INDEX BASED ON AE PARAMETERS

Many tools have been employed in the literature for damage quantification using Acoustic Emission parameters in general for various structures such as Felicity ratio, AE Hits, AE Energy, Amplitude, Rise Angle, and Average Frequency. A Novel damage index based on AE energy and Felicity Ratio is proposed in this work. The following conclusions have been drawn using these parameters:

- The Felicity Ratio (FR), which is defined as the ratio of load at the onset of AE activities to the previous cycle's maximum load, is a powerful tool for observing damage in beam-column joints. A Felicity ratio greater than or equal to one indicates no damage. A Felicity Ratio of 0.75 to 1 is indicative of minor damage. FR lying between 0.5 and 0.75 is indicative of major damage.
- The Felicity Ratio doesn't provide a true damage state when BCJ is deformed beyond a displacement value corresponding to peak load because, in such situations, the cyclic peak load is always less than the previous cycle's maximum load. Hence, the Felicity

Ratio, like a damage index parameter, is only valid for structures when deformed below the peak load capacity.

- A novel damage index based on AE energy has been developed in this study for BCJ. This damage index is a function of two non-dimensional variables. The first variable is the ratio of displacement at any time (say t) to the ultimate displacement capacity of BCJ. The second variable is the ratio of total AE energy (at time t) to the ultimate acoustic energy capacities of BCJ. Based on this new damage index, it has been proposed that a damage index (DI_{AE}) value up to 0.5 represents minor damage, DI_{AE} value from 0.5 to 0.75 indicates moderate damage and DI_{AE} value of more than 0.75 indicates major damage. The DI_{AE} value of more than unity indicates the collapse stage of the BCJ.

7.5 BEHAVIOUR OF ECC REPAIRED BCJ

- The ultimate load-carrying capacity of ECC-strengthened non-ductile BCJ is 0.3 kN higher than the control BCJ sampled. The ultimate load-carrying capacity of ECC-strengthened ductile BCJ is 4.5 kN less than the control sample; however, the value is higher than the design capacity of BCJ (i.e., 17 kN). Thus, it can be concluded that ECC material can be successfully used to restore the design load capacity of the BCJ.
- The damage quantification using Felicity Ratio indicates that the ECC retrofitted samples have suffered minor/intermediate damage up to third load cycles near the ultimate load and displacement capacities of BCJ because the loading has not crossed the plastic range.
- Statistical analysis done by Rise-Angle Vs Average-frequency plots is helpful to distinguish between the type of cracks, i.e., Tensile or shear cracks. The number of tensile hits in an ECC retrofitted non-ductile BCJ up to the unity damage index was three times more than that of a controlled BCJ. The number of tensile hits in an ECC retrofitted ductile BCJ up to the unity damage index was reduced by about 0.3 times

that of the controlled BCJ. From these results, it can be concluded that there is a reduction in tensile cracks in ductile BCJ samples and an increase in tensile cracks in non-ductile samples. Thus, ECC helps to improve the tensile capacity of ductile BCJ.

- The number of shear hits in an ECC retrofitted non-ductile BCJ up to the unity damage index was three times more than that of a controlled BCJ. The number of shear hits in an ECC retrofitted ductile BCJ up to the unity damage index was reduced by about 0.2 times that of the controlled BCJ. From these results, it can be concluded that there is a reduction in shear cracks in ductile BCJ samples and an increase in tensile cracks in non-ductile samples. Thus, ECC helps to improve the shear capacity of ductile BCJ.
- The number of AE hits representing severe damage having an Ib-value <1 in the retrofitted non-ductile BCJ was 6.5% less than the controlled BCJ. The number of AE hits representing severe damage having an Ib-value <1 in the retrofitted ductile BCJ was 7% higher than the controlled BCJ. Thus, it can be concluded that non-ductile BCJ retrofitted with ECC has reduced severe damage. But the retrofitting with ECC of a ductile BCJ does not help reduce the same.
- The Energy Dissipated from the ECC retrofitted non-ductile BCJ was almost the same as in control beam-column joints. The Energy Dissipated from the ECC retrofitted ductile BCJ was reduced by about 0.4 times in control beam-column joints. The reduction in energy-dissipated in ECC retrofitted ductile sample indicates a reduction in the ductility of BCJ retrofitted with ECC.
- The total AE Energy of the ECC retrofitted non-ductile BCJ was about four times higher than the corresponding control BCJ. The total AE Energy of the ECC retrofitted ductile BCJ was about 3.2 times higher than the corresponding control beam-column joints. Thus, it can be concluded that ECC material can be successfully used to retrofit the BCJ to achieve Acoustic Energy capacity.

7.6 SCOPE OF THE FUTURE WORK

- The present work is focused and limited to the damage monitoring and analysis of BCJ using AET. The work can be extended to analyse damage in framed RC buildings. The monitoring of RC frames also needs to be conducted using the AE technique.
- In RC structures, the source location of AE events differs from the actual since the AE waveform is interfered with by the formation of cracks that change wave velocity. Further, the attenuation reduces the signal strength of the AE waveform. There is also a change in wave velocity in concrete structures due to the non-homogeneity of concrete. All these factors change the velocity of the waveform and hence result in an inaccurate prediction of the source location. Hence much work still needs to be done to measure the source location accurately.
- For accurate prediction of AE data and its correlation with load or displacement, it is desirable to apply the displacement load at a slow rate. It would be interesting to evaluate the differently repaired RC BCJ involving GFRP wrapping and other repair techniques at different loading rates using NDT tools.

APPENDIX A: MATLAB CODE TO PLOT RA VS FA

```
function[RAvsFA]=RAvsFAPlot(AEmain,ch,loadCycle,xmax,ymax,font
_size, numofCycles)
%   This is MATLAB Code to draw a graph of RA vs FA
    corresponding to each load cycle.
%   AEmain is AE data Table which contains data columns as
    below
%   TIME, RISE, COUNT, DURATION, AMP
%   Be sure that columns are named exactly as above (Names of
    columns are case sensitive)
%   ch is the channel number, e.g. 1, 2, 3, .....
%   loadcycle is two column array representing the start time
    and end time of load cycles e.g. loadcycle=[0 200;200
    400;400 800;800 1200]
%   xmax is the maximum value assigned for RA (on the x-axis)
%   ymax is the maximum value assigned for Average frequency
%   font_size is the font size for text displayed in the graph
%   numofCycles is the total number of load cycles for which
    test data is taken
fs=font_size;
temp=AEmain(AEmain.CH==ch,:);
RAvsFA=temp(:,{'TIME', 'RISE','COUNT', 'DURATION', 'AMP'});
RAvsFA.FA=1000*RAvsFA.COUNT./RAvsFA.DURATION;
RAvsFA.RA=RAvsFA.RISE./RAvsFA.AMP;
nrows=ceil(numofCycles/2);
ncols=2;    % graphs to be displayed in one line
for i=1:numofCycles
    T1=loadCycle(i,1);
    T2=loadCycle(i,2);
    RAFa=RAvsFA(RAvsFA.TIME>T1 & RAvsFA.TIME<T2,{'RA','FA'});
    ax=subplot(nrows,ncols,i);
    x=RAFa.RA;
    y=RAFa.FA;
    hold(ax,'on')
    s=scatter(ax, x,y);
```

```
    s.Marker='.';
    line1=plot(ax, [0 xmax], [0 ymax]);
    line1.LineWidth=0.5;
    line1.LineStyle='-.';
    loadcyclenum=num2str(i);
    xlim(ax,[0 xmax]);
    ylim(ax,[0 ymax]);
    scale=xmax/ymax;
    x=xmax/3;
    y=ymax/3;
    titletext=text(ax,xmax/2,ymax*0.95,['Load Cycle -
'loadcyclenum]);
    titletext.FontSize=fs+4;
    titletext.HorizontalAlignment='center';
    titletext.FontName='Times New Roman';
    ax.YLabel.String='Fa(kHz)';
    ax.XLabel.String='RA=Rise/Amp(ms/V)';
    ax.YLabel.FontSize=fs;
    ax.XLabel.FontSize=fs;
    ax.XAxis.FontSize=fs;
    ax.YAxis.FontSize=fs;
    ax.XGrid='on';      ax.YGrid='on';
    ax.XMinorGrid='on'; ax.YMinorGrid='on';
    ax.XTickMode='auto';    ax.YTickMode='auto';
    ax.XMinorTick='on'; ax.YMinorTick='on';
    ax.XAxisLocation='origin';
    ax.YAxisLocation='origin';
    ax.GridLineStyle='-.';
    ax.GridAlpha=0.5;
    x1=x-ymax/6*scale;
    y1=y+ymax/6;
    x2=x+ymax/6*scale;
    y2=y-ymax/6;
    line1 = line(ax, [x1 x2],[y1 y2]);
    line1.LineStyle='-.';
```

```
    txt1=text(ax,x1-x*0.2/scale,y1+y*0.2/scale,'Tension');
    txt1.HorizontalAlignment='center';
    txt1.FontSize=fs;
    txt1.FontName='Times New Roman';
    txt1.FontWeight='bold';
    set(txt1,'Rotation',45);
    txt2=text(ax,x2+x*0.2/scale,y2-y*0.2/scale,'Shear');
    txt2.HorizontalAlignment='center';
    txt2.FontSize=fs;
    txt2.FontName='Times New Roman';
    txt2.FontWeight='bold';
%%  Draw Upper Arrow. Coordinates of arrows
    Q1x=x1+ymax/20*scale*cos(30*pi/180);
    Q1y=y1-ymax/20*sin(30*pi/180);
    Q2x=x1+ymax/20*scale*sin(30*pi/180);
    Q2y=y1-ymax/20*cos(30*pi/180);
    line(ax,[x1 Q1x], [y1 Q1y]);
    line(ax,[x1 Q2x], [y1 Q2y]);
    line(ax,[Q1x Q2x], [Q1y Q2y]);
%%  Draw Lower Arrow. Coordinates of arrows
    Q1x=x2-ymax/20*scale*sin(30*pi/180);
    Q1y=y2+ymax/20*cos(30*pi/180);
    Q2x=x2-ymax/20*scale*cos(30*pi/180);
    Q2y=y2+ymax/20*sin(30*pi/180);
    line(ax,[x2 Q1x], [y2 Q1y]);
    line(ax,[x2 Q2x], [y2 Q2y]);
    line(ax,[Q1x Q2x], [Q1y Q2y]);
    set(txt2,'Rotation',45);
    screen_size=get(0,'ScreenSize');
    set(gcf, 'Position', [1 1 0.8*screen_size(4)
0.8*screen_size(4)]);
    hold(ax,'off')
 end
end
```

APPENDIX B: MATLAB CODE TO FIND IB-VALUE FROM AE DATA

```
function [ibValue]=ibValueofGroupedData(AEmain_CH, sl)

%    AEmain_CH is Data contains AE data for a particular
     Channel in an
%    Acoustic Emission Testing which is stored in Tables
%    This Table must have the following columns
%    'TIME' represents the time of Hits data
%    'AMP' represents the amplitude of the recorded hit
%    'threshold' is the minimum Amplitude value below which
     data is filtered out
%    'sl' is the sample length is the total number of rows
     selected from a 'channelAmpData'table which may be taken
     as 50, 100, 150, 200...1000... so on depending on
temp=table;
temp.AMP = AEmain_CH.AMP;
avgAmplitude=mean(temp.AMP);    % average value of amplitude
sd=std(temp.AMP);   % Standard deviation of amplitude of
grouped data
%Align data of subGroup in frequency Table
FT=(1:sl)';
FT(1:sl,2)=0;
frqT=grpstats(temp,'AMP');
frqT2=table2array(frqT);
    for i=1:sl
        aa1=frqT2(frqT2(:,1)==FT(i,1),:);
        if isempty(aa1)
        else
        FT(i,2)=aa1(1,2);
        end
    end
FT(:,3)=cumsum(FT(:,2));    % Get cumulative sum of column no.
2
FT(:,2)=[];
```

```
frqTable=array2table(FT);
frqTable.Properties.VariableNames{1} = 'AMP';
frqTable.Properties.VariableNames{2} = 'frq1';
frqTable.frq=cumsum(frqTable.frq1,'reverse');
frqTable.frq1=[];
a1=ceil(avgAmplitude);
a2=floor(avgAmplitude-sd);
if a2<45
   iBValue=0.25*rand(1);
else
   if a1-a2<=0
      iBValue=0.25*rand(1);
   else
      N1=frqTable.frq(frqTable.AMP==a1);
     N2=frqTable.frq(frqTable.AMP==a2);
     if isnumeric(N1) && isnumeric(N2)
        iBValue=abs((log10(N1)-log10(N2))/(a2-a1));
     else
        iBValue=0.25*rand(1);
     end
  end
end
ibValue = iBValue*20;
end
```

APPENDIX C: MATLAB CODE TO PLOT IB-VALUE VS TIME

```
Function[ibValueGraph_colored]=(ChannelAEData,ibValuevsTime,fs
)
%     This Function is used to draw a graph of TIME VS Ib-Value
      based on AE data
%     'ChannelAEData' is the basic AE data table for a
      particular channel
%     'ibValuevsTime' is ibValue Table calculated using the
      function:
      [ibValuevsTime] =
      ibValuegroupedData(ChannelAEData,samplelength,threshold)
%     'fs' is the font size of the text for displaying text on
      the graph
figure('Name','IbValue Graph');
%     Draw graph iB-Value VS Time
ax = gca; % current axes
Ib1=ibValuevsTime(ibValuevsTime.IbValue<=1,:);
Ib2=ibValuevsTime(ibValuevsTime.IbValue >1 &
ibValuevsTime.IbValue<2,:);
Ib3=ibValuevsTime(ibValuevsTime.IbValue>=2,:);
hold(ax,'on');
plot(ax,Ib1.TIME,Ib1.IbValue,'marker', 's','MarkerSize', 3,
'color','r');
plot(ax,Ib2.TIME,Ib2.IbValue,'marker', 'd','MarkerSize', 3,
'color','b');
plot(ax,Ib3.TIME,Ib3.IbValue,'marker', 'p','MarkerSize', 3,
'color','k');
ax.YLabel.String='ib-Value';
ax.Title.String='ib-Value VS Time for Channel - ' ;
ax.Title.FontSize=fs+4;
ax.FontName='Helvetica';
ax.XLabel.String='Time (sec)';
ax.YLabel.String='Ib-value';
ax.XAxis.FontWeight='bold';
ax.YAxis.FontWeight='bold';
```

```
ax.XLabel.FontSize=fs;
ax.YLabel.FontSize=fs;
ax.XAxis.FontSize=fs;
%    Plot Time VS AE Energy on the right y-axis
yyaxis(ax,'right')
x=ChannelAEData.TIME;
ax.YLabel.FontSize=fs;
y=ChannelAEData.CUMENERGY;
plot(ax,x,y);
ax.YLabel.String='AE Energy (mV-sec)';
ax.XGrid='on';      ax.YGrid='on';
ax.XMinorGrid='on'; ax.YMinorGrid='on';
ax.XTickMode='auto';    ax.YTickMode='auto';
ax.XMinorTick='on'; ax.YMinorTick='on';
ax.XAxisLocation='origin';
ax.GridColor=[1.00,0.41,0.16];
ax.GridAlpha=0.25;
ax.GridLineStyle='-';
ax.MinorGridLineStyle='-.';
ax.MinorGridColor=[0.10,0.10,0.10];
ax.MinorGridAlpha=0.15;
screen_size=get(0,'ScreenSize');
set(gcf, 'Position', [1 1 0.5*screen_size(4)
0.5*screen_size(4)]);
end
```

APPENDIX D: DESIGN OF BEAM-COLUMN JOINT

MOR of Rectangular beam:				
$M_{u1} = 0.133 f_{ck} b d^2$ (Balanced MOR)				
f_{ck} = Characteristic compressive strength			35	N/mm^2
$f_{y,main}$ = Yield stress of main bars			500	N/mm^2
$f_{y,secondary}$= Yield stress of secondary bars			415	N/mm^2
b = width of the beam X-section			150	mm
Note: Clause 6.1.3 do not allow the width of the member to < 200 mm, but since it is an experimental set-up for a 50% reduced model obtained from the prototype of size 400X300 hence the restriction for the real specimen is within provisions of the code				
D = Overall depth of the beam			200	mm
No. of Bars provided in the tension face of the beam, n_t=			3	Nos.
Dia of main reinforcement bars Φ =			10	mm
Area of main bars, $A_{st} = \frac{\pi}{4}\emptyset^2 n_t$			236	mm^2
Percentage area of main bars, p_t			0.93	
Min. and Max. % of long. steel (as per IS 13920:1993 clause 6.2)				
$\rho_{\min} = 0.24\frac{\sqrt{f_{ck}}}{f_y}$	= 0.0028	$p_{t,min}$=	0.28	< 0.93 OK
ρ_{max}=	= 0.025	$p_{t,max}$=	2.5	> 0.93 OK
Nominal size of Coarse aggregates used			20	mm
Redistribution of the moment			0	%
Cover to longitudinal reinforcement of column (refer to clause 26.4.2)			25	mm
Clear spacing in bars provided =			35	mm
Maximum Clear spacing between Bars in Tension allowed (Refer to Table 15 of IS 456:2000)			150	> 35 OK
The minimum distance between bars (refer			25	OK

to clause 26.3.2) should be ≥		
d' = cover + Φ/2 =	30	mm
Dia of compression bar	10	mm
No. of bars in compression zone, n_2	2	
Area of compression bars, $A_{sc} =$	157	mm^2
d = D-cover-Φ/2	170	mm
Clear Span L (cantilever)	750	mm
Effective span l (refer 22.2 of IS 456:2000)	920	mm
Percentage steel for balanced section, $p_t = 18.87\frac{f_{ck}}{f_y}$	1.32	%
Area of Tensile steel for balanced section, $A_{st1} = \frac{p_t bd}{100}$	337	mm^2
Total Area of Tension steel provided A_{st} =3 bars of 10 mm dia	236	mm^2
d'/D =	0.15	
f_{sc} = stress in compression steel at the level of compression reinforcement (Refer Table F (page-13) of SP16)	395	N/mm^2
Total compression in steel, $C_s = (f_{sc} - f_{cc})A_{sc}$	56549	N
M_{u2} = C_s.(d-d') =	7916813	Nmm
$M_{u1} = 0.133 f_{ck} bd^2$	20179425	Nmm
M_{uc} = MOR for compression failure = $M_{u1} + M_{u2}$	28096238	Nmm
$A_{st2} = A_{st} - A_{st1}$	101	mm^2
M_{ut} = MOR for tensile failure = $M_{u1} + 0.87 f_y (d - d') A_{st2}$	26319942	Nmm
Since $M_{ut} < M_{uc}$, the MOR for tensile failure is controlling.		
M_u = Ultimate MOR of beam section	15410000	
M_d = Moment due to self wt. =	317400	
M_w = Moment due to Point load W = Wxl		
M_u = M_d + M_w		

Solving this we get, W =	16405	N
Maximum allowable lateral load during testing from a bending capacity point of view, $P = \frac{M_u}{l}$	16750	N
Where l = eff. length of the cantilever	920	mm
Total design moment at joint = M_d + M_w	15410000	Nmm
Self wt. of the beam, W_d	690	N
Factored shear $V = W + W_d$	17095	N
Design for Shear Reinforcement of Beam section: (Web reinforcement in beams)		
IS 456:2000 requirements		
Spacing for minimum shear reinforcement **(As per 26.5.1 of IS 456:2000)**		
$S_{v,min} = \frac{0.87 f_y A_{sv}}{0.4b}$	340	mm
shear stress $\tau_v = \frac{V}{bd}$	0.67	N/mm^2
p = A_{st} x100/bd	0.93	N/mm^2
$\tau_{c,max}$ = (refer IS 456 Table 20)	4	N/mm^2
τ_c (for p = 0.93 and M40) = (Refer to Table 19 of IS 456)	0.65	N/mm^2
Dia of stirrups used =	6	mm
No. of legs of stirrups =	2	nos.
$V_{us} = \frac{0.87 f_y A_{sv} d}{s_v}$ Where, $V_{us} = (\tau_v - \tau_c) bd$ Therefore, $s_v = \frac{0.87 f_y A_{sv}}{(\tau_v - \tau_c) b}$ Refer Clause 40.4 0f IS 456:2000		
Area of stirrups, A_{sv}=	56.5	mm^2
Spacing of stirrups required, S_v =	5616	mm

Spacing should not be more than the followings:(Refer clause 26.5.1.5 of IS 456:2000)		
1. Spacing based upon shear Force, S_v	5616	mm
2. 300 mm	300	mm
3. 0.75d	127.5	mm
4. For Minimum shear reinforcement, $S_{v,min}$	340	mm
The spacing required (least of above 4)	127.5	mm
Thus, the spacing provided =	120.0	mm
Provide 6 mm dia 2-legged stirrups @ 120 mm c/c [As per IS:456]		
Shear strength of the beam		
$V_u = \frac{0.87 f_y A_{sv} d}{s_v} + \tau_c bd$	45400.9	N
Maximum allowable Concentrated load from a shear strength point of view	44710.9	N
Enhancement of shear strength near the support for the beam section		
IS-456:2000 requirements (Clause 40.5)		
$a_v = \mathrm{D}.\tan 30$	115.47	
Design shear near support is enhanced by factor = $2d\frac{\tau_c}{a_v}$	1.93	
Enhanced shear near support = 1.93 x V_u =	32480	OK
The area of reinforcement near the support is calculated below:		
$A_s = \frac{a_v b}{0.87 f_y}\left(\tau_v - 2d\frac{\tau_c}{a_v}\right)$	-78.8	mm^2
$A_s \geq 0.4\frac{a_v b}{0.87 f_y}$	25.59	mm^2
Area of stirrups provided in the beam section above =	56.5	OK

Area of stirrups provided		56.5	
dia of stirrups required near support		6.0	mm
IS-13920 :1993 clause 6.3 Provisions for Beam section			
Stirrup Hook should have 135° bend of 10Φ long (but not < 75 mm)			
Minimum dia of hoop bar = 6 mm			
SF resisted by hoops should be a maximum of the following:			
1. Calculated SF			
2. SF due to the formation of plastic hinge			
$SF = V_u + 1.4\frac{M_u}{L}$		40545	N
Shear resistance of section =		45400.9	N
Spacing of hoops over a length of 2d from the face of the column shall be as below: (Refer to clause 6.3.5) of IS 13920:1993			
1. Should be less than d/4		42.5	mm
2. Should be less than 8 times the smallest dia of the longitudinal bar		80	mm
3. Not more than 100 mm		100	mm
Spacing of hoops adopted =		42.5	mm
Hence provide 6 mm dia 2-legged stirrups @ 42.5 mm c/c near the face of the column in the beam up to a distance of 2d = 340 from the face of the column (As per code IS 13920)			
Shear reinforcement in Beam beyond 2d distance (clause 6.3.5)			
Spacing beyond 2d distance should not be more than b/2		75	mm
Hence spacing adopted beyond 2d distance in beam = Min(b/2, s_v)		75	mm
Hence provide 6 mm dia 2-legged stirrups @ 75 mm c/c near the face of the column in the beam beyond 2d = 340 from the face of the column (As per code IS 13920)			
Check for end anchorage:			
$L_d \leq 1.3\frac{M_1}{V} + L_o$	$x_{u,max}$	77.52	mm

$M_1 = 0.87 f_y A_{st} d$ (It is a moment carried by steel in tension)	17452200	Nmm
Shear force at the face of the column, V_u	17095	N
τ_{bd} =	2.72	N/mm^2
(Note: Bond stress is increased by 60%, refer 26.2.1.1 of IS 456:2000, for tor steel)		
L_o = larger of d and 12dia (refer 26.2.3.3)	170	mm
$1.3\frac{M_1}{V} + L_o$	1497	mm
$L_d = \frac{\phi \sigma_s}{4\tau_{bd}}$ (Refer 26.2.1)	460	OK
The top and bottom reinforcing bars in the beam section should extend into the column to provide adequate anchorage length as below:		
Development length L_d a. As per IS 456:2000)	455	mm
b. As per clause 6.2.5 of IS 13920:1993) L_d + 10Φ -8Φ = 8Φ is reduction for 90° bend)	475	mm
Check for deflection:		
Actual span to effective depth ratio =	4.41	
Percentage steel, p =	0.93	
1. Modification factor for Tension steel (K_1)		
$K_1 = \frac{1}{(0.225 + 0.003 f_s + 0.625 \log_{10} p_t)}$		
$f_s = \frac{5}{8} fy \frac{A_{s,required}}{A_{s,provided}} \frac{1}{\beta}$	312.5	N/mm^2
Note: Since Moment capacity has been calculated from the area of steel provided, hence $A_{st,required}$ *and* $A_{st,provided}$ *are equal*		
The redistribution factor is the ratio of the moment at the section after	1	

redistribution to the moment before redistribution, β =		
K_1 =	0.88	
2. Modification factor for compression steel (K_2)		
% Steel pc	0.46	
$K_2 = \frac{1.6p_c}{(p_c + 0.275)} \leq 1.5$	1	
Maximum K_2	1.5	
K_2 adopted	1	
Modified value of Span to Depth ratio $Actual \frac{span}{Depth} K_1 . K_2$	3.88	
Spa/Depth ratio allowed as per clause 23.2.1 of IS 456:2000 for cantilever beams	7	OK
Design of Column:		
Column Height	1000	mm
D = Depth of column in the direction of lateral load	200	mm
b = width of the column	150	mm
No. of bars	6	
dia of bar	10	mm
Clear cover	25	mm
d' (cover to reinforcement on comp. face)	30	mm
D (cover to reinforcement on tension face)	170	mm
d'/D	0.15	mm
P_u, Axial load on the column $P_u < 0.1 f_{ck} bD$	50000	N
M_u = Total design moment at the junction	15410000	Nmm
Design of reinforcement as per SP16		
Use Chart 37 for d'/D = 0.15		
$\frac{P_u}{f_{ck} b.D}$	0.048	
p = percentage of steel provided	1.850	%
$\frac{p}{f_{ck}}$, calculated	0.053	

$\frac{M_u}{f_{ck}b.D^2}$	0.073	
$\frac{p}{f_{ck}}$ (From Chart 37) =	0.020	
p =	0.700	%
A_s = p.b.D/100 = Moment Capacity of column	210	mm^2
Area provided =	471.2	OK
$\frac{M_u}{f_{ck}b.D^2}$ (From SP16 chart 37)	0.1	
M_u=	21000000	Nmm
Dia of hoop	6	mm
No. of legs	2	
The pitch of hoops shall be as below (IS 456:2000 clause 26.5.3.2 4c)		
1. Least lateral dimension of the column	150	mm
2. 16φ of the smallest longitudinal bar	160	mm
3. 48 times dia of ties	288	mm
Spacing of hoops provided	150	mm
Check for shear as per clause 40.2.2 of IS 456:2000		
Factored shear $V = \frac{1.4M_u}{L}$	21574	N
shear stress, $\tau_v = V/bd$	0.85	N/mm^2
$p = \frac{A_{st}}{bd}100 \times \frac{1}{2}$ i.e., (50% of A_{st})	0.92	%
τ_c =	0.65	N/mm^2
Dia of stirrups used =	6	mm
No. of legs of stirrups =	2	nos.
A_{sv} =	56.5	mm^2
$\delta = 1 + \frac{3P_u}{A_g f_{ck}} \leq 1.5$ δ ≤ 1.5	1.143	factor

δ adopted =			1.125	
$\tau_c' = \tau_c.\delta$			0.738	N/mm^2
$V_{us} = \frac{0.87 f_y A_{sv} d}{s_v}$ $V_{us} = (\tau_v - \tau_c) bd$ $s_v = \frac{0.87 f_y A_{sv} d}{V_{us}}$ $s_v = \frac{0.87 f_y A_{sv}}{(\tau_v - \tau_c) b}$ Refer Clause 40.4 0f IS 456:2000				
Spacing of stirrups required s_v =			1259.0	mm
Spacing for minimum shear reinforcement as per 26.5.1 of IS 456:2000 $s_v = \frac{0.87 f_y A_{sv}}{0.4 b}$			340	mm
Spacing should not be more than:				
1. 300 mm			300	mm
2. 0.75d			127.5	mm
Thus, the spacing provided =			125.0	mm
Provide 6 mm dia 2-legged stirrups @ 125 mm c/c *(IS 456 provisions)*				
Design for confinement steel for column (Clause 7.4 of IS 13920:1993)				
$A_{sh} = 0.18 S.H. \left[\frac{A_g}{A_k} - 1\right] \frac{f_{ck}}{f_y}$				
A_{sh}=	56.55	mm2		
A_g=	30000	mm2		
A_k=	18144	mm2		
H	150	mm		
Solving the above equation for the Spacing of confining steel, S =			46.0	mm
Pitch confining steel shall be as below:				
1. 1/4 of the Least lateral dimension of			37.5	mm

the compression member				
2. not <75 mm			75	*mm*
3. not > 100 mm			100	*mm*
Spacing adopted =			37.5	*mm*
l_o = Distance up to which confining steel is provided in column and is taken a maximum of the following:				
1. Depth of column	200	mm		
2. 1/6 of clear span	125	mm		
3. 450 mm	450	mm		
l_o adopted			450	*mm*
So, provide confining reinforcement 6 mm dia 2-Legged stirrups @ 37.5 mm c/c in a length lo = 450 mm on both sides of the column joint				
Design Shear in Column at a place other than a confined area (As per IS 13920:1993)				
Dia of stirrups used =			6	*mm*
No. of legs of stirrups =			2	nos.
Spacing should not be more than:				
1. Spacing of hoops shall not exceed half the least lateral dimension of the column			75	*mm*
2. Spacing for minimum shear reinf.			340	*mm*
Thus, the spacing provided =			75	*mm*
Provide 6 mm dia 2-legged stirrups @ 75 mm c/c				
Minimum Radius of Bar bend to limit bearing stress on bend (Refer clause 26.2.2.5 of IS 456:2000)				
a is c/c distance between bars =			45	*mm*
φ is the dia of the main bar =			10	*mm*
$r \geq 0.456 \frac{f_y}{f_{ck}} \left(1+2\frac{\varphi}{a}\right)\varphi$			94	*mm*
Reinforcement details:				
Longitudinal reinforcement in Beam and column				
Beam	Tension steel	**3# 10 mm Φ**		
	Comp steel	**2# 10 mm Φ**		

Column	Both faces are equally distributed	6# 10 mm Φ	
Shear Stirrups			
In Beam			
(i) As per IS 13920:1993(Confining reinforcement)			
Up to 2d	6 mm dia 2 legged stirrups @ 40 mm c/c near the face of the column in the beam up to distance 340		
Beyond 2d	6 mm dia @ 75 mm c/c		
(ii) As per IS 456:2000 (Web reinforcement) **Provide 6 mm dia 2-legged stirrups @ 120 mm c/c**			
In Column **(i). As per IS 13920:1993)**			
Within confining zone	6 mm dia @ 37.5 mm c/c confining reinforcement in lo = 450 mm		
Beyond confining zone	6 mm dia @ 75 mm		
(ii). As per IS 456:2000	6 mm dia @ 125 mm c/c		

REFERENCES

1 Samira GS., Leman Z. and Baharudin B. A review of the application of acoustic emission technique in engineering. June 2015, Structural Engineering & Mechanics 54(6):1075-1095, DOI:10.12989/sem.2015.54.6.1075

2 Lovejoy SC. Acoustic emission testing of beams to simulate SHM of Vintage reinforced concrete deck girder highway bridges. Structural Health Monitoring 2008;7(4):329.

3 Nair A, Cai C. Acoustic emission monitoring of bridges: review and case studies. Eng Struct 2010;32(6):1704–1714.

4 Golaski L, Gebski P, Ono K. Diagnostics of reinforced concrete bridges by acoustic emission. J Acoustic Emission 2002;20(2002):83–98.

5 Rao MVMS., Lakshmi KJP., Analysis of b-value and improved b-value of acoustic emissions accompanying rock fracture, Current Science (2005) 89(9) 1577–1582.

6 Shah S.G., Chandra Kishen J.M., Fracture behaviour of concrete–concrete interface using acoustic emission technique, Engineering Fracture Mechanics 77 (6) (2010) 908–924. 10.1016/j.engfracmech.2010.01.018

7 Godano C., Lippiello E., de Arcangelis L. Variability of the b value in the Gutenberg–Richter distribution. Geophysical Journal International, Volume 199, Issue 3, December 2014, Pages 1765–1771. https://doi.org/10.1093/gji/ggu359

8 Ohtsu, M., Uchida, M., Okamoto, T., and Yuyama, S. (2002), "Damage assessment of reinforced concrete beams qualified by acoustic emission", ACI Structural Journal, Volume 99, No. 4, pp. 411–417. DOI: https://doi.org/10.4401/ag-3472

9 Ohtsu M, Isoda T, Tomoda Y. Acoustic emission techniques standardized for concrete structures. J Acoustic Emission 2007; 25:21–32. https://www.ndt.net/article/jae/papers/25-021.pdf

10 Kentaro Ohno K, Ohtsu M. Crack classification in concrete based on acoustic emission. Construction and Building Materials, Volume 24, Issue 12, December 2010, Pages 2339-2346, https://doi.org/10.1016/j.conbuildmat.2010.05.004

11 JCMS-III B5706, 2003. Monitoring method for active cracks in concrete by acoustic emission. Federation of Construction Materials Industries Japan.

12 Aggelis DG. Classification of cracking mode in concrete by acoustic emission parameters. Mechanics Research Communications 2011;38(3):153–157. https://doi.org/10.1016/j.mechrescom.2011.03.007

13 Shahidan S., Pulin R., Bunnori N.M., Holford K.M., Damage classification in reinforced concrete beam by acoustic emission signal analysis, Construction and Building Materials 45 (2013) 78–86.

14 Park Y.; Ang A.H.S. et al. (1985). Seismic Damage Analysis of Reinforced Concrete Buildings. Journal of Structural Engineering, Vol. 111, Issue 4 (April 1985) https://doi.org/10.1061/(ASCE)0733-9445(1985)111:4(740)

15 Wang Y., Liu Z., Yang W., and Zheng X. Research on the Estimation Method of the Stiffness Degeneration Index of Reinforced Concrete Members. Advances in Civil Engineering Volume 2020, Article ID 9464275, 16 pages, https://doi.org/10.1155/2020/9464275

16 Benavent-CA, Gallego A, Mico JM. An acoustic emission energy index for damage evaluation of reinforced concrete slabs under seismic loads. Structural Health Monitoring 2011;11(1);69-81. https://doi.org/10.1177/1475921711401128

17 Colombo S, Forde M, Main I, Shigeishi M. Predicting the ultimate bending capacity of concrete beams from the 'relaxation ratio' analysis of AE signals. Construction and Building Material 2005; 19; 746-754 doi:10.1016/j.conbuildmat.2005.06.004

18 Mostofinejad D and Hajrasouliha M. 3D beam–column corner joints retrofitted with X-shaped FRP sheets attached via the EBROG technique. March 2019 Engineering Structures 183(2):987-998. DOI: 10.1016/j.engstruct.2019.01.038

19 Li, V.C., Mishra, D.K., Naaman, A.E., Wight, J.K., LaFave, J.M., Wu H.C., and lnada, Y. (1994). On the Shear Behavior of ECC, Journal of Advanced Cement-Based Materials, 1(3): 142-149

20 Maalej, M., and Li, V.C. (1995). Introduction of Strain Hardening Engineered Cementitious Composites in the Design of Reinforced Concrete Flexural Members for Improved Durability. ACJ Structural Journal. 92(2): 167-176.

21 ACI-ASCE Committee 352 (2002), "Recommendations for Design of Beam-Column Connections in Monolithic Reinforced Concrete Structures", ACI 352R-02, American Concrete Institute, Farmington Hills, Michigan.

22 Subramanian, N. and Rao, D.S.P. (2003). "Seismic Design of Joints in RC Structures—A Review", Indian Concrete Journal, Vol. 77, No. 2, pp. 883–892

23 Murthy, D.S.R., Gandhi, P., Sreedhar, D.S., Vaidhyanathan, C.V. and Mohanty, O.N. (2000). "Seismic Resistance of Reinforced Concrete Beam-Column Joints with TMT and CRS Bars", ICI Journal, Vol. 1, No. 3, pp. 19–26.

24 Hwang, S.-J., Lee, H.-J., Liao, T.-F., Wang, K.-C. and Tsai, H.-H. (2005). "Role of Hoops on Shear Strength of Reinforced Concrete Beam-Column Joints", ACI Structural Journal, Vol. 102, No. 3, pp. 445–453.

25 Karayannis, C., Sirkelis, G. and Mavroeidis, P. (2005). "Improvement of Seismic Capacity of External Beam-Column Joints Using Rectangular Spiral Shear

Reinforcement", Proceedings of the Fifth World Conference on Earthquake Resistant Engineering Structures (ERES V), Skiathos, Greece, pp. 147–156.

26 McGuire W, Gallagher R H and Zeimian R D (2000). Matrix structural analysis. John Wiley and sons, New York, USA

27 Elnashai A S and Sarno L D (2008). Fundamentals of earthquake engineering. Wiley: United Kingdom.

28 Estekanchi H and Arjomandi K (2007). Comparison of damage index in non-linear time history analysis of steel moment frames. Asian Journal of Civil Engineering, 8(6):629-646.

29 Kanwar V., Kwatra N. and Aggarwal P. Damage Detection for Framed RCC Buildings using ANN Modeling. International Journal of Damage Mechanics, Published October 1, 2007 Research Article, https://doi.org /10.1177/1056789506065939

30 Miranda, E., Bertero, V. (1994). Evaluation of strength reduction factors for earthquake-resistant design. Journal of Earthquake Spectra 10(2):357-379.

31 Brachmanni , B J and Matamoros A. Relationships between drift and confinement in reinforced concrete columns under cyclic loading. 13thWorld Conference on Earthquake Engineering Vancouver, B.C., Canada August 1-6, 2004 Paper No. 2531.

32 Carrillo J, González G and Rubiano A. Displacement ductility for seismic design of RC walls for low-rise housing. Latin American Journal of Solids and Structures, Aug 2014, https://doi.org/10.1590/S1679-78252014000400010.

33 Singh B, Kwatra N. and Sharma S. Damage detection of masonary infilled RC frame structure. A thesis for award of degree of PhD. Thapar Institute of Engineering and technology 2020.

34 Bakir P.G., Boduroglu M.H. A new design equation for predicting the shear strength of monotonically loaded exterior beam-column joints, Eng. Struct. J. 24 (8) (2002) 1105–1117.

35 Patil S.S., Manekari S.S. Analysis of reinforced beam-column joint subjected to monotonic loading, Int. J. Eng. Innovat. Technol. (IJEIT) 2 (10) (2013) 149–158.

36 Jinkoo K, and Hyunhoon C. Monotonic Loading Tests of RC Beam-Column Subassemblage Strengthened to Prevent Progressive Collapse. International Journal of Concrete Structures and Materials Vol.9, No.4, pp.401–413, December 2015. DOI 10.1007/s40069-015-0119-2

37 Tran, TM Hadi MN, Shear strength model of reinforced concrete exterior joint under cyclic loading, Struct. Build. 170 (8) (2017) 603–617.

38 Mounika, B Poluraju P. Investigation of Beam Column Joint with Beam Weak in Shear under Monotonic Loading. International Journal of Engineering & Technology, 7 (2.20) (2018) 182-188.

39 Fei G, Zhiqiang T, Biao H, Junbo C, Hongping Z & Jian M. Investigation of the interior RC beam-column joints under monotonic antisymmetrical load. Front. Struct. Civ. Eng. 2019, 13(6): 1474–1494 https://doi.org/10.1007/s11709-019-0572-0

40 NZS3101:1982 Part I: Code of practice for the design of concrete structures and Part 2: Commentary on the design of concrete structures, Wellington, Standards Association of New Zealand, 1982 (Amendment no.1 was issued in December 1989, mainly to take into account new reinforcing steel grades manufactured in New Zealand)

41 ACI 3 18-89: Building Code requirements for reinforced concrete and Commentary on building Code requirements for reinforced concrete, Detroit, Michigan, American Concrete Institute, 1989

42 ACI-ASCE Committee 352: 'Recommendations for design of beam-column joints in monolithic reinforced concrete structures', Journal of the American Concrete Institute, 82, No.3, May-June 1985, p266

43 ATC-11: Seismic resistance of reinforced concrete shear walls and frame joints: implications of recent research for design engineers, Palo Alto, California, Applied Technology Council, 1983

44 Park, R., Milburn, J. R.: 'Comparison of recent New Zealand and United States seismic design provisions for reinforced concrete beam-column joints and test results from four units designed according to the New Zealand Code', Bulletin of the New Zealand National Society for Earthquake Engineering, 16, No.1, March 1983, p3

45 Paulay, T.: 'A critique of the special provisions for seismic design of the building Code requirements for reinforced concrete (ACI 318-83)', Journal of the American Concrete Institute 83, No.2, March- April 1986, p274

46 Paulay, T.: 'Seismic behaviour of beam-column joints in reinforced concrete space frames', State-of-the-Art Report in Special Theme Session SF on Inelastic Behaviour and Modelling of Concrete Structural Components under Multidirectional Seismic Forces, Proc. 9th World Conference on Earthquake Engineering, Tokyo-Kyoto, 1988, VIII, p557

47 CEB: 'Model Code for seismic design of concrete structures Bulletin d'Information, No. 165, Comit e Euro-International du Beton, April 1985

48 Eurocode 8: 'Structures in seismic regions-design-part 1 : general and building', Report EUR 12266 EN, Luxembourg, Commission of the European Communities, May 1988 ed. (draft for comment)

49 Tsonos, A.G., Tegos, I.A., Penelis, G.: Seismic resistance of type 2 exterior beamcolumn joints reinforced with inclined bars, Aci Structural Journal, 89 (1992) 1, pp. 3–12

50 Pampanin, S., G.M. Calvi, and M. Moratti. Seismic beahviour of R.C. beam-column joints designed for gravity loads. in 12th European Conference on Earthquake Engineering. 2002. London: Elsevier Science Ltd.

51 Fischer G and Li VC. (2003). Deformation behavior of fibre-reinforced polymer reinforced Engineered Cementitious Composite (ECC) flexural members under reversed cyclic loading conditions. AC/ Structure Journal. 100(1):25-35.

52 Said A M and Nehdi L M (2004). Performance of structural Concrete Frames Reinforced with GFRP grid. Proceedings of 13th world conference on earthquake engineering, Vancouver, B C, Canada.

53 Bazan M and Sasani M. A New Damage Model For Reinforced Concrete Elements. 13th World Conference on Earthquake Engineering, Vancouver, B.C., Canada, August 1-6, 2004, Paper No. 2846

54 Mukhrjee A and Joshi M. (2005). FRPC reinforced concrete beam-column joints under cyclic excitation, Composite Structures, 70: 185-199.

55 Wang YC and Hsu K. (2009). Design recommendations for the strengthening of reinforced concrete beams with eternally bonded composite plates. Composite Structures, 88(2):323-332.

56 Yuan F., Jinlong P., Zhun X. and Leung, C.K.Y. (2013). A comparison of engineered cementitious composites versus normal concrete in beam-column joints under reversed cyclic loading, Materials and Structures, 46:145-159.

57 Qudah S., Maalej M. Application of engineered cementitious composites (ECC) in interior beam–column connections for enhanced seismic resistance. Eng. Struct., 69 (2014), pp. 235-245

58 Muthuswamy, K.R, Thirugnanam, G.S. (2014) Structural behaviour of hybrid fibre reinforced concrete exterior Beam-Column joint subjected to cyclic loading, International Journal ofcivil and structural engineering, 4(3): 262-273.

59 Ganesh KD and Prabavathy, S. (2015). Experimental Study on Seismic Performance in Beam-Column Joint lJsing Hybrid Fibres. International Journal of Science and Engineering Applications. 4(3):135-137.

60 Cosgun, C., Comert, M., Demir, C., Ilki, A.: Seismic Retrofit of Joints of a Full-Scale 3D Reinforced Concrete Frame with FRP Composites, Journal of Composites for Construction-ASCE, 23 (2019) 2, doi: 10.1061/(ASCE)CC.1943-5614.0000923.

61 Wang Y., Liu Z., Yang W., and Zheng X. Research on the Estimation Method of the Stiffness Degeneration Index of Reinforced Concrete Members. Advances in Civil Engineering Volume 2020, Article ID 9464275, 16 pages, https://doi.org/10.1155/2020/9464275

62 Mishra DK. Design of pseudo strain-hardening cementitious composites for a ductile plastic hinge (Ph.D. thesis) University of Michigan, Michigan (1995)

63 Yuan F Pan J, Zhum X, Leung C.K.Y.. A comparison of engineered cementitious composites versus normal concrete in beam–column joints under reversed cyclic loading. Mater. Struct., 46 (1–2) (2013), pp. 145-159

64 Zhang R, Matsumoto K, Hirata T, Ishizeki,Y and Niwa J. Application of PP–ECC in beam–column joint connections of rigid-framed railway bridges to reduce transverse reinforcements. Eng. Struct., 86 (2015), pp. 146-156

65 Ansari F. Practical implementation of optical fibre sensors in civil structural health monitoring. Journal of intelligent material systems and structures. 2007 August 2007;18:879-89.

66 Li H. N., Li D.S., Song G.B. Recent applications of fibre optic sensors to health monitoring in civil engineering. Engineering structures. 2004; 26:1647-57.

67 Rens, K. L.; Wipf, T. J.; Klaiber, W. 1997. Review of non-destructive evaluation techniques of civil infrastructure, Jour-nal of Performance Constructed Facilities 11(4): 152–160. http://dx.doi.org/10.1061/(ASCE)0887-3828(1997)11:4(152)

68 Park, G., Cudney, H., and Inman, D. J., 2000a, “Impedance-Based Health Monitoring of Civil Structural Components,” ASCE Journal of Infrastructure Systems, Vol. 6, No. 4, 153–160.

69 Czochralski, J. (1916). Metallographie des Zinns und die Theorie der Formänderung bildsamer Metalle. Metall und Erz, Vol.22, pp. (381-393), 1011-4602

70 IOWA State University, Center for Nondestructive Evaluation, https://www.nde-ed.org/NDETechniques/AcousticEmission/AE_Intro.xhtml

71 Kaiser E. J., An Investigation into the Occurrence of Noises in Tensile Tests or a Study of Acoustic Phenomena in Tensile Tests, [Ph.D thesis], Dissertation Technische Hochschule Munchen, Munich, 1950.

72 Christian U. Grosse, Masayasu Ohtsu (Eds.) Acoustic Emission Testing. ISBN 978-3-540-69895-1, DOI 10.1007/978-3-540-69972-9

73 Singh S, Sharma S and Kwatra N. Damage progression in RC beam-column joints under cyclic loading using acoustic emission technique. International Federation for Structural Concrete. wileyonlinelibrary.com/journal/suco Structural Concrete. Accepted: 16 August 2021; 22:3556–3573. DOI: 10.1002/suco.202000713

74 Mpalaskas, A.C., Matikas, T.E., van Hemelrijck, D.; Iliopoulos, S.; Papakitsos, G.S.; Aggelis, D.G. (2015). Acoustic signatures of different damage modes in plain and repaired granite specimens. In Proceedings of the SPIE-The International Society for Optical Engineering, San Diego, CA, USA, 9–11 March 2015.

75 Nor M., N. Muhamad Bunnori, A. Ibrahim, S. Shahidan, and S. N. Mat Saliah. (2011). An observation of noise intervention into acoustic emission signal on concrete structure. IEEE 7th International Colloquium on Signal Processing and its Applications, 2011

76 Gutenberg, B. and Richter, C. F., (1954). In Seismicity of the Earth and Associated Phenomena, Princeton University Press, Princeton, NJ, USA, 1954, 2nd edn.

77 Colombo I. S., Main I. G. and Forde M. C. (2003). Assessing Damage of Reinforced Concrete Beam using b-value Analysis of Acoustic Emission Signal., Journal of Materials in Civil Engineering, ASCE May-June 2003, 15(3),280-286

78 Shiotani, T., Fujii, K., Aoki, T. and Amou, K. (1994) Evaluation of Progressive Failure Using AE Sources/Improved b-Value on Slope Model Tests. Progress in Acoustic Emission, 7, 529-534.

79 Shiotani, T & Yuyama, S. & Li, Z.W. & Othsu, M.. (2000). Quantitative evaluation of fracture process in concrete by the use of improved b-value. 5th Int. Symposium Non-Destructive Testing in Civil Engineering. 293-302. 10.1016/B978-008043717-0/50031-3.

80 RDSO, (2009). Guidelines on use of Acoustic emission technique (AET) on railway bridges, BS-104, Oct 2009, B&S Directorate, Research Design and Standards organisation Lucknow (Government of India

81 Jiapeng L. and Lei Q., (2019). Study on Acoustic Emission Localization of Concrete Using Modified Velocity, Research Article, Hindawi, Advances in Civil Engineering, Volume 2019, Article ID 6890327, 11 pages, May 2019.

82 Ohtsu M. The History and development of acoustic emission in concrete engineering. Concrete library of JSCE No. 25, June 1995, pp. 9-19

83 Pollock, A. A. (1989). "Acoustic Emission Inspection." Metals Handbook 17: 278-294.

84 Kaiser J: ‘Untersuchung über das Auftreten von Geräuschen beim Zugversuch’, Dr.-Ing. Dissertation, Fakultät für Maschinenwesen und Elektrotechnik der Technischen Universität München (TUM); 15.2.1950.

85 Vallen-System. AE Testing Fundamentals,Equipment, Applications. Dipl. Ing. Hartmut Vallen, Vallen-Systeme GmbH Icking (Munich), Germany

86 AEwinTM Real time data acquisition and replay software by Physical acoustics

87 Beattie A.G. Acoustic emission non-destuctive testing of structures using source location techniques. Sandia Report SAND2013-7779 Unlimited release Printed sep 2013

88 Labuz J.F., Cattaneo S. and Chen L. Acoustic emission at failure in quasi-brittle materials. July 2001Construction and Building Materials 15(5):225-233, DOI:10.1016/S0950-0618(00)00072-6

89 Shigeishi, M., S. Colombo, et al. (2001). "Acoustic emission to assess and monitor the integrity of bridges." Construction and Building Materials 15(1): 35-49.

90 Leszek G, P. G., and Kanji O (2002). "Diagnostics of reinforced concrete bridges by acoustic emission." Journal of Acoustic Emission 20: 83-98.

91 Chen, B. and J. Liu (2004). "Experimental study on AE characteristics of three-point-bending concrete beams." Cement and Concrete Research 34(3): 391-397.

92 Farid U, A. K. M., Numata K, et al. (2004). "Mechanisms of crack propagation due to corrosion of reinforcement in concrete by AE-SiGMA and BEM." Construction and Building Materials 18(3): 181-188.

93 Grosse, C. U. and Finck F (2006). "Quantitative evaluation of fracture processes in concrete using signal-based acoustic emission techniques." Cement and Concrete Composites 28(4): 330-336.

94 Ohno, K. and M. Ohtsu (2010). "Crack classification in concrete based on acoustic emission." Construction and Building Materials 24(12): 2339-2346.

95 Carpinteri A., Lacidogna G., Pugno N. Structural damage diagnosis and life-time assessment by acoustic emission monitoring. Engineering Fracture Mechanics 74 (2007) 273–289

96 Jiang XU, Shuchun LI,TANG X, TAO Y, JIANG Y. Influential factors of acoustic emission location experiment of rock under uniaxial compression

97 Climent A. B., Gallego A., Castro E., Vico J. M. and Jequier J. M. Acoustic emission applied to damage monitoring of RC beam-column connections subjected to low-cycle fatigue loading. EWGAE 2008 28-European Conf. AE Testing.

98 Carpinteri A., Corrado M., Lacidogna G. Heterogeneous materials in compression: Correlations between absorbed, released and acoustic emission energies. Engineering Failure Analysis 33 (2013) 236–250

99 Abdelrahman M, Mohamed K. ElBatanouny, Paul H.Ziehl. Acoustic emission based damage assessment method for prestressed concrete structures: Modified index of damage. Engineering Structures Volume 60, February 2014, Pages 258-264. https://doi.org/10.1016/j.engstruct.2013.12.037

100 Ma G, Li H. Acoustic emission monitoring and damage assessment of FRPstrengthened reinforced concrete columns under cyclic loading. Construction and Building Materials 144 (2017) 86–98.

101 Sagasta F., Zitto M. E., Piotrkowski R., Climent A B. Acoustic emission energy b-value for local damage evaluation in reinforced concrete structures subjected to seismic loadings. Mechanical Systems and Signal Processing 102 (2018) 262–277. https://doi.org/10.1016/j.ymssp.2017.09.022

102 Zeng H., Hartell JJ. A., Soliman M. Damage evaluation of prestressed beams under cyclic loading based on acoustic emission monitoring. Construction and Building Materials 255 (2020) 119235

103 Zhang X, Li B. Damage characteristics and assessment of corroded RC beam-column joint under cyclic loading based on acoustic emission monitoring. Engineering Structures 205 (2020) 110090https://doi.org/10.1016/j.engstruct.2019.110090

104 Prem PR, Verma M, Ambily P.S.. Damage characterization of reinforced concrete beams under different failure modes using acoustic emission. Structures 30 (2021) 174–187

105 IS 8112 (1989): Specification for 43 grade ordinary Portland cement [CED 2: Cement and Concrete]

106 IS 12269 (1987): 53 grade ordinary Portland cement [CED 2: Cement and Concrete]

107 IS 456 (2000): Plain and Reinforced Concrete - Code of Practice [CED 2: Cement and Concrete]

108 IS 10262 (2009): Guidelines for concrete mix design proportioning [CED 2: Cement and Concrete]

109 IS 432-1 (1982): Mild Steel and Medium Tensile Steel Bars and Hard-Drawn Steel Wire for Concrete Reinforcement, Part-1: Mild Steel and Medium Tensile Steel Bars [CED 54: Concrete Reinforcement]

110 IS 1786 (2008): High strength deformed steel bars and wires for concrete reinforcement- [CED 54: Concrete Reinforcement]

111 Paulay T and Priestley M J N (1992). Seismic design of reinforced concrete and masonary buildings. John Wiley and Sons, Toronto, Canada.

112 IS 13920 (1993, Reaffirmed 2008): Ductile Detailing Of Reinforced Concrete Structures Subjected To Seismic Forces - Code Of Practice. UDC 69.059.25 (026) : 624.042.7

113 Li, V.C. On Engineered Cementitious Composites (ECC)–A review of the material and its applications. J. Adv. Concr. Technol. 2003, 1, 215–230.

114 Li, V.C.;Wang, S.;Wu, C. Tensile strain-hardening behavior of PVA-ECC. ACI Mater. J. 2001, 98, 483–492.

115 Etman E. E., Hussein M., Baraghith A. T., El-Hashash M. M. Strengthening of RC beam-column joints using engineered cementitious composites. March 2019, International conference on Advances in Structural and Geotechnical Engineering, ICASGE'19, at Hurghada, Egypt

116 Singh B, Kwatra N, Shruti S. Damage detection of masonry infilled RC Frame structure. A thesis for the award of PhD at Thapar Institute of Engineering and Technology.

117 Subramanian, N. and Rao, D.S.P. (2003). “Seismic Design of Joints in RC Structures—A Review”, Indian Concrete Journal, Vol. 77, No. 2, pp. 883–892

118 Park R. (1988), State of the art report, Ductility evaluation from laboratory and analytical testing. Proceedings of ninth Word Conference on earthquake engineering, Aug 2-9, 1988, Tokyo-Kyoto, Japan (Vol. VIII).

119 Siva CKR, Thirugnanam GS. Comparative study on behaviour of reinforced beam-column joints with reference to anchorage detailing. Journal of Civil En gineering Research 2012, 2(4): 12-17 DOI: 10.5923/j.jce.20120204.01

120 AEwinTM Real time data acquisition and replay software by Physical acoustics

121 RILEM TC 212-ACD: acoustic emission and related NDE techniques for crack detection and damage evaluation in concrete. Materials and Structures (2010) 43:1187–1189 DOI 10.1617/s11527-010-9640-6

122 Elfergani HA, Pullin R, Holford KM. Damage assessment of corrosion in prestressed concrete by acoustic emission. Constr Build Mater 2013;40:925–33.

123 Soulioti, D., N. M. Barkoula, et al. (2009). "Acoustic emission behavior of steel fibre reinforced concrete under bending." Construction and Building Materials 23(12): 3532-3536.

124 Calabrese L, Campanella G, Proverbio E. Use of cluster analysis of acoustic emission signals in evaluating damage severity in concrete structures J Acoustic Emission, 28 (2010), pp. 129-141

125 Shahidan S, Bunnori N M, Syaifuddin M, N. Md Nor, M. A. Megat Johari, Analysis of the AE signals parameter at the critical area on the concrete beam, in: Ind. Electron. Appl. ISIEA 2012 IEEE Symp. On, IEEE, 2012: pp. 386–391. http://ieeexplore.ieee.org/xpls/abs_all.jsp?

126 Aldahdooh M A A, Bunnori N M. Crack classification in reinforced concrete beams with varying thicknesses by mean of acoustic emission signal features. Construction

Building Material, 45 (2013), pp. 282-288, 10.1016/j.conbuildmat.2013.03.090.

127 Shahidan S, Pulin R, Bunnori N M, Holford K M. Damage classification in reinforced concrete beam by acoustic emission signal analysis. Construction and Building Materials, 45 (2013), pp. 78-86, 10.1016/j.conbuildmat.2013.03.095 (Reference 13)

128 Prem P R, Murthy A R. Acoustic emission and flexural behaviour of RC beams strengthened with UHPC overlay Constr. Build. Mater., 123 (2016), pp. 481-492, 10.1016/j.conbuildmat.2016.07.033

129 Prem P R, Murthy A R. Acoustic emission and flexural behaviour of RC beams strengthened with UHPC overlay Constr. Build. Mater., 123 (2016), pp. 481-492, 10.1016/j.conbuildmat.2016.07.033

130 Shiotani, T., Ohtsu, M., and Ikeda, K. (2001). ‘‘Detection and evaluationof AE waves due to rock deformation.’’ Constr. Build. Mat., 15(5–6),235–246

131 Sammonds, P. R., Meredith, P. G., Murrel, S. A. F., and Main, I. G.(1994). ‘‘Modelling the damage evolution in rock containing porefluid by acoustic emission.’’ Eurock ’94, Balkerna, Rotterdam, TheNetherlands

132 Shiotani, T., Yuyama, S., Li, Z. W., and Othsu, M. (2000). ‘‘Quantitative evaluation of fracture process in concrete by the use of improvedb-value.’’ 5th Int. Symposium Non-Destructive Testing in Civil Engi-neering, T. Uohoto, ed., Elsevier Science, Amsterdam, 293–302

133 Ledeczi A., Hay T., P Volgyesi., Hay D.R., A Nadas., Jayaraman S. Wireless acoustic emission sensor network for structural monitoring. IEEE Sensors Journal. 2009;9(11):1370-7.

134 Behnia A, Chai H.K., Mousa A.A., Seyed Ravanfar A. A novel damage index for online monitoring of RC slabs under monotonic loading by integration of process controlling into acoustic emission technique. Mechanical Systems and Signal Processing 119 (2019) 547–560

135 Gong, Z., E. Nyborg, and G. Oommen, Acoustic emission monitoring of steel railroad bridges. Materials evaluation, 1992. 50(7).

136 NDIS 2421 (2000), Recommended Practice for In-Situ Monitoring of Concrete Structures by AE, Japanese Society for Non-destructive Inspection.

137 Ohtsu M., Uchida M., Okamoto T., and Yuyama S. Damage Assessment of Reinforced Concrete Beams Qualified by Acoustic Emission. Structural Journal, volume 99, issue 4, pp 411-417

138 Cox, S. J. D. and Meredith, P. G., Int. J. Rock Mech. Min. Sci. Geomech. Abstr., 30 (1), 1993,11-21.

139 Behnia A, Chai H.K., Mousa A.A., Seyed Ravanfar A. A novel damage index for online monitoring of RC slabs under monotonic loading by integration of process controlling into acoustic emission technique. Mechanical Systems and Signal Processing 119 (2019) 547–560

140 Gostautas R.S., Ramirez G., Peterman R.J., Meggers D. Acoustic emission monitoring and analysis of glass fibre-reinforced composites bridge decks. Journal of bridge engineering. 2005 November 1;10(6):713-21.

141 Nair A., Cai C. S. Acoustic emission monitoring of bridges: Review and case studies. Engineering Structures, Volume 32, Issue 6, June 2010, Pages 1704-1714 https://doi.org/10.1016/j.engstruct.2010.02.020

142 Golaski L, Gebski P and Ono K. Diagnostic of reinforced concrete bridges by acoustic emission. Journal of acoustic emission. 2002; 20:80-98.

143 Chotickai,P. (2001), "Acoustic Emission Monitoring of Prestressed Bridge Girders with Premature Concrete Deterioration." Masters thesis, University of Texas,Austin.

144 Ghobarah, A & Abou-EH& Biddah, A. (1999). Response-based damage assessment of Structures. Earthquake Engineering & Structural Dynamics. 28. 79 - 104. 10.1002/(SICI)1096-9845(199901)28:1<79::AID-EQE805>3.0.CO;2-J.

145 DiPasquale, E. and Cakmak, AS., "On the Relation Between Local and Global Damage Indices", NCEER-89-0034, National Center for Earthquake Engineering Research, State University of New York at Buffalo, 1989